On-shell methods and positive geometry

Akshay Yelleshpur Srikant

a dissertation
presented to the faculty
of princeton university
in candidacy for the degree
of Doctor of Philosophy

recommended for acceptance
by the Department of
Physics

Adviser: Nima Arkani-Hamed

September 2020

Abstract

The past few decades have seen the development of a number of techniques for calculating scattering amplitudes without recourse to quantum fields and Feynman diagrams. These are broadly referred to as on-shell methods. The development of these methods has birthed a new perspective on scattering amplitudes. In many cases they can be thought of as differential forms with special properties on constrained spaces - i.e. as differential forms on so called positive geometries. The constraints of positivity suffice to completely determine the singularity structure of the S-matrix in these cases. This thesis is focused on understanding the emergence of known physics from positive geometries, computations in this new formalism and developments in on shell methods for theories involving massive particles. The first two chapters study the amplituhedron which is the positive geometry relevant to $\mathcal{N} = 4$ super Yang-Mills. They focus on understanding the constraints of positivity and on seeing the physics of unitarity emerge from it. The next chapter develops geometric and on-shell techniques for understanding the properties of one loop integrals from the integrand in Feynman parameter space. The final chapter takes a step closer to the real world and develops an on-shell formalism for computing amplitudes in the bosonic, electroweak sector of the Standard Model. This includes an on-shell understanding of the Higgs mechanism within the context of the Standard Model.

Contents

Acknowledgments

This thesis would have been impossible without the support, guidance and encouragement of a large number of amazing people. I feel a serious dearth of synonyms for the word "thanks". First and foremost, it has been a privilege to work with Nima Arkani-Hamed. It is hard to overstate the magnitude of debt I owe him. It has long surpassed trans-Planckian scales. I have benefited from his deep intuition, extensive knowledge and patient guidance. I have never ceased to be amazed at his breadth and depth of knowledge, both of which extend well beyond physics. His knack for getting to the heart of a problem and constant source of innovative ideas ensured that every single meeting with him concluded on a hopeful note. His unmatched enthusiasm for physics and his spirit of inquiry have been a constant source of motivation for me throughout graduate school. He will undoubtedly continue to be a source of inspiration for the rest of my life.

Scientific progress is rarely the result of a solo venture. This thesis too, has been influenced by numerous interactions. It is my pleasure to thank Jaroslav Trnka for being an amazing collaborator, teacher and for offering valuable advice for the past few years. I am grateful to him for agreeing to be a reader for this thesis. I thank my other collaborators, Cameron Langer and Brad Bachu for their contributions to this thesis. I thank Chris Tully and Igor Klebanov for agreeing to serve on my committee. I am indebted to the Department of Physics at Princeton and the Institute for Advanced Study for providing an excellent academic environment and conducive places to do research. Finally, I have learnt a lot from discussions with a number of people including Aaron Hillman, Wayne Zhao, Ellis Yuan, Ziming Ji and Himanshu Khanchandani.

On a more personal note, I am fortunate to have been surrounded by amazing friends who were a constant source of love and support. I thank Sravya for being a fixture of my life at Princeton. You've been with me through thick and thin. I thank Sravya, Sumegha and Niranjani for putting up with my increasingly frequent visits to their house. It has been a home away from home for me because you have always been the most gracious of hosts and excellent company. I thank my roommates Arjun and Akshay for making my house much

more lively and fun. I thank all my other friends for the numerous potlucks, trips, board game sessions and more. These have ensured that graduate school will be a phase of my life that I will recall fondly. Being largely unaffected by a global pandemic has brought into sharp focus the privileges of my life. This is in no small part due to the tireless efforts of my parents. I would be remiss if I failed to thank my parents Nandini and Srikant, my sister Manjari and my brother-in-law Ajay for all their love, encouragement and support.

0

Introduction

The principles of Poincaré invariance and quantum mechanics are the pillars of 20th century fundamental physics. Since any theory of physics must be consistent with these principles, it is logical to look for a framework in which they are unified. The unification of these principles in a manifestly local and unitary fashion led to the birth of quantum field theory. The quantity of greatest interest in any quantum field theory is the scattering matrix or S-matrix. The ability to compute scattering amplitudes, which are elements of the S-matrix,

using Feynman rules derived from a Lagrangian was one of the earliest successes of Quantum field theory. The taming of infinities of loop integrals by the development of techniques like the renormalization group further entrenched the position of Quantum field theory in fundamental physics. However the complexity of the computations of scattering amplitudes seemed to grow exponentially with the number of particles involved, particularly in the case of massless particles. This is exemplified by the 6 page computation of $2 \to 4$ gluon amplitude in [1]. Surprisingly, this huge result could be condensed into a single line. More surprisingly the single line result with slight modifications was also the result for the $2 \to n$ MHV gluon scattering [2]. In the next few decades, this stunning simplicity fuelled explosive progress in understanding of scattering amplitudes. It is now well understood that the complexity of the calculations stemmed entirely from the presence of gauge degrees of freedom - corresponding to the longitudinal polarizations of the gluon. The Feynman rules compute of an intermediate quantity - which we call the Feynman amplitude - that then needs to be contracted with polarization vectors to obtain the physical scattering amplitude. Indeed, all the complexity disappears in the final result for gluons of transverse polarizations.

The simplicity of the final amplitude precipitated the development of a multitude of techniques, broadly referred to as "on-shell methods", whose aim was compute the physical scattering amplitude directly without recourse to Feynman rules. The goal was to avoid computing the Feynman amplitude altogether and directly arrive at the final, simple expression by using only on-shell quantities and physical principle. Consequently, these techniques make no references to Lagrangians, path integrals and quantum fields. Scattering amplitudes

are thought of as functions of the external kinematic data which were severely constrained by physical principles like locality, unitarity, causality, global and spacetime symmetries. These developments were largely restricted to theories involving only massless particles as these were the theories plagued by gauge redundancy.

One of the earliest on-shell techniques are the unitarity based methods [3]. They were used to evaluate loop integrals which were impossible by traditional, Feynman diagrammatic techniques. In the next decade, new recursion relations like BCFW [4, 5] and CSW [6] enabled the computation of four and higher point amplitudes beginning with three point amplitudes - which were completely fixed by Poincarè invariance. The singularity structure of the S-matrix was a slave to the principles of locality and unitarity. These determined the locations of the poles, their residues, the location of branch points and the discontinuities across the corresponding branch cuts.

Symmetries play a pivotal role in constraining the S-matrix. They impose stringent constraints on scattering amplitudes (examples of which include charge conservation and Poincarè symmetry) or relate different processes (an example of this is supersymmetry). It is extremely beneficial to choose the representation of the external kinematics such that the amplitudes have simple transformation laws under the relevant symmetry groups. The choice of spinor helicity variables (which correspond to the transverse polarizations of the gluons) in the gluon amplitude makes the Little group transformation of amplitudes explicit. This made the resulting expression simple. The use of twistor variables makes the conformal properties of scattering amplitudes obvious while the momentum twistors make the dual conformal symmetry manifest. The new expressions also

promoted alternative ways of thinking about scattering amplitudes, particularly in $\mathcal{N} = 4$ SYM [7].

On-shell methods have proven to be spectacularly successful in $\mathcal{N} = 4$ super Yang-Mills (SYM). The vast symmetry group of the theory permitted an all loop extension of BCFW recursion relations [8]. Exploitation of this symmetry has also led to the discovery of the underlying Grassmannian structure [9] of the theory. Each amplitude corresponds to a differential form on a Grassmannian. Grassmannians corresponding to higher point amplitudes are constructed by gluing together those corresponding to lower point amplitudes. A convenient diagrammatic implementation of these rules, called on-shell diagrams replaces Feynman diagrams in this theory. While symmetries suffice to fix three point amplitudes, four and higher point amplitudes are constructed by gluing together three point amplitudes in a manner dictated by unitarity.

The Grassmannian formulation of scattering amplitudes in planar $\mathcal{N} = 4$ SYM made possible a fundamental reformulation of our understanding of scattering amplitudes. It shifted the role of locality and unitarity from guiding principles to emergent properties. The underlying fundamental principle was positivity. The amplituhedron was a geometric object whose boundaries were determined by the requirements of positivity. This in turn determines the singularities of scattering amplitudes. The amplituhedron was just the first example of a positive geometry in connection with scattering amplitudes. This was followed by the discovery of positivity in several other contexts - the associahedron in biadjoint scalar field theory, in conformal field theory, in effective field theory and in ϕ^4 theory.

The ideas outlined so far set the stage for the work presented in this thesis.

The body of work has a number of important frontiers. The amplituhedron is well defined and the central problem now lies in solving the positivity constraints. Understanding precisely how perturbative unitarity emerges from these positivity constraints will provide valuable prototype for emergent unitarity. Furthermore, a complete understanding of the constraints is now the central problem and is crucial in understanding the physics of $\mathcal{N} = 4$ SYM. While the amplituhedron geometrizes the loop integrands of the theory, we are still far away from a geometric understanding of loop integrals. It is essential to look for geometric structure in loop integrals, beginning with the simplest case of one loop integrals. The bulk of research in the field of scattering amplitudes over the last few decades has focused on theories with only massless particles. Yet, an understanding of massive particles is essential for any complete theory of Nature. Understanding massive theories and their physics from a purely on-shell perspective is an essential preliminary step. This thesis represents research done towards these goals. The following section provides a brief overview of its contents.

0.1 Overview of the thesis

In chapter 1, we review the definition of the amplituhedron and the essential concepts of canonical forms. We use this definition to present a proof of perturbative unitarity for planar $\mathcal{N} = 4$ SYM, following from the geometry of the amplituhedron. This proof is valid for amplitudes of arbitrary multiplicity n, loop order L and MHV degree k. This is based on the following paper:

A. Yelleshpur Srikant, *Emergent unitarity from the amplituhedron*,

JHEP 01 (2020), 069

In chapter 2, we use the examine the definition of the amplituhedron and attempt to understand mutual positivity. The definition of the amplituhedron in terms of sign flips involves both one-loop constraints and the "mutual positivity" constraint. To gain an understanding of the all-loop integrand of $\mathcal{N} = 4$ sYM requires understanding the crucial role played by mutual positivity. This paper is an attempt towards developing a procedure to introduce the complexities of mutual positivity in a systematic and controlled manner. As the first step in this procedure, we trivialize these constraints and understand the geometry underlying the remaining constraints to all loops and multiplicities. We present a host of configurations which correspond to various faces of the amplituhedron. The results we derive are valid at all multiplicities and loop orders for the maximally helicity violating (MHV) configurations. These include detailed derivations for the results in [10]. We conclude by indicating how one might move beyond trivial mutual positivity by presenting a series of configuration which re-introduce it bit by bit. This is based on the following papers

- C. Langer and A. Yelleshpur Srikant, *All-loop cuts from the Amplituhedron*, **JHEP 1904**, 105 (2019)

- N. Arkani-Hamed, C. Langer, A. Yelleshpur Srikant and J. Trnka, *Deep Into the Amplituhedron: Amplitude Singularities at All Loops and Legs*, **Phys. Rev. Lett. 122**, no. 5, 051601 (2019)

Chapter 3 is devoted to understanding the geometry of Feynman parameter space. Spherical contours introduced in [11] translate the concept of "discontinuity across a branch cut" to Feynman parameter space. In this paper, we fur-

ther explore spherical contours and connect them to the computation of leading IR divergences of 1 loop graphs directly in Feynman parameter space. These spherical contours can be used to develop a Feynman parameter space analog of "Leading Singularities" of loop integrands which allows us to develop a method of determining Feynman parameter integrands without the need to sum over Feynman diagrams in momentum space. Finally, we explore some interesting features of Feynman parameter integrands in $\mathcal{N} = 4$ SYM. This is based on the following paper which is currenty under review by **JHEP**

A. Yelleshpur Srikant,*Spherical Contours, IR Divergences and the geometry of Feynman parameter integrands at one loop*

Chapter 4 is devoted to the development of an on-shell formalism for the bosonic sector of the standard model.We describe a new approach towards the development of an entirely on-shell description of the bosonic electroweak sector of the Standard Model and the Higgs mechanism. We write down on-shell three particle amplitudes consistent with Poincaré invariance and little group covariance. Tree-level, four particle amplitudes are determined by demanding consistent factorization on all poles and correct UV behaviour. We present expressions for these $2 \to 2$ scattering amplitudes using massive spinor helicity variables. We show that on-shell consistency conditions suffice to derive relations between the masses of the $W^{\pm}, Z$, the Weinberg angle and the couplings. This provides a completely on-shell description of the Higgs mechanism without any reference to the vacuum expectation value of the Higgs field. This is based on the following paper which is currently under review by JHEP.

B. Bachu and A. Yelleshpur, *On-Shell Electroweak Sector and the Higgs Mechanism*

1

Emergent Unitarity from the amplituhedron

1.1 Introduction

Unitarity is at the heart of the traditional, Feynman diagrammatic approach to calculating scattering amplitudes. It is built into the framework of quantum field theory. Modern on-shell methods provide an alternative way to calculate

scattering amplitudes. While they eschew Lagrangians, gauge symmetries, virtual particles and other redundancies associated with the traditional formalism of QFT, unitarity remains a central principle that needs to be imposed. It has allowed the construction of loop amplitudes from tree amplitudes via generalized Unitarity methods [3, 12–15] and the development of loop level BCFW recursion relations [5, 8]. These on-shell methods have been particularly fruitful in planar $\mathcal{N} = 4$ SYM and led to the development of the on-shell diagrams in [9] and the discovery of the underlying Grassmannian structure. Locality and unitarity seemed to be the guiding principles which dictated how the on-shell diagrams glued together to yield the amplitude. The discovery of the amplituhedron in [16], [17] revealed the deeper principles behind this process - positive geometry. Positivity dictated how the on-shell diagrams were to be glued together. The resulting scattering amplitudes were miraculously local and unitary!

This discovery of the amplituhedron was inspired by the polytope structure of the six point NMHV scattering amplitude, first elucidated in [18] and expanded upon in [19]. This motivated the original definition of the amplituhedron which was analogous to the definition of the interior of a polygon. The tree amplituhedron $\mathcal{A}_{n,k,0}$ was defined as the span of k planes Y^I_α, living in $(k+4)$ dimensions. Here $I = \{1, \ldots, k+4\}$ and $\alpha = \{1, \ldots k\}$.

$$Y^I_\alpha = C_{\alpha a} \mathcal{Z}^I_a \tag{1.1}$$

where $\mathcal{Z}^I_a$ $(a = 1, \ldots n)$ are positive external data in $(k+4)$ dimensions. In this context, positivity refers to the conditions $det\left\{\mathcal{Z}_{a_1}, \ldots \mathcal{Z}_{a_{k+4}}\right\} \equiv \langle \mathcal{Z}_{a_1} \ldots \mathcal{Z}_{a_{k+4}} \rangle > 0$ if $a_1 < \cdots < a_{k+4}$ and $C_{\alpha a} \in G_+(k,n)$. $G_+(k,n)$ is the positive Grassmannian

defined as the set of all $k \times n$ matrices with ordered, positive $k \times k$ minors. For more details on the properties of the positive Grassmannian, see [9, 20–22] and the references therein. The scattering amplitude can be related to the differential form with logarithmic singularities on the boundaries of the amplituhedron. The exact relation along with the extension of eq.(1.1) to loop level can be found in [16].

The amplituhedron thus replaced the principles of unitarity and locality by a central tenant of positivity. Tree level locality emerges as a simple consequence of the boundary structure of the amplituhedron, which in turn is dictated by positivity. The emergence of unitarity is more obscure. It is reflected in the factorization of the geometry on approaching certain boundaries. This was proved for $\mathcal{A}_{4,0,L}$ in [17]. The extension of this proof to amplitudes with arbitrary multiplicity using (1.1) is cumbersome and requires the use of the topological definition of the amplituhedron introduced in [23]. In the following section, we review this definition in some detail along with some properties of scattering amplitudes relevant to this chapter. We also expound the relation between the amplituhedron and scattering amplitudes. The rest of the chapter is structured as follows. In Section [1.3], we present a proof of unitarity of scattering amplitudes for 4 point amplitudes of planar $\mathcal{N} = 4$ SYM, using the topological definition of the amplituhedron. This serves as a warm up to Section [1.4] in which we provide a proof which is valid for MHV amplitudes of any multiplicity. Finally, in Section 1.5 we show how the proof of the previous section can be extended to deal with the complexity of higher k sectors.

1.2 Review of the topological definition of $\mathcal{A}_{n,k,L}$

The scattering amplitudes extracted from the amplituhedron defined as in (1.1), using the procedure outlined in [16], reproduce the Grassmannian integral form of scattering amplitudes presented in [20–22, 24, 25]. These necessarily involve the auxiliary variables $C_{\alpha a}$. In contrast, the topological definition of the amplituhedron can be stated entirely in terms of the $4D$ momentum twistors (first introduced in [18]). Consequently, this yields amplitudes that can be thought of as differential forms on the space of momentum twistors. In this section, we will review the basic concepts involved in the topological definition of the amplituhedron. We begin with a review of momentum twistors and their connection to momenta in Section [1.2.1] and proceed to the topological definition of the amplituhedron in Section [1.2.2]. We then explain how amplitudes are extracted from the amplituhedron in Section [1.2.3] and finally, in Section [1.2.4], we set up the statement of the optical theorem in the language of momentum twistors. This is the statement we will prove in the main body of the chapter.

1.2.1 Momentum twistors

Momentum twistor space is the projective space $\mathbb{CP}^3$. A connection to physical momenta can be made by writing them in the coordinates of an embedding $\mathbb{C}^4$ as $Z_a = \left(\lambda_{a\,\alpha}, \mu_a^{\dot{\alpha}}\right)$. Here $(\lambda, \tilde{\lambda})$ are the spinor helicity variables which trivialize the on-shell condition.

$$p_{a\,\alpha\dot{\alpha}} \equiv \lambda_{a\,\alpha}\tilde{\lambda}_{a\,\dot{\alpha}} \implies p_a^2 = \det(\lambda_a, \lambda_a)\det(\tilde{\lambda}_a, \tilde{\lambda}_a) = 0$$

$\mu_a^{\dot{\alpha}} = x_a^{\alpha\dot{\alpha}}\lambda_{a\alpha}$ where the dual momenta x_a are defined via $p_a = x_a - x_{a-1}$ and trivialize conservation of momentum. Thus the point x_a in dual momentum space is associated to a line in momentum twistor space. Scattering amplitudes in $\mathcal{N} = 4$ SYM involve momenta p_a which are null ($p_a^2 = 0$) and are conserved ($\sum_a p_a = 0$). Momentum twistors are ideally suited to describe the momenta involved in these amplitudes because they trivialize both these constraints. Figure 1.1 summarizes the point-line correspondence between points in dual momentum space and lines in momentum twistor space. Thus all the points of the

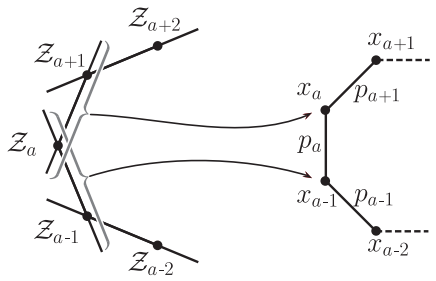

Figure 1.1: A representation of the relationship between momenta and momentum twistors, taken from [26].

form

$$Z_a = \left(\lambda_{a\,\alpha},\, x_a^{\alpha\dot{\alpha}}\lambda_{a\alpha}\right) \tag{1.2}$$

are associated to the momentum p_a. Note that these Z_a are different from the calligraphic $\mathcal{Z}_a$ used in 1.1(the connection between the two is that Z_a are obtained by projecting the $\mathcal{Z}_a$ through the $k-$plane Y in 1.1). Thus, a set of on-shell momenta $\{p_1, \ldots p_n\}$ satisfying $\sum_{a=1}^{n} p_a = 0$ can be represented by an ordered set of momentum twistors $\{Z_1, \ldots Z_n\}$. Each line $Z_a Z_{a+1}$ corresponds to the point x_a in dual momentum space as shown in Fig 1.1.

Each loop momentum ℓ_a can also be associated to a line in momentum twistor space. We denote these lines by $(AB)_a$, where A and B are any representative points. This helps us distinguish loop momenta from other external momenta. We can express Lorentz invariants in terms of determinants of momentum twistors using the relation

$$(x_a - x_b)^2 = \frac{\langle a-1ab-1b\rangle}{\langle a-1a\rangle\langle b-1b\rangle} \tag{1.3}$$

with $\langle abcd\rangle = \det\ \{Z_a, Z_b, Z_c, Z_d\}$ and $\langle ab\rangle = \det\ \{I_\infty, Z_a, Z_b\}$ where I_∞ is the infinity twistor [21, 26]. Finally, we connect the invariants involving the $\mathcal{Z}_a^I$ with the four bracket via

$$\langle Z_a Z_b Z_c Z_d\rangle = \epsilon_{I_1\ldots I_{k+4}} Y_1^{I_1}\ldots Y_k^{I_k}\mathcal{Z}_a^{I_{k+1}}\mathcal{Z}_b^{I_{k+2}}\mathcal{Z}_c^{I_{k+3}}\mathcal{Z}_d^{I_{k+4}}$$

We will utilize this connection later in Section [1.5.4].

1.2.2 Topological definition

The amplituhedron $\mathcal{A}_{n,k,L}$ is a region in momentum twistor space which can be cut out by inequalities. The region depends on the integers n, k and L which specify the $n-$point, N^{k}MHV amplitude. n is the number external legs of the amplitude and correspondingly the number of momentum twistors which are involved in the definition of the amplituhedron. We denote these by $\{Z_1, \ldots Z_n\}$. L is the number of loops and we have the lines, $(AB)_1, \ldots\ldots (AB)_L$ corresponding to the L loop momenta $\ell_1, \ldots \ell_L$. k appears below in the inequalities that define $\mathcal{A}_{n,k,L}$.

Tree level conditions

The first set of conditions that define the amplituhedron involve only the external momentum twistors Z_a and we refer to these as the "tree-level" conditions. They are listed below along with some comments about each condition.

- The external data must satisfy the following positivity conditions.

$$\langle ii+1jj+1\rangle > 0 \quad i = 1, \dots n \tag{1.4}$$

  We adopt an ordering $(1, \dots n)$ in all definitions. We must also define a twisted cyclic symmetry for this ordering with

$$Z_{n+i} \equiv (-1)^{k-1} Z_i \tag{1.5}$$

  This definition is required to ensure that $\langle ii+1n1\rangle > 0$ for odd k and $\langle ii+1n1\rangle < 0$ for even k. We will see below that this is crucial to obtain the right number of sign flips.

- We require that the sequence

$$S^{\text{tree}} : \{\langle 1234\rangle, \langle 1235\rangle \dots \langle 123n\rangle\} \text{ has } k \text{ sign flips.} \tag{1.6}$$

  Note that the ordering $(1, \dots n)$ is crucial for the above condition to make sense. Using (1.4), (1.6) and the reasoning in Appendix [B], we can conclude that all sequences of the form

$$\big\{\langle ii+1i+2i+3\rangle, \dots \langle ii+1i+2n\rangle, (-1)^{k-1}\langle ii+1i+21\rangle, \dots \langle ii+1i+2i-1\rangle(-1)^{k-1}\big\}$$

with $i = 1, \ldots n$ have k sign flips. The use of (1.5) is crucial in arriving at this conclusion. Since all the sequences $\{\langle ii+1i+2j\rangle\}_{j=i+3}^{j=i-1}$ have the same number of flips (with the appropriate twisted cyclic symmetry factors), we can use any of them in place of the sequence $\{\langle 123i\rangle\}_{i=4}^{i=n}$. In the rest of the chapter, we will the sequence which is most convenient to the situation.

Loop level conditions

The next set of conditions involve both the external data and the loops $(AB)_a$ and we refer to these as "loop level" conditions.

- Each loop $(AB)_a$ must satisfy a positivity condition analogous to (1.4)

$$\langle (AB)_a ii+1\rangle > 0 \quad i = 1, \ldots n \tag{1.7}$$

  Note that we must include the twisted cyclic symmetry factor $(-1)^{k-1}$ here as well. Once again, this implies that $\langle (AB)_a n1\rangle > 0$ for odd k and $\langle (AB)_a 1n\rangle > 0$ for even k.

- We require that sequence

$$S^{\text{loop}} : \{\langle (AB)_a 12\rangle, \langle (AB)_a 13\rangle, \ldots \langle (AB)_a 1n\rangle\} \text{ has } k+2 \text{ flips.} \tag{1.8}$$

  Following a line of reasoning similar to that in 1.2.2, we can show that all sequences of the form

$$\left\{\langle (AB)_a ii+1\rangle, \ldots \langle (AB)_a in\rangle, \langle (AB)_a i1\rangle(-1)^{k-1}, \ldots \langle (AB)_a ii-1\rangle(-1)^{k-1}\right\}$$

with $i = 1, \ldots n$ have the same number of sign flips. We will make use of these sequences as convenient in the rest of the chapter.

Mutual positivity condition

The final condition is a relation involving multiple loop momenta $(AB)_a$. We must have

$$\langle (AB)_a (AB)_b \rangle > 0 \qquad \forall a, b = \{1, \ldots L\} \tag{1.9}$$

For multi loop amplitudes, the conditions above amount to demanding that each loop $(AB)_a$ is in the one-loop amplituhedron (i.e. it satisfies conditions (1.7) and (1.8)) and also the mutual positivity condition (1.9). Finding a solution to all these inequalities is tantamount to computing the $n-$point N^{k}MHV amplitude. The complexity of solving the mutual positivity condition shows up even in the simplest case of $n = 4$. Indeed, its solution is at the heart of the four point problem, as explained in [17].

The topological definition is well suited to exploring cuts of amplitudes (which correspond to saturating some of the inequalities in (1.4) - (1.9) by setting them to be equal to zero). This formalism has been exploited to investigate the structure some cuts of amplitudes that are inaccessible by any other means. The results of some classes of these "deep" cuts are obtained to all loop orders in [10, 27].

1.2.3 Amplitudes and integrands as Canonical Forms

The inequalities (1.4) - (1.9) define a region in the space of momentum twistors. The goal of the amplituhedron program is to be able to obtain the amplitude from purely geometric considerations. More precisely, we can obtain the tree level amplitude and the loop level integrand for planar $\mathcal{N} = 4$ SYM. In contrast to generic quantum field theories, the planar integrand in $\mathcal{N} = 4$ SYM is a well defined, rational function as shown in [8, 28]. The conjecture here is that the Canonical form associated to the amplituhedron is the loop integrand. The Canonical form associated to a region is the differential form with logarithmic singularities on all the boundaries of that region. For more details on Canonical forms, their properties and precise definitions, see [29]. The discovery of amplituhedron-like geometric structures (for e.g. [30–33]) in other theories lends further support to the idea that amplitudes can be thought of as differential forms on kinematic spaces. Some consequences of this are explored in [34]. It is interesting to note that a topological definition of the amplituhedron has been found directly in momentum space [35]. This allows for the possibility of expressing $\mathcal{N} = 4$ SYM amplitudes as differential forms in momentum space rather than momentum twistor space.

It is illustrative to show the calculation of the canonical form for the simple case of $\mathcal{A}_{4,0,1}$. This canonical form should be the 4-point, one-loop MHV inte-

grand. The defining inequalities are

$$\begin{aligned} &\underline{\text{Tree Level :}}\ \langle 1234\rangle > 0 \\ &\underline{\text{Loop Level :}}\ \langle AB12\rangle > 0,\ \langle AB23\rangle > 0,\ \langle AB34\rangle > 0,\ \langle AB14\rangle > 0, \\ &\qquad\qquad \langle AB13\rangle < 0,\ \langle AB24\rangle < 0 \end{aligned} \tag{1.10}$$

Since $A, B \in \mathbb{C}^4$, we can expand these in a basis consisting of $\{Z_1, Z_2, Z_3, Z_4\}$. However, A, B are arbitrary points on the line AB which corresponds to the loop momentum. Since any linear combination (A', B') of the points A and B is also on the same line, there is a $GL(2)$ redundancy in the choice of A and B. Fixing this redundancy, we arrive at the following parametrization.

$$A = Z_1 + \alpha_1 Z_2 + \alpha_2 Z_3 \qquad B = -Z_1 + \beta_1 Z_3 + \beta_2 Z_4$$

The solution to the inequalities in (1.10) is

$$\alpha_1 > 0 \qquad \alpha_2 > 0 \qquad \beta_1 > 0 \qquad \beta_2 > 0$$

The boundaries are located at $\alpha_1 = \alpha_2 = \beta_1 = \beta_2 = 0$ and the differential form with logarithmic singularities on all the boundaries is just

$$\frac{d\alpha_1}{\alpha_1}\frac{d\alpha_2}{\alpha_2}\frac{d\beta_1}{\beta_1}\frac{d\beta_2}{\beta_2} = \frac{\langle ABd^2A\rangle\langle ABd^2B\rangle}{\text{Vol}(GL(2))}\frac{\langle 1234\rangle^2}{\langle AB12\rangle\langle AB23\rangle\langle AB34\rangle\langle AB14\rangle}$$

This is the integrand for the 1-loop four point MHV amplitude as conjectured.

At higher points, the situation is more complicated cases. There are multiple ways in which the sequence S^{loop} (1.8) can have $k+2$ sign flips. It is useful to

triangulate the complete region by enumerating all such patterns. This procedure works extremely well for $n-$point MHV amplitudes and is fleshed out in Section [7] of [23]. Specifically, if we parametrize

$$A_a = Z_1 + \alpha_1 Z_i + \alpha_2 Z_{i+1} \quad B_a = -Z_1 + \beta_1 Z_j + \beta_2 Z_{j+1} \tag{1.11}$$

with $\alpha_i > 0$, $\beta_i > 0$, we have $\frac{\langle (AB)_a 1i\rangle}{\langle (AB)_a 1i+1\rangle} = -\frac{\alpha_1}{\alpha_2}$ and $\frac{\langle (AB)_a 1j\rangle}{\langle (AB)_a 1j+1\rangle} = -\frac{\beta_1}{\beta_2}$. The sequence $\{\langle (AB)_a 1i\rangle\}$ has two sign flips, one occurring between $\langle (AB)_a 1i\rangle$ and $\langle (AB)_a 1i+1\rangle$ and the second between $\langle (AB)_a 1j\rangle$ and $\langle (AB)_a 1j+1\rangle$. Summing over all $i < j = \{1, \ldots n\}$ covers all the positions of the flips. The canonical form for this region is the integrand of the $n-$ point MHV amplitude.

$$\sum_{i<j} \langle ABd^2A\rangle \langle ABd^2B\rangle \frac{\langle AB(1ii+1 \cap 1jj+1)\rangle^2}{\langle AB1i\rangle\langle AB1i+1\rangle\langle ABii+1\rangle\langle AB1j\rangle\langle AB1j+1\rangle\langle ABjj+1\rangle}$$

For another derivation of this integrand, please refer to [8].

Finally, an important property of these forms is that they are all projectively well defined. They are invariant under the re-scaling $Z_i \to t_i Z_i$ of each external leg. We will make use of this property in Section [1.5].

1.2.4 Unitarity and the Optical theorem

The relationship between the singularity structure of scattering amplitudes and unitarity has been the subject of a lot of work. [3, 12–15, 28, 36–38]. It is well known that the branch cut structure of amplitudes is intimately tied to perturbative unitarity. This is encapsulated in the optical theorem which related the discontinuity across a double cut to the product of lower loop amplitudes.

The presence of branch points in loop amplitudes is due to the pole structure of the integrand. This is governed by the boundary structure of the amplituhedron. The structure of boundaries and their relation to branch points has been studied extensively in [39–46]. The discontinuity across a branch cut is calculated by the residue on an appropriate boundary of the amplituhedron. The optical theorem thus translates into a statement about the factorization of the residue on this boundary. We expect this factorization to emerge as a consequence of the positive geometry.

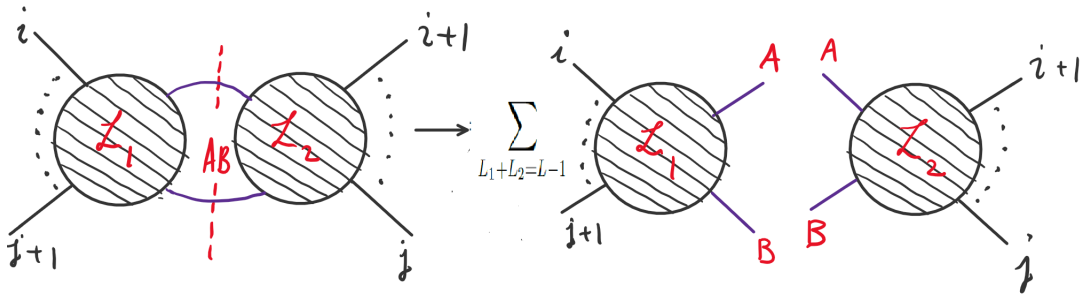

Figure 1.2: Structure of a unitarity cut of MHV amplitudes. The loop (AB) is cut and the residue factorizes as shown.

Let us begin by rewriting the optical theorem, specifically for $\mathcal{N} = 4$ SYM in the language of momentum twistors. For now, we will focus on MHV amplitudes. We are interested in the case where one of the loops, AB, cuts the lines $ii+1$ and $jj+1$ and all other loops (which we denote by $(AB)_a$) remain uncut. Thus we are calculating the residue of the $n-point$ MHV amplitude on the cut $\langle ABii+1\rangle = \langle ABjj+1\rangle = 0$. It is convenient to parametrize AB as

$$A = Z_i + xZ_{i+1} + w_1 Z_\star \qquad B = yZ_j + Z_{j+1} + w_2 Z_\star \tag{1.12}$$

where $Z_\star$ is an arbitrary reference twistor. The terms in the L-loop integrand which contribute to this cut (which has the required poles) can be written as

$$\mathcal{M}_n^L = \frac{\langle ABd^2A\rangle\langle ABd^2B\rangle}{\langle ABii+1\rangle\langle ABjj+1\rangle}\prod_{a=1}^{L-1}\langle(AB)_a d^2A_a\rangle\langle(AB)_a d^2B_a\rangle f(x,y,w_1,w_2,(AB)_a)$$

The dependence of f on the external twistors has been suppressed. The residue of $\mathcal{M}_n^L$ on the cut $\langle ABii+1\rangle = \langle ABjj+1\rangle = 0$ is

$$Res_{w_1=w_2=0}\,\mathcal{M}_n^L = \frac{dx\,dy}{g(x,y)}\prod_{a=1}^{L-1}\langle(AB)_a d^2A_a\rangle\langle(AB)_a d^2B_a\rangle f(x,y,0,0,(AB)_a) \quad (1.13)$$

where $g(x,y)$ is a Jacobian which is irrelevant to our purposes. Unitarity predicts that the function $f(x,y,0,0,(AB)_a)$ is related to lower point amplitudes (see figure 1.2) and is of the form

$$f(x,y,0,0,(AB)_a) = \sum_{L_1+L_2=L-1}\mathcal{M}_{\mathcal{L}}^{L_1}(Z_{j+1},\dots Z_i,A,B)\mathcal{M}_{\mathcal{R}}^{L_2}(B,A,Z_{i+1},\dots,Z_j) \quad (1.14)$$

We will show that this structure emerges from the geometry of the amplituhedron. We will first present a proof for the four point case. This is just a rewriting of the proof found in [17] using the topological definition. This proof will then admit a generalization to amplitudes of higher multiplicity.

1.3 Proof for 4 point Amplitudes

In this section we will examine the unitarity cut $\langle AB12\rangle = \langle AB34\rangle = 0$, at four points and show that the residue can be written as a product of lower loop, 4-point amplitudes. Specifically, we will show that the defining conditions of

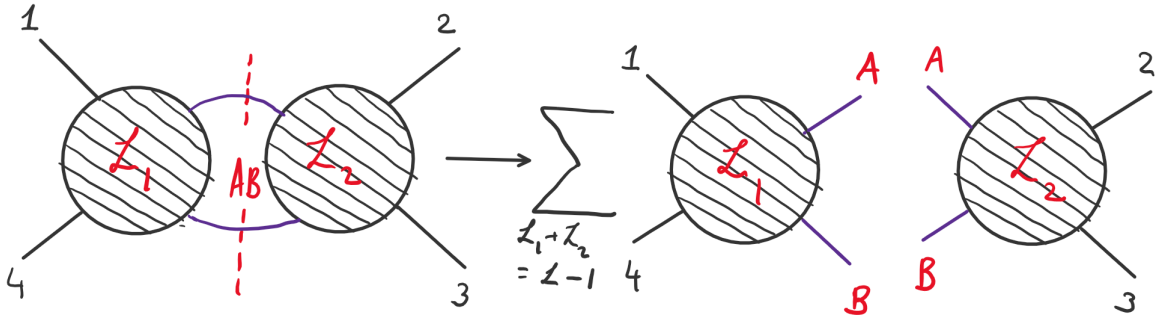

Figure 1.3: Structure of the unitarity cut at 4 points

the amplituhedron (1.4) - (1.8) can be replaced by two disjoint set of conditions which define a "left amplituhedron" with external data $\{Z_1, A, B, Z_4\}$ and a "right" amplituhedron with external data $\{A, Z_2, Z_3, B\}$. We will show that the mutual positivity conditions in (1.9) which seemingly connect the "left" and "right" amplituhedra are automatically satisfied once the defining conditions for the "left" and "right" amplituhedra are met. This suffices to prove that the canonical form on the cut is

$$\sum_{L_1+L_2=L-1} \mathcal{M}_{\mathcal{L}}^{L_1}(Z_1, A, B, Z_4)\ \mathcal{M}_{\mathcal{R}}^{L_2}(B, A, Z_2, Z_3)$$

where $\mathcal{M}_{\mathcal{L}}^{L_1}(Z_1, A, B, Z_4)$ and $\mathcal{M}_{\mathcal{R}}^{L_2}(B, A, Z_2, Z_3)$ are the canonical forms of the "left" and "right" amplituhedra respectively. A suitable parametrization of (AB) is

$$A = Z_1 + xZ_2 \qquad B = yZ_3 + Z_4 \tag{1.15}$$

This ensures the cut conditions are satisfied. To compute the canonical form on the cut, we must solve the remaining inequalities. The tree level constraints

(1.4), (1.6) trivially imply $\langle 1234\rangle > 0$. The remaining loop level conditions in (1.7) and (1.8) impose $\langle AB13\rangle < 0$ and $\langle AB14\rangle > 0$ which ensure $x > 0, y > 0$. Denoting the uncut loops as $(AB)_a$ with $a = 1, \ldots L-1$, the remaining inequalities are loop positivity conditions,

$$\langle (AB)_a jj+1\rangle > 0 \qquad \forall j = 1, \ldots 4, \tag{1.16}$$

mutual positivity among the uncut loops

$$\langle (AB)_a (AB)_b\rangle > 0, \tag{1.17}$$

and mutual positivity with the cut loop

$$\langle AB A_a B_a\rangle = \langle A_a B_a 13\rangle y + \langle A_a B_a 14\rangle + \langle A_a B_a 23\rangle xy + \langle A_a B_a 24\rangle x > 0. \tag{1.18}$$

Here we have used the parametrization (1.15) for A and B. The consequences of this inequality are best understood by considering the related quantity $(\langle (AB)_a 2B\rangle \langle (AB)_a A3\rangle)$. Using (1.15) for A and B, we can rewrite this as follows.

$$\begin{aligned}
&(\langle (AB)_a 2B\rangle \langle (AB)_a A3\rangle) \\
&= (\langle A_a B_a 24\rangle + \langle A_a B_a 23\rangle y)\,(\langle A_a B_a 13\rangle + \langle A_a B_a 23\rangle x) \\
&= \langle AB A_a B_a\rangle \langle A_a B_a 23\rangle - \langle A_a B_a 14\rangle \langle A_a B_a 23\rangle + \langle A_a B_a 13\rangle \langle A_a B_a 24\rangle \\
&= \langle AB A_a B_a\rangle \langle A_a B_a 23\rangle + \langle (A_a B_a 1 \cap A_a B_a 2) 34\rangle \\
&= \langle AB A_a B_a\rangle \langle A_a B_a 23\rangle + \langle A_a B_a 12\rangle \langle A_a B_a 34\rangle
\end{aligned} \tag{1.19}$$

The above equation implies $\langle (AB)_a 2B\rangle\langle (AB)_a A3\rangle > 0$ as each term on the right hand side is individually positive due to (1.16) and (1.18). The two possible solutions are

$$\langle (AB)_a 2B\rangle > 0 \qquad \langle (AB)_a A3\rangle > 0 \tag{1.20}$$

and

$$\langle (AB)_a 2B\rangle < 0 \qquad \langle (AB)_a A3\rangle < 0 \tag{1.21}$$

A particular loop $(AB)_a$ may satisfy either (1.20) or (1.21). In a generic case, there will be L_1 loops, $(AB)_{a_1}$ which obey (1.20) and $L_2 = L - L_1 - 1$ loops, $(AB)_{a_2}$ which obey (1.21). There are no restrictions on what values L_1 and L_2 can take. Consequently, the complete region satisfying the inequalities (1.16) and (1.18) is a sum over all values of L_1 and L_2 with $L_1 + L_2 = L - 1$. We will now show that the canonical form for a region with fixed L_1 and L_2 can be written as a product of forms for amplituhedra $\mathcal{A}_{4,0,L_1}$ and $\mathcal{A}_{4,0,L_2}$. From Fig. 1.3, it is clear the the external data corresponding to the left amplitude is the set $\{Z_1, A, B, Z_4\}$. Any loops $(AB)_{a_1}$ which belongs to this amplituhedron must

satisfy the defining conditions 1.4, 1.6, 1.7, 1.8.

$$\underline{\text{Tree Level}} \qquad \langle 1AB4\rangle = \langle AB14\rangle = \langle 1234\rangle > 0 \text{ from 1.15} \tag{1.22}$$

$$\underline{\text{Loop level}} \qquad \langle (AB)_{a_1} 1A\rangle = x\,\langle (AB)_{a_1} 12\rangle > 0 \qquad \langle (AB)_{a_1} B4\rangle = y\langle (AB)_{a_1} 34\rangle > 0$$

Both of these follow from (1.15) and (1.16)

$\langle (AB)_{a_1}\, AB\rangle > 0$ from (1.18)

The sequence $\{\langle (AB)_{a_1} 1A\rangle, \langle (AB)_{a_1} 1B\rangle, \langle (AB)_{a_1} 14\rangle\}$ has 2 sign flips

$\underline{\text{Mutual positivity}} \qquad \langle (AB)_{a_1} (AB)_{a_1'}\rangle > 0$ (1.17),

The flip condition is the only one left to be verified and follows from the Plücker relation

$$\langle (AB)_{a_1} 1B\rangle\langle (AB)_{a_1} 23\rangle - \langle (AB)_{a_1} 2B\rangle\langle (AB)_{a_1} 13\rangle = \langle (AB)_{a_1} 12\rangle\langle (AB)_{a_1} B3\rangle \tag{1.23}$$

This can be derived by noting that the 5 twistors $\{B, A_{a_1}, B_{a_1}, Z_1, Z_2\}$ are linearly dependent which leads to the condition

$$\langle BA_{a_1} B_{a_1} 1\rangle Z_2 \,+\, \langle A_{a_1} B_{a_1} 12\rangle B \,+\, \langle B_{a_1} 12B\rangle A_{a_1} \,+\, \langle 12BA_{a_1}\rangle B_{a_1} \,+\, \langle 2BA_{a_1} B_{a_1}\rangle Z_1 = 0.$$

Contracting this with $(AB)a_1 Z_3$ yields (1.23). Note that the RHS of (1.23) is negative since $\langle (AB)_{a_1} B3\rangle = -\langle (AB)_{a_1} 34\rangle < 0$ while the signs of the terms in the LHS are

$$\{\langle (AB)_{a_1} 23\rangle, \langle (AB)_{a_1} 2B\rangle, \langle (AB)_{a_1} 13\rangle\} \tag{1.24}$$

$$\{ \quad + \quad , + \quad , \quad - \quad \}$$

This forces $\langle (AB)_a 1B\rangle < 0$ and ensures that the sequence in (1.22) has 2 flips.

Similarly, the external data for the right is the set $\{A, Z_2, Z_3, B\}$ and a loop $(AB)_{a_2}$ which belongs to it satisfies the following conditions.

$$\begin{aligned}
&\underline{\text{Tree Level}} \qquad \langle A23B\rangle = \langle AB23\rangle > 0 \qquad (1.25)\\
&\underline{\text{Loop level}} \qquad \langle (AB)_{a_2} A2\rangle = \langle (AB)_{a_2} 12\rangle > 0 \qquad \langle (AB)_{a_2} 23\rangle > 0\\
&\qquad\qquad\qquad \langle (AB)_{a_2} 3B\rangle = \langle (AB)_{a_2} 34\rangle > 0\\
&\qquad\qquad\qquad \text{The sequence } \{\langle (AB)_{a_2} A2\rangle, \langle (AB)_{a_2} A3\rangle, \langle (AB)_{a_2} AB\rangle\} \text{ has 2 sign flips}\\
&\underline{\text{Mutual positivity}} \qquad \langle (AB)_{a_2} (AB)_{a_2'}\rangle > 0,
\end{aligned}$$

Clearly, the conditions (1.22) and (1.25) define the amplituhedra $\mathcal{A}_{4,0,L_1}$ and $\mathcal{A}_{4,0,L_2}$ with canonical forms $\mathcal{M}_{\mathcal{L}}^{L_1}(Z_1, A, B, Z_4)$ and $\mathcal{M}_{\mathcal{R}}^{L_2}(B, A, Z_2, Z_3)$ respectively. To complete the proof that the canonical form on the cut is just the product of these forms, we must show that that mutual positivity between the loops $(AB)_{a_1}$ and $(AB)_{a_2}$ imposes no further constraints. To see this, we can expand the loop $(AB)_{a_1}$ in terms of $\{Z_1, A, B, Z_4\}$

$$A_{a_1} = Z_1 + \alpha_1 A + \alpha_2 B \qquad B_{a_1} = -Z_1 + \beta_1 B + \beta_2 Z_4$$

and compute $\langle (AB)_{a_1} (AB)_{a_2}\rangle$ which yields,

$$\begin{aligned}
\langle (AB)_{a_1} (AB)_{a_2}\rangle = \quad & y\langle (AB)_{a_2} 1B\rangle \beta_1 + \langle (AB)_{a_2} 14\rangle \beta_2 + \langle (AB)_{a_2} 1A\rangle (\alpha_1) + \langle (AB)_{a_2} AB\rangle \alpha_1\beta_1\\
& + \langle (AB)_{a_2} A4\rangle a_{21}\beta_2 + \langle (AB)_{a_2} 1B\rangle (a_{22}) + \langle (AB)_{a_2} B4\rangle a_{22}\beta_2 \qquad (1.26)
\end{aligned}$$

The positivity of all the terms except for $\langle (AB)_{a_2} A4\rangle$ and $\langle (AB)_{a_2} B1\rangle$ immedi-

ately follows from (1.25). For these two, we have

$$\langle (AB)_{a_2} A4\rangle = \langle (AB)_{a_2} A(B - y3)\rangle = \langle (AB)_{a_2} AB\rangle - y\langle (AB)_{a_2} A3\rangle > 0$$
$$\langle (AB)_{a_2} 1B\rangle = \langle (AB)_{a_2} (A - x2)B\rangle = \langle (AB)_{a_2} AB\rangle - x\langle (AB)_{a_2} 2B\rangle > 0$$

Therefore, $\langle (AB)_{a_1} (AB)_{a_2}\rangle > 0$ imposes no new constraints and the canonical form on the cut factorizes into $\mathcal{M}_{\mathcal{L}}$ and $\mathcal{M}_{\mathcal{R}}$.

1.4 Proof for MHV amplitudes of arbitrary multiplicity

We will extend the above results to amplitudes of arbitrary multiplicity. However, the existence of higher k sectors beginning with $n = 5$ complicates the proof. In this section we will focus on a proof of unitarity for MHV amplitudes. This allows us to sketch the essentials of the proof without additional complications. In the next section, we modify the proof to account for higher k sectors.

We are examining the residue of the MHV amplituhedron $\mathcal{A}_{n,0,L}(Z_1, \ldots, Z_n)$ on the cut $\langle ABii+1\rangle = \langle ABjj+1\rangle = 0$. For the rest of the chapter, we will assume $j \neq i+1$*. The defining conditions for the amplituhedron $\mathcal{A}_{n,0,L}\{Z_1, \ldots Z_n\}$

*In the singular case of $j = i + 1$, the amplitude factorizes into a 3-point MHV or $\overline{\text{MHV}}$ amplitude a $n + 1$ point MHV amplitude. The 3 point case is degenerate and the use of momentum twistors ensures that all the defining conditions(on-shell and momentum conservation) are always satisfied. There are no further constraints that need to be imposed

are

$$\begin{aligned}
&\underline{\text{Tree Level}} \quad && \langle ijkl\rangle > 0 \text{ for } i<j<k<l \\
&\underline{\text{Loop level}} \quad && \langle ii+1\rangle > 0 \\
& && \text{The sequence } S = \{\langle i+1\, i+2\rangle, \ldots \langle i+1\, n\rangle, -\langle i+1\, 1\rangle, \cdots - \langle i+1\, i\rangle\} \\
& && \text{has 2 sign flips.} \\
&\underline{\text{Mutual Positivity}} \quad && \langle (AB)_a (AB)_b\rangle > 0 \qquad \forall a,b \in \{1,\ldots L\}
\end{aligned} \tag{1.27}$$

Here, $\langle ij\rangle \equiv \langle (AB)_a ij\rangle$. We have chosen to look at the flip pattern of a particularly convenient sequence. All other related sequences will also have the same number of flips as mentioned in Section [1.2.2].

There are clearly many patterns of signs for which the sequences S has two sign flips. We refer to each pattern as a configuration of the amplituhedron. A configuration for the MHV amplituhedron is specified by giving the signs of all entries of the sequence S. We would like to show that for each configuration, the canonical form can be written as the product of canonical forms of a left and right amplituhedron. To begin, we we can parametrize the cut loop AB as

$$A = Z_i + x\, Z_{i+1} \qquad B = y\, Z_j + Z_{j+1} \tag{1.28}$$

To show that the canonical form on this cut can written as a product of canonical forms for lower loop, "left" and "right" MHV amplituhedra $\mathcal{A}^{\mathcal{L}}_{n_1,0,L_1}$ and $\mathcal{A}^{\mathcal{R}}_{n_2,0,L_2}$ (with $L_2 = L - L_1 - 1$), we need precise definitions of these objects. This is provided in the following section.

1.4.1 Left and right Amplituhedra

The left amplituhedron $\mathcal{A}_{n_1,0,L_1}$

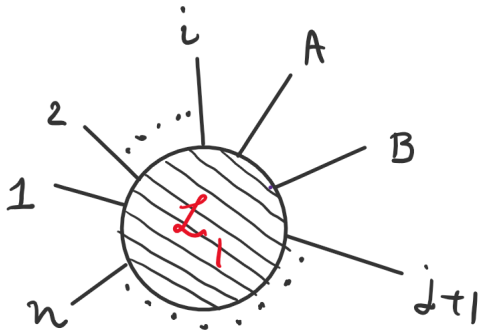

Figure 1.4: The left amplituhedron

The left amplituhedron $\mathcal{A}_{n_1,0,L_1}$ is defined by three sets of conditions similar to (1.27). In this case, the external data, as seen from Fig 1.4 is the set $\mathcal{L} = \{Z_1, \ldots Z_i, A, B, Z_{j+1}, \ldots, Z_n\}$. Letting a, b, c, d denote elements of this set and $\langle ij \rangle \equiv \langle (AB)_a ij \rangle$, the defining conditions are

$$\underline{\text{Tree Level}} \qquad \forall a < b < c < d \in \mathcal{L}$$

$$\langle abcd \rangle > 0, \;\; \langle iAab \rangle > 0, \;\; \langle ABab \rangle > 0, \;\; \langle Bj+1ab \rangle > 0$$

These are satisfied if $x > 0$ and $y > 0$.

$$\underline{\text{Loop Level}} \qquad \langle aa+1 \rangle > 0, \langle iA \rangle > 0, \langle AB \rangle > 0, \langle Bj+1 \rangle > 0$$

The sequence $S_L = \{\langle iA \rangle, \langle iB \rangle, \langle ij+1 \rangle, \ldots \langle in \rangle, -\langle i1 \rangle, \cdots - \langle ii-1 \rangle\}$

has 2 sign flips

$$\underline{\text{Mutual Positivity}} \qquad \langle (AB)_a (AB)_b \rangle > 0.$$

The above sequence lends itself to easy comparison with the sequence S in (1.27). However, for consistency, we must also verify that the following sequences have the same number of sign flips as S_L.

$$\begin{aligned}
&\{\langle AB\rangle, \langle Aj+1\rangle, \ldots, -\langle Ai\rangle\}\\
&\{\langle Bj+1\rangle, \langle Bj+2\rangle, \ldots, -\langle BA\rangle\}\\
&\qquad\vdots\\
&\{\langle i-1i\rangle, \langle i-1A\rangle, \cdots - \langle i-1i-2\rangle\}
\end{aligned}$$

This ensures that the definition of the amplituhedron is independent of the choice of sequence, similar to Section [1.2.2]. The positivity conditions on the loop data ensures that all the first and last entries of these sequences are positive. Furthermore any two sequences in the above set, all of which are of the form $\{\langle ak\rangle\}$ and $\{\langle a+1k\rangle\}$, satisfy

$$\langle ak\rangle\langle a+1k+1\rangle - \langle ak+1\rangle\langle a+1k\rangle = \langle aa+1\rangle\langle kk+1\rangle > 0 \tag{1.29}$$

The equality of sign flips now follows from the analysis in Appendix [B]. This shows that the left amplituhedron can be consistently defined at tree level. The mutual positivity and the loop level positivity conditions for all the loops in the left amplituhedron are automatically satisfied because of (1.28) and (1.27). The flip condition defines the criterion for any uncut loop $(AB)_a$ to be in the left amplituhedron. We will present a detailed analysis in Section [1.4.2].

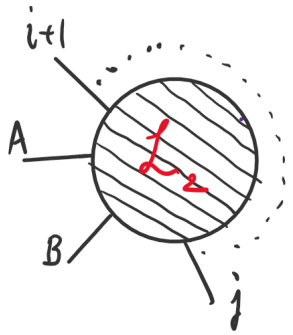

Figure 1.5: The right amplituhedron

THE RIGHT AMPLITUHEDRON $A_{n_2,0,L_2}$

The external data for the right amplituhedron $\mathcal{A}_{n_2,0,L_2}$ is $\mathcal{R} = \{A, Z_{i+1}, \ldots, Z_j, B\}$ and the defining inequalities are listed below. $a, b, c, d \in \mathcal{R}$ and $\langle ij \rangle \equiv \langle (AB)_a ij \rangle$ with $(AB)_a$ being an uncut loop.

$$\begin{aligned}
\underline{\text{Tree Level}} \quad & \langle abcd \rangle > 0, \ \langle Ai+1ab \rangle > 0, \ \langle abjB \rangle > 0, \\
& \langle ABab \rangle > 0 \qquad \text{with } a < b < c < d \\
\underline{\text{Loop Level}} \quad & \langle Ai+1 \rangle > 0, \ \langle jB \rangle > 0, \ \langle aa+1 \rangle > 0 \\
& \text{The sequence } S_R = \{\langle i+1i+2 \rangle, \ldots \langle i+1j \rangle, \langle i+1B \rangle, -\langle i+1A \rangle\} \\
& \text{has 2 sign flips} \\
\underline{\text{Mutual Positivity}} \quad & \langle (AB)_a (AB)_b \rangle > 0
\end{aligned} \tag{1.30}$$

Once again, for consistency we should verify that

$$
\begin{aligned}
&S_1 : \{\langle Ai+1\rangle, \langle Ai+2\rangle, \ldots, \langle AB\rangle\} \\
&S_2 : \{\langle i+2i+3\rangle, \langle i+2i+4\rangle, \ldots, -\langle i+2i+1\rangle\} \\
&\vdots \\
&S_{2+j-i} : \{-\langle BA\rangle, -\langle Bi+1\rangle, \cdots - \langle Bj\rangle\}
\end{aligned}
$$

all have the same number of sign flips as S_R. The proof is identical to the one for the left amplituhedron. The tree level, mutual positivity and loop level positivity conditions are once again guaranteed by (1.28) and (1.27) and an analysis of the flip condition is in Section [1.4.2].

1.4.2 Factorization on the unitarity cut

It was shown in the last section that the two sets $\mathcal{L} = \{Z_1, \ldots, Z_i, A, B, Z_{j+1}, \ldots, Z_n\}$ and $\mathcal{R} = \{A, Z_{i+1}, \ldots Z_j, B\}$ define positive external data and that the loop level positivity conditions are satisfied. We need to analyze every configuration of the amplituhedron and show that for each configuration, an uncut loop belongs to the left or the right amplituhedron. The similar analysis for the 4 point case, performed in Section [1.3], was much simpler owing to the fact there there was only one possible sign pattern for the sequence, $\{\langle AB12\rangle, \langle AB13\rangle, \langle AB14\rangle\}$. Here, the presence of multiple compatible sign patterns increases the complexity of the proof and no simple relation like (1.19) exists. It is natural to label the configurations of $\mathcal{A}_{n,0,L}(Z_1, \ldots Z_n)$ by looking at the sign patterns in the se-

quence S as explained below.

$$S = \{\langle i+1 i+2\rangle, \quad \dots \quad \langle i+1 j\rangle | \langle i+1 j+1\rangle, \quad \dots \quad -\langle i+1 i\rangle\}$$

Note that the flip pattern of this sequence determines whether the loop $(AB)_a$ belongs to the original amplituhedron which has external data $\{Z_1, \dots Z_n\}$. Consequently, it doesn't involve the points A and B. We have divided the sequence in a suggestive way. The *left* half of S looks very similar to S_R (1.30). It is natural to label the different flip patterns of S as S_{ablr} where $a, b = \pm$ are the signs of $\langle i+1 j\rangle$ and $\langle i+1 j+1\rangle$ and l, r are the number of flips in the left and right parts of S.

In order to compare S_L (1.29) to S, we introduce the sequence

$$S'_L = \{\langle i+1 A\rangle, \langle i+1 B\rangle, \langle i+1 j+1\rangle, \cdots -\langle i+1 i-1\rangle\} \tag{1.31}$$

and call the number of flips in this sequence k'_L flips. The motivation behind introducing this is that S_L and S'_L are connected by the Plücker relation (similar to (1.29))

$$\langle ik\rangle\langle i+1 k+1\rangle - \langle ik+1\rangle\langle i+1 k\rangle = \langle ii+1\rangle\langle kk+1\rangle \; > \; 0 \tag{1.32}$$

Following the analysis in Appendix[B], the relation between k_L and k'_L is determined entirely by the signs of the first and last elements

$$\begin{pmatrix} \langle iA\rangle & -\langle ii-1\rangle \\ \langle i+1 A\rangle & -\langle i+1 i-1\rangle \end{pmatrix} = \begin{pmatrix} + & + \\ - & \langle i-1 i+1\rangle \end{pmatrix}$$

where k_L is the number of sign flips in S_L. If $\langle i-1i+1\rangle > 0$, then $k_L = k'_L - 1$ otherwise $k_L = k'_L$.

S now looks almost like a juxtaposition of S_R and S'_L. Each flip pattern of S determines whether the corresponding loop $(AB)_a$ belongs to the left or the right amplituhedron as shown below.

- $S_{++20} = \{+, \ldots 2 \text{ flips} \cdots + | + \ldots 0 \text{ flips} \cdots +\}$

The sequence S_R clearly has 2 sign flips since

$$-\langle i+1A\rangle > 0 \text{ and } \langle i+1j\rangle > 0,\ \langle i+1j+1\rangle > 0 \implies \langle i+1B\rangle > 0$$

S'_L has one sign flip since

$$\langle i+1A\rangle > 0,\ \langle i+1B\rangle > 0, \langle i-1i+1\rangle > 0.$$

Furthermore $k_L = k'_L - 1 = 0$ and the loop $(AB)_a$ belongs only to the right amplituhedron.

- $S_{++02} = \{+, \ldots 0 \text{ flips } \cdots + | + \ldots 2 \text{ flips } \cdots +\}$

S_R obviously has 0 sign flips. If $\langle i-1i+1\rangle > 0$, $k_L = k'_L + 1 = 2$ and if $\langle i-1i+1\rangle < 0$, $k'_L = k_L = 2$. In both cases, the loop belongs to the left amplituhedron and not the right.

- $S_{+-01} = \{+, \ldots 0 \text{ flips} \cdots + | - \ldots 1 \text{ flip} \cdots +\}$

If $\langle i+1B\rangle > 0$, then the sequence S_R has 0 flips and the loop doesn't belong to the right amplituhedron. If $\langle i-1i+1\rangle > 0$, $k'_L = 3$ and $k_L = k'_L - 1 = 2$.

Otherwise, $k'_L = 2$ and $k_L = k'_L = 2$. Thus irrespective of the sign of $\langle i-1\, i+1\rangle$, the loop $(AB)_a$ belongs to the left amplituhedron.

If $\langle i+1 B\rangle < 0$, then S_R has 2 sign flips and it can be shown that $k_L = 0$ by analysis similar to the cases above. This $(AB)_a$ belongs to the right amplituhedron.

- $S_{-+10} = \{+, \ldots 1 \text{ flip } \cdots -|+\ldots 0 \text{ flips } \cdots +\}$

In this case, S_R has two flips and S'_L has one flip irrespective of the sign of $\langle i+1B\rangle$. Since $k_L = k'_L - 1$, we have $k_L = 0$ and the loop belongs to the right amplituhedron.

- $S_{--11} = \{+, \ldots 1 \text{ flip } \cdots -|-\ldots 1 \text{ flip } \cdots +\}$

Once again, it is simple to show that S_R has two sign flips and S_L has 0 sign flips in this configuration.

Trivialized mutual positivity

We have shown that for every configuration of the amplituhedron, each loop belongs either to the left or the right. While we can consistently define left and right amplituhedra, it remains to be shown that the mutual positivity between a loop $(AB)_{\mathcal{L}}$, $(\mathcal{L} = 1, \ldots L_1)$ in the left amplituhedron and a loop $(AB)_{\mathcal{R}}$ $(\mathcal{R} = 1, \ldots L_2)$ in the right amplituhedron doesn't impose any extra constraints.

This is easiest to see if we expand each loop $(AB)_{\mathcal{L}}$ and $(AB)_{\mathcal{R}}$ using (1.11) as

$$A_{\mathcal{R}} = A + \alpha_1 Z_{r_1} + \alpha_2 Z_{r_1+1} \qquad B_{\mathcal{R}} = -A + \beta_1 Z_{r_2} + \beta_2 Z_{r_2+1}$$
$$A_{\mathcal{L}} = A + \alpha_3 Z_{l_1} + \alpha_4 Z_{l_1+1} \qquad B_{\mathcal{L}} = -A + \beta_3 Z_{l_2} + \beta_4 Z_{l_2+1}$$

with $r_1 < r_2 \in \{A, Z_{i+1}, \ldots, Z_j, B\}$ and $l_1 < l_2 \in \{Z_1, \ldots Z_i, A, B, Z_{j+1}, \ldots, Z_n\}$. On expanding $\langle (AB)_{\mathcal{L}} (AB)_{\mathcal{R}} \rangle$, every term is of the form $\langle l_1 l_2 r_1 r_2 \rangle$ with ${}_1 < l_2 < r_1 < r_2$. Since the external data are positive, i.e. $\langle ijkl \rangle > 0$ for $i < j < k < l$, we are assured that $\langle (AB)_{\mathcal{L}} (AB)_{\mathcal{R}} \rangle > 0$.

This completes the proof of factorization for MHV amplituhedra on the unitarity cut. In the next section, we will extended this proof to the higher k sectors.

1.5 Proof for higher k sectors

The proof of unitarity for higher k is similar in spirit to that for the MHV sector. However, there are a lot additional details that we must take into account. Firstly, we must modify (1.14) to include products of "left" and "right" amplituhedra with different k. Suppose the left amplitude has g_L negative helicity gluons and the right amplitude has g_R negative helicity gluons, then we have $g_L + g_R = g + 2$. With the MHV degrees defined as $k_L = g_L - 2, k_R = g_R - 2, k = g - 2$, this equation reads $k_L + k_R = k$. Recall that we introduced the function $f(x, y, 0, 0, (AB)_a)$ in (1.13) and stated the optical theorem in terms of it. Including sectors of different k, this becomes,

$$f(x, y, 0, 0, (AB)_a) = \sum_{k_L + k_R = k} \sum_{L_1 + L_2 = L-1} \mathcal{M}_{\mathcal{L}}^{k_L, L_1} \mathcal{M}_{\mathcal{R}}^{k_R, L_2} \tag{1.33}$$

We expect that unitarity emerges from a factorization property of the geometry in a manner similar to the MHV case. In order to make this statement more precise, we will have to define analogues of the left and right MHV amplituhedra for N^{k}MHV external data. $\mathcal{A}_{n,k,L}$, the N^kMHV amplituhedron defined by

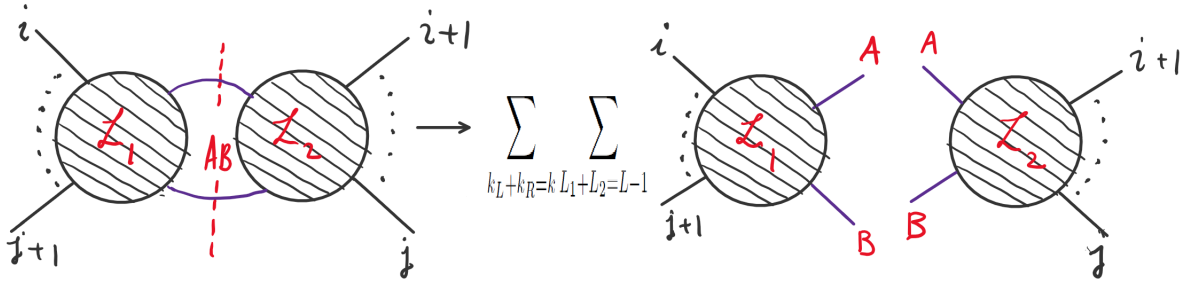

Figure 1.6: Unitarity cut for an N^{k}MHV amplitude

the conditions

$$\begin{aligned}
&\underline{\text{Tree level}} && \langle ii+1jj+1\rangle > 0,\ \langle ii+1n1\rangle(-1)^{k-1} > 0 \text{ and the sequence} \\
&&& S^{\text{tree}} : \left\{\langle ii+1i+2i+3\rangle, \ldots \langle ii+1i+2i-1\rangle(-1)^{k-1}\right\} \text{ has } k \text{ sign flips.} \\
&\underline{\text{Loop level}} && \langle (AB)_a ii+1\rangle > 0,\ \langle ABn1\rangle(-1)^{k-1} > 0 \text{ and the sequence} \\
&&& S^{\text{loop}} : \{\langle (AB)_a 12\rangle, \langle (AB)_a 13\rangle, \ldots \langle (AB)_a 1n\rangle\} \text{ has } k+2 \text{ sign flips.} \\
&\underline{\text{Mutual Positivity}} && \langle (AB)_a (AB)_b\rangle > 0
\end{aligned} \tag{1.34}$$

We can use any sequence $\{\langle ABki\rangle\}$ instead of $\{\langle AB1i\rangle\}$ as explained in Section [1.2.2].

It is worth re-emphasizing that we wish to prove that the canonical form on the cut (which is computed by solving the inequalities (1.34) for the uncut loops $(AB)_a$ along with $\langle ABii+1\rangle = \langle ABjj+1\rangle = 0$) can be written as in (1.33). For this to happen, we want to show that the set of inequalities in (1.34) can be replaced by two sets of inequalities which define lower loop amplituhedra, $\mathcal{A}^{\mathcal{L}}_{n_1,k_L,L_1}$ and $\mathcal{A}^{\mathcal{R}}_{n_2,k_R,L_2}$. It is not essential that the external data for these is a subset of $\{Z_1, \ldots Z_n\}$. In particular they can be rescaled by factors $Z_i \to \sigma(i)Z_i$ and still yield the same canonical form due to projective invariance as discussed

in Section [1.2.3]. In fact, as we show below, this rescaling plays a crucial role in ensuring that the left and right amplituhedra have k of both even and odd parity.

On the unitarity cut ($\langle ABii+1\rangle = \langle ABjj+1\rangle = 0$ with $i+1 \neq j$), there is a natural division of the external data into "left" and "right" sets, $\{Z_1, \ldots, Z_i, A, B, Z_{j+1}, \ldots, Z_n\}$ and $\{A, Z_{i+1}, \ldots, Z_j, B\}$. However, insisting that this be the external data for the left and right amplituhedra imposes too many constraints. To see this, suppose that the "left" set has MHV degree k_L. We must have $\langle ABn1\rangle(-1)^{k_L-1} > 0$. But (1.34) implies that $\langle ABn1\rangle(-1)^{k-1} > 0$. This forces $(-1)^{k+k_L} > 0$ and restricts k_L to be the same parity as k. Similarly for the right set, we have $\langle j-1jBA\rangle(-1)^{k_R-1} > 0$ and again (1.34) implies $\langle ABj-1j\rangle > 0$ which forces $(-1)^{k_R} > 0$. In order to avoid these extra constraints on k_L and k_R, we must allow for arbitrary signs on the Zs and define two the sets of external data as

$$\begin{aligned}\mathcal{L} &= \{\sigma_L(1)Z_1, \ldots \sigma_L(i)Z_i, \sigma_L(A)A, \sigma_L(B)B, \sigma_L(j+1)Z_{j+1}, \ldots, \sigma_L(n)Z_n\}\\ \mathcal{R} &= \{\sigma_R(A)A, \sigma_R(i+1)i+1, \ldots, \sigma_R(j)j, \sigma_R(B)B\}\end{aligned} \tag{1.35}$$

where $\sigma(k) = \pm 1$. These signs will be determined by conditions like (1.34) which define the left and right amplituhedra along with the appropriate twisted cyclic symmetry. We will then show that the canonical form for every configuration in $\mathcal{A}_{n,k,L}$ can be mapped into a product of canonical forms on suitably defined left and right amplituhedra $\mathcal{A}^{\mathcal{L}}_{n_1,k_L,L_1}$ and $\mathcal{A}^{\mathcal{R}}_{n_2,k_R,L_2}$.

1.5.1 The left and right amplituhedra

The left amplituhedron $\mathcal{A}^{\mathcal{L}}_{n_1,k_L,L_1}$

We must demand that the set $\mathcal{L}$ satisfies all the conditions in (1.34). In addition, this must also be compatible with the fact that the Z_i are the external data for $\mathcal{A}_{n,k,L}$.

$$\begin{aligned}
&\langle aa+1bb+1\rangle \sigma_L(a)\sigma_L(a+1)\sigma_L(b)\sigma_L(b+1) > 0 \\
&\langle ABaa+1\rangle \sigma_L(A)\sigma_L(B)\sigma_L(a)\sigma_L(a+1) > 0 \\
&\forall\, a,b \in \{1,\ldots,i-1,j+1,\ldots,n-1\}
\end{aligned} \tag{1.36}$$

AB and the Zs automatically satisfy $\langle aa+1bb+1\rangle > 0$ and $\langle ABaa+1\rangle > 0$. Thus we have, $\sigma_L(a)\sigma_L(a+1)\sigma_L(b)\sigma_L(b+1) > 0$ and $\sigma_L(A)\sigma_L(B)\sigma_L(a)\sigma_L(a+1) > 0$. Furthermore, we have new constraints on A and B coming from

$$\begin{aligned}
&\langle iABj+1\rangle \sigma_L(i)\sigma_L(A)\sigma_L(B)\sigma_L(j+1) > 0 \\
&\langle iAkk+1\rangle \sigma_L(i)\sigma_L(A)\sigma_L(k)\sigma_L(k+1) > 0 \\
&\langle Bj+1kk+1\rangle \sigma_L(B)\sigma_L(j+1)\sigma_L(k)\sigma_L(k+1) > 0
\end{aligned} \tag{1.37}$$

Finally, since the set $\mathcal{L}$ is the external data for $\mathcal{A}^{\mathcal{L}}_{n_1,k_L,L_1}$, it must satisfy a twisted cyclic symmetry

$$\langle aa+1n1\rangle \sigma_L(a)\sigma_L(a+1)\sigma_L(n)\sigma_L(1)(-1)^{k_L-1} > 0 \tag{1.38}$$

Since $\langle aa{+}1n1\rangle(-1)^{k-1} > 0$, consistency requires $(-1)^{k+k_L}\sigma_L(a)\sigma_L(a{+}1)\sigma_L(n)\sigma_L(1) > 0$. This divides into two cases

- $(-1)^{k+k_L} < 0$

An allowed set $\{\sigma_L(k)\}$ satisfying (1.36) and (1.38) is

$$\begin{aligned}&\{\sigma_L(1),\ldots,\sigma_L(i),\sigma_L(A),\sigma_L(B),\sigma_L(j+1),\ldots,\sigma_L(n)\}\\&=\{+,\quad\ldots\ ,\quad+,\quad?\quad,\ ?\quad,\quad-\quad,\ldots,\quad-\quad\}\end{aligned}$$

with $\sigma_L(A)$ and $\sigma_L(B)$ undetermined. (1.36) requires $\sigma_L(A)\sigma_L(B) > 0$ and the constraints in (1.37) read

$$\langle iABj+1\rangle < 0 \qquad \langle iAkk+1\rangle\sigma_L(A) > 0 \qquad \langle Bj+1kk+1\rangle\sigma_L(B) < 0$$

The solutions to these constraints are

$$\begin{aligned}&\mathcal{L}_1 : \sigma_L(A) > 0,\ \sigma_L(B) > 0 \ \text{ with } \langle iAkk+1\rangle > 0,\ \langle Bj+1kk+1\rangle < 0,\ \langle iABj+1\rangle < 0\\&\mathcal{L}_2 : \sigma_L(A) < 0,\ \sigma_L(B) < 0 \ \text{ with } \langle iAkk+1\rangle < 0,\ \langle Bj+1kk+1\rangle > 0,\ \langle iABj+1\rangle < 0\end{aligned}$$

- $(-1)^{k+k_L} > 0$

In this case $\{\sigma_L(k)\}$ satisfying (1.36) and (1.38) is

$$\begin{aligned}&\{\sigma_L(1),\ldots,\sigma_L(i),\sigma_L(A),\sigma_L(B),\sigma_L(j+1),\ldots,\sigma_L(n)\}\\&=\{+,\quad\ldots\ ,\quad+,\quad?\quad,\ ?\quad,\quad+\quad,\ldots,\quad+\quad\}\end{aligned}$$

which again requires $\sigma_L(A)\sigma_L(B) > 0$ and turns (1.37) into

$$\langle iABj+1\rangle > 0 \qquad \langle iAkk+1\rangle\sigma_L(A) > 0 \qquad \langle Bj+1kk+1\rangle\sigma_L(B) > 0.$$

This has the following solutions

$$\mathcal{L}_3 : \sigma_L(A) > 0,\ \sigma_L(B) > 0 \ \text{ with } \langle iAkk+1\rangle > 0,\ \langle Bj+1kk+1\rangle > 0,\ \langle iABj+1\rangle > 0$$
$$\mathcal{L}_4 : \sigma_L(A) < 0,\ \sigma_L(B) < 0 \ \text{ with } \langle iAkk+1\rangle < 0,\ \langle Bj+1kk+1\rangle < 0,\ \langle iABj+1\rangle > 0$$

Each of these regions is characterized by particular signs for $\langle iAkk+1\rangle$ and $\langle Bj+1kk+1\rangle$ along with a pattern of sign flips for the sequence

$$S_L^{\text{tree}} : \left\{\langle i-1iAB\rangle\sigma_L(B), \langle i-1iAj+1\rangle\sigma_L(j+1), \ldots \langle i-1iAi-2\rangle(-1)^{k_L-1}\sigma_L(i-2)\right\}.$$

Each region allows parametrization of the line (AB) as $A = \pm Z_i \pm xZ_{i+1}$ and $B = \pm yZ_j \pm Z_{j+1}$ with $x > 0, y > 0$. In the table below, we list the different possibilities.

Region	A	B	S_L^{tree}
$\mathcal{L}_1$	$\pm Z_i + xZ_{i+1}$	$-yZ_j \pm Z_{j+1}$	$\left\{+, \ldots, (-1)^{k_L}\right\}$
$\mathcal{L}_2$	$\pm Z_i - xZ_{i+1}$	$yZ_j \pm Z_{j+1}$	$\left\{-, \ldots, (-1)^{k_L-1}\right\}$
$\mathcal{L}_3$	$\pm Z_i + xZ_{i+1}$	$yZ_j \pm Z_{j+1}$	$\left\{+, \ldots, (-1)^{k_L}\right\}$
$\mathcal{L}_4$	$\pm Z_i - xZ_{i+1}$	$-yZ_j \pm Z_{j+1}$	$\left\{-, \ldots, (-1)^{k_L-1}\right\}$

Table 1.1: Parametrization of (AB) in the four regions

It is crucial to remember that the canonical form is independent of the choice of $\sigma(i)$ and parametrization of A and B. In all these cases the canonical form is that of $\mathcal{A}_{n_1,k_L,L_1}$.

THE RIGHT AMPLITUHEDRON $\mathcal{A}^{\mathcal{R}}_{n_2,k_R,L_2}$

A similar analysis of the effects of (1.34) on the set $\mathcal{R}$ yields the following constraints on $\{\sigma_R\}$.

$$\begin{aligned}
&\sigma_R(a)\sigma_R(a+1)\sigma_R(b)\sigma_R(b+1) > 0 \\
&\sigma_R(A)\sigma_R(i+1)\sigma_R(k)\sigma_R(k+1)\langle Ai+1kk+1\rangle > 0 \\
&\sigma_R(j)\sigma_R(B)\sigma_R(k)\sigma_R(k+1)\langle jBkk+1\rangle > 0 \\
&\sigma_R(B)\sigma_R(A)\sigma_R(k)\sigma_R(k+1)\langle BAkk+1\rangle(-1)^{k_L-1} > 0 \\
&\sigma_R(A)\sigma_R(B)\sigma(i+1)\sigma_R(j)\langle ABi+1j\rangle > 0
\end{aligned} \tag{1.39}$$

These conditions are satisfied by

$$\begin{aligned}
&\{\sigma_R(1),\ldots,\sigma_R(i),\sigma_R(A),\sigma_R(B),\sigma_R(j+1),\ldots,\sigma_R(n)\} \\
&= \{+, \quad \ldots \ , \quad +, \quad ? \quad , \ ? \ , \quad + \quad ,\ldots, \quad + \quad \}
\end{aligned}$$

with $\sigma_R(A)$ and $\sigma_R(B)$ having solutions depending on k_R.

- $(-1)^{k_R} > 0$

$\mathcal{R}_1 : \sigma_R(A) > 0,\ \sigma_R(B) > 0$ with $\langle Ai+1kk+1\rangle > 0,\ \langle jBkk+1\rangle > 0,\ \langle ABi+1j\rangle > 0$

$\mathcal{R}_2 : \sigma_R(A) < 0,\ \sigma_R(B) < 0$ with $\langle Ai+1kk+1\rangle < 0,\ \langle jBkk+1\rangle < 0,\ \langle ABi+1j\rangle > 0$

- $(-1)^{k_R} < 0$

$$\mathcal{R}_3 : \sigma_R(A) > 0,\ \sigma_R(B) < 0 \text{ with } \langle Ai+1kk+1\rangle > 0,\ \langle jBkk+1\rangle < 0,\ \langle ABi+1j\rangle < 0$$

$$\mathcal{R}_4 : \sigma_R(A) < 0,\ \sigma_R(B) > 0 \text{ with } \langle Ai+1kk+1\rangle < 0,\ \langle jBkk+1\rangle > 0,\ \langle ABi+1j\rangle < 0$$

Once again, each region is characterized by different pattern of sign flips of the sequence

$$S_R^{\text{tree}} : \{\langle Ai+1i+2i+3\rangle\sigma_R(i+3), \ldots, \langle Ai+1i+2B\rangle\sigma_R(B)\}$$

where we have ignored an overall factor of $\sigma_R(A)\sigma_R(i+1)\sigma_R(i+2)$. We list the various parametrizations and sign patterns of S_R^{tree} below.

Region	A	B	S_R^{tree}
$\mathcal{R}_1$	$Z_i \pm xZ_{i+1}$	$\pm yZ_j + Z_{j+1}$	$\{+, \ldots, +\}$
$\mathcal{R}_2$	$-Z_i \pm xZ_{i+1}$	$\pm yZ_j - Z_{j+1}$	$\{+, \ldots, +\}$
$\mathcal{R}_3$	$Z_i \pm xZ_{i+1}$	$\pm yZ_j - Z_{j+1}$	$\{+, \ldots, -\}$
$\mathcal{R}_4$	$-Z_i \pm xZ_{i+1}$	$\pm yZ_j + Z_{j+1}$	$\{-, \ldots, +\}$

Table 1.2: Parametrization of (AB) in the four regions

The canonical form is independent of the choice of $\sigma(i)$ and parametrization of A and B.

1.5.2 Factorization of the external data

We will show that, on the unitarity cut, for every allowed sign flip pattern of the sequence S^{tree}, there exist regions $\mathcal{L}_i, \mathcal{R}_i$ such that S_L^{tree} and S_R^{tree} have the flip patterns necessary for $\mathcal{A}^{\mathcal{L}}_{n_1,k_L,L_1}$ and $\mathcal{A}^{\mathcal{R}}_{n_2,k_R,L_2}$. The analysis that follows is similar to the one is Section [1.4.2]. The sequence S_R is similar to the *left* part of S^{tree} and can be compared directly. In order to compare S_L^{tree} with S^{tree}, it is necessary to introduce another sequence $S_L'^{\text{tree}}$. This is analogous to what we did

in (1.31).

$$S_L^{\prime\text{tree}} : \left\{\langle i+2iAB\rangle\sigma_L(B), \langle i+2iAj+1\rangle\sigma_L(j+1), \ldots, \langle i+2iAi-2\rangle\sigma_L(i-2)(-1)^{k_L-1}\right\}$$

Let k, k_L, k'_L, k_R be the number of flips in $S_L^{\text{tree}}, S_L^{\prime\text{tree}}, S_R^{\text{tree}}, S^{\text{tree}}$ respectively. k_L and k'_L are related to each other due to the following Plücker relations

$$\begin{aligned}&\sigma_L(B)\sigma_L(j+1)\left(\langle i-1iAB\rangle\langle i+2iAj+1\rangle - \langle i-1iAj+1\rangle\langle i+2iAB\rangle\right)\\ &= \sigma_L(B)\sigma_L(j+1)\langle i-1iAi+2\rangle\langle iABj+1\rangle > 0\end{aligned}$$

and

$$\begin{aligned}&\langle i-1iAk\rangle\langle i+2iAk+1\rangle - \langle i-1iAk+1\rangle\langle i+2iAk\rangle\\ &= \langle i-1iAi+2\rangle\langle iAkk+1\rangle > 0\end{aligned}$$

It is easy to see that these hold in all regions $(\mathcal{L}_i, \mathcal{R}_i)$. As shown in Appendix[B], we can conclude that the relation between k_L and k'_L depends only on the signs of first and last terms which are encoded in the matrix below.

$$\begin{aligned}M &= \begin{pmatrix}\text{sign}(\langle i-1iAB\rangle) & \text{sign}(\langle i-2i-1iA\rangle)(-1)^{k_L}\\ \text{sign}(\langle i+2iAB\rangle) & \text{sign}(\langle i-2iAi+2\rangle)(-1)^{k_L}\end{pmatrix} \\ &\equiv \begin{pmatrix}+ & +\\ \text{sign}(\langle iAaa+1\rangle)\text{sign}(\langle Ai+1aa+1\rangle) & \text{sign}(\langle i-2ii+1i+2\rangle)\end{pmatrix}\end{aligned} \tag{1.40}$$

The relation between k_L and k'_L is tabulated below.

It is helpful to label all the allowed flip patterns of S^{tree} as S_{ab}^{tree} where a and

sign($\langle iAaa+1\rangle$)	sign($\langle Ai+1aa+1\rangle$)	sign($\langle i-2ii+1i+2\rangle$)	$k_L - k'_L$
+	+	+	0
+	+	-	1
+	-	+	-1
+	-	-	0
-	+	+	-1
-	+	-	0
-	-	+	0
-	-	-	1

Table 1.3: Relation between k_L and k'_L determined according to Appendix [B]

b are the signs of $\langle ii+1i+2j\rangle$ and $\langle ii+1i+2j+1\rangle$ respectively. The different possibilities are shown below.

$$S^{\text{tree}} : \left\{\langle ii+1i+2i+3\rangle, \ldots \langle ii+1i+2j\rangle \middle| \langle ii+1i+2j+1\rangle, \ldots, \langle ii+1i+2i-1\rangle (-1)^{k-1}\right\}$$

$$S^{\text{tree}}_{++} : \left\{+ \quad k_1 \quad + \middle| + \quad k_2 \quad (-1)^k\right\}$$

$$S^{\text{tree}}_{+-} : \left\{+ \quad k_1 \quad + \middle| - \quad k_2 \quad (-1)^k\right\}$$

$$S^{\text{tree}}_{-+} : \left\{+ \quad k_1 \quad - \middle| + \quad k_2 \quad (-1)^k\right\}$$

$$S^{\text{tree}}_{--} : \left\{+ \quad k_1 \quad - \middle| - \quad k_2 \quad (-1)^k\right\}$$

For each configuration, S^{tree}_{ab}, the sequences $S_{\mathcal{L}}$ and $S_{\mathcal{R}}$ have the following signs depending on the region $(\mathcal{L}_i, \mathcal{R}_i)$.

S_{++}^{tree}	$\mathcal{R}_1$	$\mathcal{R}_2$	$\mathcal{R}_3$	$\mathcal{R}_4$
$\mathcal{L}_1$	(k_2+1, k_1)	(k_2-1, k_1)	(k_2+1, k_1+1)	(k_2-1, k_1+1)
$\mathcal{L}_2$	(k_2-1, k_1)	(k_2+1, k_1)	(k_2-1, k_1+1)	(k_2+1, k_1+1)
$\mathcal{L}_3$	(k_2, k_1)	(k_2, k_1)	(k_2, k_1+1)	(k_2, k_1+1)
$\mathcal{L}_4$	(k_2, k_1)	(k_2, k_1)	(k_2, k_1+1)	(k_2, k_1+1)

Table 1.4: (k_L, k_R) in all regions for the configuration S_{++}

For the configuration S_{++}, we have $k_1 + k_2 = k$. Thus regions which satisfies $k_L + k_R = k$ are $(\mathcal{L}_1, \mathcal{R}_4), (\mathcal{L}_2, \mathcal{R}_3), (\mathcal{L}_3, \mathcal{R}_1), (\mathcal{L}_3, \mathcal{R}_2), (\mathcal{L}_4, \mathcal{R}_1), (\mathcal{L}_4, \mathcal{R}_2)$. For

S_{+-}^{tree}	$\mathcal{R}_1$	$\mathcal{R}_2$	$\mathcal{R}_3$	$\mathcal{R}_4$
$\mathcal{L}_1$	(k_2, k_1)	(k_2, k_1)	(k_2, k_1+1)	(k_2, k_1+1)
$\mathcal{L}_2$	(k_2, k_1)	(k_2, k_1)	(k_2, k_1+1)	(k_2, k_1+1)
$\mathcal{L}_3$	(k_2+1, k_1)	(k_2-1, k_1)	(k_2+1, k_1+1)	(k_2-1, k_1+1)
$\mathcal{L}_4$	(k_2-1, k_1)	(k_2+1, k_1)	(k_2-1, k_1+1)	(k_2+1, k_1+1)

Table 1.5: (k_L, k_R) in all regions for the configuration S_{+-}

the configuration S_{+-}, we have $k_1 + k_2 = k - 1$. Thus regions which satisfies $k_L + k_R = k$ are $(\mathcal{L}_1, \mathcal{R}_3), (\mathcal{L}_1, \mathcal{R}_4), (\mathcal{L}_2, \mathcal{R}_3), (\mathcal{L}_2, \mathcal{R}_4), (\mathcal{L}_3, \mathcal{R}_1), (\mathcal{L}_4, \mathcal{R}_2)$.

S_{-+}^{tree}	$\mathcal{R}_1$	$\mathcal{R}_2$	$\mathcal{R}_3$	$\mathcal{R}_4$
$\mathcal{L}_1$	(k_2+1, k_1+1)	(k_2-1, k_1+1)	(k_2+1, k_1)	(k_2-1, k_1)
$\mathcal{L}_2$	(k_2-1, k_1+1)	(k_2+1, k_1+1)	(k_2-1, k_1)	(k_2+1, k_1)
$\mathcal{L}_3$	(k_2, k_1+1)	(k_2, k_1+1)	(k_2, k_1)	(k_2, k_1)
$\mathcal{L}_4$	(k_2, k_1+1)	(k_2, k_1+1)	(k_2, k_1)	(k_2, k_1)

Table 1.6: (k_L, k_R) in all regions for the configuration S_{-+}

For the configuration S_{-+}, we have $k_1 + k_2 = k - 1$. Thus regions which satisfies $k_L + k_R = k$ are $(\mathcal{L}_1, \mathcal{R}_3), (\mathcal{L}_2, \mathcal{R}_4), (\mathcal{L}_3, \mathcal{R}_1), (\mathcal{L}_3, \mathcal{R}_2), (\mathcal{L}_4, \mathcal{R}_1), (\mathcal{L}_4, \mathcal{R}_2)$.

S_{--}^{tree}	$\mathcal{R}_1$	$\mathcal{R}_2$	$\mathcal{R}_3$	$\mathcal{R}_4$
$\mathcal{L}_1$	(k_2, k_1+1)	(k_2, k_1+1)	(k_2, k_1)	(k_2, k_1)
$\mathcal{L}_2$	(k_2, k_1+1)	(k_2, k_1+1)	(k_2, k_1)	(k_2, k_1)
$\mathcal{L}_3$	(k_2+1, k_1+1)	(k_2-1, k_1+1)	(k_2+1, k_1)	(k_2-1, k_1)
$\mathcal{L}_4$	(k_2-1, k_1+1)	(k_2+1, k_1+1)	(k_2-1, k_1)	(k_2+1, k_1)

Table 1.7: (k_L, k_R) in all regions for the configuration S_{--}

For the configuration S_{--}, we have $k_1 + k_2 = k$. Thus regions which satisfies $k_L + k_R = k$ are $(\mathcal{L}_1, \mathcal{R}_3), (\mathcal{L}_1, \mathcal{R}_4), (\mathcal{L}_2, \mathcal{R}_3), (\mathcal{L}_2, \mathcal{R}_4), (\mathcal{L}_3, \mathcal{R}_2), (\mathcal{L}_4, \mathcal{R}_1)$.

We see that for every configuration S_{ab}^{tree}, there are regions $(\mathcal{L}_i, \mathcal{R}_i)$ that satisfy $k_L + k_R = k$. Thus every configuration in the original amplituhedron can be covered by these regions consistent with the expected factorization. The remaining regions exist because they are related to amplitudes via inverse soft factors and have identical canonical forms. However, these are not necessary to cover all regions of the original amplituhedron.

1.5.3 Factorization of loop level data

At loop level, we need to show that each loop $(AB)_a$ belongs either to the left or the right amplituhedron. The relevant sequences are (denoting $\langle (AB)_a ij\rangle$ as $\langle ij\rangle$)

$$S_R^{\text{loop}} = \big\{\langle i+1\, i+2\rangle\sigma_R(i+2), \ldots, \langle i+1\, j\rangle\sigma_R(j), \langle i+1 B\rangle\sigma_R(B), (-1)^{k_r-1}\langle i+1 A\rangle\sigma_R(A)\big\}$$
$$S_L^{\text{loop}} = \big\{\langle iA\rangle\sigma_L(A), \langle iB\rangle\sigma_L(B), \langle ij+1\rangle\sigma_L(j+1), \ldots, \langle ii-1\rangle\sigma_L(i-1)(-1)^{k_l-1}\big\}$$

Similar to before, it will be convenient to introduce the sequence $S_L^{\prime\text{loop}}$

$$S_L^{\prime\text{loop}} = \big\{\langle i+1A\rangle\sigma_L(A), \langle i+1B\rangle\sigma_L(B), \langle i+1\, j+1\rangle\sigma_L(j+1), \ldots, \langle i+1\, i-1\rangle\sigma_L(i-1)(-1)^{k_l-1}\big\}$$

Let the number of flips in S_R^{loop} and S_L^{loop} be k_r and k_l respectively. These are *not* k_R and k_L, which are the number of flips in the tree level sequences S_R^{tree} and S_L^{tree} respectively. The flip patterns of S_{tree} can be organized as follows.

$$
\begin{array}{lccccccc}
S^{\text{loop}}: & \big\{\langle i+1\, i+2\rangle, \langle i+1\, i+3\rangle, \ldots, \langle i+1\, j\rangle & \big| & \langle i+1\, j+1\rangle, \ldots, \langle i+1\, i\rangle (-1)^{k-1} & \big\} \\
S^{\text{loop}}_{++}: & \big\{ \quad + \quad & k_1 & + & \big| & + \quad & k_2 & (-1)^k \quad \big\} \\
S^{\text{loop}}_{+-}: & \big\{ \quad + \quad & k_1 & + & \big| & - \quad & k_2 & (-1)^k \quad \big\} \\
S^{\text{loop}}_{-+}: & \big\{ \quad + \quad & k_1 & - & \big| & + \quad & k_2 & (-1)^k \quad \big\} \\
S^{\text{loop}}_{--}: & \big\{ \quad + \quad & k_1 & - & \big| & - \quad & k_2 & (-1)^k \quad \big\}
\end{array}
$$

We showed in the previous section that on the unitarity cut, the external data factorizes such that $k_L + k_R = k$ with $k_L, k_R \in \{0, \ldots k\}$. It is trivially true that each loop belongs either to the left or the right amplituhedron. We must show that if a loop $(AB)_a$ belongs to the left amplituhedron, then it cannot belong to the right amplituhedron. First, note that in each configuration, we will have $k_l = k_2 + l$ and $k_r = k_1 + r$ with $r, l = 1$ or 2. Now suppose that $(AB)_a$ belongs to both the left and right amplituhedra. Then we must have $k_l = k_L + 2$ and $k_r = k_R + 2$. Expressing k_l and k_r in terms of k_1, l, k_2 and r, and using $k_L + k_R = k$, we get

$$
l + r = \begin{cases} 4 \text{ if } k_1 + k_2 = k \\ \\ 5 \text{ if } k_1 + k_2 = k - 1 \end{cases}
$$

Clearly, $l + r = 5$ is impossible since $l, r = 1$ or 2. We just need to show that $l + r = 4$ is impossible. Note that this is possible only if $l = r = 2$. In this case,

the following hold true.

$$\big(\langle i+1j\rangle\sigma_R(j), \langle i+1B\rangle\sigma_R(B), (-1)^{k_r}\big) \sim (-1)^{k_r}(+,-,+)$$

$$\begin{aligned} & (\langle i+1A\rangle\sigma_L(A), \langle i+1B\rangle\sigma_L(B), \langle i+1j+1\rangle\sigma_L(j+1)) \\ = \quad & \big(-\sigma_L(A)\sigma_R(A), -(-1)^{k_r}\sigma_R(B)\sigma_L(B), \langle i+1j+1\rangle\sigma_L(j+1)\big) \\ = \quad & (+,-,+) \text{ or } (-,+,-) \end{aligned}$$

In all these cases, we must have $\sigma_R(A)\sigma_R(B)\sigma_L(A)\sigma_L(B)(-1)^{k_R} < 0$. It is easy to verify from Section [1.5.1] that this is always false. Thus each loop belongs solely to the left or the right ampltuhedron.

1.5.4 Mutual positivity

To complete the proof of factorization, we need to show that the mutual positivity between a loop in $\mathcal{A}^{\mathcal{L}}_{n_1,k_L,L_1}$ and one in $\mathcal{A}^{\mathcal{R}}_{n_2,k_R,L_2}$ is automatically satisfied. This is easier to see while working with $(k+2)$ dimensional data. We can rewrite all the four brackets using $\mathcal{Z}'s$ and the $k-$plane Y as described in Section [1.2.1]. For more details, see Section [7] of [23]. A loop in the left amplituhedron can be parametrized as a k_L+2 plane $Y^L_1 \dots Y^L_{k_L} A_a B_a$.

$$Y^L_\nu = (-1)^{\nu-1}\sigma_L(A)\, A + \alpha_\nu\, \sigma_L(i_\nu)\, \mathcal{Z}_{i_\nu} + \beta_\nu\, \sigma_L(\nu+1)\, Z_{i_{\nu+1}} \tag{1.41}$$

$$A_a = (-1)^{k_L+1}\sigma_L(A)\, A + \alpha_{k_L+1}\, \sigma_L(i_{k_L+1})\mathcal{Z}_{i_{k_L+1}} + \beta_{i_{k_L+1}}\, \sigma_L(i_{k_L+1}+1)\, \mathcal{Z}_{i_{k_L+1}+1}$$

$$B_a = (-1)^{k_L+2}\sigma_L(A)\, A + \alpha_{k_L+2}\, \sigma_L(i_{k_L+2})\, \mathcal{Z}_{i_{k_L+2}} + \beta_{i_{k_L+2}}\, \sigma_L(i_{k_L+2}+1)\, \mathcal{Z}_{i_{k_L+2}+1}$$

with $\nu = \{1, \ldots k_L\}$, $\mathcal{Z}_{i_\nu} \in \{\mathcal{Z}_1, \ldots \mathcal{Z}_i, A, B, \mathcal{Z}_{j+1}, \mathcal{Z}_n\}$ and $i_1 < i_2 < \ldots i_{K_L} + 2$.

Similarly, a loop in the right amplituhedron can be thought of as a $k_R + 2$ plane $Y_1^R \ldots Y_{k_R}^R A_b B_b$ and parametrized as

$$
\begin{aligned}
Y_\mu^R &= (-1)^{\mu-1}\sigma_R(A)\, A + \alpha_\mu\, \sigma_R(i_\mu)\, Z_{i_\mu} + \beta_\mu\, \sigma_R(\mu+1)\, \mathcal{Z}_{i_{\mu+1}} \qquad (1.42)\\
A_b &= (-1)^{k_R+1}\sigma_R(A)\, A + \alpha_{k_R+1}\, \sigma_R(i_{k_R+1})\mathcal{Z}_{i_{k_R+1}} + \beta_{i_{k_R+1}}\, \sigma_R(i_{k_R+1}+1)\, \mathcal{Z}_{i_{k_R+1}+1}\\
B_b &= (-1)^{k_R+2}\sigma_R(A)\, A + \alpha_{k_R+2}\, \sigma_R(i_{k_R+2})\, \mathcal{Z}_{i_{k_R+2}} + \beta_{i_{k_R+2}}\, \sigma_R(i_{k_R+2}+1)\, \mathcal{Z}_{i_{k_R+2}+1}
\end{aligned}
$$

with $\mu \in \{1, \ldots k_R\}$, $\mathcal{Z}_{i_\mu} \in \{A, \mathcal{Z}_{i+1}, \ldots, \mathcal{Z}_j, B\}$ and with $j_1 < j_2 < \ldots j_{k_R+2}$.

This reduces the mutual positivity condition $\langle Y^L (AB)_a Y^R (AB)_b \rangle > 0$ to a condition involving $k+4$ brackets of the form $\langle ijklm \rangle$. It is easy to see that with positive $k+4$ dimensional data ($\langle i_1 \ldots i_{k+4} \rangle$ when $i_1 < i_2 < \ldots i_{k+4}$), mutual positivity is guaranteed. The signs $\sigma_L(k)$ and $\sigma_R(k)$ are crucial in making this work.

1.6 Conclusions

We have shown that unitarity can be an emergent feature. The positivity of the geometry inevitably leads to amplitudes identical to those derived from a unitary quantum field theory. This lends further support for the conjecture that the amplituhedron computes all the amplitudes of $\mathcal{N} = 4$ SYM. It also suggests that the notion of positivity is more fundamental than those of unitarity and locality which are the cornerstones of the traditional framework of quantum field theory.

2

Deep into the Amplituhedron

2.1 Introduction

The amplituhedron is a geometric object that is conjectured to encode all the perturbative scattering amplitudes of planar $\mathcal{N} = 4$ sYM. First introduced in [16], the original definition of this object was built on the discovery of the structures of the positive Grassmannian uncovered in [9] as well as the observation in [18] associating the NMHV tree amplitude to the volume of a particular

polytope in momentum twistor space. The amplituhedron realizes a similar geometric picture for general tree amplitudes and loop integrands, associating to each positive geometry a (conjecturally unique) "canonical differential form" defined by having logarithmic singularities on all its boundaries [29]. The computation of scattering amplitudes in planar $\mathcal{N} = 4$ is equivalent to determining a triangulation of the amplituhedron, so that different representations of amplitudes correspond to different geometric triangulations of the space. There is nontrivial evidence [47–49] that this geometric construction can be extended to the nonplanar sector of the theory, as the essential analytic properties of the loop integrand, namely logarithmic singularities and no poles at infinity [50], have been observed to hold beyond the planar limit.

Understanding this geometry $\mathcal{A}_{n,k,L}$ for all multiplicities n, helicity configurations k and loop orders L is an open problem, and many different directions have been explored. The connections between the tree level amplituhedron and the Yangian symmetry of $\mathcal{N} = 4$ have been explored in [51], while a triangulation-independent understanding of the geometry has been studied from several different perspectives [52–54], primarily for NMHV trees. An explicit description of how the BCFW cells triangulate the tree-level space was given in [55] while an alternative sign flip reformulation of the $m = 1$ amplituhedron was given in [56]. A manifestly Yangian invariant diagrammatic formulation using so-called "momentum twistor diagrams" was introduced in [57] and used to study the structure of the one-loop geometry in [58]. The higher loop-level geometry of the amplituhedron was explored in detail in [**?**, 40] and an attempt to completely understand the geometry at four points and progressively higher loops can be found in [59–61]. However, important open questions regarding the

technical details of triangulating the amplituhedron remain. Moreover, while the original definition provided a deeper understanding of the positive Grassmannian and on-shell diagrammatic structure of scattering amplitudes in $\mathcal{N} = 4$ sYM, it was still slightly unsatisfactory since all these structures were associated to an auxiliary space not directly tied to the kinematic data.

The introduction of the topological definition of the amplituhedron in [23] completely resolved this issue, revealing the geometric structure of the amplitudes directly in kinematic space. In this new formulation, the amplitudes and loop integrands could now be thought of as differential forms in momentum twistor space depending on the loop integration variables as well as the external data. Recently, it was discovered that the scattering amplitudes in other theories may also be written as differential forms on the space of kinematical data, see e.g, [30, 33, 34].

The topological definition also makes it clear that the inequalities that define the multi-loop amplituhedron fall into two categories. The first set of conditions constrains the variable associated with each loop to live in the one-loop amplituhedron, while the second set of conditions enforces mutual positivity among the different loops. This division provides us with greater control on the source of complexity – the mutual positivity. A full understanding of the interplay between these two conditions is still lacking. However, as a starting point we begin by analyzing special configurations which completely trivialize mutual positivity. These cuts are exactly the opposite of the all-loop cuts considered in [17], which focus on cutting propagators involving external data. Moreover, we begin an investigation of the effects of mutual positivity by introducing this non-triviality in stages.

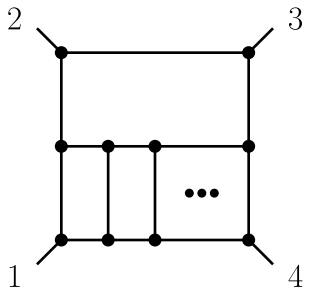

Figure 2.1: A subclass of diagrams which contribute to the cuts considered in this chapter.

One way to understand the geometry of the all-loop amplituhedron is by exploring different cuts of the loop integrand. In addition to specifying the structure of the amplituhedron's boundaries, these cuts allow us to access all-loop order information about the loop integrand which seems out of reach using any other known method. In this chapter, we utilize the reformulation of the amplituhedron outlined in [23] to explore a few faces of the all-loop MHV amplituhedron. These will involve cutting the maximal number of internal propagators involving loop momenta and thus trivializing the mutual positivity conditions between loops. As an example, in terms of Feynman diagrams, at four points, our cut will include (but is not limited to) summing over all diagrams of the form shown in Figure 2.1. In this sense the cuts we consider in this work probe the contributions of the most complicated multi-loop Feynman diagrams to the loop integrand involving the highest number of internal propagators. We will derive compact expressions for these cuts which are valid at all loop orders and, moreover, for an arbitrary number of external particles.

The chapter is structured as follows. In Section 2.2, we will briefly review the amplituhedron and explain the geometry of the different cuts that we analyze in

this chapter. In Section 2.3, we explore cuts which involve cutting $4L-4$ propagators. We derive expressions for these cuts and verify their correctness against known results. In Section 2.4, we derive the results for $2L-4$ cut propagators which in [10] were named the "deepest cuts" of the amplituhedron. Finally, in Section 2.6, we present a few preliminary results which involve solving nontrivial mutual positivity conditions. We consider the nontrivial deformations away from the deepest cuts, as well as generalized ladder cuts which are n-point extensions of the four-point results of [17].

2.2 Geometry of the Amplituhedron

Although it was initially defined in terms of a generalization of the positive Grassmannian [9], the amplituhedron can be defined entirely in terms of sign flip conditions on intrinsically four-dimensional data [23]. The external kinematic data for any massless scattering process is completely specified by the (null) external momenta $\{p_1, \ldots, p_n\}$ satisfying momentum conservation, and the helicities of the interacting particles. The external momenta can be completely specified by giving n unconstrained momentum twistors $\{Z_1, \ldots Z_n\}$ as introduced in [18]. In $\mathcal{N} = 4$ sYM, it suffices to give the N^kMHV degree k instead of specifying the individual helicities. Additionally, at L loops the loop integration variables are given by L lines $\mathcal{L}_\alpha = (AB)_\alpha$, $\alpha = 1, \ldots, L$, each of which can be specified by two points say, A_α and B_α. In terms of these variables, the

amplituhedron is the region which satisfies the following conditions:

$$\begin{aligned}
&\langle ii+1jj+1\rangle > 0, \qquad \forall i<j, \\
&\{\langle 1234\rangle, \langle 1235\rangle, \ldots \langle 123n\rangle\} \text{ has } k \text{ sign flips}, \\
&\langle (AB)_\alpha ii+1\rangle > 0 \qquad \forall \alpha \in \{1, \ldots L\}, \\
&\{\langle (AB)_\alpha 12\rangle, \ldots, \langle (AB)_\alpha 1n\rangle\} \qquad \text{has } k+2 \text{ sign flips}, \\
&\langle (AB)_\alpha (AB)_\beta\rangle > 0, \qquad \forall\ \alpha < \beta \text{ and } \alpha, \beta \in \{1, \ldots L\}.
\end{aligned} \tag{2.1}$$

The L-loop integrand for the N^{k}MHV helicity configuration is the unique degree $4(k+L)$ differential form in $(Z_i, (AB)_\alpha)$ with logarithmic singularities on all boundaries of the space. For the MHV ($k=0$) helicity configuration, the sign flip conditions on the sequence $\{\langle (AB)_\alpha 1i\rangle\}_{i=2,\ldots,n}$ can be reformulated in a slightly different form in terms of the planes $\bar{i} \equiv (i{-}1ii{+}1)$ dual to the points Z_i [23]. For the MHV L-loop integrand we can equivalently impose the following set of conditions:

$$\begin{aligned}
&\langle ii+1jj+1\rangle > 0, \\
&\langle (AB)_\alpha\, \bar{i}\, \bar{j}\rangle > 0, \qquad \forall\, i<j, \\
&\langle (AB)_\alpha (AB)_\beta\rangle > 0, \qquad \forall\ \alpha < \beta \text{ and } \alpha, \beta \in \{1, \ldots L\},
\end{aligned} \tag{2.2}$$

where we introduced the shorthand notation $\langle (AB)_\alpha \bar{i}\bar{j}\rangle \equiv \langle (AB)_\alpha (i{-}1ii{+}1) \cap (j{-}1jj{+}1)\rangle$ to denote the intersection of the planes $\bar{i}$ and $\bar{j}$. From these definitions, it is clear that solving the problem at L-loops amounts to solving the problem at one-loop together with the mutual positivity conditions $\langle (AB)_\alpha (AB)_\beta\rangle > 0$. In this chapter, we are interested in some faces of the amplituhedron which

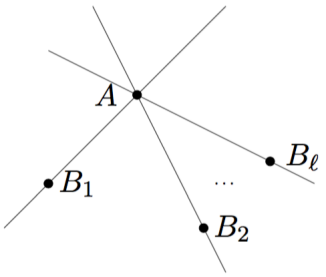

Figure 2.2: Intersecting cut

trivialize all mutual positivity constraints i.e., we approach the boundary where $\langle (AB)_\alpha (AB)_\beta \rangle = 0$ for all $\alpha < \beta$. Generically, this set of constraints has two solutions which are related by parity i.e., the exchange of points$\leftrightarrow$planes. The first solution is a configuration of lines, all of which intersect at a single point A as shown in Figure 2.2. We refer to this solution as the *intersecting cut*.

It is worthwhile to understand the counting of the number of degrees of freedom left on this boundary. We start with L loops and hence $4L$ degrees of freedom. Making each loop pass through a point requires two constraints. Naïvely, this would require $2L$ constraints. However, the point at which all the lines intersect is not specified. Hence we only need $2L-3$ conditions, and the resulting form has degree $(2L+3)$. The remaining conditions on the loop lines are

$$\langle AB_\alpha \bar{i}\bar{j} \rangle > 0. \tag{2.3}$$

These are completely independent of each other and the problem essentially reduces to L copies of the one-loop problem. These inequalities determine the allowed locations of A (which has three degrees of freedom) and also the allowed configuration of each line AB_α for a given A (each B_α has two degrees of free-

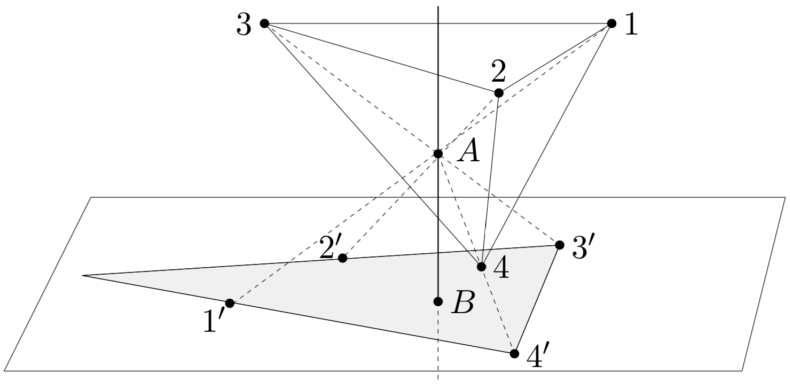

Figure 2.3: Projection through A at four points.

dom left). We seek a cell decomposition of A-space such that for each cell in A space, the geometry of B_α is fixed. By projecting through the common intersection point A one possible one-loop configuration at, say, four points is given in Figure 2.3 (the full L-loop configuration is simply L copies of this geometry).* In this picture we see that A lives inside a tetrahedron with vertices $Z_1, \ldots, Z_4$ while B lives inside the triangle with vertices Z'_3, Z'_4 and $(23)' \cap (14)'$. The triangulation of the intersecting cut is given by the set of all such configurations consistent with the inequalities defining the amplituhedron. Note that since the mutual positivity has been trivialized we expect that we will be able to write the canonical form such that it factorizes into a form for each cell in A space and a product of forms for each loop AB_α. Schematically, we have

$$\Omega^{\text{cut}} = \sum_A \Omega_A \prod_{\alpha=1}^{L} \Omega_{B_\alpha}, \tag{2.4}$$

*Of course, at this point there is no reason to think that the configuration of Figure 2.3 is actually consistent with the inequalities defining the amplituhedron. However, as we shall demonstrate in Section 2.4 this geometry does contribute to the intersecting cut.

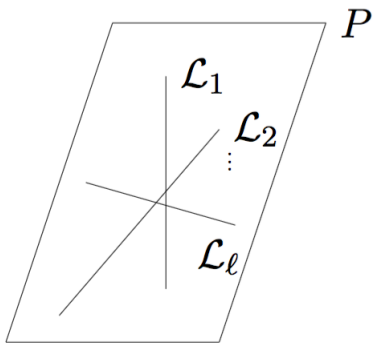

Figure 2.4: All in plane cut

where in this expression (and in many that follow) we suppress the measure of integration, which for the L-loop intersecting cut amounts to omitting the common factors $\langle A\mathrm{d}^3A\rangle \prod_{\alpha=1}^{L}\langle AB_\alpha \mathrm{d}^2 B_\alpha\rangle$ from all expressions.

The second solution to $\langle (AB)_\alpha (AB)_\beta\rangle = 0$ is the configuration in which all lines are coplanar but do not necessarily intersect at the same point shown in Figure 2.4. We refer to this solution as the coplanr cut.

Let us denote the common plane by $(A_1A_2A_3)$. In this case, the remaining constraints read

$$\langle (A_1A_2A_3)B_\alpha \overline{ij}\rangle > 0. \tag{2.5}$$

Since it is easier to work with points than to work with planes, we can dualize the above configuration. This involves the dual point $A^I = \epsilon^{IJKL}A_1^J A_2^K A_3^L$. The dual of the condition in (2.5) is

$$\langle AB_\alpha ij\rangle > 0. \tag{2.6}$$

We see that the dual configuration is now a set of lines AB_α, all of which intersect at a point but satisfy $\langle AB_\alpha ij\rangle > 0$ rather than $\langle AB_\alpha \bar{i}\bar{j}\rangle > 0$ as in (2.3). This demonstrates that the two cuts are distinct from each other.

To find the canonical form for the configuration in Fig. 2.4, we can find the canonical form associated to the dual inequalities (2.6) and dualize the form, exchanging $Z \leftrightarrow W$. Here we are assuming that the dual of the canonical form of the dual region is equal to the canonical form of the original region. We refer the reader to [29] for more details. Operationally, it is somewhat easier to compare our results for the coplanar cut to cuts of the corresponding parity conjugate, "$\overline{\text{MHV}}$" integrand, where by "$\overline{\text{MHV}}$" here we mean the integrand obtained by dualizing $Z \leftrightarrow W$. Note, however, that this is not quite the actual $\overline{\text{MHV}}$ integrand since this object is defined by setting $k = n-2$ in the full definition of the amplituhedron. The relationships can be summarized by

$$\begin{aligned} &\text{MHV intersecting} \leftrightarrow \text{"}\overline{\text{MHV}}\text{" coplanar ,} \\ &\text{"}\overline{\text{MHV}}\text{" intersecting} \leftrightarrow \text{MHV coplanar.} \end{aligned} \tag{2.7}$$

Thus we can view the set of conditions $\langle AB_\alpha ij\rangle > 0$ as defining the intersecting cut of the "$\overline{\text{MHV}}$" integrand, which is dual (by exhanging $Z \leftrightarrow W$) to the coplanar cut of the MHV integrand. Similarly, the MHV intersecting cut can be viewed as the dual of the "$\overline{\text{MHV}}$" coplanar cut. To keep notation consistent in the rest of this chapter we will write all results in terms of the intersection point A, regardless of whether we are considering the intersecting or coplanar cut. Explicit formulae for the two coplanar cuts are obtained by dualizing expressions (2.56) and (2.81). Before solving these two cuts, however, we will first

consider an even simpler set of geometries where the intersecting/coplanar lines satisfy additional constraints.

2.3 $4L-4$ Cuts of Amplitudes

2.3.1 Intersecting cut

In this section, we will focus on a configuration of lines $(AB)_\alpha$ $\alpha = 1, \dots L$, all of which intersect at a common point A. Additionally, we will demand that some of them pass through the points Z_i. Let us suppose that AB_α for some α passes through Z_1. The constraints that this imposes are given by a special case of (2.5), i.e. $\langle A1\overline{ij}\rangle > 0$. It is straightforward to show this implies that $\{\langle A123\rangle, \langle A134\rangle, \dots, \langle A1n2\rangle\}$ must all have the same sign. Geometrically, this implies that after projecting through Z_1, the point A lies in the polygon with vertices $\{\hat{Z}_2, \hat{Z}_3, \dots, \hat{Z}_n\}$ (where the hats indicate the projection through Z_1). We can thus express $A = c_2 Z_2 + \dots c_n Z_n$ with $c_i > 0$. Similarly, for a line passing through $Z_{i_\alpha} B$ we have the constraint that $\langle Aii{+}1i{+}2\rangle$, $\langle Aii{+}2i{+}3\rangle$, …, $\langle Ain(-1)\rangle$, … and $\langle Ai(-(i{-}2))(-(i{-}1))\rangle$ all have the same sign. In this case, we can write

$$A = -c_1 Z_1 - c_2 Z_2 - \dots + c_{i+1} Z_{i+1} \dots + c_n Z_n, \tag{2.8}$$

with $c_i > 0$.

Thus each line $(AB)_\alpha$ which passes through some point Z_{i_α} imposes constraints on the possible positions of the intersection point A. These are all linear inequalities on the $\mathbf{P}^3$ in which A lives. Therefore they cut out some poly-

tope, provided the inequalities are mutually consistent. To check for the consistency, it suffices to keep track of the sign pattern in the expansion of A in terms of the Z_i. For example, passing through Z_1 forces the pattern to be $(?++\cdots+)$ or $(?--\cdots-)$ and Z_2 forces $(-?++\cdots+)$ or $(+?--\cdots-)$, where the ? means that there are no constraints on the sign of that coefficient. We will now demonstrate this in detail for a few examples.

Let us begin with the the simplest case of $n = 4$ points and two loops. Here we have two lines AB_1 and AB_2, and we demand that these pass through Z_1 and Z_2. We can expand

$$A = c_1 Z_1 + c_2 Z_2 + c_3 Z_3 + c_4 Z_4. \tag{2.9}$$

Passing through Z_1 imposes the pattern $(?+++)$ or $(?---)$ on the signs of the coefficients c_i,

$$c_2 > 0\,, c_3 > 0\,, c_4 > 0, \text{ or } c_2 < 0\,, c_3 < 0\,, c_4 < 0. \tag{2.10}$$

Similarly, passing through Z_2 imposes the pattern $(-?++)$ or $(+?--)$. We see that the only consistent patterns are $(-+++)$ or $(+---)$. These are equivalent up to an overall sign and we can write $A = -Z_1 + c_2 Z_2 + c_3 Z_3 + c_4 Z_4$. This is indeed a polytope as stated above. Namely, it is a tetrahedron with vertices Z_2, Z_3, Z_4 and $-Z_1$.

Still working with two loops, we can consider the configuration that results from demanding that the lines pass through Z_1 and Z_3. The patterns imposed on the c_i are $(?+++)$ or $(?---)$ from Z_1 and $(--?+)$ or $(++?-)$ from Z_3.

To obtain a consistent pattern from these, we would need to make one of the c_i vanish. This results in a degenerate configuration and is not allowed for generic loop momenta. Thus there are no consistent patterns and the cut must vanish. We know that this is indeed the case, as shown in [16]. We will also verify this and more general predictions in Section 2.3.2.

While still working at two loops, we can easily generalize the above results to arbitrary n. If the two lines pass through Z_1 and Z_2, then, we have

$$A = -Z_1 + c_2 Z_2 + c_3 Z_3 + \cdots + c_n Z_n. \tag{2.11}$$

Hence A is in the convex hull of $\{Z_2, \ldots, -Z_1\}$ which we denote as $A \in \text{Conv}[Z_2, Z_3, \ldots, -Z_1]$.

We can further generalize to the configuration of lines passing through Z_i and Z_j (with $i < j$), with the result that

$$A \in \text{Conv}\left[Z_j, \ldots Z_n, -Z_1, \cdots - Z_{i-1}\right] \quad \text{and} \quad A \in \text{Conv}\left[Z_i, Z_{i+1} \ldots Z_{j-1}, Z_j\right], \tag{2.12}$$

provided neither is degenerate. Finally, for the most general case in which L lines $(AB)_1$, …, $(AB)_L$ pass through $Z_{i_1}, \ldots Z_{i_L}$, respectively, the above discussion shows that we can have $A \in \text{Conv}\left[Z_{i_L}, Z_{i_L+1}, \ldots, Z_n, -Z_1, \ldots, -Z_{i_1-1}\right]$, $A \in \text{Conv}\left[Z_{i_1}, \ldots, Z_{i_2}\right]$, $A \in \text{Conv}\left[Z_{i_2}, \ldots, Z_{i_3}\right]$, up to $A \in \text{Conv}\left[Z_{i_{L-1}} \ldots Z_{i_L}\right]$, barring degeneracy.

2.3.2 Verification

In this section, we will verify all predictions made in Section 2.3.1 for two loops. We do this by computing the cuts directly from the two loop MHV integrand

which can be expressed in terms of a cylic sum of the double pentagons introduced in [26]. We denote the following diagram as $(ijkl)$:

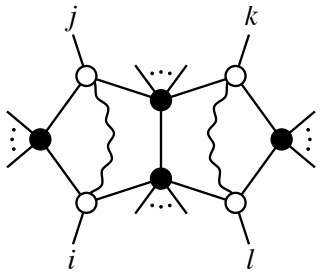

This picture represents the formula

$$(ijkl) = \frac{\langle AB\overline{ij}\rangle}{\langle ABi{-}1i\rangle\langle ABii{+}1\rangle\langle ABj{-}1j\rangle\langle ABjj{+}1\rangle\langle ABCD\rangle} \tag{2.13}$$

$$\times\frac{\langle CD\overline{kl}\rangle\langle ijkl\rangle}{\langle CDk{-}1k\rangle\langle CDkk{+}1\rangle\langle CDl{-}1l\rangle\langle CDll{+}1\rangle}, \tag{2.14}$$

where the two loop lines are (AB) and (CD). The MHV two-loop integrand can be expressed as a sum of double pentagons,

$$\mathcal{A}^{\text{2-loop}}_{n,\text{MHV}} = \sum_{i<j<k<l<i} (ijkl). \tag{2.15}$$

We follow the same order as in the last section and begin with $n = 4$. In this case the integrand can be expressed in terms of two double boxes

$$\Omega_4 = \frac{\langle AB\mathrm{d}^2A\rangle\langle AB\mathrm{d}^2B\rangle\langle CD\mathrm{d}^2C\rangle\langle CD\mathrm{d}^2D\rangle\langle 1234\rangle^3}{\langle AB14\rangle\langle AB12\rangle\langle AB34\rangle\langle ABCD\rangle\langle CD12\rangle\langle CD23\rangle\langle CD34\rangle} + \tag{2.16}$$

$$\frac{\langle AB\mathrm{d}^2A\rangle\langle AB\mathrm{d}^2B\rangle\langle CD\mathrm{d}^2C\rangle\langle CD\mathrm{d}^2D\rangle\langle 1234\rangle^3}{\langle AB14\rangle\langle AB12\rangle\langle AB23\rangle\langle ABCD\rangle\langle CD14\rangle\langle CD23\rangle\langle CD34\rangle}. \tag{2.17}$$

Taking the residue such that AB passes through Z_1 and CD through Z_2, we

get[†]

$$\Omega_{4,\text{cut}} = \frac{\langle A \mathrm{d}^3 A\rangle \langle 1234\rangle^3}{\langle A123\rangle\langle A134\rangle\langle A412\rangle\langle A423\rangle}, \tag{2.18}$$

where A is the point of intersection of AB and CD. This is precisely the canonical form for the simplex with vertices $Z_2, Z_3, Z_4, -Z_1$ as expected from Section 2.3.1.

We can also make AB pass through Z_1 and CD through Z_3. Taking residues appropriately, we find the residue on the cut vanishes

$$\Omega_{4,\text{cut}} = \frac{\langle 1234\rangle^3}{\langle C142\rangle\langle C134\rangle\langle C312\rangle\langle C234\rangle} + \frac{\langle 1234\rangle^3}{\langle C142\rangle\langle C123\rangle\langle C314\rangle\langle C234\rangle} = 0, \tag{2.19}$$

exactly as predicted in Section 2.3.1 and [16].

At five points, we next consider the cut where AB passes through Z_1 and CD through Z_2. Only three double pentagons contribute to this cut.

$$(5123) \xrightarrow[D\to Z_2]{B\to Z_1} \frac{\langle C \mathrm{d}^3 C\rangle\langle 5123\rangle\langle 4512\rangle\langle 1234\rangle}{\langle C145\rangle\langle C512\rangle\langle C123\rangle\langle C234\rangle} \tag{2.20}$$

$$(5124) \xrightarrow[D\to Z_2]{B\to Z_1} -\frac{\langle C \mathrm{d}^3 C\rangle\langle 5124\rangle^2\langle 2345\rangle}{\langle C145\rangle\langle C512\rangle\langle C234\rangle\langle C245\rangle} \tag{2.21}$$

$$(4123) \xrightarrow[D\to Z_2]{B\to Z_1} \frac{\langle C \mathrm{d}^3 C\rangle\langle 1234\rangle^2\langle 1345\rangle}{\langle C134\rangle\langle C145\rangle\langle C123\rangle\langle C234\rangle}. \tag{2.22}$$

$$\tag{2.23}$$

It is easy to check that this is indeed a triangulation of the cyclic polytope with vertices $Z_2, Z_3, Z_4, Z_5, -Z_1$ as expected from Section 2.3.1.

More generally, at two loops if we have AB passing through Z_a and CD pass-

[†]Henceforth where appropriate we will sometimes suppress the measure of loop integration.

ing through Z_b, the following double pentagons contribute:

$$(ajbl) \xrightarrow[D\to Z_b]{B\to Z_a} \frac{\langle Aa\left(\overline{a}\cap\overline{j}\right)\rangle\langle Ab\left(\overline{b}\cap\overline{l}\right)\langle abjl\rangle\rangle}{\langle A\overline{a}\rangle\langle Aaj-1j\rangle\langle Aajj+1\rangle\langle A\overline{b}\rangle\langle Abl-1l\rangle\langle Abll+1\rangle} \tag{2.24}$$

$$(ajkb) \xrightarrow[D\to Z_b]{B\to Z_a} \frac{\langle Aa\left(\overline{a}\cap\overline{j}\right)\rangle\langle Ab\left(\overline{k}\cap\overline{b}\right)\langle ajkb\rangle\rangle}{\langle A\overline{a}\rangle\langle Aaj-1j\rangle\langle Aajj+1\rangle\langle A\overline{b}\rangle\langle Abk-1k\rangle\langle Abkk+1\rangle} \tag{2.25}$$

$$(iabl) \xrightarrow[D\to Z_b]{B\to Z_a} \frac{\langle Aa\left(\overline{i}\cap\overline{a}\right)\rangle\langle Ab\left(\overline{b}\cap\overline{l}\right)\langle iabl\rangle\rangle}{\langle A\overline{a}\rangle\langle Aai-1i\rangle\langle Aaii+1\rangle\langle A\overline{b}\rangle\langle Abl-1l\rangle\langle Abll+1\rangle} \tag{2.26}$$

$$(iakb) \xrightarrow[D\to Z_b]{B\to Z_a} \frac{\langle Aa\left(\overline{i}\cap\overline{a}\right)\rangle\langle Ab\left(\overline{k}\cap\overline{b}\right)\langle iakb\rangle\rangle}{\langle A\overline{a}\rangle\langle Aai-1i\rangle\langle Aaii+1\rangle\langle A\overline{b}\rangle\langle Abk-1k\rangle\langle Abkk+1\rangle}. \tag{2.27}$$

The form on this cut is then

$$\Omega = \sum_{j=a+1}^{b-1}\sum_{l=b+1}^{a-1}(ajbl) + \sum_{j=a+1}^{b-2}\sum_{k=j+1}^{b-1}(ajkb) + \sum_{l=b+1}^{a-2}\sum_{i=l+1}^{a-1}(iabl) + \sum_{i=b+1}^{a-2}\sum_{k=a+1}^{b-1}(iakb) \tag{2.28}$$

We expect this to be a triangulation corresponding to the sum of the forms for the two cyclic polytopes $\mathrm{Conv}[Z_a,\dots Z_b]$ and $\mathrm{Conv}[Z_b,\dots Z_n,-Z_1,\dots,-Z_a]$. To verify this, we need the canonical form of a cyclic polytope. A triangulation of this form is given by $\Omega_1+\Omega_2$, where [29]

$$\Omega_1 = \sum_{i=a+1}^{b-2}[aii+1b], \qquad \text{and} \qquad \Omega_2 = \sum_{i=b+1}^{a-2}[bii+1a], \tag{2.29}$$

where we define

$$[abcd] \equiv \frac{\langle abcd\rangle^3}{\langle Aabc\rangle\langle Abcd\rangle\langle Acda\rangle\langle Adab\rangle}. \tag{2.30}$$

We have verified up to $n = 20$ that this prediction holds true in every case. However, the double pentagon expansion provides a triangulation of the two

polytopes which is different from (2.29). Furthermore, there is no obvious subset of terms in the double pentagon form which triangulates either the polytope $\text{Conv}[Z_a, \dots Z_b]$ or $\text{Conv}[Z_b, \dots Z_n, -Z_1, \dots, -Z_a]$ separately. This of course follows from the known fact that the double pentagon expansion of the integrand, although term-by-term local, is not a triangulation in the usual mathematical sense because it involves points living outside the amplituhedron. Understanding exactly how this representation of the integrand covers the amplituhedron, even on this special cut, is an interesting open question which we leave to future work.

2.3.3 Coplanar cut

In this section we will focus on the coplanar cut of the MHV integrand. Since we are considering coplanar lines, we cannot demand that they pass through the Z_i. This is impossible for generic configurations of external data. However, there exists a natural analog of making the lines AB_α pass through Z_i. Consider the planes $(i{-}1ii{+}1)$, which are dual to the points Z_i. These intersect the plane $(A_1A_2A_3)$ in lines as shown in Figure 2.5.

We can identify the lines $(AB)_\alpha$ with these lines. To understand why this is a natural analog, it is helpful to look at the dual picture. Recall that the dual of a set of coplanar lines is a set of lines intersecting at a point. The dual of a line lying in the plane $(i{-}1ii{+}1)$ is a line passing through the point Z_i. Thus the dual of the configuration shown in Figure 2.5 is a set of lines intersecting at a point and passing through Z_i, Z_j and Z_k. For the rest of this section, we will be working with the dual configuration and demanding the constraints $\langle ABij\rangle > 0$ as explained in Section 2.2. We will denote the dual of the common

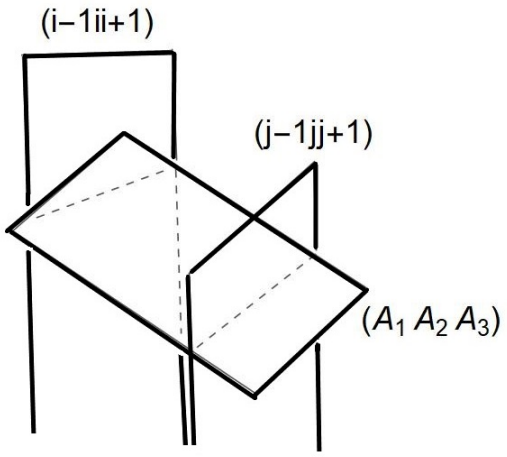

Figure 2.5: The dotted lines are common plane $(A_1A_2A_3)$ intersecting $(i{-}1ii{+}1)$ and $(j{-}1jj{+}1)$.

plane $A_1A_2A_3$ by the point A.

The coplanar cut is strikingly different from the intersecting cut. It lacks the rich structure of deeper cuts that we saw in Section 2.3.1. The first result which sets the two cuts apart is that we cannot make AB_α pass through non consecutive Z_i. To see this, it suffices to look at the constraints imposed by passing through Z_a and Z_b for $b > a$. Let us suppose that passing through a imposes $\langle Aaij\rangle > 0$. Passing through b then requires $\langle Abij\rangle < 0$ since $a < b$ and we must have a consistent sign for $\langle Aabj\rangle$. Now, if there exists c such that $a < c < b$ we have a contradiction, and therefore such a configuration of lines does not belong to the one-loop amplituhedron.

Consequently, configurations of lines passing through three or more of the Z_i are also disallowed since this will necessarily involve two non consecutive Z_i.

ℓ	total # of topologies	possible contributions	%
4	8	4	50
5	34	20	58.8
6	229	146	63.8
7	1873	1248	66.6
8	19 949	13 664	68.5
9	247 856	172 471	69.6
10	3 586 145	2 530 903	70.6

Figure 2.6: Number of topologies contributing on the cut through ten loops [10].

2.4 $2L-4$ Cuts of Amplitudes

We now tackle the problem of finding the form for the cut $\langle (AB)_\alpha (AB)_\beta \rangle = 0$ with no other constraints imposed. As discussed in [10] this cut is hopelessly complicated from a local diagram expansion. We can be slightly more quantitative about the complexity of this cut by estimating how many local diagrams contribute at, say, $n = 4$ points using known results available from the soft collinear bootstrap program [62–64]. From the ancillary files in [64] the number of dual conformal invariant (DCI) integrals that have enough internal propagators to possibly contribute on the cut can be counted through ten loops, with the number of topologies given in Figure 2.6 which is taken from [10]. Note in particular that the *total* number of diagrams is given by symmetrizing in all loop momenta and cycling through external labels. Of course, simply having enough internal propagators is not sufficient to say that a given diagram actually has support on our cuts, since there may be compensating DCI numerators which cancel some internal propagators and/or kill the residue. Thus, the numbers shown in the "possible contributions" column of Figure 2.6 are

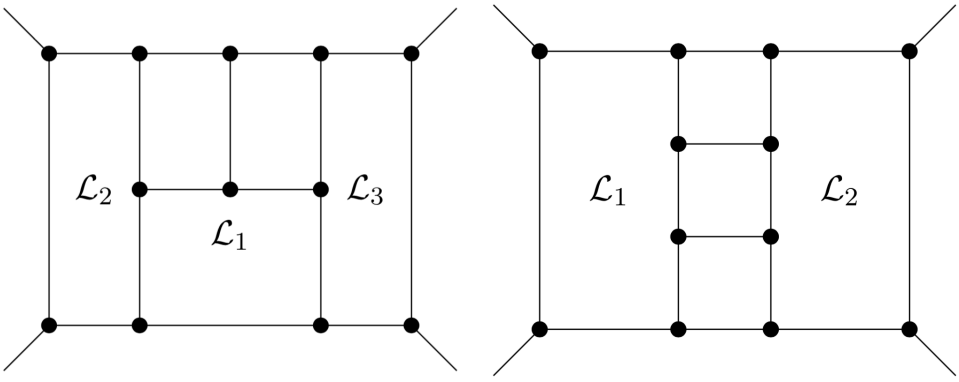

Figure 2.7: The two local diagrams at five loops which have the necessary number of internal propagators but nevertheless do not contribute to the $(2L-4)$-dimensional cuts. Here we label the lines $\mathcal{L}_\alpha = (AB)_\alpha$.

overestimates of the actual contributions, as can be seen by, for example, a more detailed consideration of the thirty-four topologies present at five loops: of these planar graphs twenty have at least the required seven internal propagators necessary to a priori contribute on the cut. However, of these twenty the two graphs shown in Figure 2.7 have the associated DCI numerators

$$N_1 = -\langle 1234\rangle^4 \langle 12(AB)_1\rangle^2 \langle (AB)_2(AB)_3\rangle^2, \tag{2.31}$$

and

$$N_2 = -\langle 1234\rangle^4 \langle (AB)_1(AB)_2\rangle^4, \tag{2.32}$$

respectively. Therefore neither of these diagrams have nonzero residue on our cut, and the correct counting at five loops is eighteen rather than twenty.

2.4.1 Four point problem

We will first focus on the intersecting cut at four points. The inequalities for the line AB_α to be in the one-loop amplituhedron are $\langle AB_\alpha \overline{ij}\rangle > 0$. These reduce to

$$\begin{aligned} &\langle AB_\alpha 12\rangle > 0, \quad \langle AB_\alpha 13\rangle < 0, \quad \langle AB_\alpha 14\rangle > 0, \\ &\langle AB_\alpha 23\rangle > 0, \quad \langle AB_\alpha 24\rangle < 0, \quad \langle AB_\alpha 34\rangle > 0. \end{aligned} \tag{2.33}$$

The inequalities that result from the coplanar cut $\langle ABij\rangle > 0$ are identical to (2.33) except for the signs of $\langle AB_\alpha 13\rangle$ and $\langle AB_\alpha 24\rangle$. However, the form for the two inequalities is identical as the case of $n = 4$ is too simple to distinguish between the two cuts. We can solve the system in (2.33) explicitly by setting

$$A = Z_1 + a_2 Z_2 + a_3 Z_3 + a_4 Z_4, \quad B_\alpha = Z_1 + x_\alpha Z_2 + y_\alpha Z_3, \tag{2.34}$$

and solving the resulting inequalities for a_2, a_3, a_4, x_α and y_α. The resulting triangulation is the union of the following four regions:

- $a_4 < 0 \qquad a_3 > 0 \qquad a_2 < 0 \qquad a_2 < x_\alpha < 0 \qquad 0 < y_\alpha < (a_3 x_\alpha)/a_2,$
- $a_4 > 0 \qquad a_3 < 0 \qquad a_2 < 0 \qquad x_\alpha < a_2 \qquad y_\alpha > 0,$
- $a_4 > 0 \qquad a_3 > 0 \qquad a_2 > 0 \qquad x_\alpha < 0 \qquad 0 < y_\alpha < a_3 x_\alpha / a_2,$
- $a_4 > 0 \qquad a_3 > 0 \qquad a_2 < 0 \qquad x_\alpha < a_2 \qquad y_\alpha > a_3 x_\alpha / a_2.$

This determines the canonical form for the region of interest in terms of a_2, a_3, a_4, x_α and y_α. It is trivial to take these expressions and rewrite them in terms of momentum twistors by solving the linear equations (3.22) for all variables. We refer the

reader to [17] for numerous example of writing down the canonical forms corresponding to regions defined by inequalities, and here give only the final expression for the four-point form:

$$\Omega_4^{(L)} = \frac{\langle 1234\rangle^3}{\langle A123\rangle\langle A124\rangle\langle A134\rangle\langle A234\rangle} \times \left(\prod_\alpha \frac{\langle A123\rangle\langle A234\rangle}{\langle AB_\alpha 12\rangle\langle AB_\alpha 23\rangle\langle AB_\alpha 34\rangle} + \prod_\alpha \frac{(-1)\langle A123\rangle\langle A124\rangle}{\langle AB_\alpha 12\rangle\langle AB_\alpha 23\rangle\langle AB_\alpha 14\rangle} + \prod_\alpha \frac{\langle A124\rangle\langle A134\rangle}{\langle AB_\alpha 12\rangle\langle AB_\alpha 34\rangle\langle AB_\alpha 14\rangle} + \prod_\alpha \frac{(-1)\langle A134\rangle\langle A234\rangle}{\langle AB_\alpha 23\rangle\langle AB_\alpha 34\rangle\langle AB_\alpha 14\rangle}\right), \tag{2.35}$$

where at four points there is only one form in A,

$$\Omega_A^{(4)} = [1234] = \frac{\langle 1234\rangle^3}{\langle A123\rangle\cdots\langle A412\rangle}, \tag{2.36}$$

which corresponds to the tetrahedron with faces Z_i [19]. This clearly shows that the form in A, Ω_A, is independent of the number of loops, L.

2.4.2 Five point coplanar cut

At five points we can algebraically solve the inequalities $\langle AB_\alpha ij\rangle > 0$ by parametrizing A and B_α as above and triangulating the space of allowed common points A for fixed geometries in B_α. As the number of inequalities to solve becomes large for higher points, this approach becomes computationally intractable. However, the geometry of the problem is quite simple: we have several intersecting lines with at most quadratic inequalities between them. This suggests that the pieces in the triangulation might in some sense be "simple." To see if this is possible we seek an alternative procedure to solve the inequalities which is completely

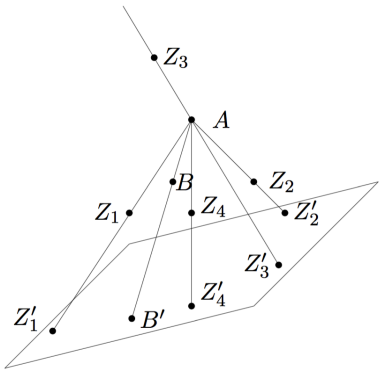

Figure 2.8: Projecting through A to get a two-dimensional configuration.

geometric rather than algebraic in nature. In fact, this reformulation of the problem is easy to find: to "triangulate" the space of allowed AB_α we should simply draw all configurations of points $\{Z_1, \ldots Z_n\}$ allowed by the inequalities $\langle AB_\alpha ij\rangle > 0$. This is efficiently accomplished by first projecting the external data and the points B_α through the common intersection point A, whence we land on the two dimensional picture of Figure 2.8 where the bracket $\langle ABij\rangle$ is positive if the point B lies to the right of the line (ij).

For a given configuration of projected positive external data $Z_1', \ldots, Z_n'$ (henceforth we omit the primes on projected variables) the conditions that AB_α is in the one-loop amplituhedron simply demand that the projected point B_α lies to the right of all lines (ij), for $i < j$. This generates a list of allowed configurations in A along with the corresponding regions in B from which we can directly write down the forms.

There are eight quadrilateral and eight triangular configurations for the four point case. Checking all possibilities against the inequalities $\langle AB_\alpha ij\rangle > 0$ for $i < j = 1, \ldots 4$, we find four allowed configurations, displayed in Figure 2.9

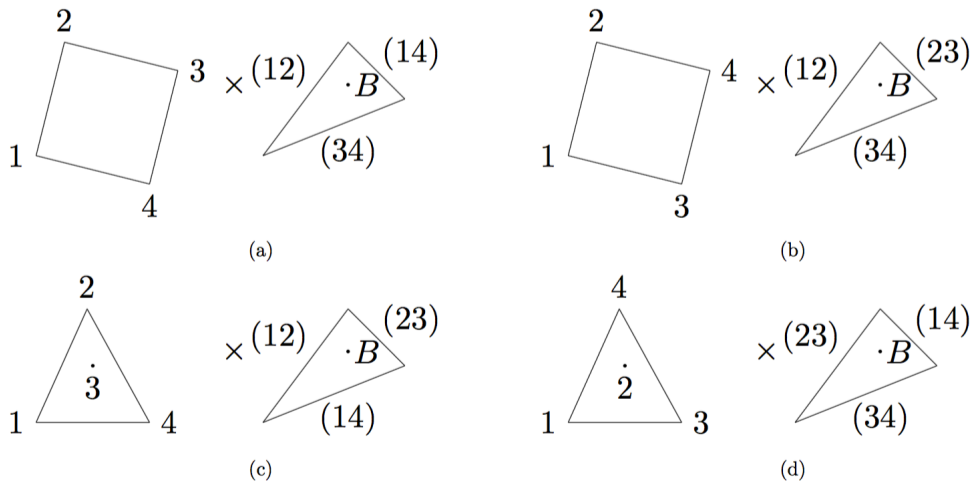

Figure 2.9: Four point configurations written as (configuration in A) and (allowed region in B).

as the list of configurations in A and the corresponding regions in B where the inequalities are satisfied. From these pictures it is trivial to write down the corresponding canonical form, and we find term-by-term agreement with the algebraic approach of the previous section. To solve the MHV coplanar (although here we are thinking of it as the "$\overline{\text{MHV}}$" intersecting) cut at five points, we can proceed by taking the four point configurations just obtained and adding a fifth point everywhere consistent with the additional five point inequalities $\langle ABi5\rangle > 0$, for $i = 1, \ldots, 4$. For example, for configuration (a) of Figure 2.9, the point Z_5 can be added in any of the regions shown in Figure 2.10, where in this picture we have labelled regions of the plane by the corresponding sign patterns of the sequence

$$\{\langle A125\rangle, \langle A135\rangle, \langle A145\rangle, \langle A235\rangle, \langle A245\rangle, \langle A345\rangle\}, \tag{2.37}$$

and only configurations which give a nonzero allowed region for B have been

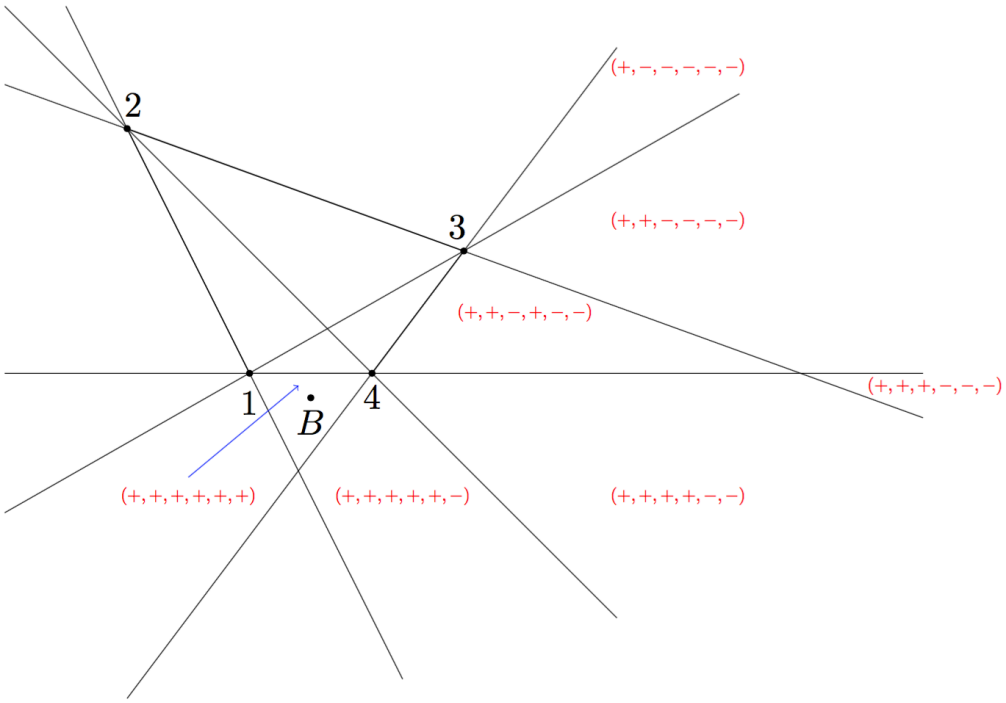

Figure 2.10: Allowed regions in the projection plane for the point Z_5', labelled by the sign sequence of (2.37).

labelled. Although a priori this gives seven distinct configurations in A, in fact several of the configurations give identical allowed regions in B and hence "glue together" naturally. If we complete this exercise for each four-point picture in Figure 2.9, the resulting list of configurations in A and allowed regions for B can be translated into the corresponding forms just as in the four point case. However, it is a less trivial exercise to compute the forms in A corresponding to configurations of the Z_i. For example, one of the allowed configurations is the simple (projected) pentagon of Figure 2.14(a), which gives for the point B_α the triangle bounded by lines (12)(15)(45). Here the codimension one boundaries in A are obviously given by all deformations making three projected points collinear, so for the pentagon with ordered vertices 12345 the poles of the form

in A are

$$\{\langle A123\rangle, \langle A234\rangle, \langle A345\rangle, \langle A451\rangle, \langle A512\rangle\}. \tag{2.38}$$

However, starting at five points we also find configurations such as in Figure 2.14(b)-(c), both of which give the region for B_α bounded by the lines (12)(15)(34), where the pole structure of the form is not as obvious. The quadrilateral configuration of Figure 2.14(b) has codimension one boundaries corresponding to the poles

$$\{\langle A123\rangle, \langle A134\rangle, \langle A345\rangle, \langle A145\rangle, \langle A235\rangle, \langle A125\rangle\},$$

as can easily be seen by deforming the picture in all ways which make three points collinear. However, for the triangular configuration as drawn in Figure 2.14(c) the relative orientation of points Z_3 and Z_4 inside the triangle is *crucial* in reconstructing the form, and we must indicate whether the brackets $\{\langle A134\rangle, \langle A234\rangle, \langle A345\rangle\}$ are required to have definite signs in order to satisfy the inequalities. The codimension one boundaries of this cell correspond to those collinear limits which do not first flip any brackets which have definite sign. For Figure 2.14(c) this gives, for example, the boundary structure corresponding to the poles

$$\{\langle A134\rangle, \langle A234\rangle, \langle A135\rangle, \langle A235\rangle, \langle A245\rangle\}.$$

The allowed regions in B_α can be classified by the pole structure of the associated form. In the four-point case we found all possible "triangles" with three poles in B corresponding to the lines $(i{-}1i), (ii{+}1)$ and $(i{+}1i{+}2)$, and a priori at n-points one would anticipate finding triangles, quadrilaterals, etc. up

to possibly n-gons for the allowed regions for B_α. Indeed, adding a fifth point everywhere in the four-point configurations consistent with the additional five point inequalities yields both quadrilaterals and pentagons in B_α. However, the corresponding sum of canonical forms for each cell does *not* reproduce the correct integrand on this cut at any loop order. The reason for this discrepancy is simple: in addition to the inequalities $\langle AB_\alpha ij\rangle > 0$ we must ensure that we are only keeping configurations that are consistent with having been projected from *positive* data. To be more explicit, consider the following five-point configuration obtained from the procedure outlined above which is consistent with the inequalities $\langle AB_\alpha ij\rangle > 0$ (here the point Z_3 must lie to the right of the line (14) and to the left of the line (25) to give the region in B_α shown)

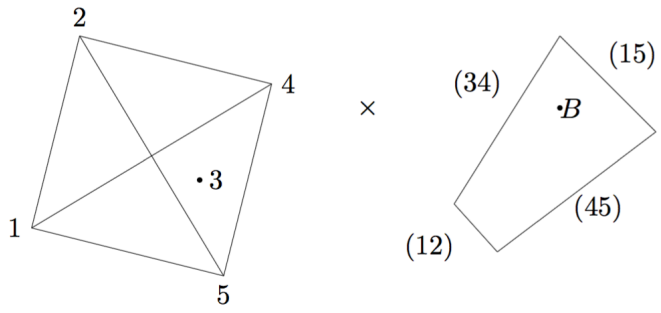

(2.39)

Naïvely this configuration contributes to the cut with a quadrilateral region for B_α with poles $\langle AB12\rangle, \langle AB34\rangle, \langle AB45\rangle$ and $\langle AB15\rangle$. However, this configuration of projected Z_i is actually *inconsistent* with having been projected from *positive* data, as a simple argument demonstrates. Namely, if we expand Z_5 in the basis $Z_1, \ldots, Z_4$ we have

$$Z_5 = \alpha_4 Z_4 - \alpha_3 Z_3 + \alpha_2 Z_2 - \alpha_1 Z_1, \tag{2.40}$$

where the positivity of the variables $\alpha_i > 0$ follows from the positivity of the external data. Expanding the bracket $\langle A135\rangle$ using (2.40) and noting that $\langle A123\rangle > 0$ and $\langle A134\rangle < 0$ (which are conditions defining this configuration) we see this implies this bracket is negative,

$$\langle A135\rangle = \alpha_4\langle A134\rangle - \alpha_3\langle A123\rangle < 0, \tag{2.41}$$

which is in contradiction to the configuration we have drawn, where $\langle A135\rangle > 0$. Thus, the configuration (2.39) cannot be obtained by the projection of positive data.

If we cross-check the list of configurations obtained by adding a fifth point to the allowed four-point cases of Figure 2.9 against the positivity constraints on the external data, the surprising result is the elimination of all geometries apart from triangles in B_α. The complete set of configurations can be constructed out of the following list:

(12)(23)(34)

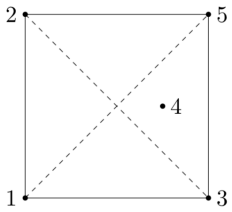

(2.42)

(12)(23)(45)

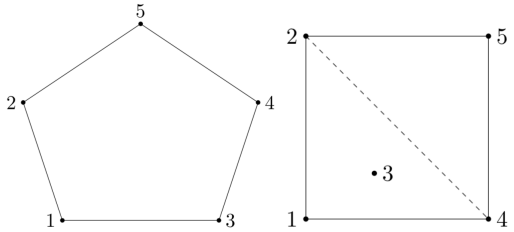

(2.43)

(12)(23)(15) 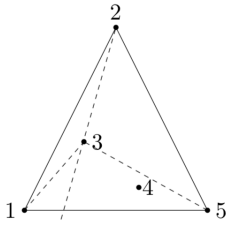 (2.44)

(12)(34)(45) 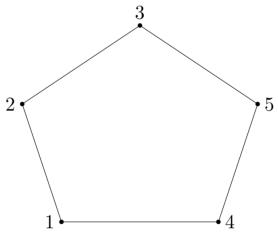 (2.45)

(12)(34)(15) 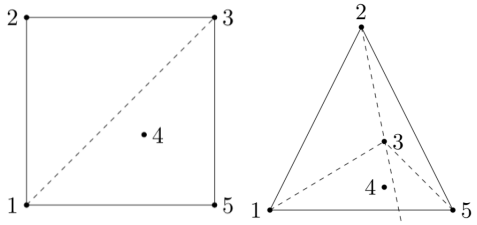 (2.46)

(12)(45)(15) 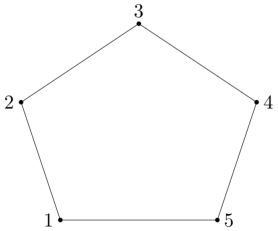 (2.47)

(23)(34)(45) 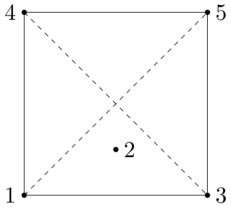 (2.48)

(23)(34)(15) 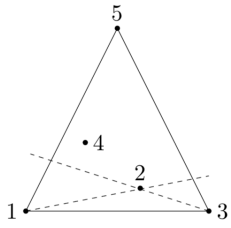 (no sign on $\langle A245 \rangle$) (2.49)

(23)(45)(15)

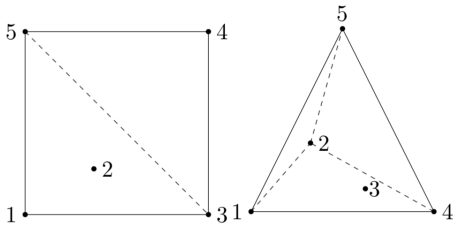

(2.50)

(34)(45)(15)

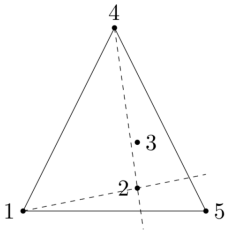

(2.51)

In these results, we have indicated the regions in B_α satisfying the one-loop inequalities by the codimension one boundaries which are lines $(ii{+}1)$ in the projection through A. The full set of allowed configurations is given by adding all reflections across the line (12) of the above list (disregarding duplicates), which is equivalent to requiring the consideration of both cases $\langle A123\rangle \gtrless 0$. Alternatively, all possibilities can be generated by constructing, for each possible B_α region, all configurations consistent with the inequalities (with no requirements on any $\langle Aijk\rangle$ bracket); this leads to exactly the same set of allowed configurations as (2.42)-(2.51), plus reflections across (12).

As already mentioned, the key aspect of the five point results (2.42)-(2.51) is that only triangles in B_α are found, despite there being no immediately obvious reason why quadrilaterals and pentagons are forbidden. In fact, if one repeats the above brute-force procedure to construct the complete set of six point geometries, the same simple result is found: only triangles in B_α satisfy the inequalities and are consistent with the positivity of external data. Although a deep explanation of why the positivity constraints demand triangle geometry for the B_α is at this point missing, in Appendix A we discuss the precise nature of

the constraints imposed on the projected data in slightly more detail. However, even without a satisfying explanation for this simplicity, we can immediately make an obvious ansatz: namely, for an *arbitrary* number of particles, the geometry in B_α is still no more complicated than triangles! As we will see below this powerful hypothesis, checked by brute force at five and six points, allows use to solve the problem completely for any n by a simple unitarity-inspired procedure. Since we know the allowed regions for the B_α, we can obtain the corresponding Ω_A from the known two loop MHV integrands (2.15) by taking residues. At higher points our triangle-hypothesis has been verified by matching our prediction for the cut against known expressions for the full integrand.

2.4.3 Coplanar cut for arbitrary multiplicities

It was shown in Section 2.3.3 that the coplanar cut allowed only a limited number of deeper cuts. In particular, we cannot have any Ω_B which allows passing through more than two Z_i. We allow for all possible Ω_B with three factors of $\langle ABii+1\rangle$ in the denominator and determine the corresponding Ω_A. Surprisingly, this turns out to be the exact form on the cut for arbitrary n and L. There can be three kinds of Ω_B with the following factors in the denominator.

- $\langle ABaa+1\rangle \langle ABbb+1\rangle \langle ABcc+1\rangle$
- $\langle ABa-1a\rangle \langle ABaa+1\rangle \langle ABbb+1\rangle$
- $\langle ABa-1a\rangle \langle ABaa+1\rangle \langle ABa+1a+2\rangle$

We can determine Ω_A for each of them by localizing the two-loop MHV integrand (2.15) appropriately and computing the residues. Since the form for A is

independent of the number of loops, this gives us the form in A for any number of loops.

Case 1: $aa{+}1$-$bb{+}1$-$cc{+}1$

We can assume $a < b < c$ and no degeneracies (i.e $b \neq a+1, c \neq b+1, a \neq c+1$) and focus on the cut $\langle ABaa{+}1\rangle = \langle ABbb{+}1\rangle = 0$, $\langle CDbb{+}1\rangle = \langle CDcc{+}1\rangle = 0$. The four double pentagons which contribute to this cut are $(abb{+}1c)$, $(a{+}1bb{+}1c)$, $(abb{+}1c{+}1)$, and $(a{+}1bb{+}1c{+}1)$. Their residues on this cut are

$$\begin{aligned}
&(abb+1c) \xrightarrow[B\to(Aaa+1\cap Abb+1)]{D\to(Acc+1\cap Abb+1)} \frac{\langle \overline{a}\,\overline{b}\,\overline{b+1}\,\overline{c}\rangle}{\langle A\overline{a}\rangle\langle A\overline{b}\rangle\langle A\overline{b+1}\rangle\langle A\overline{c}\rangle} \\
&(a+1bb+1c) \xrightarrow[B\to(Aaa+1\cap Abb+1)]{D\to(Acc+1\cap Abb+1)} \frac{\langle \overline{a+1}\,\overline{b}\,\overline{b+1}\,\overline{c}\rangle}{\langle A\overline{a+1}\rangle\langle A\overline{b}\rangle\langle A\overline{b+1}\rangle\langle A\overline{c}\rangle} \\
&(abb{+}1c{+}1) \xrightarrow[B\to(Aaa+1\cap Abb+1)]{D\to(Acc+1\cap Abb+1)} \frac{\langle \overline{a}\,\overline{b}\,\overline{b+1}\,\overline{c+1}\rangle}{\langle A\overline{a}\rangle\langle A\overline{b}\rangle\langle A\overline{b+1}\rangle\langle A\overline{c+1}\rangle} \\
&(a+1bb+1c+1) \xrightarrow[B\to(Aaa+1\cap Abb+1)]{D\to(Acc+1\cap Abb+1)} \frac{\langle \overline{a+1}\,\overline{b}\,\overline{b+1}\,\overline{c+1}\rangle}{\langle A\overline{a+1}\rangle\langle A\overline{b}\rangle\langle A\overline{b+1}\rangle\langle A\overline{c+1}\rangle}.
\end{aligned} \tag{2.52}$$

Here the bar represents the dual ($\overline{a} = (a{-}1aa{+}1)$). The sum of these four terms can be compactly written as

$$\Omega_1 = \frac{\langle (Aaa{+}1 \cap Abb{+}1)cc{+}1\rangle\langle a{-}1aa{+}1a{+}2\rangle\langle b{-}1bb{+}1b{+}2\rangle\langle c{-}1cc{+}1c{+}2\rangle}{\langle A\overline{a}\rangle\langle A\overline{a+1}\rangle\langle A\overline{b}\rangle\langle A\overline{b+1}\rangle\langle A\overline{c}\rangle\langle A\overline{c+1}\rangle} \tag{2.53}$$

This is an octahedron with vertices

$$\begin{aligned}
&(\overline{a},\,\overline{b},\,\overline{c}), (\overline{a},\,\overline{b},\,\overline{c+1}), (\overline{a},\,\overline{b+1},\,\overline{c}), (\overline{a},\,\overline{b+1},\,\overline{c+1}), (\overline{a+1},\,\overline{b},\,\overline{c}), \\
&(\overline{a+1},\,\overline{b},\,\overline{c+1}), (\overline{a+1},\,\overline{b+1},\,\overline{c}), \text{ and } (\overline{a+1},\,\overline{b+1},\,\overline{c+1}).
\end{aligned}$$

The numerator puts a zero on all the other co-dimension 2 singularities. The

facets are obvious from the expression.

Case 2: $a{-}1a{-}aa{+}1{-}bb{+}1$

A similar calculation shows that the form can be written as

$$\Omega_2 = \frac{\langle Aabb{+}1\rangle\langle b{-}1bb{+}1b{+}2\rangle\langle a{-}2a{-}1aa{+}1\rangle\langle a{-}1aa{+}1a{+}2\rangle}{\langle A\overline{a{-}1}\rangle\langle A\bar{a}\rangle\langle A\overline{a{+}1}\rangle\langle A\bar{b}\rangle\langle A\overline{b{+}1}\rangle} \tag{2.54}$$

This is a polytope with vertices

$(\overline{a-1}, \bar{a}, \bar{b}), (\overline{a-1}, \bar{a}, \overline{b+1}), (\overline{a-1}, \overline{a+1}, \bar{b}), (\overline{a-1}, \overline{a+1}, \overline{b+1}), (\bar{a}, \overline{a+1}, \bar{b})$, and $(\bar{a}, \overline{a+1}, \overline{b+1})$.

Again, the numerator puts a zero on all other co-dimension two singularities and the facets are obvious.

Case 3: $a{-}1a{-}aa{+}1{-}a{+}1a{+}2$

Finally, we have

$$\Omega_3 = \frac{\langle a{-}2a{-}1aa{+}1\rangle\langle a{-}1aa{+}1a{+}2\rangle\langle aa{+}1a{+}2a{+}3\rangle}{\langle A\overline{a{-}1}\rangle\langle A\bar{a}\rangle\langle A\overline{a{+}1}\rangle\langle A\overline{a{+}2}\rangle}. \tag{2.55}$$

This is a tetrahedron with vertices $(\overline{a-1}, \bar{a}, \overline{a+1}), (\overline{a-1}, \bar{a}, \overline{a+2})$, $(\overline{a-1}, \overline{a+1}, \overline{a+2})$, and $(\overline{a+1}, \bar{a}, \overline{a+2})$.

The full form at L-loops and arbitrary number of particles n is given by summing over all possible triangles in B_α. Note that the key aspect of this calculation was the fact that only triangles in B_α appear in the expansion (2.4). If quadrilaterals and higher polygons appeared it would not, in general, be possible to fully fix the forms in A just from the two-loop integrand. However, in this problem once we know the result on the cut can be expressed as a sum of

triangles in B_α it is trivial to obtain the coefficients of the individual triangles. In particular, the triangles labelled by boundaries $(i{-}1i),(ii{+}1),(i{+}1i{+}2)$ are fixed by setting some set of the $B_\alpha = Z_i$ and the rest to $B_\beta = Z_{i+1}$. On this further cut of the integrand only this triangle can contribute. For example at two loops for the triangle $(12),(23),(34)$ the form in A is fully fixed by solving the geometry when we cut $\langle AB_1 12\rangle = \langle AB_1 23\rangle = 0$ and $\langle AB_2 23\rangle = \langle AB_2 34\rangle = 0$ i.e., $B_1 = Z_2$ and $B_2 = Z_3$. For the triangles $(i{-}1i),(ii{+}1),(jj{+}1)$ we fix the coefficients by setting some $B_\alpha = Z_i$ and the rest to $B_\beta = (ii{+}1)\cap(Ajj{+}1)$. At two loops we can explicitly check that matching on this cut is sufficient to fix the coefficient of the triangle, matching on the other possible cuts $B_\alpha = Z_i$,$B_\beta = (i{-}1i)\cap(Ajj{+}1)$ and $B_\alpha = (i{-}1i)\cap(Ajj{+}1)$, $B_\beta = (ii{+}1)\cap(Ajj{+}1)$ is automatic.

Proceeding in this way we obtain the full result for the n-point cut:

$$\Omega_n^{(L)} = \frac{1}{L!}\sum_{i<j<k}\left(\frac{\langle A(ii{+}1)\cap(Ajj{+}1)kk{+}1\rangle\langle i{-}1ii{+}1i{+}2\rangle\langle j{-}1jj{+}1j{+}2\rangle\langle k{-}1kk{+}1k{+}2\rangle}{\langle Ai{-}1ii{+}1\rangle\langle Aii{+}1i{+}2\rangle\langle Aj{-}1jj{+}1\rangle\langle Ajj{+}1j{+}2\rangle\langle Ak{-}1kk{+}1\rangle\langle Akk{+}1k{+}2\rangle}\right.$$
$$\left.\times\prod_{\alpha=1}^{L}\frac{\langle A(ii{+}1)\cap(Ajj{+}1)kk{+}1\rangle}{\langle AB_\alpha ii{+}1\rangle\langle AB_\alpha jj{+}1\rangle\langle AB_\alpha kk{+}1\rangle}\right). \tag{2.56}$$

As discussed in Section 2.2, the final result (2.56) is the correct formula for the $\overline{\text{MHV}}$ intersecting cut. To obtain the form for the MHV coplanar cut, we have to dualize (2.56). As discussed in [10] the dual formula can be written

$$\tilde{\Omega}_n^{(L)} = \sum_{i=1}^{n-2}\sum_{j=i+1}^{n-1}\sum_{k=j+1}^{n}\{i,j,k\}\wedge\prod_{\alpha=1}^{L}\frac{\mathrm{d}\mu_{\mathcal{L}_\alpha}\langle\langle P(i,j,k)\rangle\rangle}{\langle\langle(AB)_\alpha ii{+}1\rangle\langle(AB)_\alpha jj{+}1\rangle\langle(AB)_\alpha kk{+}1\rangle\rangle}, \tag{2.57}$$

where $\mathrm{d}\mu_{\mathcal{L}_\alpha}$ is the measure of the line $\mathcal{L}_\alpha$ on the plane P, and we define

$$\{i,j,k\} \equiv \frac{\mathrm{d}\mu_P \langle\langle P(i,j,k)\rangle\rangle}{\langle Pi\rangle\langle Pi{+}1\rangle\langle Pj\rangle\langle Pj{+}1\rangle\langle Pk\rangle\langle Pk{+}1\rangle}, \tag{2.58}$$

and

$$\langle\langle P(i,j,k)\rangle\rangle \equiv \langle ii{+}1P\cap(jj{+}1)P\cap(kk{+}1)\rangle, \tag{2.59}$$

where $\mathrm{d}\mu_P$ is the measure of the plane P. In terms of the point A and the planes $\bar{Z}_i$, the result (2.57) can be schematically interpreted as in Figure 2.15, where $\{i,j,k\}$ is the canonical form associated to a cube with facets associated to the lines $(ii{+}1)$ $(jj{+}1)$ and $(kk{+}1)$ and the form in B_α corresponds to a triangle in the plane with (the projections of) these lines. Note that, for example, in the case when $j = i{+}1$ and $k = i{+}2$ the geometry (and corresponding form) in (the dual of) P smoothly degenerates to a tetrahedron.

2.4.4 Verification of $\Omega_n^{(L)}$

We have verified that the expression for $\Omega_n^{(L)}$ matches the coplanar cut of the two-loop MHV integrand up to $n = 20$. We also verified that $\Omega_n^{(L)}$ reproduces the cut of the three-loop MHV integrand given in [26] up to (and including) $n = 7$.

2.4.5 Intersecting cut

Five points

We now consider the MHV intersecting cut where all lines intersect in a common point A. Naïvely, one might hope that the simplicity of (2.56) is mirrored

in this cut as well. However, the lack of complexity in the coplanar cut arose from the fact that the only allowed regions in the B_α were triangles. This is clearly impossible for the intersecting cut due to the results of Section 2.3.1 which show non-vanishing residues for the intersecting lines $(AB)_\alpha$ passing through any number of external points. It is also straightforward to verify that, for example, the three-loop five point integrand has a non-vanishing residue on the cut where $B_1 = Z_2$ and $B_2 = Z_4$ which no triangle in B_α can possibly reproduce. Instead, at five points we make the following ansatz:

$$\Omega = \sum_{\text{triangles } i} f_{t_i}(A) t_i(B_\alpha) + \sum_{\text{quadrilaterals } i} f_{q_i}(A) q_i, \tag{2.60}$$

where the forms in B_α for the quadrilaterals have four poles and the numerators are determined by demanding unit leading singularities and vanishing on spurious singularities. For example, for the quadrilateral q_1 which corresponds to the region shown in Figure 2.16 bounded by the lines $(12), (23), (34), (45)$, the form is

$$q_1((12),(23),(34),(45)) = \prod_\alpha \frac{(\langle AB_\alpha 45\rangle\langle A123\rangle\langle A234\rangle - \langle AB_\alpha 3(45)\cap(A23)\rangle)}{\langle AB_\alpha 12\rangle\langle AB_\alpha 23\rangle\langle AB_\alpha 34\rangle\langle AB_\alpha 45\rangle}. \tag{2.61}$$

This form gives the correct residues on $B_\alpha = Z_2, Z_3, Z_4$ and the numerator vanishes on spurious boundaries $B_\alpha = (12)\cap(A34)$ and $B_\alpha = (23)\cap(A45)$ (but does not vanish on $B_\alpha = (12)\cap(A45)$). If we complete the exercise the forms for

the additional quadrilaterals are given by:

$$
\begin{aligned}
q_2((12),(23),(34),(15)) &= \prod_\alpha \frac{\langle AB_\alpha 12\rangle\langle A135\rangle\langle A234\rangle + \langle AB_\alpha 34\rangle\langle A123\rangle\langle A125\rangle}{\langle AB_\alpha 12\rangle\langle AB_\alpha 23\rangle\langle AB_\alpha 34\rangle\langle AB_\alpha 15\rangle}, \\
q_3((12),(23),(45),(15)) &= \prod_\alpha \frac{\langle AB_\alpha 12\rangle\langle A145\rangle\langle A235\rangle + \langle AB_\alpha 45\rangle\langle A123\rangle\langle A125\rangle}{\langle AB_\alpha 12\rangle\langle AB_\alpha 23\rangle\langle AB_\alpha 45\rangle\langle AB_\alpha 15\rangle}, \\
q_4((12),(34),(45),(15)) &= \prod_\alpha \frac{\langle AB_\alpha 15\rangle\langle A124\rangle\langle A345\rangle - \langle AB_\alpha 34\rangle\langle A125\rangle\langle A145\rangle}{\langle AB_\alpha 12\rangle\langle AB_\alpha 34\rangle\langle AB_\alpha 45\rangle\langle AB_\alpha 15\rangle}, \\
q_5((23),(34),(45),(15)) &= \prod_\alpha \frac{\langle AB_\alpha 3(45)\cap(A23)\rangle\langle A145\rangle - \langle AB_\alpha 45\rangle\langle A135\rangle\langle A234\rangle}{\langle AB_\alpha 23\rangle\langle AB_\alpha 34\rangle\langle AB_\alpha 45\rangle\langle AB_\alpha 15\rangle}.
\end{aligned}
\tag{2.62}
$$

The coefficients of the quadrilaterals can be fixed from the two-loop result by considering particular cuts. For example, only the quadrilateral $q_1((12),(23),(34),(45))$ contributes on the cut where $B_1 = Z_2$ and $B_2 = Z_4$. This residue for the two-loop MHV integrand on the intersecting cut is

$$
\begin{aligned}
f_{q_1}(A) = &- \frac{\langle 1234\rangle^2\langle 1245\rangle}{\langle A123\rangle\langle A124\rangle\langle A145\rangle\langle A234\rangle} + \frac{\langle 1235\rangle\langle 1245\rangle\langle 1345\rangle}{\langle A123\rangle\langle A125\rangle\langle A145\rangle\langle A345\rangle} \\
&- \frac{\langle 1234\rangle\langle 1235\rangle\langle 2345\rangle}{\langle A123\rangle\langle A125\rangle\langle A234\rangle\langle A345\rangle} - \frac{\langle 1234\rangle\langle 1345\rangle\langle 2345\rangle}{\langle A123\rangle\langle A145\rangle\langle A234\rangle\langle A345\rangle} \\
&- \frac{\langle 1245\rangle\langle 2345\rangle^2}{\langle A125\rangle\langle A234\rangle\langle A245\rangle\langle A345\rangle}.
\end{aligned}
\tag{2.63}
$$

However, this expression is deceptively complicated as a little algebra reveals that an equivalent form of the residue is simply

$$
f_{q_1}(A) = \frac{\langle 1245\rangle^3}{\langle A124\rangle\langle A245\rangle\langle A451\rangle\langle A512\rangle}. \tag{2.64}
$$

An even faster way to fix (or alternatively double-check the derivation just given) the coefficient of $q_1((12),(23),(34),(45))$ is by considering the following cut

of the three-loop five point integrand available in local form in [26]: if we set $B_1 = Z_2, B_2 = Z_3, B_3 = Z_4$ (which again isolates the coefficient of the quadrilateral) it is easily verified that the residue of the three-loop form on this cut is exactly (2.64). The rest of the cuts are just as trivial; introducing the shorthand notation

$$[abcd] = \frac{\langle abcd\rangle^3}{\langle Aabc\rangle \cdots \langle Adab\rangle}, \tag{2.65}$$

the coefficients of the additional quadrilaterals are

$$f_{q_2}(A) = [1345], \qquad f_{q_3}(A) = [2345], \qquad f_{q_4}(A) = [1234], \qquad f_{q_5}(A) = [1235]. \tag{2.66}$$

To fix the triangle coefficients we need only demand consistency on additional cuts. If we cut $B_1 = Z_1$ and $B_2 = Z_2$, the triangle with edges $(12), (23), (15)$ as well as the quadrilaterals q_2 and q_3 contribute. Therefore, we demand that the residue on the cut, which is

$$\begin{aligned}&\frac{\langle 1234\rangle^2\langle 1235\rangle}{\langle A123\rangle\langle A125\rangle\langle A134\rangle\langle A234\rangle} + \frac{\langle 1234\rangle\langle 1235\rangle\langle 1245\rangle}{\langle A123\rangle\langle A125\rangle\langle A145\rangle\langle A234\rangle} \\ &- \frac{\langle 1234\rangle^2\langle 1245\rangle\langle A135\rangle}{\langle A123\rangle\langle A125\rangle\langle A134\rangle\langle A145\rangle\langle A234\rangle} + \frac{\langle 1245\rangle^2\langle 2345\rangle}{\langle A125\rangle\langle A145\rangle\langle A234\rangle\langle A245\rangle},\end{aligned} \tag{2.67}$$

matches the sum of the forms corresponding to the triangle t_3 and quadrilaterals q_2, q_3,

$$f_{t_3}(A) + f_{q_2}(A) + f_{q_3}(A). \tag{2.68}$$

Using (2.66) this fixes the form in A for the triangle t_3 to be surprisingly simple:

$$f_{t_3}(A) = [1235]. \tag{2.69}$$

Checking all such cuts fixes the rest of the triangle coefficients. It is trivial to verify that at three loops the coefficients of all triangles and quadrilaterals are the same as at two loops. The final result at five points is:

$$
\begin{aligned}
\Omega_5 = &+ [1234] \prod_\alpha \frac{\langle A123\rangle\langle A234\rangle}{\langle AB_\alpha 12\rangle\langle AB_\alpha 23\rangle\langle AB_\alpha 34\rangle} \\
&+ [5123] \prod_\alpha \frac{(-1)\langle A123\rangle\langle A125\rangle}{\langle AB_\alpha 12\rangle\langle AB_\alpha 23\rangle\langle AB_\alpha 15\rangle} \\
&+ [1245] \prod_\alpha \frac{\langle A125\rangle\langle A145\rangle}{\langle AB_\alpha 12\rangle\langle AB_\alpha 45\rangle\langle AB_\alpha 15\rangle} \\
&+ [2345] \prod_\alpha \frac{\langle A234\rangle\langle A345\rangle}{\langle AB_\alpha 23\rangle\langle AB_\alpha 34\rangle\langle AB_\alpha 45\rangle} \\
&+ [3451] \prod_\alpha \frac{(-1)\langle A345\rangle\langle A145\rangle}{\langle AB_\alpha 34\rangle\langle AB_\alpha 45\rangle\langle AB_\alpha 15\rangle} \\
&+ [1245] \prod_\alpha \frac{\langle AB_\alpha 45\rangle\langle A123\rangle\langle A234\rangle - \langle AB_\alpha 3(45)\cap(A23)\rangle\langle A124\rangle}{\langle AB_\alpha 12\rangle\langle AB_\alpha 23\rangle\langle AB_\alpha 34\rangle\langle AB_\alpha 45\rangle} \\
&+ [3451] \prod_\alpha \frac{\langle AB_\alpha 12\rangle\langle A135\rangle\langle A234\rangle + \langle AB_\alpha 34\rangle\langle A123\rangle\langle A125\rangle}{\langle AB_\alpha 12\rangle\langle AB_\alpha 23\rangle\langle AB_\alpha 34\rangle\langle AB_\alpha 15\rangle} \\
&+ [2345] \prod_\alpha \frac{\langle AB_\alpha 12\rangle\langle A145\rangle\langle A235\rangle + \langle AB_\alpha 45\rangle\langle A123\rangle\langle A125\rangle}{\langle AB_\alpha 12\rangle\langle AB_\alpha 23\rangle\langle AB_\alpha 45\rangle\langle AB_\alpha 15\rangle} \\
&+ [1234] \prod_\alpha \frac{\langle AB_\alpha 15\rangle\langle A124\rangle\langle A345\rangle - \langle AB_\alpha 34\rangle\langle A125\rangle\langle A145\rangle}{\langle AB_\alpha 12\rangle\langle AB_\alpha 34\rangle\langle AB_\alpha 45\rangle\langle AB_\alpha 15\rangle} \\
&+ [5123] \prod_\alpha \frac{\langle AB_\alpha 3(45)\cap(A23)\rangle\langle A145\rangle - \langle AB_\alpha 45\rangle\langle A135\rangle\langle A234\rangle}{\langle AB_\alpha 23\rangle\langle AB_\alpha 34\rangle\langle AB_\alpha 45\rangle\langle AB_\alpha 15\rangle}.
\end{aligned}
\tag{2.70}
$$

This has been directly checked against the two and three-loop integrands evaluated on the intersecting cut. Note that all triangles of the form $((i{-}1i),(ii{+}1),(i{+}1i{+}2))$ appear in this expression, while the five triangles not of this form do not contribute at five points.

Six points

At six points it can be verified that on the cut $B_1 = Z_2, B_2 = Z_4, B_3 = Z_5$ the three-loop integrand has nonzero residue. This implies that at the very least pentagons are necessary, since in our factorized ansatz only the pentagon with edges $((12),(23),(34),(45),(56))$ can possibly contribute on this cut. Writing down the general ansatz

$$\Omega_6 = \sum_{\text{triangles } i} f_{t_i}(A) t_i(B_\alpha) + \sum_{\text{quadrilaterals } i} f_{q_i}(A) q_i(B_\alpha) + \sum_{\text{pentagons } i} f_{p_i}(A) p_i(B_\alpha), \tag{2.71}$$

it is clear that once the forms in A multiplying the pentagons are fixed it will be trivial to determine the forms for the quadrilaterals and triangles simply by demanding consistency on lower dimensional cuts. For example, once we compute cuts of the three-loop integrand and find that the coefficients of $p_1(12,23,34,45,56)$ and $p_2(12,23,34,45,16)$ are given by

$$f_{p_1}(A) = [1256] \qquad \text{and} \qquad f_{p_2}(A) = [4561], \tag{2.72}$$

we can look at the two-loop integrand and cut $B_1 = Z_2$ and $B_2 = Z_4$, where only these two pentagons and the quadrilateral $q_1(12,23,34,45)$ contribute:

$$\text{residue on cut} = f_{q_1}(A) + f_{p_1}(A) + f_{p_2}(A), \tag{2.73}$$

which implies $f_{q_1}(A) = [1245]$, which is exactly the coefficient of this quadrilateral at five points. From these results we can immediately guess (and subse-

quently verify) the pattern: for the quadrilaterals

$$(i{-}1i, ii{+}1, i{+}1i{+}2, i{+}2i{+}3)$$

the corresponding forms in A are $[i{-}1ii{+}2i{+}3]$, for the pentagons $(i{-}1i, \ldots, i{+}3i{+}4)$ the forms are $[i{-}1ii{+}3i{+}4]$ and for triangles

$$(i{-}1i, ii{+}1, i{+}1i{+}2)$$

the forms are $[i{-}1ii{+}1i{+}2]$. Checking the set of these cuts fixes the coefficients of all pentagons at six points as well as all quadrilaterals except those *not* of the form

$$(i{-}1i, ii{+}1, i{+}1i{+}2, i{+}2i{+}3),$$

e.g., the quadrilateral $(12, 23, 34, 56)$. However, it is easy to verify that all such quadrilaterals of this type, as well as the triangles not of the form $(i{-}1i, ii{+}1, i{+}1i{+}2)$, do not contribute to the integrand. For example, consider the cut $B_1 = Z_2, B_2 = Z_3$ of the two-loop integrand. Naïvely the following geometries contribute:

$$\begin{aligned}\text{residue on cut} =& t(12,23,34) + q(12,23,34,45) + q(12,23,34,56) + q(12,23,34,16) \\ &+ p(12,23,34,45,56) + p(12,23,34,45,16) + p(12,23,34,56,16).\end{aligned} \tag{2.74}$$

However if we substitute the known forms in A we find this kills the coefficient of $q(12,23,34,56)$

$$\begin{aligned}&\text{residue on cut} = [1234] + [1245] + f_q(12,23,34,56) + [6134] + [1256] + [6145] + [5634]\\ &\implies f_q(12,23,34,56) = 0.\end{aligned} \tag{2.75}$$

A similar argument kills the quadrilateral $q(12,23,45,56)$ and all quadrilaterals of this type. The final expression for the six point integrand at L loops is:

$$\begin{aligned}&\sum_{i=1}^{6}[i{-}1ii{+}1i{+}2]\prod_{\alpha=1}^{L}\frac{\langle Ai{-}1ii{+}1\rangle\langle Aii{+}1i{+}2\rangle}{\langle AB_\alpha i{-}1i\rangle\langle AB_\alpha ii{+}1\rangle\langle AB_\alpha i{+}1i{+}2\rangle}\\ &+\sum_{i=1}^{6}[i{-}1ii{+}2i{+}3]\prod_{\alpha=1}^{L}\frac{N_{\text{quadrilateral}}(i)}{\langle AB_\alpha i{-}1i\rangle\langle AB_\alpha ii{+}1\rangle\langle AB_\alpha i{+}1i{+}2\rangle\langle AB_\alpha i{+}2i{+}3\rangle}\\ &+\sum_{i=1}^{6}[i{-}1ii{+}3i{+}4]\prod_{\alpha=1}^{L}\frac{N_{\text{pentagon}}(i)}{\langle AB_\alpha i{-}1i\rangle\langle AB_\alpha ii{+}1\rangle\langle AB_\alpha i{+}1i{+}2\rangle\langle AB_\alpha i{+}2i{+}3\rangle\langle AB_\alpha i{+}3i{+}4\rangle},\end{aligned} \tag{2.76}$$

where $N_{\text{quadrilateral}}(i)$ and $N_{\text{pentagon}}(i)$ are the (unique) numerators which have unit leading singularities on codimension two boundaries such as $B_\alpha = Z_i, Z_{i+1}, Z_{i+2}, Z_{i+3}$ and vanish on spurious singularities such as $B_\alpha = (i{-}1i)\cap(Ai{+}1i{+}2)$. We give explicit expressions for the form for the k-gon below.

Arbitrary multiplicities

From the six point result it is clear what our ansatz should be at n points: all triangles, quadrilaterals, pentagons, ..., up to $(n{-}1)$-gons which have only consecutive poles contribute on the cut. The form in A for the ith k-gon is given by

$[i{-}1, i, i{+}k{-}2, i{+}k{-}1]$ where $(i{-}1, i)$ labels the first edge and $(i{+}k{-}2, i{+}k{-}1)$ labels the last edge. The form is then

$$\begin{aligned}\Omega_n = &\sum_{i=1}^{n}[i{-}1ii{+}1i{+}2]\prod_{\alpha=1}^{L}\frac{\langle Ai{-}1ii{+}1\rangle\langle Aii{+}1i{+}2\rangle}{\langle AB_\alpha i{-}1i\rangle\langle AB_\alpha ii{+}1\rangle\langle AB_\alpha i{+}1i{+}2\rangle}\\ &+\sum_{i=1}^{n}[i{-}1ii{+}2i{+}3]\prod_{\alpha=1}^{L}\frac{N_{\text{quadrilateral}}(i)}{\langle AB_\alpha i{-}1i\rangle\langle AB_\alpha ii{+}1\rangle\langle AB_\alpha i{+}1i{+}2\rangle\langle AB_\alpha i{+}2i{+}3\rangle}\\ &+\sum_{i=1}^{n}[i{-}1ii{+}3i{+}4]\prod_{\alpha=1}^{L}\frac{N_{\text{pentagon}}(i)}{\langle AB_\alpha i{-}1i\rangle\langle AB_\alpha ii{+}1\rangle\langle AB_\alpha i{+}1i{+}2\rangle\langle AB_\alpha i{+}2i{+}3\rangle\langle AB_\alpha i{+}3i{+}4\rangle}\\ &+\cdots\\ &+\sum_{i=1}^{n}[i{-}1, i, i{+}n{-}3, i{+}n{-}2]\prod_{\alpha=1}^{L}\frac{N_{(n-1)-\text{gon}}(i)}{\langle AB_\alpha i{-}1i\rangle\langle AB_\alpha ii{+}1\rangle\cdots\langle AB_\alpha i{+}n{-}3, i{+}n{-}2\rangle},\end{aligned} \tag{2.77}$$

or more succinctly

$$\Omega_n = \sum_{k=1}^{n-1}\sum_{i=1}^{n}[i{-}1, i, i{+}k{-}2, i{+}k{-}1]\prod_{\alpha=1}^{L}\frac{N_{k-\text{gon}}(i)}{\langle AB_\alpha i{-}1i\rangle\langle AB_\alpha ii{+}1\rangle\cdots\langle AB_\alpha i{+}k{-}2, i{+}k{-}1\rangle}. \tag{2.78}$$

It is straightforward to verify that assuming (2.78) is true at e.g., seven points is consistent with computing cuts of the two- and three-loop integrands, even without having the explicit form of the hexagons in B_α. In fact, however, it is trivial to obtain the forms for any k-gon either using the procedure outlined in [65] or alternatively by simple triangulation. For a k-gon with the vertices

$$Z_i, Z_{i+1}, \ldots, Z_{i+k-2}, (i{-}1i)\cap(A, i{+}k{-}2, i{+}k{-}1)$$

an expression for the form is given by

$$\Omega_{k\text{-gon}} = \sum_{j=2}^{k-2} \frac{\langle Aij\widehat{j{+}1}\rangle^2}{\langle Aij\rangle\langle Aj\widehat{j{+}1}\rangle\langle A\widehat{j{+}1}i\rangle}, \tag{2.79}$$

where we define

$$\hat{Z}_{j+1} = \begin{cases} Z_{j+1}, & j \neq k-2, \\ (i{-}1i)\cap(Aijj{+}1), & j = k-2. \end{cases} \tag{2.80}$$

The final expression for the intersecting cut is then:

$$\Omega_n = \sum_{k=1}^{n-1}\sum_{i=1}^{n}[i{-}1, i, i{+}k{-}2, i{+}k{-}1]\prod_{\alpha=1}^{L}\left(\sum_{j=2}^{k-2}\frac{\langle Aij\widehat{j{+}1}\rangle^2}{\langle Aij\rangle\langle Aj\widehat{j{+}1}\rangle\langle A\widehat{j{+}1}i\rangle}\right). \tag{2.81}$$

Geometrically the solution can be described as (tetrahedron in A)$\times$(polygon in B_α) as in Figure 2.17, which is directly reproduced from [10].

2.4.6 Verification of intersecting cut

The result (2.81) has been checked against the expressions for the two- and three-loop MHV integrands given in [26] through $n = 10$ points.

2.5 Coplanar - intersecting cuts and path dependence

An obvious degeneration of the above configurations would be to demand that all the lines lie in a plane and intersect each other. Here, we will see that the order in which the limit is taken determines the result. Recall that the form in (2.56) is actually the form of the dual configuration in which all the dual lines

are intersecting and we demand that they satisfy $\langle AB_\alpha ij\rangle > 0, \forall i,j$. We can now take the limit $\langle A123\rangle = \langle AB_\alpha 12\rangle = 0$ or $\langle A123\rangle = \langle AB_\alpha 23\rangle = 0$ which forces all the lines AB_α (which already intersect at A) to lie in the common plane (123). We can perform a similar procedure on the form in (2.81). We will show below that the results are significantly different.

First consider the intersecting cut. To make the configuration collapse to the plane (123), we need a pole $\langle A123\rangle$ in addition to either $\langle AB_\alpha 12\rangle$ or $\langle AB_\alpha 23\rangle$. Note that there are two solutions to $\langle AB_\alpha 12\rangle = \langle AB_\alpha 23\rangle = 0$, one in which (AB_α) passes through Z_2 and the other in which it lies in the plane (123). However, since all the regions in B_α are polygons, they are designed to have singularities only on their vertices. Thus the numerator is designed to kill the singularity in which the line lies in the plane (123). This is precisely the singularity we are looking for. Hence we can achieve this limit only if the pole $\langle A123\rangle$ is present, which severely restricts the number of terms that can contribute to this cut. In fact, it is easy to see that only the triangles can contribute. Thus, we are left with the result that at L loops and n, points, if A lies in the plane (123), the corresponding region in B_α must be either the triangle (12)(23)(34) or $(n1)(12)(23)$.

We can derive the same result directly from the amplituhedron. Since we are interested in a configuration of coincident, coplanar lines in the MHV amplituhedron, we can parametrize them as follows

$$A = Z_1 + a_2 Z_2 + a_3 Z_3$$

$$B_\alpha = Z_1 + b_\alpha Z_2$$

and demand $\langle AB\bar{i}\bar{j}\rangle > 0$. The mutual positivity is trivialized and the form is just the product of the form for each B_α. It is not hard to see that the final result is

$$\Omega^{cc} = \frac{1}{a_2 a_3}\left(\prod_{\alpha=1}^{L}\frac{1}{(a_2 - b_\alpha)} + \prod_{\alpha=1}^{L}\frac{1}{b_\alpha}\right). \tag{2.82}$$

The first term corresponds to the triangle $(n1)(12)(23)$ and the second to $(12)(23)(34)$.

In contrast with this simple result, the coplanar cut yields a far more complex residue. Indeed whenever B_α is in any triangle whose edge is either (12) or (23), the corresponding region in A has the pole $\langle A123\rangle$ required to collapse the configuration into the (123) plane.

2.6 Moving beyond trivial mutual positivity

The results in equations (2.56), (2.81) and (2.82) are valid for an arbitrary number of loops. While analytic all-loop results are few and far between, it is essential to realize that it was possible to obtain these results only because of the trivial mutual positivity condition. It is essentially equivalent to solving a one-loop problem. In this section, we begin exploring a few different configurations in which the mutual positivity conditions are not completely trivialized. We see that the associated geometries are far richer and the corresponding canonical forms more complex. In Section 2.6.1, we consider generalized ladder cuts where we cut only external propagators, while in Section 2.6.2 we examine several cuts which are directly related to the intersecting and coplanar cuts.

2.6.1 Ladder cuts

We consider the cut where our loops $(AB)_\alpha$, $\alpha = 1, \dots L$ all intersect one line, say (12). Concretely, we are looking to find the form on the cut $\langle AB_\alpha 12\rangle = 0$. Let us write our form as

$$\Omega = \prod_{\alpha=1}^{L} \langle (AB)_\alpha \mathrm{d}^2 A_\alpha\rangle \langle (AB)_\alpha \mathrm{d}^2 B_\alpha\rangle \frac{1}{\langle (AB)_\alpha 12\rangle} f[(AB)_\alpha].$$

We expand $A_\alpha = Z_1 + x_\alpha Z_2 + z_\alpha Z_\star$ and take the residue $z_\alpha \to 0$ to obtain the ladder cut:

$$\Omega^{\text{ladder}} = \prod_{\alpha=1}^{L} \mathrm{d}x_\alpha \langle (AB)_\alpha \mathrm{d}^2 B_\alpha\rangle f[(AB)_\alpha]\Big|_{A_\alpha = 1 + x_\alpha 2}. \tag{2.83}$$

We will determine Ω^{ladder} from the geometry of the amplituhedron. We can satisfy all but the mutual postivity condition by putting each loop $(AB)_\alpha$ in a Kermit

$$\begin{aligned} A_\alpha &= Z_1 + x_\alpha Z_2 \\ B_\alpha &= -Z_1 + y_\alpha (Z_{i_\alpha} + w_\alpha Z_{i_\alpha + 1}), \end{aligned} \tag{2.84}$$

so that each cell is labelled by L integers $\{i_1, \dots, i_L\}$. Indeed, the conditions $\langle (AB)_\alpha i i+1\rangle > 0$ and the sign flip criterion are satisfied and each $(AB)_\alpha$ is in the one-loop amplituhedron so long as $x_\alpha, y_\alpha, w_\alpha > 0$. It remains to work out the implications of mutual positivity $\langle (AB)_\alpha (AB)_\beta\rangle > 0$. Inserting (2.84) we

find

$$\langle (AB)_\alpha (AB)_\beta \rangle = -\langle A_\alpha A_\beta B_\alpha B_\beta \rangle \tag{2.85}$$
$$= y_\alpha y_\beta (x_\alpha - x_\beta) \left[\langle 12 i_\alpha i_\beta \rangle + w_\alpha \langle 12\, i_\alpha{+}1 i_\beta \rangle + w_\beta \langle 12\, i_\alpha\, i_\beta{+}1 \rangle + w_\alpha w_\beta \langle 12\, i_\alpha{+}1\, i_\beta{+}1 \rangle \right].$$

Depending on the relative positions of α and β, we have the following cases:

- $i_\alpha < i_{\alpha+1} < i_\beta < i_{\beta+1}$

In this case, we have $\langle 12 i_\alpha i_\beta \rangle > 0$, $\langle 12 i_{\alpha+1}\, i_\beta \rangle > 0$, $\langle 12 i_\alpha\, i_{\beta+1} \rangle > 0$ and $\langle 12 i_{\alpha+1}\, i_{\beta+1} \rangle > 0$. Hence (2.85) reduces to

$$(x_\alpha - x_\beta) > 0. \tag{2.86}$$

- $i_\alpha < i_{\alpha+1} = i_\beta < i_{\beta+1}$

In this case, $\langle 12 i_\alpha i_\beta \rangle > 0$, $\langle 12 i_{\alpha+1}\, i_\beta \rangle = 0$, $\langle 12 i_\alpha\, i_{\beta+1} \rangle > 0$ and $\langle 12 i_{\alpha+1}\, i_{\beta+1} \rangle > 0$ and (2.85) again reduces to

$$(x_\alpha - x_\beta) > 0. \tag{2.87}$$

- $i_\alpha = i_\beta < i_{\alpha+1} = i_{\beta+1}$

This configuration makes (2.85) collapse to

$$(w_\beta - w_\alpha)(x_\alpha - x_\beta) > 0. \tag{2.88}$$

At L loops, we will have $3L$ variables $x_\alpha, y_\alpha, w_\alpha$ satisfying the inequalities above. Let us denote by $g_{\{i_1 \ldots i_L\}}(x_\alpha, w_\alpha)$ the canonical form associated with the L-loop

configuration. Note that the y_α factor out of the problem since they are unconstrained variables. We can write

$$\Omega^{\text{ladder}} = \sum_{\{i_1 \ldots i_L\}} \prod_\alpha \frac{\mathrm{d}y_\alpha}{y_\alpha}\, \mathrm{d}x_\alpha\, \mathrm{d}w_\alpha\, g_{\{i_1 \ldots i_L\}}\,(x_\alpha, w_\alpha), \tag{2.89}$$

where $\sum_{\{i_1 \ldots i_L\}}$ stands for a sum over all configurations at L loops. To compute the canonical form for this space, we need to triangulate it. However, in order to add the canonical forms associated with different pieces in the triangulation, we need to write the form of each piece in a coordinate invariant way. The variables x_α are the same for all cells but the y_α and w_α are cell dependent. We can obtain coordinate invariant expressions by noting that the point of intersection of the line (AB) with the plane $(1Z_iZ_{i+1})$ is by the Schouten identity

$$(AB) \cap (1Z_iZ_{i+1}) = \langle ABii+1\rangle Z_1 - \langle AB1i+1\rangle Z_i + \langle AB1i\rangle Z_{i+1}. \tag{2.90}$$

Comparing with (2.84), we read off

$$y = \frac{\langle AB1i{+}1\rangle}{\langle ABii{+}1\rangle} \qquad y\,w = -\frac{\langle AB1i\rangle}{\langle ABii{+}1\rangle} \implies w = -\frac{\langle AB1i\rangle}{\langle AB1i{+}1\rangle}. \tag{2.91}$$

From the measure associated with the Kermit, we have

$$\frac{\mathrm{d}y\,\mathrm{d}w}{y\,w} = \frac{\langle AB\mathrm{d}^2B\rangle\langle A1ii{+}1\rangle^2}{\langle AB1i\rangle\langle AB1i{+}1\rangle\langle ABii+1\rangle} \implies \frac{\mathrm{d}y\,\mathrm{d}w}{y} = -\frac{\langle AB\mathrm{d}^2B\rangle\langle A1ii{+}1\rangle^2}{\langle AB1i{+}1\rangle^2\langle ABii{+}1\rangle}.$$

With this, we can write Ω^{ladder} in an invariant way as

$$\begin{aligned}\Omega^{\text{ladder}} =&(-1)^L \sum_{\{i_1 \ldots i_L\}} \prod_{\alpha} \frac{\mathrm{d}x_\alpha \langle A_\alpha 1 i_\alpha i_\alpha{+}1\rangle^2}{\langle (AB)_\alpha 1 i_\alpha{+}1\rangle^2 \langle (AB)_\alpha i_\alpha i_\alpha{+}1\rangle} \\ &\times g_{\{i_1 \ldots i_L\}}\left(x_\alpha, -\frac{\langle (AB)_\alpha 1 i_\alpha\rangle}{\langle (AB)_\alpha 1 i_\alpha{+}1\rangle}\right).\end{aligned} \tag{2.92}$$

Let us work out a few examples at low loop orders to get a better idea of how to write the form explicitly. The first case $L = 1$ is trivial, since $g(x, w) = 1/(xw)$ and we have

$$\begin{aligned}\Omega^{\text{ladder}} =& -\sum_i \frac{\langle A_1 i i{+}1\rangle^2}{\langle AB1i{+}1\rangle^2 \langle ABii{+}1\rangle} \frac{1}{x} \frac{-1}{\frac{\langle AB1i\rangle}{\langle AB1i{+}1\rangle}} \\ =&\frac{1}{x} \sum_i \frac{\langle A1ii{+}1\rangle^2}{\langle AB1i\rangle \langle AB1i{+}1\rangle \langle ABii{+}1\rangle}.\end{aligned} \tag{2.93}$$

At two loops, the function $g_{\{i_1,i_2\}}$ is

$$\begin{cases} \dfrac{1}{w_1 w_2 x_2 (x_1 - x_2)}, & \text{if } i_1 < i_2, \\ \dfrac{1}{w_1 w_2 x_1 (x_1 - x_2)}, & \text{if } i_1 > i_2, \\ \dfrac{1}{x_2(x_1 - x_2)} \dfrac{1}{w_1(w_2 - w_1)} + \dfrac{1}{x_1(x_2 - x_1)} \dfrac{1}{w_2(w_1 - w_2)}, & \text{if } i_1 = i_2. \end{cases}$$

Moving to three loops, for the set $\{i_1, i_2, i_3\}$ there are three possibilities: (i) all three indices are distinct, (ii) Two of the indices are equal, or (iii) all three indices are equal. For each possibility, the indices can be ordered in a variety of ways. Furthermore, in the degenerate cases we must break these orderings into smaller pieces in order to triangulate the space. For example, if $i_1 = i_2$ we must consider both cases $x_{i_1} < x_{i_2}$ and $x_{i_1} > x_{i_2}$ separately. Repeating this for an

arbitrary number of loops it is easy to see that one possible triangulation which covers all possibilities exactly once is given by specifying the following:

- A partition $N = \{N_1, \dots N_m\}$ of L i.e., $\sum_i N_i = L$ and $N_i \geq 1$ along with an associated set of integers $\mathcal{J}_N = \{j_1, \dots j_m\}$ of equal length such that $3 \leq j_1 < j_2 < \cdots \leq n-1$. The integer N_i represents how many of the loops $(AB)_\alpha$ are in the Kermit labelled by $[1\,2\,3; 1\,j_i\,j_{i+1}]$
- A permutation $\Pi = \{\pi_1 \dots \pi_L\}$ of $\{1, \dots L\}$.

The sum over all the cells is carried out by summing over all possible $\mathcal{N}, J_\mathcal{N}, \Pi$. For the sake of compactness, we define another quantity

$$W[s, e, \Pi, j] \equiv \frac{1}{w_{\pi_s}(w_{\pi_{s+1}} - w_{\pi_s}) \cdots (w_{\pi_e} - w_{\pi_{e-1}})}\Big|_{w_{\pi_\alpha} = \frac{-\langle (AB)_{\pi_\alpha} 1j\rangle}{\langle (AB)_{\pi_\alpha} 1j+1\rangle}}. \tag{2.94}$$

In terms of this function, the form for the ladder cut can be written as

$$\begin{aligned}
\Omega^{\text{ladder}} =& (-1)^L \sum_{N, J_N, \Pi} \frac{1}{x_{\pi_L}(x_{\pi_{L-1}} - x_{\pi_L}) \dots (x_{\pi_1} - x_{\pi_2})} \\
&\times \left(\prod_{\alpha=1}^{N_1} \frac{\langle A_{\pi_\alpha} 1 j_1 j_1{+}1\rangle^2}{\langle (AB)_{\pi_\alpha} 1 j_1{+}1\rangle^2 \langle (AB)_{\pi_\alpha} j_1 j_1{+}1\rangle} \right) W[1, N_1, \pi, j_1] \\
&\times \left(\prod_{\alpha=1+N_1}^{N_2} \frac{\langle A_{\pi_\alpha} 1 j_2 j_2{+}1\rangle^2}{\langle (AB)_{\pi_\alpha} 1 j_2{+}1\rangle^2 \langle (AB)_{\pi_\alpha} j_2 j_2{+}1\rangle} \right) W[1{+}N_1, N_1{+}N_2, \pi, j_2] \\
&\times \vdots \\
&\times \left(\prod_{\alpha=1+N_1+\cdots+N_{m-1}}^{N_m} \frac{\langle A_{\pi_\alpha} 1 j_m j_m{+}1\rangle^2}{\langle (AB)_{\pi_\alpha} 1 j_m{+}1\rangle^2 \langle (AB)_{\pi_\alpha} j_m j_m{+}1\rangle} \right) \\
&\times W[1{+}N_1{+}\cdots{+}N_{m-1}, N_m, \pi, j_m].
\end{aligned} \tag{2.95}$$

2.6.2 Extra free lines

In this section, we will consider a series of cuts in which the configuration of lines $(AB)_\alpha$ are minor modifications to the coplanar and collinear cut. In each case, we consider an extra line which allows for non trivial mutual positivity. In order of increasing difficulty, some of the types of cuts we consider involve the following configurations of lines:

- **Cut 1**: $L-1$ loops intersecting in a common point A, with each line passing through one of the external Z_i. We can denote these lines as Ai. An additional line passes through some Z_j, but does not intersect the lines Ai in A. Denoting this line by Bj, the non trivial mutual positivity conditions are $\langle AiBj\rangle > 0$.

- **Cut 2**: $L-1$ loops Ai, intersecting in a common point A and passing through some Z_i with the L^{th} line CD completely free. Here, the addtional constraint is $\langle CDAi\rangle > 0$.

- **Cut 3**: $L-1$ loops AB_α which intersect at A with the L^{th} line CD intersecting two of the lines AB_i and AB_j resulting in the non trivial constraint $\langle AB_\alpha CD\rangle > 0$ with $\alpha \neq i, j$.

- **Cut 4**: $L-1$ loops intersecting in a common point A with the L^{th} line completely free. This is a generalization of the above cut.

The first two cuts are generalizations of the $(4L-4)$-cuts of Section 2.3.1 while the next two are related to the $(2L-4)$ cuts of Section 2.4.

Cut 1:

Here, the configuration of lines Ai is the same as in Section 2.3.1, with modifications for the L^{th} loop as shown in Figure 2.18. We begin by solving this problem at four and five points to illustrate the complications presented by mutual positivity.

A generic configuration at four points includes L_1 lines passing through Z_1, L_2 lines passing through Z_2, L_3 through Z_3 and L_4 through Z_4. This cut has already computed in [17] using a slightly different approach. Here, we will merely present a simple example of a three-loop cut with lines $A1$ and $A2$ intersecting at A and passing through Z_1 and Z_2 respectively.The third loop ($B3$) passes through Z_3 but is otherwise unconstrained. We can be parametrize the points A and B as

$$A = Z_1 - a_2 Z_2 - a_3 Z_3 - a_4 Z_4, \qquad B = Z_1 - b_2 Z_2 + b_3 Z_3 - b_4 Z_4. \tag{2.96}$$

The constraints $\langle A1\bar{i}\bar{j}\rangle > 0$,$\langle A2\bar{i}\bar{j}\rangle > 0$ and $\langle B3\bar{i}\bar{j}\rangle > 0$ are trivially satisfied by $a_i > 0$ and $b_2, b_4 > 0$. We are left with the mutual positivity conditions

$$\begin{aligned} -\langle A1B3\rangle &= (a_4 b_2 - a_2 b_4)\langle 1234\rangle < 0, \\ -\langle A2B3\rangle &= (a_4 - b_4)\langle 1234\rangle < 0. \end{aligned} \tag{2.97}$$

The canonical form associated to these inequalities is trivial to obtain:

$$\Omega = \frac{\langle 1234\rangle^4 \langle B123\rangle \langle A\mathrm{d}^3 A\rangle \langle B\mathrm{d}^3 B\rangle}{\langle A123\rangle\langle A124\rangle\langle AB23\rangle\langle AB13\rangle\langle B124\rangle\langle B134\rangle\langle B234\rangle}, \tag{2.98}$$

which matches the three-loop integrand evaluated on the same cut and agrees with the general result for the corner cut in [**?**]. Note the presence of the poles

$\langle AB13\rangle$ and $\langle AB23\rangle$ is due to the mutual positivity constraint. This demonstrates that this condition is introducing new physical boundaries into the geometry.

Moving on to five points, we begin with $L = 3$. Consider the configuration of the cyclic polytope cut of Section 2.3.1, where we have lines $A1$ and $A2$ which intersect at A and additionally pass through Z_1 and Z_2. The third loop $(AB)_3 = (1B)$ passes through Z_1 but does not intersect the other lines in A. The point B has two degrees of freedom since it is constrained to lie on the line $(1B)$. By imposing the inequalities

$$\langle A\alpha\bar{i}\bar{j}\rangle > 0, \quad \alpha = 1, 2, \qquad \langle 1B\bar{i}\bar{j}\rangle > 0, \qquad \langle A21B\rangle > 0, \tag{2.99}$$

on the points A and B, the associated canonical form is

$$\begin{aligned}\Omega_5^{(3)}|_{\text{cut 1}} =& \frac{-\langle A\mathrm{d}^3A\rangle\langle 1B\mathrm{d}^2B\rangle}{\langle A145\rangle\langle A134\rangle\langle B145\rangle\langle B125\rangle\langle AB12\rangle\langle A345\rangle\langle A123\rangle\langle B134\rangle} \\ &\times\big(\langle A123\rangle\langle B134\rangle\langle 1245\rangle^2\langle 1345\rangle^2 + \langle A145\rangle\langle B145\rangle\langle 1234\rangle^2\langle 1235\rangle^2 \\ &\quad + \langle A145\rangle\langle B123\rangle\langle 1345\rangle^2\langle 1235\rangle\langle 1245\rangle\big).\end{aligned} \tag{2.100}$$

Next consider the corresponding $L = 4$ configuration where the first three loops are $A\alpha$ for $\alpha = 1, 2, 3$, and the fourth line is $(AB)_4 = (1B)$. As we found in Section 2.3.1, the point A must be in the tetrahedron with vertices $Z_3, Z_4, Z_5, -Z_1$. Here we can parametrize the two points A and B as

$$A = Z_1 + a_3Z_3 + a_4Z_4 + a_5Z_5 \qquad B = -Z_2 + b_3Z_3 + b_4Z_4. \tag{2.101}$$

Demanding that the inequalities

$$\langle A\alpha\bar{i}\bar{j}\rangle > 0, \qquad \langle 1B\bar{i}\bar{j}\rangle > 0, \qquad \langle AB\alpha 1\rangle > 0, \quad \alpha = 1,2,3, \tag{2.102}$$

are satisfied, we find the associated canonical form

$$\begin{aligned}\Omega_5^{(4)}|_{\text{cut 1}} =& \frac{\langle A\mathrm{d}^3 A\rangle\langle 1B\mathrm{d}^2 B\rangle}{\langle A345\rangle\langle A145\rangle\langle A135\rangle\langle A134\rangle\langle B145\rangle\langle B125\rangle\langle B134\rangle\langle AB12\rangle\langle AB13\rangle} \\ &\times\big(\langle A135\rangle^2\langle B134\rangle^2\langle 1245\rangle^2\langle 1345\rangle - \langle A135\rangle\langle A145\rangle\langle B123\rangle\langle B134\rangle\langle 1245\rangle\langle 1345\rangle^2 \\ &- \langle A134\rangle\langle A135\rangle\langle B135\rangle\langle B134\rangle\langle 1245\rangle^2\langle 1345\rangle + \langle A134\rangle^2\langle B125\rangle^2\langle 1345\rangle^3 \\ &+ \langle A123\rangle\langle A145\rangle\langle B145\rangle\langle B134\rangle\langle 1235\rangle\langle 1345\rangle^2 \\ &- \langle A134\rangle\langle A135\rangle\langle B124\rangle\langle B125\rangle\langle 1345\rangle^3\big).\end{aligned} \tag{2.103}$$

In both these cases, we can see the poles due to mutual positivity. The all-loop extension of this configuration with $L-1$ lines $A1, A2, \ldots A(L{-}1)$ passing through $1, \ldots (L{-}1)$, respectively, and the L^{th} line $(AB)_L = (1B)$ passing through Z_1 but not A can be similarly obtained on a case-by-case basis. However, we do not yet have an analytic expression valid for all L.

Cut 2:

We now lift the constraint that the extra line passes through one of the external points. However, we will still consider the configuration where $L-1$ lines $A1, A2, \ldots A(L{-}1)$ pass through $1, \ldots (L{-}1)$, respectively, so the configuration is identical to that of Fig. 2.18 with the line $(Cj) \to (CD)$. The relevant in-

equalities are

$$\langle CD\bar{i}\bar{j}\rangle > 0 \qquad \langle AkCD\rangle > 0 \qquad \langle Ak\bar{i}\bar{j}\rangle > 0 \qquad k = 1, \ldots L. \tag{2.104}$$

We parametrize CD by putting it in the Kermit:

$$C = Z_1 + \alpha_1 Z_a + \alpha_2 Z_{a+1}, \tag{2.105}$$

$$D = -Z_1 + \beta_1 Z_b + \beta_2 Z_{b+1}. \tag{2.106}$$

The one-loop constraints $\langle CD\bar{i}\bar{j}\rangle > 0$ enforce positivity of α_i and β_i. As before, the one-loop conditions on the lines Ai, which are independent of the line CD imply that A must lie in the cyclic polytope Conv $[L, L+1, .. -1]$. The mutual positivity conditions reduce to a single condition,

$$\begin{aligned}\langle AkCD\rangle =& \langle Ak1b\rangle\beta_1 + \langle Ak1b{+}1\rangle\beta_2 + \langle Ak1a\rangle\alpha_1 + \langle Akab\rangle\alpha_1\beta_1 + \langle Akab{+}1\rangle\alpha_1\beta_2 \\ &+ \langle Ak1a{+}1\rangle\alpha_2 + \langle Aka{+}1b\rangle\alpha_2\beta_1 + \langle Aka{+}1b{+}1\rangle\alpha_2\beta_2.\end{aligned} \tag{2.107}$$

Although we do not have a complete understanding of this system of inequalities, in some simple cases an analytical solution is possible. For example, for $n = 4$ the free loop line CD is in the Kermit $[123; 134]$, and the form is given by

$$\Omega_4^{(4)}|_{\text{cut}} = \frac{\langle A\mathrm{d}^3 A\rangle\langle CD\mathrm{d}^2 C\rangle\langle CD\mathrm{d}^2 D\rangle\langle 1234\rangle^3}{\langle A123\rangle\langle A234\rangle\langle A134\rangle\langle A124\rangle\langle CD14\rangle\langle CD23\rangle\langle CD34\rangle\langle CDA2\rangle\langle CDA1\rangle}$$
$$\times\big(-\langle CD34\rangle\langle A123\rangle\langle A124\rangle + \langle A123\rangle\langle A234\rangle\langle CD14\rangle$$
$$+\langle A134\rangle\langle CD12\rangle\langle A234\rangle - \langle A134\rangle\langle A124\rangle\langle CD23\rangle\big). \tag{2.108}$$

Cuts 3 and 4:

Finally, we can also consider cuts which relax conditions on the $2L-4$ cuts discussed in Section 2.3. For example, we can consider $L-1$ loops intersecting in a common point A (but not passing through any external Z_i), and the L^{th} line intersecting two of the loops $(AB)_i$ and $(AB)_j$, as pictured in Figure 2.19. The $L=3$ configuration is simply the coplanar cut discussed above, but $L=4$ is more interesting. Here we can take the first three loop lines to intersect, and the fourth line to cut $(AB)_1$ and $(AB)_2$. We can write $(AB)_\alpha = AB_\alpha$ for $\alpha = 1,2,3$ and for the fourth loop $(AB)_4 = (B_1B_2)$. The inequalities defining the four-loop amplituhedron become

$$\langle AB_\alpha \bar{i}\bar{j}\rangle > 0, \qquad \langle B_1B_2\bar{i}\bar{j}\rangle > 0, \qquad \langle AB_1B_2B_3\rangle > 0, \tag{2.109}$$

where there is only a single remaining mutual positivity condition. Parametrizing the intersection point A and the points B_1, B_2, B_3 as in Section 2.4,

$$\begin{aligned} A &= Z_1 + a_2Z_2 + a_3Z_3 + a_4Z_4, \qquad B_\alpha = Z_1 + x_\alpha Z_2 + y_\alpha Z_3, \quad \alpha = 1,3 \\ B_2 &= Z_1 + x_2Z_3 + y_2Z_4, \end{aligned} \tag{2.110}$$

(where we choose a different parametrization for B_2 so the configuration is not too degenerate) we get several quadratic inequalities and a single cubic inequality,

$$\begin{aligned}\langle AB_1B_2B_3\rangle = &[x_1y_3 + x_3(x_2 - y_1) - x_1x_2]\, a_4 + (x_1y_2 - x_2x_3)\, a_3 + (x_2y_3 - y_1y_2)\, a_2 \\ &+ y_1y_2x_3 - x_1y_2y_3 > 0.\end{aligned} \tag{2.111}$$

Completing the triangulation we get for the canonical form

$$\Omega_4^{(L)}|_{\text{cut}} = \frac{\langle A\mathrm{d}^3A\rangle \prod\limits_{\alpha=1,3} \langle AB_\alpha \mathrm{d}^2B_\alpha\rangle\langle B_1B_2\mathrm{d}^2B_1\rangle\langle B_1B_2\mathrm{d}^2B_2\rangle N\left(AB_\alpha, B_1B_2\right)}{\prod\limits_{\alpha=1,3}\prod\limits_{i=1}^{4}\left(\langle AB_\alpha ii{+}1\rangle\right)\prod\limits_{i=1}^{4}\left(\langle B_1B_2ii{+}1\rangle\right)\langle AB_1B_2B_3\rangle}, \tag{2.112}$$

where the numerator $N\left(AB_\alpha, B_1B_2\right)$ is a sum with several hundred terms. We have verified the result of this calculation matches the full four-point four-loop integrand, which is a sum of eight local diagrams, symmetrized over all loop momenta and cyclically summed over external legs and given explicitly in momentum twistor variables in [65], evaluated on this cut.

The same cut at five points is also solvable with the amplituhedron, although we have yet to find a particularly simple representation of the canonical form which suggests a generalization to higher points and loops. We plan to revisit these problems as well as generalized corner cuts in future work.

2.7 Conclusion

The all-loop amplituhedron is a remarkable mathematical object capturing the complicated loop-level structure of scattering amplitudes in planar $\mathcal{N} = 4$ sYM in geometric form directly in the physical kinematic space. This chapter has been concerned with the practical application of this geometric picture to make predictions about the MHV loop integrand, valid for any number of particles and any number of loops, which are completely hidden in the usual unitarity or recursion-based methods. In particular we studied a series of cuts which probed the part of the loop-integrand which is, in the Feynman diagram expansion, encoded in the subset of diagrams with many internal propagators which have complicated branch-cut structure. We found remarkably simple expressions for the canonical forms for these "maximally intersecting" cuts. The topological winding formulation of the amplituhedron of [29] was crucial in deriving our results. In fact without this sign flip picture even a qualitative description of the canonical forms (2.81) and (2.56), the central results of this chapter, would likely be impossible. However, from the perspective of the amplituhedron, the factorization of the canonical forms on the intersecting and coplanar cuts is completely trivial and follows directly from the definition of the geometry. However, our analysis reveals an even greater simplicity than one would naïvely guess: for the intersecting cut the allowable space for the intersection point is naturally triangulated by a simple collection of tetrahedra, while the remaining degrees of freedom of the loop lines live inside a polygon.

This work is a continuation of a systematic exploration of the facets of the amplituhedron for all n, k, L. As such, there are a number of avenues for fur-

ther investigation: first, there are the unfinished cuts presented in Section 2.6.2 which gradually relax some of the constraints imposed on the maximally intersecting cuts we solved. The most interesting (and complicated) extension of the all-loop results presented here involve $L-1$ lines intersecting in a common point A with the L^{th} line free; solving this cut would amount to a complete understanding of the MHV two-loop geometry. Although the direct product form of the solutions obtained to all-loop orders will of course not remain, preliminary considerations suggest that simple geometrical decompositions of the canonical forms do persist to these more generic cuts. Another natural starting point for further work is to consider the same maximally intersecting cuts for $k \geq 1$ i.e., different helicity sectors. For example, by parity conjugation the NMHV five-point coplanar cut is simply the R-invariant [12345] multiplying the result derived in this chapter at five points. In the general n, k case although the product form will remain, the sign flip conditions change for both the external data and the loop momentum variables; however, it is likely that just as in the MHV configuration considered here, these problems will ultimately reduce to finding the right way of understanding the corresponding one-loop geometries for arbitrary n, k. Finally, there is another class of facets of the amplituhedron which are of physical interest. These involve unitarity cuts which trivialize the inequalities involving external data while leaving the mutual positivity conditions untouched. An example of these are the "corner cuts" computed in [**?**] at four points where loop lines pass through either Z_i or $(i-1ii+1)$. A detailed understanding of such corner cuts, along with complete knowledge of the structure of the integrand on the maximally intersecting cuts initiated here, would be invaluable to the goal of reconstructing the full loop integrand directly from the

amplituhedron.

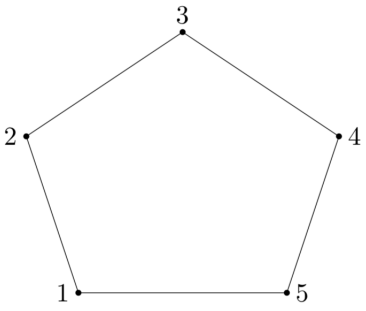

0.3
(a)
b

Figure 2.11

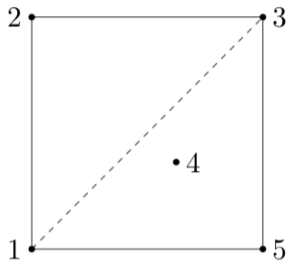

0.3
(a)
b

Figure 2.12

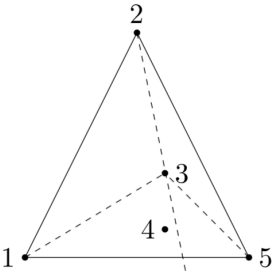

0.3
(a)
b

Figure 2.13

Figure 2.14: (a) Pentagonal configuration 12345 with the region bounded by the lines (12)(45)(15) for B_α; (b) Quadrilateral configuration with the region bounded by lines (12)(15)(34) for B_α; (c) Triangular configuration giving the same region for B_α as (b).

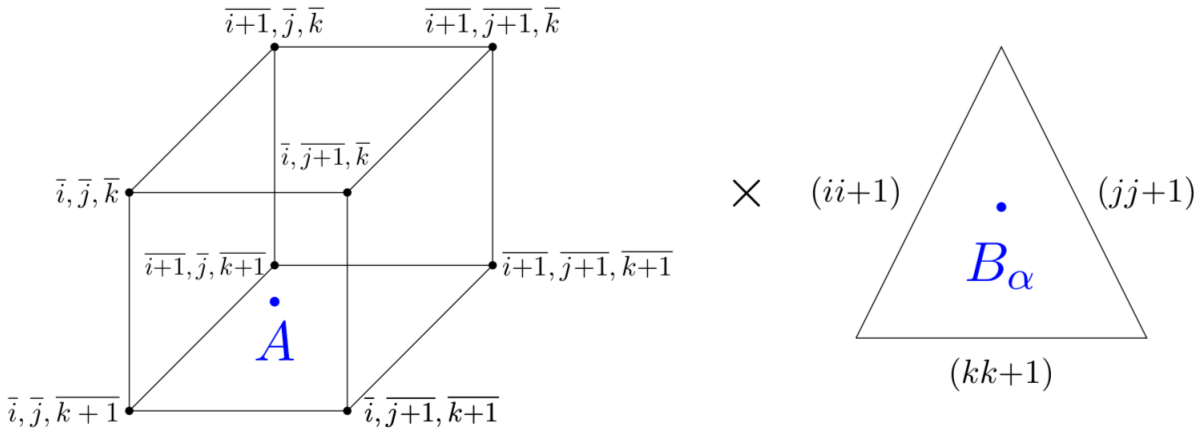

Figure 2.15: The geometry of (the geometric dual of) the coplanar cut at n points.

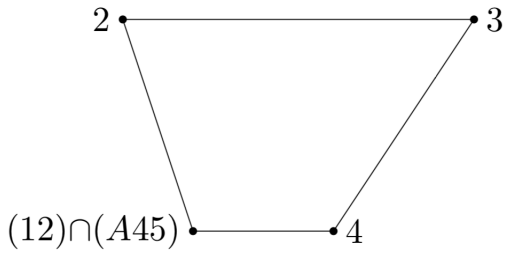

Figure 2.16: The region bounded by lines $(12), (23), (34)$ and (45) whose canonical form is given by (2.61).

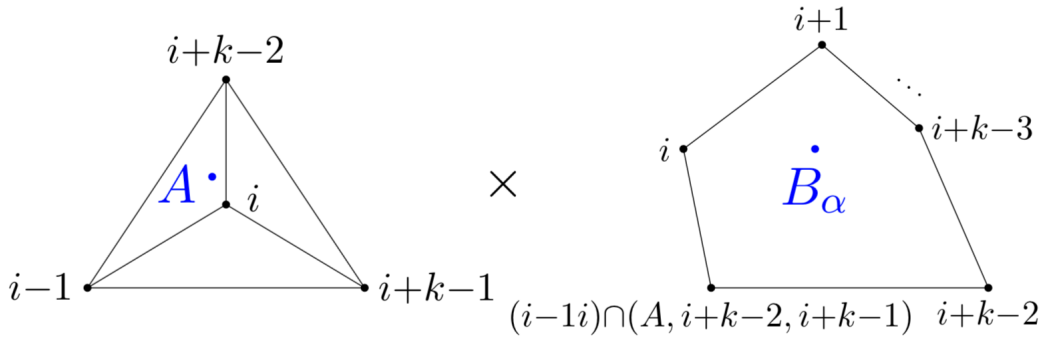

Figure 2.17: n-point geometry for the intersecting cut.

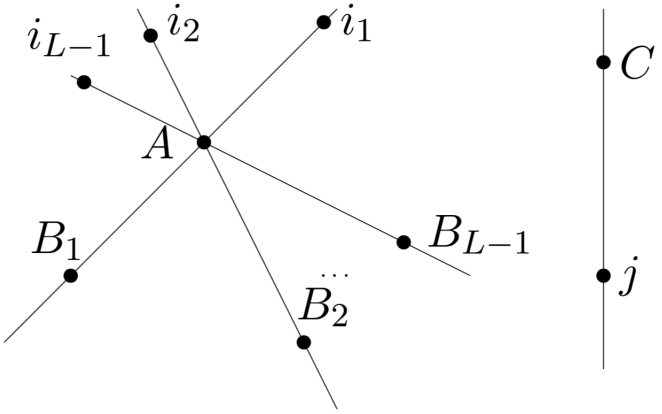

Figure 2.18: Cut 1, where $L-1$ loops intersect in a common point A as well as $L-1$ points $Z_{i_1}, \ldots, Z_{i_{L-1}}$, and the L^{th} loop intersects an additional point Z_j.

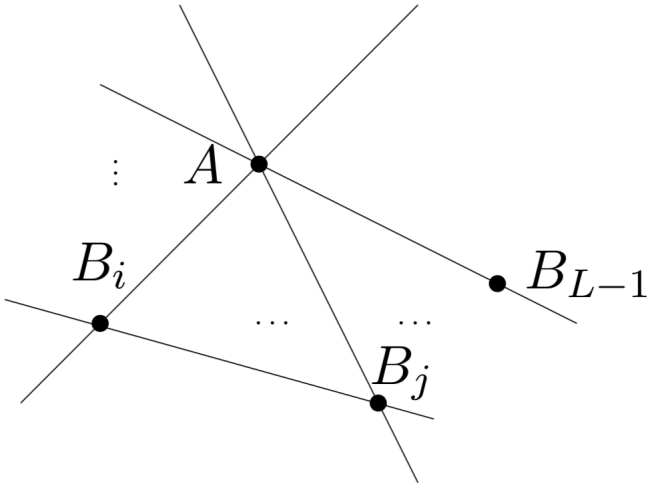

Figure 2.19: Cut 3 where $L-1$ loops intersect in a common point A, and the L^{th} loop intersects lines i and j.

3

Spherical contours, IR divergences and the geometry of Feynman parameter integrands at one loop

3.1 Introduction

A connection between the singularity structure of one-loop integrals and the projective geometry of their associated Feynman parameter integrand was established in [11]. One of the central results of this chapter was the introduction of a new kind of residue in Feynman parameter space - associated with "spherical contours " - operations involving only the one-loop integrand - which capture information about discontinuities of the integrals across various branch cuts . It was shown that this calculus based operation also has an algebraic interpretation. The purpose of this chapter is to provide some additional details on this algebraic interpretation and also explore IR divergent integrals as the authors of [11] largely focused on finite integrals.

The structure of the chapter is as follows. We begin by discussing some preliminaries of Feynman parametrization and setting up the notation for the rest of the chapter. In Section [3.3], we investigate IR divergent integrals in Feynman parameter space. We motivate and develop a new kind of "residue" opera-

tion which computes the leading IR divergence of one loop amplitudes. We use the simple example of a scalar $n-$gon integral to demonstrate the procedure. We then use the embedding space formalism [66] to consider general one loop integrals and demonstrate that this procedure correctly reproduces the leading IR divergences. Section [3.4] involves a discussion of the algebraic structure of spherical residues. In particular, we provide expressions for the new numerators of spherical residues of integrands. We then prove a few essential properties of spherical residues. In Section [3.5], we outline a method to construct one - loop integrands using spherical residues. Finally, we conclude by examining some appealing features of Feynman parameter integrands in $\mathcal{N} = 4$ SYM in [3.6].

3.2 Feynman Parametrization revisited

Although Feynman parametrization is a familiar trick, let us begin by discussing it in a more geometric way. This will highlight some of the features of Feynman parameter integrals which are important for the rest of the chapter. Consider the scalar one-loop integrals of the form (μ^2 is the mass scale introduced in dimensional regularization)

$$I_n = (\mu^2)^{\nu - LD/2} \int \prod_{k=1}^{L} \frac{d^D \ell_k}{i\pi^{D/2}} \prod_{j=1}^{n} \frac{1}{(-q_j^2 + m_j^2)^{\nu_j}} \qquad \nu = \sum_{j=1}^{n} \nu_j \tag{3.1}$$

Here each q_j is a linear combination of the external momenta p_k and the loop momenta ℓ_k. A straightforward Feynman parametrization yields (see [67–69])

$$I_n = (\mu^2)^{\nu - LD/2} \frac{\Gamma(\nu - LD/2)}{\prod_{j=1}^{n} \Gamma(\nu_j)} \int_0^\infty d^n x \; \delta(1 - \sum_i x_i) \prod_{j=1}^{n} x_j^{\nu_j - 1} \frac{\mathcal{U}^{\nu - (L+1)D/2}}{\mathcal{F}^{\nu - LD/2}} \tag{3.2}$$

where $\mathcal{U}$ and $\mathcal{F}$ are functions of the Feynman parameters x_j and depend on the particular integral being evaluated. They are functions of the external momenta and are connected to the propagators appearing in eq(3.1) via the polynomial

$$\sum_{j=1}^{n} x_j(-q_j^2+m_j^2) = -\sum_{r,s=1}^{L} \ell_r^\mu M_{r,s}\ell_{s\mu} + 2\sum_{r=1}^{L} l_r^\mu Q_{r\mu} + J$$

where J contains all the terms independent of the loop momenta. Then,

$$\mathcal{U} = \det M \qquad\qquad \mathcal{F} = \det M(J + Q.M^{-1}.Q)$$

$\mathcal{U}$ and $\mathcal{F}$ are called the Symanzik polynomials. It will be of interest to note that at one loop, $\mathcal{U}$ and $\mathcal{F}$ are homogeneous linear and quadratic polynomials respectively. The Symanzik polynomials can also be calculated efficiently by using graphical rules. For more details on these rules, we refer the reader to [67].

It is illuminating to consider an alternate derivation of this result. Let us first introduce Schwinger parameters α_i

$$\frac{1}{(-q_i^2+m_i^2)^{\nu_i}} = \int_0^\infty d\alpha_i\, e^{-\alpha_i(-q_i^2+m_i^2)\nu_i} \tag{3.3}$$

Inserting this in eq(3.1), we can perform the Gaussian integrals over all the loop momenta. The result is

$$I_n = (\mu^2)^{\nu-LD/2}\frac{i^{-\nu-1}\pi^2}{\prod_{j=1}^n \Gamma(\nu_j)}\int_0^\infty d\alpha_1\ldots d\alpha_n \prod_{j=1}^n \alpha_j^{\nu_j-1}\frac{1}{U^{D/2}}e^{i\frac{F}{U}-i\sum_j m_j^2\alpha_j} \tag{3.4}$$

where U and F are polynomials in the α_i. They are homogeneous and like the Symanzik polynomials $\mathcal{U}$ and $\mathcal{F}$, linear and quadratic respectively. For more

details, see [67, 70].

We can now introduce new variables via $\alpha_i = \eta x_i$. Since there are $n+1$ new variables, we must impose a constraint on the x_i which we take to be $\sum_{i\in S} x_i = 1$ where $S \subset \{1, \ldots n\}$ which changes eq(3.4) to

$$I_n = (\mu^2)^{\nu - LD/2} \frac{i^{-\nu-1}\pi^2}{\prod_{j=1}^n \Gamma(\nu_j)} \int_0^\infty dX\, d\eta\, \eta^{n-1} \left(\eta^{\nu-n-2} \prod_{j=1}^n x_j^{\nu_j - 1} \frac{1}{U^{D/2}} e^{i\,\eta \left(\frac{F}{U} - i \sum_j m_j^2 x_j\right)} \right)$$

where $dX = dx_1 \ldots dx_n\, \delta(1 - \sum_{i\in S} x_i)$. This result is called the Cheng-Wu theorem [71]. In particular, this implies that we could set any one of the Feynman parameters x_i to 1. The vector $X = (x_1, \ldots, x_n)$ can be thought of as a point in projective space and the measure $dx_1 \ldots dx_n\, \delta(1 - \sum_{i\in S} x_i)$ can be better written as

$$\langle X\, d^{n-1} X \rangle \equiv \epsilon_{\mu_1 \ldots \mu_n} X^{\mu_1}\, dX^{\mu_2} \ldots dX^{\mu_n}.$$

The textbook result of Feynman parametrization eq(3.2) is obtained by setting $S = \{1, \ldots n\}$. For the rest of the chapter, we will only work with integrals with the factors $\nu_i = 1$ and write all the Feynman parameter integrals in a projective manner as shown below (the factor of $(\mu^2)^{n-LD/2}$ is omitted) .

$$I_n = \Gamma(n - LD/2) \int \frac{\langle X\, d^{n-1} X \rangle\, \mathcal{U}^{n-(L+1)\,D/2}}{\mathcal{F}^{n-L\,D/2}}$$

The homogeneity properties of $\mathcal{U}$ and $\mathcal{F}$ are essential in making the integrals projectively well defined.

Throughout this chapter we will use three kinds of variables to describe the external momenta - dual momenta, momentum twistors [18] and embedding

space momenta [66]. Dual momenta y_i^μ are defined by

$$p_i^\mu = y_i^\mu - y_{i-1}^\mu \qquad y_{ij}^\mu \equiv y_i^\mu - y_j^\mu.$$

In the rest of the chapter, we focus on one-loop integrals and associate the dual variable y with the loop momentum. Momentum twistors, Z_i, introduced in [18], are convenient to describe null momenta in 4D. They are defined by associating a line $Z_{i-1}Z_i$ with each y_i. The scalar y_{ij}^2 is related to the $SL(4,R)$ invariant $\langle i-1ij-1j\rangle \equiv \epsilon_{ABCD}Z_{i-1}^A Z_i^B Z_{j-1}^C Z_j^D$. Each loop momentum variable is associated to a line AB in twistor space which is to be integrated over using the measure $\langle ABd^2A\rangle\langle ABd^2B\rangle$. For more details, see [26]

A vector y^μ in D-dimensional Minkowski space is mapped to a null vector $Y^M = (1, y^2, y^\mu)$ in embedding space. Here, we have specified the components in light-cone co-ordinates, i.e. $Y^+ = 1, Y^- = y^2$ and $Y^\mu = y^\mu$. The metric is $g_{+-} = g_{-+} = -1/2$ and $g_{\mu\nu} = \eta_{\mu\nu}$ with all other entries zero. The invariants $y_{ij}^2 = -2Y_i.Y_j$. In particular, for null momenta, we have $Y_i.Y_{i+1} = 0$. The integral eq(3.1) can be written as

$$I_n = (\mu^2)^{\nu - LD/2} \int \frac{[d^4Y]}{(Y.Y_1)^{\nu_1}\dots(Y.Y_n)^{\nu_n}} \tag{3.5}$$

The measure $[d^4Y] = \frac{d^6Y\delta(Y.Y)}{\mathrm{Vol}(GL(1))}$. For more details, see [11, 66].

For the particular case of planar one-loop integrals, simple expressions are available for the Symanzik polynomials. While $\mathcal{U}$ depends on the details of the

numerator, $\mathcal{F}$ depends only on the pole structure.

$$\mathcal{F} = \sum_{i<j} x_i x_j \, y_{ij}^2 = X.Q.X$$

where Q_{ij} can be expressed in any of the three equivalent forms y_{ij}^2 ,$\langle i-1ij-1j\rangle$ or $Y_i.Y_j$.

3.3 1-LOOP IR DIVERGENCES

The infrared (IR) structure of gauge theories has been the subject of a great amount of study. Long range forces which lead to early and late time interactions in a scattering process make the very definition of an S-Matrix difficult. For recent work on these issues, see [72, 73]. One of the main reasons for these difficulties is the contribution of IR divergent loop integrals to scattering amplitudes. These integrals are usually dealt with via dimensional regularization. In $D = 4 - 2\epsilon$ dimensions, at one-loop, soft and collinear divergences appear as $\frac{1}{\epsilon}$ poles and overlapping soft-collinear divergences lead to $\frac{1}{\epsilon^2}$ poles. At L-loops, the leading divergence is $\frac{1}{\epsilon^{2L}}$.

The structure of these divergences is well understood in gauge theories. It has been shown that they have a universal (independent of the number of external particles) structure which is captured by the factorization formula

$$\mathcal{M}_n = S\left(\{k_i\}, \mu, \epsilon\right) \times \prod_{i=1}^{n} J_i\left(k_i, \mu, \epsilon\right) \times h_n(\{k_i\}, \mu)\,. \tag{3.6}$$

Here $\mathcal{M}_n$ is the full $n-$particle amplitude divided by the corresponding tree amplitude, μ is the factorization scale (an arbitrary scale chosen to separate

soft and hard momenta) and ϵ is the dimensional regularization parameter. In writing this, we have followed the notation in [74]. h_n is a finite function corresponding to hard scattering, S is a color dependant function which encodes the soft singularities and J_i are functions encoding the collinear singularities along the k_i directions. In general, these are all complicated matrices in color and spin space. For a review of factorization properties and the structure of IR divergences in QCD and other gauge theories, see [75, 76].

The factorization in eq(3.6) has introduced an arbitrary scale μ which distinguishes between hard and soft momenta. This scale is unphysical and amplitudes cannot depend on it. Consequently, $\mathcal{M}_n$ satisfies a renormalization group equation

$$\mu \frac{d}{d\mu} S\left(\{k_i\}, \mu, \epsilon\right) = -\Gamma S\left(\{k_i\}, \mu, \epsilon\right) \tag{3.7}$$

with Γ being the anomalous dimensions matrix. It encodes the structure of IR divergences in the theory. For more details, we refer the reader to the review [77].

In planar theories and conformal theories like $\mathcal{N} = 4$, the all-loop solution to the RG equations is easy to obtain. Surprisingly, the full four point amplitude in $\mathcal{M}_4$ is completely fixed by the structure of IR divergences. It can be written as [78]

$$\mathcal{M}_4 = \exp\left[-\frac{1}{8}\sum_{l=1}^{\infty} a^l \left(\frac{\gamma_K^{(l)}}{(l\epsilon)^2} + \frac{2\mathcal{G}_0^{(l)}}{l\,\epsilon}\right) \sum_{i=1}^{4} \left(\frac{\mu^2}{-s_{i,i+1}}\right)^{l\,\epsilon}\right] \tag{3.8}$$

where a is related to the coupling and the number of colours, l is the number

of loops and $\gamma_K^{(l)}$ and $\mathcal{G}_0^{(l)}$ are constants that are not fixed by the RG equations. The cusp anomalous dimension is $\Gamma_{\mathcal{M}_n} = \sum_l a^l \gamma_K^{(l)}$. At one-loop, it is simply the coefficient of $\frac{1}{\epsilon^2}$. At higher points, while the structure of the IR divergences doesn't change, the full amplitude is different from 3.8 and involves remainder functions. Techniques from integrability provide all order results for $\Gamma_{\mathcal{M}_n}$ [79] which has been tested via perturbative computations extensively [80–83]. The IR divergences are related to the UV divergences of lightlike cusps of Wilson loops [84, 85]. The UV divergences of these Wilson loops are controlled by the same anomalous dimension, justifying the name "cusp" anomalous dimension.

The focus of this chapter is in understanding the origin of IR divergences and in developing a method to compute the cusp anomalous dimension directly in Feynman parameter space (in 4 spacetime dimensions). The first step is to gain an understanding of one-loop integrals. The complete structure of IR divergences in a theory depends on the particle content of the theory. We will not delve into these issues here and will focus solely on the properties of individual integrals. The next few paragraphs serve to provide intuition for analyzing IR divergences in Feynman parameter space.

It is well known that IR divergences arise when the loop momentum ℓ becomes collinear with an external massless momentum p_i, i.e. $\ell.p_i \to 0$ (soft) or when it becomes collinear to two consecutive null external momenta $\ell.p_{i-1} = \ell.p_i = 0$. Soft-collinear divergences arise when both these conditions are satisfied simultaneously. Let us consider the concrete example of a 4D massless box integral in momentum space and the corresponding Feynman parameter integral (in dimensional regularization with $D = 4 - 2\epsilon$).

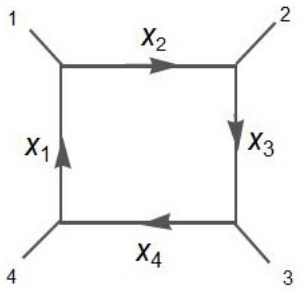

$$
\begin{aligned}
I_4 \quad &= \int \frac{d^D\ell}{i\pi^{D/2}} \, \frac{1}{\ell^2\,(\ell-p_2)^2\,(\ell-p_2-p_3)^2\,(\ell+p_1)^2} \\
&= \int \prod_{i=1}^{4} dx_i\,\Gamma\,(2+\epsilon)\,\frac{\delta(x_1+x_2+x_3+x_4-1)}{(x_1x_3\,s+x_2x_4\,u)^{2+\epsilon}}
\end{aligned}
$$

where $s = (p_1+p_2)^2$ and $u = (p_1+p_4)^2$. This integral is of course well known and has been evaluated in dimensional regularization in $D = 4-2\epsilon$ dimensions (reintroducing the factors of μ^2) [86, 87].

$$
I_4 = \frac{\Gamma(1+\epsilon)\Gamma^2(1-\epsilon)}{\Gamma(1-2\epsilon)s\,u}\left(\frac{2}{\epsilon^2}\left[(-\mu^{-2}s)^{-\epsilon}+(-\mu^{-2}u)^{-\epsilon}\right]-\log^2\frac{s}{u}-\pi^2\right)+\mathcal{O}(\epsilon)
$$

The presence of the $\frac{1}{\epsilon^2}$ terms indicated an IR divergence. A more transparent analysis using a massive regulator instead of dimensional regularization reveals that the divergence coming from the regions $\ell^2 = (\ell-p_2)^2 = (\ell+p_1)^2 = 0$ is of the form $\frac{1}{su}(\log^2\frac{m^2}{s}+\log^2\frac{m^2}{u})$. We refer the reader to section 7 in [88].

We can thus precisely characterize the leading IR divergent region in momentum space as being associated with three propagators going on-shell. A similar characterization in Feynman parameter space should involve the Feynman parameters corresponding to these three propagators, x_1, x_2 and x_3. To motivate

such a characterization, recall the definition of the Schwinger parameter α

$$\frac{1}{p^2} = \int_0^\infty d\alpha\, e^{-\alpha\, p^2}$$

Near the upper limit of the integral, i.e. for large α, a configuration with $p^2 \approx 0$ would be the most relevant. We might hope that the large α limit probes soft momenta. Since Feynman parameters are related to Schwinger parameters by $x_i = \frac{\alpha_i}{\sum_i \alpha_i}$, the limit $\alpha_i \to \infty$ corresponds to $x_i \to 1$ non - projectively or $x_i \to \infty$ projectively.

Furthermore, we can manipulate I_4 to understand the relationship between the consecutive massless legs and IR divergences. We can use Lorentz invariance to transform to a frame in which $p_1^\mu = (1,0,0,0)$ and $p_2^\mu = (0,1,0,0)$. Here, the components have been specified in light-cone frame as $(p_i^+, p_i^-, p_i^1, p_i^2)$. Hence $p_1^2 = p_2^2 = 0$ is automatic. If we work in the soft region where $\ell^2 \approx 0$, we can write $\ell.p_1 \approx l_+$ and $\ell.p_2 \approx l_-$. In this case, we can schematically write the integral as follows

$$I_4 \approx \int \frac{1}{2p_2.p_3} \frac{d^2\ell_\perp}{(\ell_+\ell_- - \ell_\perp^2)} \frac{d\ell_-}{\ell_-} \frac{d\ell_+}{\ell_+} \tag{3.9}$$

(where we have set $\epsilon = 0$*). The soft collinear region is the region in which all three propagators go on shell. $\ell_+ \approx 0$, $\ell_- \approx 0$ and $\ell_\perp^2 \approx \ell_+\, \ell_-$. In combination with the intuition in the previous paragraph, this suggests that the region in Feynman parameter space which gives rise to the divergence is $x_2 \approx x_1 x_3$

*Formally, the integral is ill defined and doesn't exist. However, it suffices to illustrate the point schematically. In the rest of the chapter, we will be interested in computing residues which are well defined and do not require a regulator.

and $x_2 \to \infty$. In this region, we should be able to observe a $\log^2$ divergence and calculate its coefficient. This should be equal to the coefficient of $\frac{1}{\epsilon^2}$ in dimensional regularization which is the cusp anomalous dimension Γ. Note that this is purely a conjecture at this point and in the next section, we will demonstrate that this region in Feynman parameter space indeed captures the essential information about the IR divergent region and can be used to calculate Γ.

3.3.1 Composite residues in momentum space

Let us begin by understanding the calculation of Γ directly in momentum space as a composite residue on the poles corresponding to three propagators going on shell. The idea of composite residues was first introduced in [89, 90]. Here, we compute this for a scalar n-gon.

$$\begin{aligned} I_n &= \int \frac{d^4\, l}{l^2(l-p_2)^2 \,\ldots\, (l+p_1)^2} \\ &= \int \frac{d^4 y}{(y-y_1)^2(y-y_2)^2 \,\ldots\, (y-y_n)^2} \end{aligned} \tag{3.10}$$

where

$$p_i = y_i - y_{i-1} \qquad y = l + x_1 \qquad (l - \sum_{i=2}^{k} p_i) = l + y_1 - y_k$$

We want to calculate the residue associated with the loop momentum ℓ being collinear to two consecutive null external momenta, i.e. $\ell.p_{i-1} = \ell.p_i = 0$. In terms of the dual momenta y_i, this is equivalent to $(y - y_i)^2 = (y - y_{i-1})^2 = (y - y_{i+1})^2 = 0$. To calculate this residue, we first parametrize y on the cut

$(y-y_i)^2=0$ by introducing spinor helicity variables (see [87] for a review).

$$y^\mu = y_i^\mu + \sigma^\mu_{\alpha\dot\alpha}\lambda^\alpha\,\tilde\lambda^{\dot\alpha} \qquad\qquad y_i^\mu - y_{i-1}^\mu = \sigma^\mu_{\alpha\dot\alpha}\lambda_i^\alpha\,\tilde\lambda_i^{\dot\alpha}$$

From this, it follows that

$$(y-y_{i-1})^2 = \langle\lambda\,\lambda_i\rangle\ \left[\tilde\lambda\,\tilde\lambda_i\right] \qquad (y-y_{i+1})^2 = \langle\lambda\,\lambda_{i+1}\rangle\left[\tilde\lambda\,\tilde\lambda_{i+1}\right]$$
$$(y-y_k)^2 = (y_i-y_k)^2 + 2\,(y_i-y_k)^\mu\sigma_{\mu\alpha\dot\alpha}(\lambda^\alpha\tilde\lambda^{\dot\alpha})$$

where $\langle a\,b\rangle = \epsilon_{\alpha\beta}a^\alpha b^\beta$ and $[\tilde a\,\tilde b] = \epsilon_{\dot\alpha\dot\beta}\tilde a^{\dot\alpha}\tilde b^{\dot\beta}$ For convenience, we expand λ in a basis consisting of λ_i and λ_{i+1} (with a similar expansion for $\tilde\lambda$).

$$\lambda = \beta\lambda_i + \gamma\,\lambda_{i+1} \qquad \tilde\lambda = \sigma\,\tilde\lambda_i + \rho\,\tilde\lambda_{i+1}$$

In terms of these variables, the measure on the cut $(y-y_i)^2=0$ is

$$\int d^4y\ \delta\left((y-y_i)^2\right) = \int \frac{d^2\lambda\,d^2\tilde\lambda}{\text{Vol}\ GL(1)} = \int d\gamma\,d\rho\,d\sigma\,\langle\lambda_i\,\lambda_{i+1}\rangle\,[\lambda_i\,\lambda_{i+1}]$$

We have used the $GL(1)$ to fix $\beta=1$. By introducing the spinor helicity variables, we are already on the cut $(y-y_i)^2=0$. This residue can now be written as

$$\text{Res}_{(y-y_i)^2=0}I_n = \int \frac{d\gamma}{\gamma}\frac{d\rho}{\rho}\frac{d\sigma}{\sigma}\frac{1}{\langle\lambda_i\,\lambda_{i+1}\rangle\,[\lambda_i\,\lambda_{i+1}]\prod_{k\neq\{i-1,i,i+1\}}((y_i-y_k)^2\ +\ 2\,(y_i-y_k)^\mu\sigma_{\mu\alpha\dot\alpha}\lambda^\alpha\tilde\lambda^{\dot\alpha})}$$

On this cut, we can now fully localize the loop momentum y_i by taking the residue of the poles $\gamma=\rho=\sigma=0$, even though we have cut only three propa-

gators. This is an example of a composite residue. Recalling that $\langle \lambda_i \, \lambda_{i+1} \rangle \, [\lambda_i \, \lambda_{i+1}] = 2 \, (y_i - y_{i-1}).(y_{i+1} - y_i) = y^2_{i-1i+1}$, the co-efficient of the IR divergence can be written as

$$\Gamma_{I_n} = \oint_{\gamma=\rho=\sigma=0} Res_{(y-y_i)^2=0} I_n = \frac{1}{y^2_{i-1,i+1} \prod_{k \neq \{i-1,i,i+1\}} y^2_{i,k}} \tag{3.11}$$

This can be compared to the full expression for the amplitudes given in [86, 91].

3.3.2 Composite residues in Feynman parameter space

We will now demonstrate that the coefficient of the log^2 divergence, as obtained in eq(3.11) can also be obtained directly in Feynman parameter space. As suggested above, the IR divergences in Feynman parameter space are associated to a triplet of consecutive Feynman parameters (x_{i-1}, x_i, x_{i+1}) and come from the region where x_i is large and $x_{i-1}x_{i+1}$ scales as x_i. We will evaluate the integral eq(3.10) in this limit and find that the result is proportional to Γ_{I_n}.

We being by writing (3.10) as a projective integral in Feynman parameter space.

$$I_n = \Gamma(n-2) \int \frac{\langle X d^{n-1} X \rangle \, \mathcal{U}^{n-4}}{\mathcal{F}^{n-2}} \tag{3.12}$$

with the Symanzik polynomials

$$\mathcal{U} = \sum_i x_i \qquad\qquad \mathcal{F} = \sum_{i<j} x_i \, x_j \, y^2_{ij} \tag{3.13}$$

Let us introduce new variables (ρ, τ) via

$$x_{i-1} = \sqrt{x_i}\,\rho\, e^{\tau} \qquad x_{i+1} = \sqrt{x_i}\,\rho\, e^{-\tau}$$

This change of variables ensures that we have the required scaling, $x_{i-1}x_{i+1} = \rho^2 x_i$ of the relevant Feynman parameters. In the limit of the limit of large x_i, the Symanzik polynomials reduce to

$$\begin{aligned}\mathcal{U} &= x_i + \mathcal{O}(\sqrt{x_i}) \\ \mathcal{F} &= x_i \left(y_{i-1i+1}^2 \rho^2 + \sum_{j\neq\{i-1,i,i+1\}} y_{ij}^2\, x_j \right) + \mathcal{O}(\sqrt{x_i}).\end{aligned}$$

Note that the quadric has factorized in this limit. This guarantees that the resulting integral over the remaining $(n-3)$ Feynman parameters (recall that the integral is projective and requires only $(n-1)$ integrations) is now rational.

$$\begin{aligned} I_n \quad &\approx \int \Big(\frac{\prod_{k\neq i-1,i+1} dx_k}{\mathrm{Vol}GL(1)}\Big)\, 2\rho\, x_i\, d\rho\, d\tau \frac{\left(x_i^{n-4}\right)\Gamma(n-2)}{x_i^{n-2}\left(y_{i-1i+1}^2\rho^2 + \sum_{j\neq\{i-1,i,i+1\}} y_{ij}^2\, x_j\right)^{n-2}} \\ &= \Gamma(n-2)\int \frac{dx_i}{x_i}\, d\tau \int \frac{\prod_{j\neq\{i-1,i,i+1\}} dx_j}{\mathrm{Vol}GL(1)} \frac{2\rho\, d\rho}{\left(y_{i-1i+1}^2\rho^2 + \sum_{j\neq\{i-1,i,i+1\}} y_{ij}^2\, x_j\right)^{n-2}} \end{aligned}$$

where we've explicitly written out a factor of Vol $GL(1)$ to indicate that the x_i are projective. The divergent factor is

$$\int \frac{dx_i}{x_i} d\tau = \frac{1}{2}\int d\log x_i\; d\log \frac{x_{i+1}}{x_{i-1}}$$

After fixing the $GL(1)$ redundancy by setting one of the $x_j = 1$, the remaining

integral is rational and can be easily evaluated.

$$2\,\Gamma(n-2)\int \frac{\prod_{j\neq\{i-1,i,i+1\}} dx_j}{\mathrm{Vol}GL(1)}\rho\, d\rho \frac{1}{\left(\rho^2+\sum_{j\neq i-1,i,i+1} x_j\right)^{n-2}} = 1$$

With this,

$$I_n \quad \approx \frac{1}{2}\int d\log x_i \; d\log\left(\frac{x_{i+1}}{x_{i-1}}\right) \; \frac{1}{y^2_{i-1,i+1}\prod_{j\neq\{i-1,i,i+1\}} y^2_{ij}}$$

where the $\approx$ sign indicates that this result is true only in the above limit. We see that there is a $\log^2$ divergence and its coefficient is identical to Γ_{I_n} computed directly as a composite residue in eq(3.11), i.e.

$$\Gamma_{I_n} = \frac{1}{2}\frac{1}{y^2_{i-1i+1}\prod_{j\neq\{i-1,i,i+1\}} y^2_{ij}} \tag{3.14}$$

3.3.3 Proof for general one-loop integrals

The proof of the previous section is valid only for scalar $n-$gon integrals. This is due to the specific form of the Symanzik polynomials in eq(3.13). In this section, we will generalize the above results to include cases with tensor numerators. We will show that the coefficient of the IR divergence obtained by computing a composite residue involving three propagators is the same as the one obtained in Feynman parameter space using the procedure outlined in Section[3.3.2]. It is easiest to work in embedding space. A generic one-loop integral with a tensor numerator has the form

$$I_n = \int \frac{T\left[Y^{n-4}\right]\left[d^4Y\right]}{(Y.Y_1)\ldots(Y.Y_n)} \tag{3.15}$$

where $T\left[Y^{n-4}\right] = T_{i_1\ldots i_n} Y^{i_1}\ldots Y^{i_n}$ is a tensor of rank $n-4$. The measure $[d^4Y] = \frac{d^6Y\delta(Y.Y)}{\mathrm{Vol}(GL(1))}$.

To calculate the coefficient of the IR divergence, we follow the same procedure as in Section [3.3.1]. We calculate the residue on the cut $Y.Y_1 = Y.Y_2 = Y.Y_3 = 0$. Since the denominator is the same as in eq(3.12), it is easy to see that the same computation goes through. The end result is,

$$\Gamma_{I_n} = \frac{T\left[Y_2^{n-4}\right]}{(Y_1.Y_3)\prod_{k\neq\{1,2,3\}} Y_2.Y_k} \tag{3.16}$$

We will now show that the same result can be obtained in Feynman parameter space by scaling the parameters as mentioned before. We begin by Feynman parametrizing the integral in (3.15)

$$I_n = \int \frac{T\left[Y^{n-4}\right][d^4Y]\,\langle X d^{n-1}X\rangle}{(Y.W)^n}$$

where $W = \sum_i x_i Y_i$. To do the integral over Y, we note that each factor of Y can be exchanged for $\frac{d}{dW}$ to get

$$\begin{aligned} I_n &= \frac{6(-1)^{n-4}}{(n-1)!} T\left[\left(\frac{d}{dW}\right)^{n-4}\right]\int \frac{[d^4Y]\,\langle X d^{n-1}X\rangle}{(Y.W)^4} \\ &= T\left[\left(\frac{d}{dW}\right)^{n-4}\right]\int \frac{\langle X d^{n-1}X\rangle}{(W.W)^2} \end{aligned}$$

where $T\left[\left(\frac{d}{dW}\right)^{n-4}\right] = T_{i_1\ldots i_{n-4}}\frac{d}{dW^{i_1}}\cdots\frac{d}{dW^{i_{n-4}}}$ and we have used

$$\int \frac{[d^4Y]}{(W.Y)^4} = \frac{1}{(W.W)^2}$$

To compare with (3.16), we set $x_1 = \sqrt{x_2}\rho e^{\tau}, x_3 = \sqrt{x_2}\rho e^{-\tau}$ and take the limit of large x_2. Once again we have $W \approx x_2 Y_2$ and $W.W \approx x_2 \left(\rho^2\, Y_1.Y_3 + \sum_{i\neq 1,2,3} x_i Y_i.Y_2\right)$. In the large x_2 limit, only the term $T[W^{n-4}] = x_2^{n-4} T[Y_2^{n-4}]$ contributes and

$$I_n \approx \int \frac{dx_2}{x_2} d\tau \frac{T[Y^{n-4}]}{(Y_1.Y_3)\prod_{i\neq 1,2,3}(Y_2.Y_i)} \int \frac{\langle X d^{n-4} X\rangle \rho d\rho}{(\rho^2 + \sum_{i\neq 1,2,3} x_i)^{n-2}}$$

The integral $\int \frac{\langle X\, d^{n-4} X\rangle \rho d\rho}{(\rho^2+\sum_{i\neq 1,2,3} x_i)^{n-2}} = \frac{1}{2(n-3)!}$ is independent of the details of the numerator. This explains why Γ_{I_n} is always rational at one-loop irrespective of the details of the integrand.

We have shown that the co-efficient of the IR divergence can be extracted from the integral by an algebraic operation directly in Feynman parameter space. There is a potential IR divergence associated with every triplet (x_{i-1}, x_i, x_{i+1}). The complete IR divergence associated with the one-loop integral (3.15) is given by summing over all such regions

$$\Gamma = \sum_{i=1}^{n} \frac{T\left[Y_i^{n-4}\right]}{(Y_{i-1}.Y_{i+1})\prod_{k\neq i-1,i,i+1} Y_i.Y_k}. \tag{3.17}$$

3.3.4 IR Finite integrals

It is instructive to understand what makes integrals IR finite in Feynman parameter space. We can see from eq(3.11) that $\Gamma = 0$ unless $T[Y_i^{n-4}] \neq 0$ for at least one $i \in \{1, \ldots n\}$. As an example, consider a well known finite integral, the chiral hexagon

$$I = \int_{AB} \frac{\langle AB13\rangle\langle AB46\rangle\langle 5612\rangle\langle 2345\rangle}{\langle AB12\rangle\langle AB23\rangle\langle AB34\rangle\langle AB45\rangle\langle AB56\rangle\langle AB16\rangle} \tag{3.18}$$

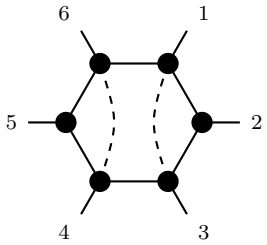

Figure 3.1: Chiral Hexagon

where we have used momentum twistor notation and $\int_{AB} = \int \langle ABd^2A\rangle\langle ABd^2B\rangle$. On Feynman parametrization, this becomes,

$$\frac{(Y_{13}.Y_{46})(W.W) - 6(W.Y_{13})(W.Y_{46})}{(W.W)^4}$$

where $W = \sum_i x_i Y_i$ and Y_{ij} is the vector in embedding space corresponding to the bi-twistor $|ij\rangle$. The numerator doesn't contain any terms of the form x_i^2 and doesn't encounter IR divergences from the collinear region.

We can now easily construct a basis of IR finite integrals in Feynman parameter space. At n-points, the numerator of a Feynman integral is a polynomial of degree $(n-4)$ in the Feynman parameters.

$$\int \langle Xd^{n-1}X\rangle \frac{T[X^{n-4}]}{(XQX)^{(n-2)}} \tag{3.19}$$

where $T[X^{n-4}] = T_{i_1\ldots i_{n-4}} X^{i_1\ldots i_{n-4}}$. The only constraint IR finiteness imposes on T is that coefficients of x_i^{n-4} should vanish for all $i \in \{1,\ldots n\}$.

At $n = 5$, this implies that there are no IR finite integrals. This is in agreement with the result that the chiral pentagons for $n = 5$ suffer from IR diver-

gences from unprotected massless corners [26].

At $n = 6$, the tensor is left with 15 independent coefficients. Further conditions can be imposed to uniquely specify a basis. For instance, we can demand that some leading singularities vanish while others are ± 1. We will develop these ideas further in Section [3.5]. But first, we need to understand the avatar of leading singularities in Feynman parameter space, which involve the notion of spherical contours.

3.4 Algebraic aspects of spherical residues

The idea of a spherical contour integral and the corresponding spherical residue was introduced in [11] to compute the discontinuities of one-loop integrands directly in Feynman parameter space. Here, we give a brief description of the procedure. Consider the following integral.

$$I_{n,k} = \int \frac{\langle X d^{n-1} X\rangle T\left[X^k\right]}{(X.Q.X)^{\frac{(n+k)}{2}}} \tag{3.20}$$

with k and n even. For any pair of Feynman parameters (x_i, x_j), there is a natural decomposition of the quadric Q into four parts,

$$\begin{aligned} X.Q.X = \quad & X_{\{ij\}}.Q_{\{ij\},\{ij\}}.X_{\{ij\}} + X_{\{ij\}}.Q_{\{ij\},\{\widehat{ij}\}}.X_{\{\widehat{ij}\}} + \\ & X_{\{\widehat{ij}\}}.Q_{\{\widehat{ij}\},\{ij\}}X_{\{ij\}} + X_{\{\widehat{ij}\}}.Q_{\{\widehat{ij}\},\{\widehat{ij}\}}.X_{\{\widehat{ij}\}} \end{aligned}$$

where

$$X_{\{ij\}} = (x_i, x_j)$$
$$X_{\{\widehat{ij}\}} = (x_1, \ldots \hat{x}_i, \ldots, \hat{x}_j \ldots x_n)$$

and the $\hat{x}_i$ indicates that the entry is missing. The integral can develop singularities at locations determined by the entries of Q (which are functions of the external momenta) and the properties of the numerator. There are possible branch point beginning at the following locations.

$$\bar{ij} = \begin{cases} r(Q^{-1}_{\{ij\},\{ij\}}) & Q_{ii} \neq 0,\ Q_{jj} \neq 0 \\ \left(\frac{Q_{ij}^2}{Q_{jj}}\right)^{-\text{sign}(Q_{ij})} & Q_{ii} = 0,\ Q_{jj} \neq 0 \\ \left(\frac{Q_{ij}^2}{Q_{ii}}\right)^{-\text{sign}(Q_{ij})} & Q_{ii} \neq 0,\ Q_{jj} = 0 \\ Q_{ij}^{-2\ \text{sign}(Q_{ij})} & Q_{ii} = 0,\ Q_{jj} = 0 \end{cases}$$

where $r(\mathbf{A}) = \frac{\mathbf{A}_{12} - \sqrt{(\mathbf{A}_{12})^2 - \mathbf{A}_{11}\mathbf{A}_{22}}}{\mathbf{A}_{12} + \sqrt{(\mathbf{A}_{12})^2 - \mathbf{A}_{11}\mathbf{A}_{22}}}$ and sign (Q_{ij}) is just the sign of the element Q_{ij}. For a complete explanation of how these arise, we refer the reader to [11]. These are actual branch points only if the residue on the spherical contour corresponding to the variables x_i and x_j is non zero. In the cases when the residue is non-zero, its value gives the discontinuity across the cut.

To compute the spherical residue, we use the following algorithm.

- Perform the transformation

$$\begin{pmatrix} x_i \\ x_j \end{pmatrix} = R \begin{pmatrix} w_i \\ w_j \end{pmatrix} - Q^{-1}_{\{ij\}\{ij\}} Q_{\{ij\}\{\widehat{ij}\}} X_{\{\widehat{ij}\}}. \tag{3.21}$$

thereby reducing the denominator to the form

$$w_i w_j + X_{\{\widehat{ij}\}} Q^{(ij)} X_{\{\widehat{ij}\}}$$

Here R is a 2×2 matrix such that $R^T Q_{\{ij\}\{ij\}} R = \begin{pmatrix} 0 & 1/2 \\ 1/2 & 0 \end{pmatrix}$.

- Integrate over the entire complex plane / Riemann sphere by setting $w_i = re^{i\theta}$ and $w_j = re^{-i\theta}$ with ranges $r \in (0, \infty)$ and $\theta \in (0, 2\pi)$.

It was shown in [11] that the whole procedure can be interpreted as an algebraic operation on the quadric, i.e. after integration the new quadric $Q^{(ij)}$ is related to the old one by

$$Q^{(ij)} = Q_{\{\widehat{ij}\}\{\widehat{ij}\}} - Q_{\{\widehat{ij}\}\{ij\}} Q^{-1}_{\{ij\}\{ij\}} Q_{\{ij\}\{\widehat{ij}\}}$$

Furthermore, the effect of performing multiple spherical contour integrals is captured by extensions of the same formula. In 4 spacetime dimensions, the maximum number of spherical contours we can perform is two (this is equivalent to cutting four propagators and fully localizing the momentum). This double spherical residue results in a quadric

$$Q^{(ijkl)} = Q_{\{\widehat{ijkl}\}\{\widehat{ijkl}\}} - Q_{\{\widehat{ijkl}\}\{ijkl\}} Q^{-1}_{\{ijkl\}\{ijkl\}} Q_{\{ijkl\}\{\widehat{ijkl}\}}$$

In order to complete the interpretation as an algebraic operation , we need to provide similar expressions for the numerators after the integrals. We will now examine the effect the spherical contour integral has on the numerators.

Linear numerator

Let's start with a Feynman parameter integral with a linear numerator,

$$I_l = \int \frac{\langle X d^{n-1} X\rangle (L.X)}{(X.Q.X)^{(n+1)/2}} \tag{3.22}$$

We want an expression for the numerator after performing a spherical contour integral along the (x_i, x_j). To perform the integral, we first decompose the numerator into parts along x_i, x_j and orthogonal pieces.

$$L.X = L_{\widehat{\{ij\}}}.X_{\widehat{\{ij\}}} + L_{\{ij\}}.(x_i, x_j)$$

Performing the transformation eq(3.21) results in an integral which we denote as

$$I_l^{(ij)} = \int \frac{\langle X_{\{\widehat{ij}\}} d^{n-3} X_{\{\widehat{ij}\}}\rangle (L^{(ij)}.X_{\{\widehat{ij}\}})}{(X_{\{\widehat{ij}\}}.Q^{(ij)}.X_{\{\widehat{ij}\}})^{(n-1)/2}} \tag{3.23}$$

with

$$L^{(ij)} = \frac{1}{\sqrt{-4 \mathrm{Det} Q_{\{ij\}\{ij\}}}} \left(L_{\widehat{\{ij\}}} - L_{\{ij\}} Q^{-1}_{\{ij\}\{ij\}} Q_{\{ij\}\{\widehat{ij}\}} \right) \tag{3.24}$$

Quadratic numerator

Consider next, the case of an integral with a quadratic numerator.

$$I_q = \int \frac{\langle X d^{n-1} X\rangle (N.X.X)}{(X.Q.X)^{(n+2)/2}} \tag{3.25}$$

To perform a spherical contour integral in the (x_i, x_j) direction, we decompose

$N^{(ij)}$ in the same way as before.

$$X.N.X = X_{\{ij\}}N_{\{ij\}\{ij\}}X_{\{ij\}} + 2N_{\{ij\}\{\widehat{ij}\}}X_{\{ij\}}X_{\{\widehat{ij}\}} + N_{\{\widehat{ij}\}\{\widehat{ij}\}}X_{\{\widehat{ij}\}}X_{\{\widehat{ij}\}}$$

We can show that the result can be written as

$$I_q^{(ij)} = \int \frac{\langle X^{(ij)} d^{n-3}X^{(ij)}\rangle (X^{(ij)}.N^{(ij)}.X^{(ij)})}{(X^{(ij)}.Q^{(ij)}.X^{(ij)})^{n/2}}$$

with

$$\begin{aligned} N^{(ij)} = \quad & Q^{(ij)}Tr(Q^{-1}_{\{ij\}\{ij\}}N_{\{ij\}\{ij\}}) + (n-2)\Big(Q_{\{\widehat{ij}\}\{ij\}}Q^{-1}_{\{ij\}\{ij\}}N_{\{ij\}\{ij\}}Q^{-1}_{\{ij\}\{ij\}}Q_{\{ij\}\{\widehat{ij}\}} \\ & -Q_{\{\widehat{ij}\}\{ij\}}Q^{-1}_{\{ij\}\{ij\}}N_{\{ij\}\{\widehat{ij}\}} - N_{\{\widehat{ij}\}\{ij\}}Q^{-1}_{\{ij\}\{ij\}}Q_{\{ij\}\{\widehat{ij}\}} + N_{\{\widehat{ij}\}\{\widehat{ij}\}}\Big) \end{aligned} \tag{3.26}$$

For more details on the calculation, we refer the reader to Appendix D.

The effect of multiple spherical contours is easy to express in this form. For e.g. a double spherical residue along directions $(ijkl)$, on the linear and quadratic numerators, results in $L^{(ijkl)}$ and $N^{(ijkl)}$ with obvious definitions.

3.4.1 Properties of Feynman integrals coming from loop integrals

In this section we elaborate on some properties satisfied by Feynman integrals. An integral of the form eq(3.20) must satisfy the following conditions if it comes from a Feynman diagram.

- The quadric Q must be degenerate for $n > 6$. This is because the entries of the quadric are all of the form $Y_i.Y_j$ where Y_i and Y_j are embedding space vectors. The embedding space corresponding to 4D spacetime is 6

dimensional. Thus the rank of Q is always 6.

- The tensor in the numerator, T must share the null space of the degenerate Q (for $n > 6$). If N is a vector in the null space of Q, i.e. $Q.N = 0$, then we must have $T.N = 0$.

It is a non trivial fact that these properties continue to hold after we perform a spherical contour integral. We can use the expressions derived above to provide a quick proof of these facts.

This is easy to show for a Feynman parameter integral with a linear numerator eq(3.22). We want to show that the new numerator shares a null space with the new quadric. i.e. for every N' such that $Q^{(ij)}.N' = 0$, we have $L'.N = 0$. To show this, suppose that N belongs to the null space of L and Q. Then we have $L.N = 0 = Q.N = 0$. It is easy to see that $N' = N_{\{\widehat{ij}\}}$ is a null vector of $Q^{(ij)}$ using the following property.

$$Q.N = 0 \implies Q_{\{\}\{ij\}}N_{\{ij\}} = -Q_{\{\}\{\widehat{ij}\}}N_{\{\widehat{ij}\}}$$

where the empty $\{\}$ can be either $\{ij\}$ or $\{\widehat{ij}\}$. Using eq(3.24) it is obvious that $L^{(ij)}.N' = 0$. Thus eq(3.22) satisfies all the conditions of a Feynman integral after a spherical contour.

This can be extended to a class of integrals of the form

$$\langle X d^{n-1} X \rangle \frac{(L.X)^{n-D}}{(X.Q.X)^{n-D/2}} \tag{3.27}$$

The spherical residue in variables (x_i, x_j) is a sum of terms of the form $(0 \leq k \leq$

$n - D$)

$$\frac{(L^{(ij)}.X)^{n-D-k/2}}{(X'Q'X')^{(D+k+2-2n)/2}}$$

See [**??**] for the detailed derivation of this result. We see that the proof for a linear numerator works here as well. An similar calculation using eq(3.26) shows that the same holds true in the case of a quadratic numerator

3.4.2 Spherical contours meet IR divergences

We have seen that the double spherical contours calculate the leading singularities. We know that leading singularities obey relations that arise from the global residue theorem [26]. These must be reflected in the double spherical contours. Let us start with the simple example of

$$I_5 = \int \frac{\langle X\, d^4X\rangle\, x_2}{(x_1x_3Q_{13} + x_1x_4Q_{14} + x_2x_4Q_{24} + x_2x_5Q_{25} + x_3x_5Q_{35})^3}$$

This integral is IR divergent and the divergence corresponds to the triplet $(x_1x_2x_3)$. Let us calculate the double spherical contours $(1423), (1425), (1324), (1325)$.

$$c_{1423} = -c_{1425} = c_{1324} = c_{1325} = -\frac{1}{2Q_{25}Q_{13}Q_{24}} \tag{3.28}$$

We see that $c_{1425} + c_{1423} = 0$ as expected from the Global residue theorem. However, $c_{1324} + c_{1325} \neq 0$ and this is precisely because of the IR divergence. Similar residue theorems are satisfied by the double spherical contours as can be checked from our expression for the 6 point MHV amplitude. Since the IR

divergence introduces non-zero composite residues, the statement of the global residue theorem must be changed to accommodate these. The spherical residue capture the usual leading singularities in Feynman parameter space and the scaling limit introduced in Sec[3.3.2] captures the composite residues. A similar analysis can be found in [92].

3.5 Constructing integrands using spherical residues

In $4D$, performing two spherical contour integrals is equivalent to putting four propagators on-shell. This fully localizes the loop momentum. The resulting object is the sum of the leading singularities associated with cutting the four propagators. Specifying the leading singularities (LS) puts constraints on the integrand. We can construct integrands from their singularities in Feynman parameter space using this technique. In this section, we will illustrate this with a few examples at 5 and 6 points. We will use our knowledge of the leading singularities of MHV amplitudes of $\mathcal{N} = 4$ SYM to construct the one-loop integrand for the 5 and 6 point amplitudes.

3.5.1 5 point integrands

At 5 points, a generic Feynman parameter integrand is

$$I_5 = \int \langle X d^4 X \rangle \, \frac{(L.X)}{(X.Q.X)^3}$$

Since we know that the only allowed poles in momentum twistor space are of the form $\langle ABii+1\rangle = 0$, we will assume that the quadric is $Q_{ij} = \langle i-1ij-1j\rangle$. The vector in the numerator $L = (l_1, l_2, l_3, l_4, l_5)$ is to be determined from

the LS. We demand that all the LS are equal and for convenience, we set them equal to 1.

We have five unique double spherical contour integrals corresponding to the five one mass LS. We denote a double spherical residue by the four associated Feynman parameters. (Note that our Feynman parameters are labeled such that the contour (ij) is equivalent to cutting propagators $\langle ABi-1i\rangle = \langle ABj-1j\rangle = 0$. The residue corresponding to (1435) is

$$\frac{2(l_5 Q_{13}Q_{24} + l_4 Q_{13}Q_{25} - l_3 Q_{14}Q_{25} + l_2 Q_{14}Q_{35} - l_1 Q_{24}Q_{35})}{Q_{13}Q_{24}Q_{25}} \tag{3.29}$$

Demanding that this be 1 imposes a constraint on the l_i. Similarly demanding that all the other LS are equal to one leads to the numerator

$$l = 1/2\,(Q_{13}Q_{14}Q_{25},\, Q_{13}Q_{24}Q_{25},\, Q_{13}Q_{24}Q_{35},\, Q_{14}Q_{24}Q_{35},\, Q_{14}Q_{25}Q_{35}) \tag{3.30}$$

We see that the leading singularities completely determine the five point amplitude in Feynman parameter space. This should be compared with eq(3.37) which was obtained by summing all the chiral pentagons at 5 points. Note that this integrand is IR divergent and has all the divergences associated with the 5 point amplitude.

We can also construct an integrand with only one non zero LS. Demanding that I_5 has support only on the cut (1425) and has unit residue results in

$$\int \langle X d^4X\rangle \frac{Q_{14}Q_{25}}{4}\frac{(x_1 Q_{13} + x_5 Q_{35})}{(XQX)^3}$$

It is easy to recognize that this is the Feynman parametrization of

$$\int_{AB} \frac{\langle AB34\rangle}{\langle AB12\rangle\langle AB23\rangle\langle AB34\rangle\langle AB45\rangle\langle AB15\rangle}$$

3.5.2 6 POINT INTEGRANDS

A generic 6 point integrand in Feynman parameter space has a quadratic numerator.

$$I_6 = \int \langle X d^5 X\rangle \frac{X.N.X}{(X.Q.X)^4}$$

N is a symmetric, rank 2 tensor. The quadric $Q_{ij} = \langle i-1ij-1j\rangle$ as usual for a one-loop integral. We can always make a change of variables to reduce it to

$$Q = \begin{pmatrix} 0 & 0 & 1 & 1 & 1 & 0 \\ 0 & 0 & 0 & u_1 & 1 & 1 \\ 1 & 0 & 0 & 0 & u_2 & 1 \\ 1 & u_1 & 0 & 0 & 0 & u_3 \\ 1 & 1 & u_2 & 0 & 0 & 0 \\ 0 & 1 & 1 & u_3 & 0 & 0 \end{pmatrix}$$

We refer the reader to Appendix E for more details. We have three kinds of leading singularities, one-mass, two-mass easy and two-mass hard. All the two mass hard leading singularities must vanish and all the remaining ones must be equal. We normalize them to unity for convenience. For computational simplic-

ity, we choose external data

$$Z_n = \left(1, n, n^2, n^3\right), \qquad n = 1, \ldots 6$$

The constraints on N arising from specifying the leading singularities suffice to fix all but 6 of the coefficients. After implementing these constraints, the integral can be written as a sum of two terms.

$$I_6 = \int \langle X d^5 X \rangle \, \frac{(X.N_1.X + X.N_2.X)}{(X.Q.X)^4}$$

with

$$\begin{aligned}
X.N_1.X = \quad & 9\left(729x_1^2 + 810x_1x_2 + 81x_2^2 + 126x_2x_3 + 45x_3^2 + 50x_3x_4 + 5x_4^2 - 648x_2x_5\right. \\
& \left. +495x_3x_5 + 50x_4x_5 + 45x_5^2 + 810x_1x_6 + 1215x_3x_6 + 207x_4x_6 + 126x_5x_6 + 81x_6^2\right) \\
X.N_2.X = \quad & 2n_{13}x_1x_3 + 2n_{14}x_1x_4 + 2n_{24}x_2x_4 + 2n_{15}x_1x_5 - 2n_{14}x_2x_5 + 2n_{15}x_2x_5 + 18n_{24}x_2x_5 \\
& -(10n_{14}x_3x_5)/9 - (10n_{26}x_3x_5)/9 + 2n_{26}x_2x_6 - 2n_{15}x_3x_6 - 18n_{24}x_3x_6 \\
& -(2n_{13}x_4x_6)/9 + (2n_{14}x_4x_6)/9 - (2n_{15}x_4x_6)/9 - 2n_{24}x_4x_6
\end{aligned}$$

The large integers that arise in this expression are due to the choice of external data. It is tedious but possible to rewrite this expression in terms of $\langle ijkl \rangle$. The integral with numerator $X.N_2.X$ is always rational and all its double spherical residues vanish. Here, we see a clear separation in Feynman parameter space of the rational part and the transcendental part.

3.6 Feynman parametrization in planar $\mathcal{N} = 4$ SYM

In this section, we examine the one-loop MHV integrand of $\mathcal{N} = 4$ SYM. It is completely determined by its leading singularities and has a well known expression in terms of chiral pentagons.

$$\mathcal{A}^{1-\text{loop}}_{\text{MHV}} = \sum_{i<j<i} \left\{ \right. \quad \left. \right\} \quad . \tag{3.31}$$

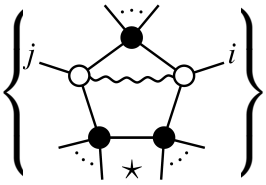

Henceforth, we denote the chiral pentagon integral shown above by (ji) which takes the following form in momentum twistor space.

$$(ji) = \int_{AB} \frac{\langle AB(j-1jj+1) \cap (i-1ii+1)\rangle \langle \star ji\rangle}{\langle ABi-1i\rangle \langle ABii+1\rangle \langle ABj-1j\rangle \langle ABjj+1\rangle \langle AB\star\rangle} \tag{3.32}$$

where $\star$ is an arbitrary bi-twistor.

There are two leading singularities, i.e. two solutions to the set of equations

$$\langle ABi-1i\rangle = \langle ABii+1\rangle = \langle ABj-1j\rangle = \langle ABjj+1\rangle = 0$$

These are the lines $Z_{[i}Z_{j]}$ and $(i-1ii+1) \cap (j-1jj+1)$. The above integrand is chiral and has vanishing support on the solution $(i-1ii+1) \cap (j-1jj+1)$. Thus an individual chiral pentagon is tailored to reproduce a leading singularity. However, it also has additional leading singularities arising from the pole $\langle AB\star\rangle$. These are not singularities of the amplitude and must cancel in the sum in eq(3.31). The cancellation of the spurious poles is not manifest and it is de-

sirable to obtain an expression for the complete amplitude which is free of spurious poles. For attempts along this line in momentum twistor space, see [65]. Here, we will derive an expression for the complete integrand in Feynman parameter space and we will see a transparent cancellation of the spurious poles. We begin with the simple case of the four point amplitude. In this case, there are 12 contributing pentagons

$$\mathcal{A}_4^{\text{MHV}} = (1,2) + (1,3) + (1,4) + \text{cyclic}$$

$$\begin{aligned}\mathcal{A}_4^{\text{MHV}} &= \int_{AB} \frac{2\langle 1234\rangle}{\langle AB12\rangle\langle AB23\rangle\langle AB34\rangle\langle AB41\rangle\langle AB\star\rangle} \times \left\{\begin{array}{l} -\langle\star 12\rangle\langle AB34\rangle + \langle\star 23\rangle\langle AB41\rangle \\ -\langle\star 34\rangle\langle AB12\rangle + \langle\star 41\rangle\langle AB23\rangle \\ +\langle AB24\rangle\langle\star 13\rangle + \langle AB13\rangle\langle\star 24\rangle \end{array}\right\} \\ &= \int \left[d^4Y\right] \langle X d^4X\rangle \frac{(Y.N)}{(W.Y)^5} \end{aligned} \tag{3.33}$$

where

$$W = x_1|12\rangle + x_2|23\rangle + x_3|34\rangle + x_4|41\rangle + x|\star\rangle$$

and N is the numerator of eq(3.33) written in embedding space. Performing the momentum integral yields the Feynman parametrization.

$$\mathcal{A}_4^{\text{MHV}} = \int \langle X d^4X\rangle \frac{1}{(W.W)^3} \left\{\begin{array}{l} -2\langle 1234\rangle x(\langle\star 13\rangle\langle\star 24\rangle - \langle X12\rangle\langle\star 34\rangle + \langle\star 23\rangle\langle\star 41\rangle) \\ +\langle 1234\rangle^2(x_1\langle\star 12\rangle + x_2\langle\star 23\rangle + x_3\langle\star 34\rangle + x_4\langle\star 41\rangle) \end{array}\right\}$$

Having obtained the Feynman parametrization, it is now straightforward to

demonstrate that $\mathcal{A}_4^{\rm MHV}$ is independent of both x and $\star$. First, note that the coefficient of x, which is quadratic in $\star$ vanishes due to a Schouten identity. The rest of the expression can be written as a total derivative.

$$\mathcal{A}_4^{\rm MHV} = -\frac{1}{2}\int \langle X d^4X\rangle \langle 1234\rangle^2 \frac{\partial}{\partial x}\left(\frac{1}{(W.W)^2}\right) = \frac{1}{2}\int \langle X d^3X\rangle \frac{1}{(\tilde{W}.\tilde{W})^2} \quad (3.34)$$

with $\tilde{W} = W\big|_{x=0}$ and the integral over the remaining Feynman parameters.

This procedure can be repeated at higher points. In each case, we find that the coefficient of the highest power of x vanishes due to a Schouten identity and the rest can be written as a total derivative which is independent of $\star$ at the boundaries. We present an expression for the 5 point amplitude. The details of the calculations are relegated to Appendix F.

$$\mathcal{A}_5^{\rm MHV} = \int \langle X d^5X\rangle \frac{\partial}{\partial x}\left(\frac{2\,n_0\,(W.\star) + \tilde{W}.\tilde{W}\,n_1 + 3\,(W.\star)n_1 x}{(\tilde{W}.\tilde{W})^3 (W.\star)^2}\right) \quad (3.35)$$

Here n_0 and n_1 are the coefficients of x^0 and x in eq(F.2). As before, the integral localizes to the boundaries where it is independent of the bi-twistor $\star$ and is given by

$$\mathcal{A}_5^{\rm MHV} = \int \langle X d^4X\rangle \frac{n}{d^3} \quad (3.36)$$

$$n = (\langle 1234\rangle\langle 1245\rangle\langle 1235\rangle x_1 + \langle 1234\rangle\langle 2345\rangle\langle 1235\rangle x_2 + \langle 1345\rangle\langle 1234\rangle\langle 2345\rangle x_3$$
$$+\langle 1345\rangle\langle 2345\rangle\langle 1245\rangle x_4 + \langle 1345\rangle\langle 1245\rangle\langle 1235\rangle x_5) \tag{3.37}$$

$$d = \tilde{W}.\tilde{W} \qquad \text{where } \tilde{W} = x_1|12\rangle + x_2|23\rangle + x_3|34\rangle + x_4|45\rangle + x_5|15\rangle$$

It is easy to see that eq(3.34) and eq(3.37) have the correct singularity structure. The presence of linear terms in the numerator of the 5 point amplitude implies the presence of IR divergences as expected. We can obtain similar expressions for the integrand at higher points. However, this has to be done on a case by case basis and we don't have a general expression.

3.7 Outlook

In this chapter we have explored the singularity structure of one-loop Feynman parameter integrands and their geometry. The spherical residue captures the notion of discontinuity and the double spherical residue that of leading singularities. Feynman parameter integrands that arise from Feynman graphs satisfy special constraints and we saw that the spherical contour remarkably preserves these properties. We have provided an algebraic description of spherical residues and given formulae which can be use to compute both them as algebraic mappings. The double spherical residue was exploited to construct Feynman parameter integrands. Composite residues in momentum space captures the leading IR divergences. The scaling procedure introduced in Section[3.3.2] to extract the leading IR divergences shows that the notion of composite residues exists even in Feynman parameter space.

The obvious next step is to extend the results of this chapter beyond one loop. It would be interesting to explore the extraction of the leading IR divergence of a two loop graph by a similar method. For some details on higher loop Feynman parametrization and IR divergences, we draw the reader's attention to [93]. While extraction of the leading IR behaviour is fascinating in its own right, it could also prove useful in calculating the cusp anomalous dimension of $\mathcal{N} = 4$ SYM which has been a topic of some interest in the past few years [80–83]. The knowledge of the relationship between cuts of Feynman graphs and discontinuities is intensely studied in momentum space (see [94, 95]). In Feynman parameter space, this amounts to an understanding of the relationship between between spherical residues and leading singularities at higher loops. This is an essential ingredient in attempting any construction of higher loop integrands. While these are some of the immediate pragmatic questions of general interest, some features of Feynman parameter integrands of $\mathcal{N} = 4$ SYM raise more provocative questions.

Section[3.6] shows the explicit independence of MHV amplitudes on spurious poles at 4 and 5 points. While this cancellation is expected even in momentum twistor space, it is simpler to observe in Feynman parameter space and isn't the consequence of a complicated identity satisfied by the external data. Another miraculous feature, seen from the 4 and 5 point one-loop integrands, eq(3.34) and eq(3.37), is that they are both manifestly positive (for positive external data). Positivity of the integrands in momentum twistor space was observed in [65]. There the positivity stemmed from the more complicated identity $\langle AB\bar{i}\bar{j}\rangle > 0$ for configurations of Z_i in the amplituhedron. Here, $\langle ijkl\rangle > 0$ for $i < j < k < l$ suffices to guarantee positivity. It is crucial to check if these fea-

tures persist beyond one loop. It would also be interesting to analyze the positivity properties of the log of the amplitude and the n-point Ratio function [96] in Feynman parameter space.

The existence of these properties seems to suggest that Feynman parameter space more than an auxiliary space introduces to aid in integration and is a natural space to study loop integrands. In the last decade, a rich geometric structure underlying scattering amplitudes of $\mathcal{N} = 4$ SYM has been uncovered [9, 16] and positive geometry [29] is at the heart of it all. It is a natural to wonder if the properties seen here are a reflection of this structure. If this were true, it suggests that Feynman parameter space has an extremely rich geometry and the properties observed thus far are only the tip of the iceberg.

4

On-shell Electroweak sector and the Higgs mechanism

4.1 Introduction

Quantum fields, path integrals and Lagrangians have been a cornerstone of 20th century theoretical physics. They have been used to describe a variety of natural phenomena accurately. Yet, it is becoming increasingly apparent that

these mathematical tools are both inefficient and insufficient. They obscure the presence of a deeper, underlying structure, particularly of scattering amplitudes in quantum field theories. The field of scattering amplitudes has undergone a paradigm shift in the past three decades. This was sparked by the discovery of the stunning simplicity of the tree-level gluon scattering amplitudes in [1, 2]. The simplicity of these amplitudes was revealed due to the use of helicity spinors, $(\lambda_\alpha, \tilde{\lambda}_{\dot{\alpha}})$ which correspond to the physical degrees of freedom of massless particles - helicity. The forbidding complexity of the Feynman diagram based calculation of tree level gluon scattering amplitudes is now understood to be an artifact of the unphysical degrees of freedom introduced by gauge redundancy. These unphysical degrees of freedom are necessary to package the physical degrees of freedom into local quantum fields in a manner consistent with Poincaré invariance [97]. The simplicity of these amplitudes fueled the development of a variety of "on-shell" techniques for computing scattering amplitudes involving massless particles. These methods do not rely on Feynman diagrams, do not suffer from gauge redundancies and do not invoke virtual particles. For an overview of these methods, see [98–102] and the references therein. However, most of this progress was limited to amplitudes involving only massless particles.

Since helicity spinors correspond to the physical degrees of freedom of massless particles, it is natural to attempt to find variables akin to these for massive particles. The physical degrees of freedom of massive particles correspond to the little group $SU(2)$ [103]. Some early generalizations can be found in [104–111]. However, the little group covariance was not manifest in these generalizations until the introduction of Spin-spinors (or massive spinor-helicity variables) in

[112]. These variables $(\lambda_\alpha^I, \tilde{\lambda}_{\dot{\alpha}}^I)$ which carry both little group indices and Lorentz indices and make the little group structure of amplitudes manifest. Information about all the $(2S+1)$ spin components of each particle is packaged into compact, manifestly Lorentz invariant expressions. Amplitudes written in terms of these variables are directly relevant to physics. This is in contrast to a Feynman diagram based computation which involves an intermediate object with Lorentz indices which must then be contracted with polarization tensors which carry the little group indices. For some interesting applications of these variables, including black holes, supersymmetric theories and double copy constructions, see [113–123].

One of the biggest successes of path integrals and the Lagrangian formulation is the development of effective field theory and the Higgs mechanism. Recently, there has been a lot of focus towards the development of on-shell methods for effective field theory and an on-shell understanding of the structure of the Standard Model (SM) [124–129]. It is worth pointing out that the aims of [124] are similar to ours but differs in the strategy employed to achieve these aims. Specifically, the authors aim to derive the constraints of electroweak symmetry breaking by specifying the IR structure of the SM and imposing perturbative unitarity. In contrast, we will derive these constraints by specifying both the UV and IR behaviour and demanding that the low energy theory has a smooth high energy limit. A completely on-shell description of the Higgs mechanism was outlined in [112] for the abelian and non-abelian gauge theories. The conventional understanding of the Higgs mechanism involves a scalar field acquiring a vacuum expectation value and vector bosons becoming massive by "eating" the goldstone modes arising from spontaneously broken symmetry. However,

the on-shell description has no mention of scalar fields, potentials and vacuum expectation values. Nevertheless, it reproduces all of the same physics. Additionally, well known results like the Goldstone Boson equivalence theorem become trivial consequences of the high energy limits of our expressions. From an amplitudes perspective, it is more natural to think of the Higgs mechanism as a unification of the massless amplitudes in the UV into massive amplitudes in the IR. In this chapter, we will focus on computing scattering amplitudes in the bosonic electroweak sector of the standard model and describing the Higgs mechanism and electroweak symmetry breaking using a completely on-shell language.

The chapter is structured as follows. We begin with a brief review of the little group, spin-spinors and their properties in Section [4.2]. We focus on constructing three particle amplitudes in the IR in Section [4.3.1] and the UV in Section [4.3.2]. In Section [4.3.4], we compute the high energy limits of the three particle amplitudes in the IR and demand that they are consistent with the three point amplitudes in the UV. This gives us the all the standard relations between the coupling constants, the masses of the Z and $W^{\pm}$ and the Weinberg angle θ_w. We also see the emergence of the custodial SO(3) symmetry in the limit in which the hypercharge coupling vanishes. Finally, in Section [4.4], we construct 4 point amplitudes in the IR by gluing together the three point amplitudes found before. We enunciate the details involved in the gluing process. We will also discover that demanding that these amplitudes have a well defined high energy limit imposes constraints on the structure of the theory.

4.2 Scattering amplitudes and the little group

4.2.1 Helicity spinors and spin-spinors

In this section, we briefly review some aspects of the on-shell approach to constructing scattering amplitudes. We will review the formalism of spin-spinors introduced in [112] whilst highlighting some features important for this chapter. One particle states are irreducible representations of the Poincare' group. They are labeled by their momentum and a representation of the little group. If the particle is charged under any global symmetry group, appropriate labels must be appended to these. In (3+1) spacetime dimensions, the little groups for massless and massive particles are $SO(2)$ and $SO(3)$ respectively.
Representations of the massless little group, $SO(2) = U(1)$ can be specified by an integer corresponding to the helicity of the massless particle. A massless one particle state is thus specified by its momentum and helicity. Under a Lorentz transformation Λ,

$$|p, h, \sigma\rangle \to w^{-2h}|\Lambda p, h, \sigma\rangle \,, \tag{4.1}$$

where σ are labels of any global symmetry group and w has the same meaning as in [97] and [112]. It is useful to introduce elementary objects $\lambda_\alpha, \tilde{\lambda}_{\dot{\alpha}}$ which transform under the little group as

$$\lambda_\alpha \to w^{-1}\lambda_\alpha \qquad \text{and} \qquad \tilde{\lambda}_{\dot{\alpha}} \to w\tilde{\lambda}_{\dot{\alpha}} \,. \tag{4.2}$$

We can use these objects to build representations with any value of h. The nat-

ural candidates for these elementary objects are the spinors which decompose the null momentum $p_{\alpha\dot{\alpha}} \equiv p_\mu \sigma^\mu_{\alpha\dot{\alpha}}$. We have

$$p_{\alpha\dot{\alpha}} = \lambda_\alpha \tilde{\lambda}_{\dot{\alpha}} \equiv |\lambda\rangle_\alpha [\tilde{\lambda}|_{\dot{\alpha}} \,. \tag{4.3}$$

Throughout the chapter we will find it convenient to make use of the following notation,

$$\lambda_\alpha \equiv |\lambda\rangle \qquad \tilde{\lambda}_{\dot{\alpha}} \equiv [\tilde{\lambda}| \qquad \lambda^\alpha \equiv \langle\lambda| \qquad \tilde{\lambda}^{\dot{\alpha}} \equiv |\tilde{\lambda}] \,.$$

For any two null momenta p_1, p_2, we can form two Lorentz invariant combinations of these spinors,

$$\langle 12\rangle \equiv \epsilon^{\alpha\beta}(\lambda_1)_\beta(\lambda_2)_\alpha \qquad\qquad [12] \equiv \epsilon^{\dot{\alpha}\dot{\beta}}(\tilde{\lambda}_1)_{\dot{\alpha}}(\tilde{\lambda}_2)_{\dot{\beta}}. \tag{4.4}$$

The massive little group is $SO(3) = SU(2)$. Its representations are well known and can be specified by the value of the Casimir operator which is restricted to values $S(S+1)$, where S is defined as the spin of the particle. The spin S representation is $2S+1$ dimensional. A massive one-particle state of spin S thus transforms as a tensor of rank 2S under $SU(2)$.

$$|p, I_1, \ldots I_{2S}, \sigma\rangle \to W_{I_1 J_1} \ldots W_{I_{2S} J_{2S}} |\Lambda p, J_1, \ldots J_{2S}, \sigma\rangle \tag{4.5}$$

The elementary objects in this case are the spinors of $SU(2)$, which are referred

to as spin-spinors. These transform as

$$\boldsymbol{\lambda}^I_\alpha \to \left(W^{-1}\right)^I_J \boldsymbol{\lambda}^J_\alpha \qquad \tilde{\boldsymbol{\lambda}}^I_\alpha \to W^I_J \, \tilde{\boldsymbol{\lambda}}^J_\alpha \,. \tag{4.6}$$

Higher representations can be built by taking tensor products of these. Decomposing the rank 2 momentum, similar to eq.(4.3), yields the requisite spinors,

$$p_{\alpha\dot{\alpha}} = \epsilon_{JI} |\boldsymbol{\lambda}\rangle^I [\tilde{\boldsymbol{\lambda}}|^J = \epsilon_{JI} \boldsymbol{\lambda}^I_\alpha \tilde{\boldsymbol{\lambda}}^J_{\dot{\beta}} \,. \tag{4.7}$$

From this we have

$$\det(p) = \det(\epsilon)\, \det(\lambda)\, \det(\tilde{\lambda}). \tag{4.8}$$

Using the fact that $\det(\epsilon) = 1$ and $\det(p) = p^2 = m^2$, we have $\det(\lambda)\, \det(\tilde{\lambda}) = m^2$. For the rest of the chapter, we will set $\det(\lambda) = \det(\tilde{\lambda}) = m^*$. We will find it convenient to suppress the little group indices on the spin-spinors. We do this according to the convention in eq. (G.2). Finally, we can construct Lorentz invariants out of spin-spinors corresponding to two massive momenta p_1, p_2 similar to eq.(4.4).

$$\langle \mathbf{12} \rangle^{IJ} \equiv \epsilon^{\alpha\beta} (\boldsymbol{\lambda}_1)^I_\beta (\boldsymbol{\lambda}_2)^J_\alpha \qquad\qquad [\mathbf{12}]^{IJ} \equiv \epsilon^{\dot{\alpha}\dot{\beta}} (\tilde{\boldsymbol{\lambda}}_1)^I_{\dot{\alpha}} (\tilde{\boldsymbol{\lambda}}_2)^J_{\dot{\beta}}. \tag{4.9}$$

*There is more freedom to set $\det \lambda = M$ and $\det \tilde{\lambda} = \tilde{M}$ such that $M\tilde{M} = m^2$, but for our purposes $M = \tilde{M} = m$ suffices.

4.2.2 Scattering amplitudes as little group tensors

Scattering amplitudes are defined as the overlap of in and out states. We have

$$\mathcal{M}(p_1, \rho_1 \dots p_n, \rho_n) = {}_{\text{out}}\langle p_1, \rho_1, \dots p_n, \rho_n | 0 \rangle_{\text{in}}$$

where we are assuming that all particles are outgoing. $\rho = (h, \sigma)$ for massless particles (eq.(4.1)) and $\rho = (\{I_1, \dots I_{2S}\}, \sigma)$ for massive ones (eq.(4.5)). Translation invariance allows us to pull out a delta function which imposes momentum conservation

$$\mathcal{M}(p_1, \rho_1 \dots p_n, \rho_n) = \delta^4(p_1 + \dots p_n) M(p_1, \rho_1, \dots, p_n, \rho_n) \tag{4.10}$$

Assuming that the asymptotic multi-particle states transform under Lorentz transformations as the tensor products of one-particle states, we have the following transformation law for the function $M(p_1, \rho_1, \dots, p_n, \rho_n)$ under a Lorentz transformation Λ.

$$M(p_a, \rho_a) \to \prod_a \left(D_{\rho_a \rho'_a}(W) \right) M((\Lambda p)_a, \rho'_a) \tag{4.11}$$

where $D_{\rho_a \rho'_a}(W) = \delta_{\sigma, \sigma'_a} \delta_{h_a, h'_a} w^{-2h_a}$ for massless particles and $D_{\rho_a \rho'_a}(W) = \delta_{\sigma, \sigma'_a} W^{I_1}_{I'_1} \dots W^{I_{2S}}_{I'_{2S}}$ for massive ones. As an example, we display the transformation law for a 4-particle amplitude where particle 1 is massive with spin 1, particle 2 is massless with helicity 5/2, particle 3 is massless with helicity -2 and

particle 4 is massive with spin 0.

$$M^{\{I_1,I_2\},\{5/2\},\{-2\},\{0\}}(p_1,p_2,p_3,p_4) \to (W_1)^{I_1}_{I_1'}\ (W_1)^{I_2}_{I_2'}\ w_2^{-5}\ w_3^4\ M^{\{I_1',I_2'\},\{5/2\},\{-2\},\{0\}}(p_1,p_2,p_3,p_4). \tag{4.12}$$

Thus, objects constructed from helicity spinors and spin spinors can correspond to scattering amplitudes only if they are Lorentz invariant and have the above transformation law under the little group. This imposes restrictions on the functional forms of objects that make up scattering amplitudes. Indeed, three point amplitudes involving all massless particles are completely fixed by this restriction. At three points, we have,

$$2p_1.p_2 = \langle 12\rangle[12] = 0 \qquad 2p_2.p_3 = \langle 23\rangle[23] = 0 \qquad 2p_3.p_1 = \langle 31\rangle[31] = 0$$

We must choose either the λ or the $\tilde{\lambda}$ to be proportional to each other. The two solutions are the MHV configuration

$$\tilde{\lambda}_1 = \langle 23\rangle\tilde{\zeta} \qquad \tilde{\lambda}_2 = \langle 31\rangle\tilde{\zeta} \qquad \tilde{\lambda}_3 = \langle 12\rangle\tilde{\zeta} \tag{4.13}$$

and the anti-MHV configuration

$$\lambda_1 = [23]\zeta \qquad \lambda_2 = [31]\zeta \qquad \lambda_3 = [12]\zeta \tag{4.14}$$

Using these, one can show that the three point amplitudes can only take the following form.

$$\begin{aligned} M^{h_1 h_2 h_3} &= g\,\langle 12\rangle^{h_1+h_2-h_3}\langle 23\rangle^{h_2+h_3-h_1}\langle 31\rangle^{h_3+h_1-h_2}\,, \qquad \text{if} \quad h_1+h_2+h_2>0 \\ &= \tilde{g}\,[12]^{h_3-h_1-h_2}[23]^{h_1-h_2-h_3}[31]^{h_2-h_3-h_1}\,, \qquad \text{if} \quad h_1+h_2+h_2>0\,. \end{aligned} \tag{4.15}$$

In cases involving one or more massive particles, Lorentz invariance and little group covariance are not sufficient to completely fix the amplitude. However, they narrow down the form of the amplitude to a finite number of terms. For an exhaustive analysis, we refer the reader to [112] and [130, 131]. In this chapter, we will discuss only the amplitudes relevant to us.

4.2.3 The high energy limit of spin-spinors

When particle energies are much higher than their masses, it is intuitive to treat them as massless. We can formalize this by expanding the spin-spinors in a convenient basis in little group space.

$$\begin{aligned} \lambda^I_\alpha = \lambda_\alpha \zeta^{-I} + \eta_\alpha \zeta^{+I} &= \sqrt{E+p}\,\zeta^+_\alpha(p)\,\zeta^{-I}(k) + \sqrt{E-p}\,\zeta^-_\alpha(p)\,\zeta^{+I}(k) \\ \tilde{\lambda}_{\dot\alpha I} = \tilde{\lambda}_{\dot\alpha}\zeta^+_I - \tilde{\eta}_{\dot\alpha}\zeta^-_I \quad &= \sqrt{E+p}\,\tilde{\zeta}^-_\alpha(p)\,\zeta^+_I(k) - \sqrt{E-p}\,\tilde{\zeta}_{\dot\alpha}(p)\,\zeta^-_I(k) \end{aligned} \tag{4.16}$$

where $\lambda, \tilde{\lambda}$ are the helicity spinors, $\zeta^{\pm I}$ are eigenstates of spin 1/2 along the momentum. We give explicit expressions for all objects involved are in Appendix [G]. Here, we just note that $\eta_\alpha, \tilde{\eta}_{\dot\alpha} \propto \sqrt{E-m} = m + \mathcal{O}(m^2)$. Taking the high energy limit corresponds to taking $m/E \to 0$. In this limit, the spin-

spinors reduce to massless helicity ones. Finally, it should be pointed out that we must take special care while taking the high energy limit of 3-point amplitudes. Owing to the special three point kinematics, factors like $\langle \mathbf{12} \rangle$ or $[\mathbf{12}]$ can tend to zero in the high energy limit.

4.3 Three particle amplitudes

3-particle amplitudes are the fundamental building blocks of scattering amplitudes. In this chapter, we are interested in analyzing the bosonic content of the standard model both in the UV and IR. The spectrum in the UV is comprised solely of massless particles. The three point amplitudes are completely determined by Poincare' invariance and little group scaling as outlined in Section [4.2]. The form of these amplitudes was given in eq.(4.15). We will use this formula to write down all the relevant 3-particle amplitudes in Section [4.3.2]. All the amplitudes in the UV obey the $SU(2)_L \times U(1)_Y$ symmetry.

The spectrum in the IR consists of massive particles and a single massless vector. 3-particle amplitudes involving massive particles are not completely fixed. They can have several contributing structures. In Section [4.3.1], we will write down all the relevant amplitudes. The amplitudes in the IR obey only a $U(1)_{\text{EM}}$ symmetry.

Finally, we will demand that the high energy limit of the IR amplitudes is consistent with the amplitudes in the UV. We will find that this consistency is possible only if the masses of particles in the IR are related in a specific way. These turn out to be the usual relations involving the Weinberg angle.

4.3.1 The IR

The spectrum in the IR consists of the following particles.

- Three massive spin 1 bosons (W^+, W^-, Z) which have masses (m_W, m_W, m_Z) and charges $(+, -, 0)$ respectively under a global symmetry group $U(1)_{EM}$. Note that W^+ and W^- are eigenstates of the $U(1)_{\rm EM}$ generator. They must have equal mass as they are related by charge conjugation.
- One massless spin 1 boson, the photon, γ which is not charged under the $U(1)_{EM}$.
- One massive scalar, the higgs, h which is also uncharged under $U(1)_{EM}$.

The only symmetry of the IR is the $U(1)_{\rm EM}$. We will now discuss all the relevant three point amplitudes in the IR. Owing to the existence of various identities amongst the spin-spinors, each amplitude can be written in a multitude of different ways. In many of the cases below, we have chosen particularly convenient ways of writing them. Different forms of the three point amplitudes lead to different expressions for four point amplitudes. The difference between these are contact terms that can be fixed by imposing other constraints on the amplitude. While the form of the contact term will depend on the form of the three point amplitudes used, the final amplitude will be the same. We will elaborate on these comments in the appropriate places below. In the rest of the chapter we will follow the convention that the bold lines in the diagrams correspond to massive particles while the unbolded lines correspond to massless ones.

$\mathbf{W^+W^-Z}$

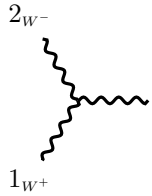

$$= \frac{e_W}{m_W^2 m_Z}\left[\langle\mathbf{12}\rangle[\mathbf{12}]\langle\mathbf{3}|p_1 - p_2|\mathbf{3}] + \text{cyc.}\right] \tag{4.17}$$

This is a form of the three point amplitude that is chosen to suit our needs. It should be noted that it can be reduced to a combination of $<>$ and $[\,]$. As an example, consider the first term in the above equation which can be re-written as follows,

$$\langle\mathbf{12}\rangle[\mathbf{12}]\langle\mathbf{3}|p_1 - p_2|\mathbf{3}\rangle = 2\left(m_1[\mathbf{12}]\langle\mathbf{23}\rangle[\mathbf{31}] - m_2[\mathbf{12}][\mathbf{23}]\langle\mathbf{31}\rangle + m_3[\mathbf{12}]\langle\mathbf{23}\rangle\langle\mathbf{31}\rangle\right) ,$$

where we made use of the Schöuten identity $\langle\mathbf{12}\rangle\mathbf{3} + \langle\mathbf{23}\rangle\mathbf{1} + \langle\mathbf{31}\rangle\mathbf{2} = 0$.

$\mathbf{W^+W^-\gamma}$

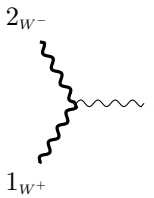

$$= e\; x_{12}^{+}\langle\mathbf{12}\rangle^2 \tag{4.18}$$

We discuss other forms of writing the same vertex in Appendix [H].

ZZh

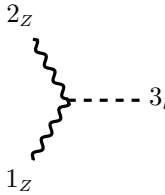

$$= \frac{e_{HZZ}}{m_Z}\langle\mathbf{12}\rangle[\mathbf{12}] + \frac{\mathcal{N}_1}{m_Z}\left(\langle\mathbf{12}\rangle^2 + [\mathbf{12}]^2\right) \tag{4.19}$$

$\mathbf{W^+W^-h}$

$$= \frac{e_{WWH}}{m_W}\langle \mathbf{12}\rangle[\mathbf{12}] + \frac{\mathcal{N}_2}{m_W}\left(\langle \mathbf{12}\rangle^2 + [\mathbf{12}]^2\right) \tag{4.20}$$

We will set $\mathcal{N}_1 = \mathcal{N}_2 = 0$ in what follows since these terms yield four point amplitudes which grow as E^2 where E is the center-of-mass energy.

---

hhh

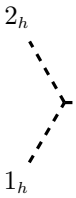

$$= e_{HHH}\, m_h \tag{4.21}$$

4.3.2 The UV

The UV spectrum of the electroweak sector of the standard model consists of the following

- One massless spin-0 particle $\Phi = \{\phi_1, \phi_2, \phi_3, \phi_4\}$ with four real degrees of freedom in the fundamental representation of $\mathrm{SO}(4) = \mathrm{SU}(2)_L \times \mathrm{SU}(2)_R$.
- One massless spin-1 particle B with charge $\frac{1}{2}$ under a global $\mathrm{U}(1)_Y$ sym-

metry group.

- Three massless spin-1 particles (W_1, W_2, W_3), in the adjoint representation of $\mathrm{SU}(2)_L$. These are not charged under the group $U(1)_Y$. In order to facilitate easy comparison to the massive particles in the IR, we will work with particle states $W^{\pm} = \frac{1}{\sqrt{2}}(W^1 \pm iW^2)$ which are eigenstates of the $U(1)_{\mathrm{EM}}$ symmetry in the IR.

The electroweak sector has an $SU(2)_L \times U(1)_Y$ symmetry. The generators of these symmetries are related to the generators of $SO(4)$ listed in Appendix [J] as follows.

$$T^1 \equiv X^1 \qquad T^2 \equiv X^2 \qquad T^3 = X^3 \qquad T^B = Y^3\,. \tag{4.22}$$

The generator of $U(1)_{\mathrm{EM}}$, which we denote by Q, can be written as a linear combination of the generators of the UV

$$e\,Q = \alpha\, g\, T^3 + \beta\, g'\, T^B, \tag{4.23}$$

where e is $U(1)_{\mathrm{EM}}$ coupling. Since $T^{\pm} = \frac{1}{\sqrt{2}}(T^1 \pm iT^2)$ are eigenstates of Q, we are free to work with the states $W^{\pm}$ in the UV. We will now list all the relevant amplitudes in the UV. The superscripts on the particles indicate the corresponding helicities.

$\mathbf{W^+W^-W^3}$

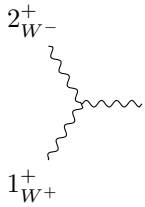

$$= g\,\frac{\langle 12\rangle^3}{\langle 23\rangle\langle 31\rangle} \tag{4.24}$$

$\mathbf{W^+\Phi\Phi}$

$$= g(T^-)_{ij}\frac{\langle 12\rangle\langle 31\rangle}{\langle 23\rangle} \tag{4.25}$$

$\mathbf{W^-\Phi\Phi}$

$$= g(T^+)_{ij}\frac{\langle 12\rangle\langle 23\rangle}{\langle 31\rangle} \tag{4.26}$$

$\mathbf{W^3\Phi\Phi}$

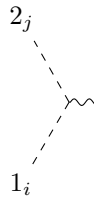

$$= g(T^3)_{ij}\frac{\langle 23\rangle\langle 31\rangle}{\langle 12\rangle} \tag{4.27}$$

These amplitudes must be proportional to a generator $T^{\{+,-,3\}}$ of the SU(2). For explicit forms of these generators, see Appendix [J].

$\mathbf{B\Phi\Phi}$

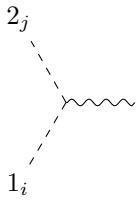

$$= g'(T^B)_{ij}\frac{\langle 23\rangle\langle 31\rangle}{\langle 12\rangle} \tag{4.28}$$

The above list doesn't contain any WWB or WBB amplitudes since the W's are not charged under the $U(1)_Y$. Note that all the above amplitudes involve particles whose helicities, h_1, h_2, h_3 are such that $\sum h_i > 0$. The amplitudes with $\sum h_i < 0$ are given by flipping $< > \to [\,]$.

4.3.3 The HE Limit of the IR

All the amplitudes in the IR listed above have one or more factors of $\frac{1}{m}$. At first glance, this seems to suggest that they blow up in the UV and cannot be matched onto any 3-particle amplitude of massless particles. However, we will see that all these factors of inverse mass drop out when we take the special 3 particle kinematics into account and carefully take the high energy limit. Many of these high energy limits are worked out in [112] and [130]. We present them here in a form compatible with our conventions. For each massive leg, in order to take the high energy limit we must first specify the component which we are interested in.

$\mathbf{W^+W^-Z}$

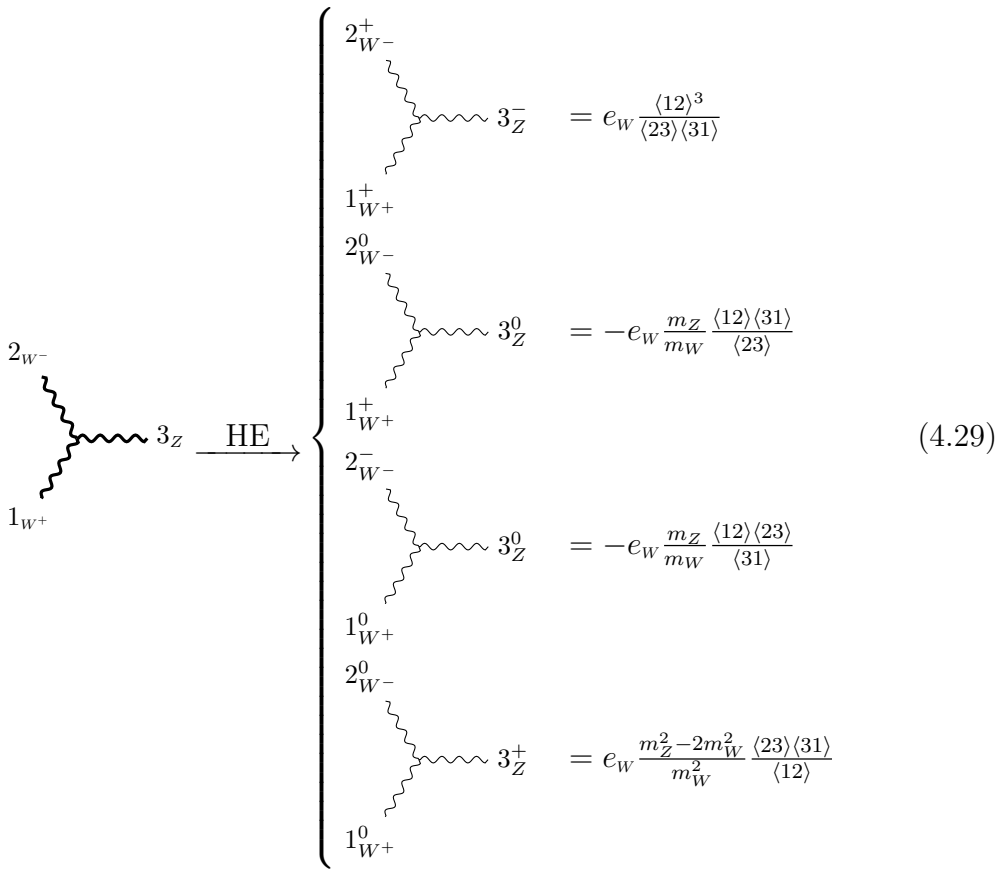

(4.29)

Amplitudes with one longitudinal mode and two transverse modes vanish in the high energy limit.

$$\mathbf{W^+W^-\gamma}$$

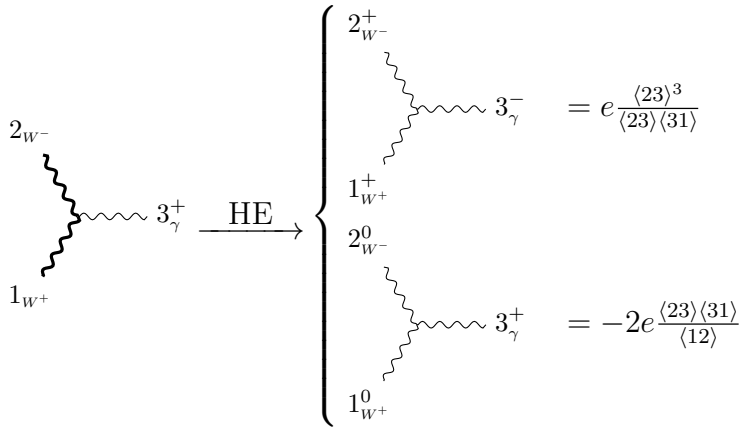

(4.30)

$\mathbf{W^+W^-h}$ and **$\mathbf{ZZh}$**

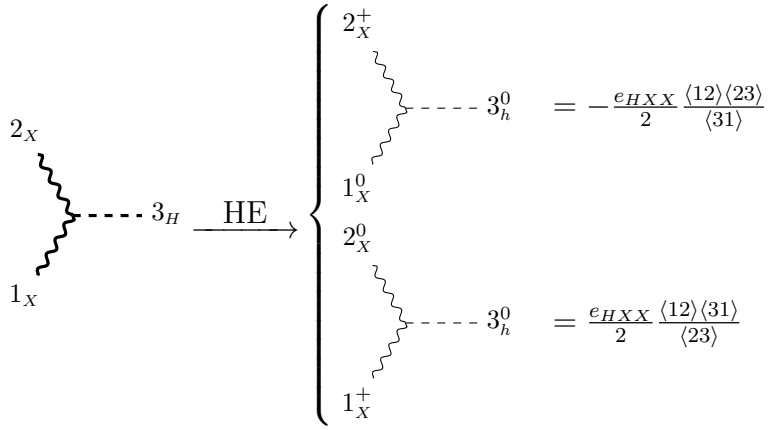

(4.31)

where $X = W, Z$. The high energy limit of amplitudes involving only one transverse mode vanish. This is consistent with the fact that we have no $WW\Phi$ amplitudes in the UV. Furthermore, the high energy limit of the all longitudinal component of these amplitudes also vanish implying that there is no Φ^3 interaction in the UV.

hhh

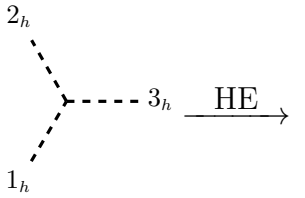

(4.32)

The hhh amplitude vanishes in the HE limit due to the explicit factor of m_h. This is again consistent with the fact that there is no Φ^3 amplitude in the UV.

4.3.4 UV-IR consistency

Thus far, we have specified the structure of the IR which consists of the interactions among the $W^{\pm}, Z, \gamma$ and h which preserve the $U(1)_{\rm EM}$ symmetry and the structure of the UV which consists of the interactions among the W^a, B, Φ which preserve the $SU(2)_L \times U(1)_Y$ symmetry. We must now ensure that they are compatible with each other. We take the high energy limit of the IR amplitudes and demand that they are equal to the appropriate amplitudes in the UV. We refer to this process as 'UV-IR matching'. This imposes many constraints and determines the couplings in the IR in terms of those in the UV. Furthermore, it also imposes constraints on the masses of the particles in the IR. To begin with, we must relate the degrees of freedom in the IR to the ones in the UV.

We assume that they are related by the following orthogonal transformation

$$\begin{pmatrix} W^+ \\ W^- \\ Z \\ \gamma \end{pmatrix} = \begin{pmatrix} \mathcal{O}_{++} & \mathcal{O}_{+-} & \mathcal{O}_{+3} & \mathcal{O}_{+B} \\ \mathcal{O}_{-+} & \mathcal{O}_{--} & \mathcal{O}_{-3} & \mathcal{O}_{-B} \\ \mathcal{O}_{Z+} & \mathcal{O}_{Z-} & \mathcal{O}_{Z3} & \mathcal{O}_{ZB} \\ \mathcal{O}_{\gamma+} & \mathcal{O}_{\gamma-} & \mathcal{O}_{\gamma 3} & \mathcal{O}_{\gamma B} \end{pmatrix} \begin{pmatrix} W^+ \\ W^- \\ W^3 \\ B \end{pmatrix} \tag{4.33}$$

Clearly, we must have $\mathcal{O}_{+-} = \mathcal{O}_{+3} = \mathcal{O}_{+B} = \mathcal{O}_{-+} = \mathcal{O}_{-3} = \mathcal{O}_{-B} = 0$. This is a result of working with the same states in the UV and IR. Orthogonality demands that the matrix be block diagonal, and so we have the simpler relation

$$\begin{pmatrix} Z \\ \gamma \end{pmatrix} = \begin{pmatrix} \cos\,\theta_w & -\sin\,\theta_w \\ \sin\,\theta_w & \cos\,\theta_w \end{pmatrix} \begin{pmatrix} W^3 \\ B \end{pmatrix} \tag{4.34}$$

for some unknown angle θ_w. All the massive particles in the IR have longitudinal components which must be generated by some some linear combination of the scalars in the UV. We assume that

$$W^{+^{(0)}} = U_{W^+ i}\Phi_i \qquad W^{-^{(0)}} = U_{W^- i}\Phi_i \qquad Z^{(0)} = U_{Zi}\Phi_i \tag{4.35}$$

The remaining linear combination of the components of Φ, $h = U_{hi}\Phi_i$ has an independent existence. Indeed, it is well known that its presence is crucial for the theory to have good UV behaviour. The high energy limit of each of the three point amplitudes in the IR must be equal to some combination of the amplitudes in the UV. This determines the masses in the IR in terms of the couplings in the UV. It also imposes some constraints on the couplings in the UV. All the constraints arising from eq.(4.29) - eq.(4.31) are determined below.

$\mathbf{W^+W^-Z}$

There are a total of 27 components to the W^+W^-Z amplitude corresponding to the $(+,-,0)$ spin component of each particle. Amplitudes with just one longitudinal mode all vanish in the high energy limit. This is consistent with the fact that there are no $WW\Phi$, $WB\Phi$, $BB\Phi$ amplitudes in the UV. The independent constraints arising from the remaining components are given below. Recall that the superscript on the particle is its helicity. These are also listed at the top of each diagram for particles 1, 2 and 3 respectively.

$(++-)$

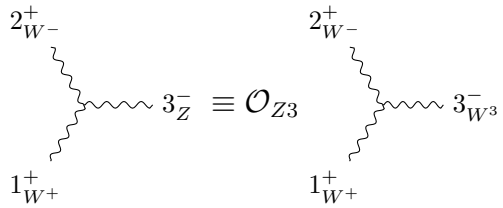

Using the expressions from eq.(4.29) and eq.(4.24), we get

$$e_W \frac{\langle 12\rangle^3}{\langle 23\rangle\langle 31\rangle} = g\,\mathcal{O}_{Z3}\,\frac{\langle 12\rangle^3}{\langle 23\rangle\langle 31\rangle} \implies e_W = g\cos\theta_w\,. \tag{4.36}$$

The absence of a W^+W^-B interaction in the UV means that there is no term proportional to $\mathcal{O}_{ZB}$ on the RHS.

$$(0\,0\,+)$$

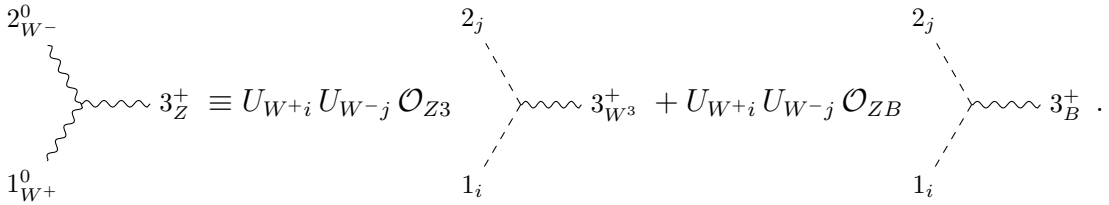

Using eq.(4.29), eq.(4.27) and eq.(4.28) in the above gives,

$$\begin{aligned} e_{_W}\frac{m_{_Z}^2-2m_{_W}^2}{m_{_W}^2}\frac{\langle 23\rangle\langle 31\rangle}{\langle 12\rangle} &= U_{W^+i}\,\left(g\,\mathcal{O}_{Z3}\,T^3_{ij}+g'\,\mathcal{O}_{ZB}\,T^B_{ij}\right)U_{W^-j}\frac{\langle 23\rangle\langle 31\rangle}{\langle 12\rangle} \\ \implies e_{_W}\frac{m_{_Z}^2-2m_{_W}^2}{m_{_W}^2} &= U_{W^+i}\left(g\cos\,\theta_w\,T^3_{ij}-g'\sin\,\theta_w\,T^B_{ij}\right)U_{W^-j}\,. \end{aligned} \tag{4.37}$$

$$(+\,0\,0)$$

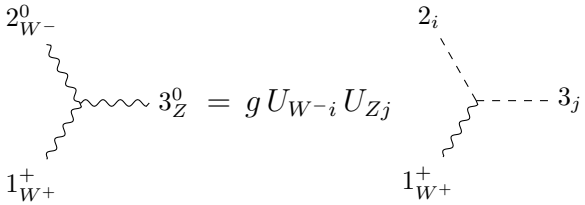

Again, eq.(4.29) and eq.(4.25) give

$$
\begin{aligned}
-e_W \frac{m_Z}{m_W} \frac{\langle 12\rangle\langle 31\rangle}{\langle 23\rangle} &= g\, U_{W^-i}\, T^-_{ij}\, U_{Zj}\, \frac{\langle 12\rangle\langle 31\rangle}{\langle 23\rangle} \\
\implies -e_W \frac{m_Z}{m_W} &= g\, U_{W^-i}\, T^-_{ij}\, U_{Zj}\,. \qquad (4.38)
\end{aligned}
$$

$\mathbf{W^+W^-\gamma}$

Since the photon is massless in the IR, the $W^+W^-\gamma$ amplitude only has 18 components. This leads to the following constraints.

$(++-)$

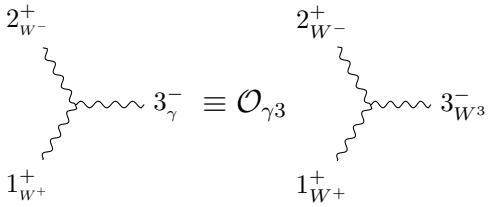

$$e_W \frac{\langle 12\rangle^3}{\langle 23\rangle\langle 31\rangle} = g\,\mathcal{O}_{\gamma\,3}\frac{\langle 12\rangle^3}{\langle 23\rangle\langle 31\rangle}$$
$$\implies e = g\sin\,\theta_w \tag{4.39}$$

$(0\,0\,+)$

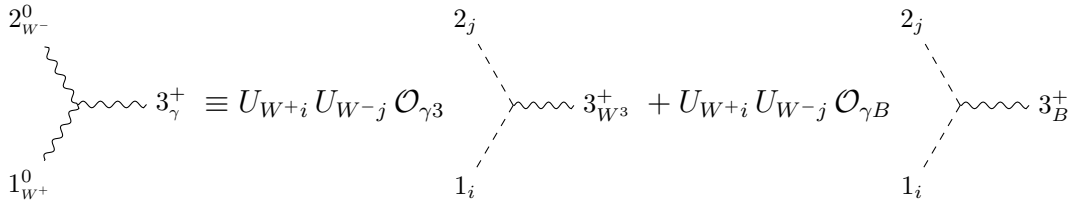

$$-2e\frac{\langle 23\rangle\langle 31\rangle}{\langle 12\rangle} = U_{W^+i}\,\left(g\,\mathcal{O}_{\gamma 3}\,T^3_{ij}\,+\,g'\,\mathcal{O}_{\gamma B}\,T^B_{ij}\,\right)U_{W^-j}\frac{\langle 23\rangle\langle 31\rangle}{\langle 12\rangle}$$
$$\implies -2e = U_{W^+i}\left(g\sin\,\theta_w T^3_{ij} + g'\cos\,\theta_w\,T^B_{ij}\right)U_{W^-j} \tag{4.40}$$

$\mathbf{W^+Z\gamma}$

Conservation of the $U(1)_{\rm EM}$ charge in the IR must be imposed. This is achieved by setting the $W^+Z\gamma$ amplitude to zero. A similar equation is given by setting the $W^-Z\gamma$ amplitude to zero.

$(0\,0\,+)$

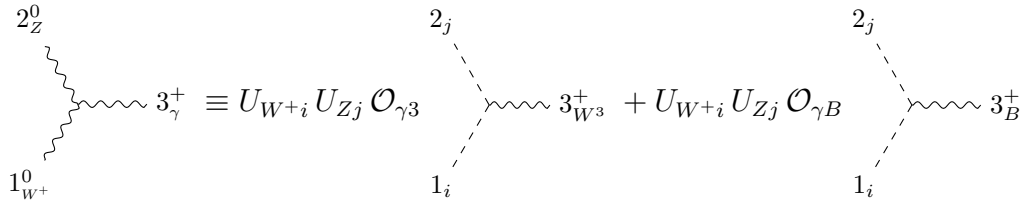

$$0 = U_{W^+i}\left(g\,\mathcal{O}_{\gamma 3}\,T^3_{ij}\;+\;g'\,\mathcal{O}_{\gamma B}\,T^B_{ij}\right)U_{Zj}\frac{\langle 23\rangle\langle 31\rangle}{\langle 12\rangle}$$

$$\implies 0 = U_{W^+i}\left(g\sin\,\theta_w\,T^3_{ij}\;+\;g'\cos\,\theta_w\,T^B_{ij}\right)U_{Zj} \tag{4.41}$$

ZZh

$(+\,0\,0)$

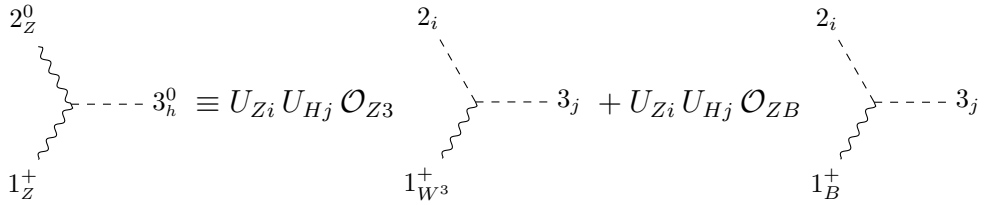

$$e_{ZZH}\frac{\langle 12\rangle\langle 31\rangle}{\langle 23\rangle} \equiv U_{Zi}\left(g\,\mathcal{O}_{Z3}\,T^3_{ij}\;+\;g'\;\mathcal{O}_{ZB}\,T^B_{ij}\,\right)U_{hj}\frac{\langle 12\rangle\langle 31\rangle}{\langle 23\rangle}$$

$$\implies e_{ZZH} = U_{Zi}\left(g\cos\,\theta_w\,T^3_{ij} - g'\sin\,\theta_w\,T^B_{ij}\,\right)U_{Hj} \tag{4.42}$$

$\mathbf{W^+W^-h}$

$(+\,0\,0)$

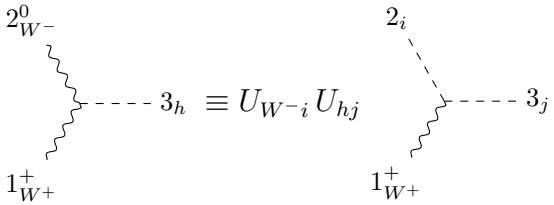

$$e_{WWH}\frac{\langle 12\rangle\langle 31\rangle}{\langle 23\rangle} \equiv g\,U_{W^-i}\,T^-_{ij}\,U_{hj}\frac{\langle 12\rangle\langle 31\rangle}{\langle 23\rangle}$$

$$\implies e_{WWH} = g\,U_{W^-i}T^-_{ij}\,U_{hj} \tag{4.43}$$

As already highlighted, eq.(4.17) and eq.(4.39) yield

$$e = g \sin\theta_w \qquad \text{and} \qquad e_W = g \cos\theta_w \tag{4.44}$$

Further, the remaining set of constraints (4.36 - 4.43) can be solved by the ansatz

$$\begin{aligned} U_{W^+} &= \frac{g}{m_W} T^- \cdot V \qquad U_{W^-} = \frac{g}{m_W} T^+ \cdot V \\ U_Z &= \frac{1}{m_Z} \left(g \, \cos\theta_w \, T^3_{ij} - g' \, \sin\theta_w \, T^B_{ij} \right) \cdot V \end{aligned} \tag{4.45}$$

where $V = \{v_1, v_2, v_3, v_4\}$. Note that despite the similarity of this equation with the usual Lagrangian based description of the Higgs mechanism, V does not have the interpretation as the vacuum expectation value of scalar field here. With the above anstaz, we find

$$\begin{aligned} v_1 = v_2 = 0\,, \qquad & \tan\theta_w = \frac{g'}{g} \\ m_Z = g\sqrt{v_3^2 + v_4^2}\,, \qquad & m_W = g\cos\theta_w \sqrt{v_3^2 + v_4^2} \\ \cos\theta_w = \frac{e_{WWH}}{e_{ZZH}} & \end{aligned} \tag{4.46}$$

We get the exact solutions as the Standard Model because we have restricted the form of the three point amplitude in eq.(4.17). Allowing for other structures will generalize the relation between m_Z and m_W. Further note that when $g' \to 0$, we have $\theta_w = 0$ and $m_Z = m_W$. Here, we see the emergence of the custodial $SU(2) = SO(3)$. The three particles $W^\pm, Z$ all have equal mass in the limit where the hypercharge coupling vanishes.

Note, the combination of generators in the anstaz (4.45) has the same form

as the generators one would associate to the $W^{\pm}$ and Z gauge fields from a field theory perspective. The generator Q associated with the photon can be found in eq.(4.41). Substituting the values in eq.(4.46), we find the familiar $Q = T^3 + T^B$ such that $Q \cdot V = 0$.

4.4 Four point amplitudes in the Electroweak sector

As we explained in the previous section, the structure of three point amplitudes is is severely restricted by Poincare' invariance and little group constraints. The construction of four point amplitudes from the three point ones requires more work. Translation invariance is assured by the delta function in eq.(4.10) and Lorentz invariance is guaranteed if we build the amplitude from the invariants in eq.(4.4) and eq.(4.9). These amplitudes must be little group tensors of the appropriate rank (or in the case of massless particles have appropriate little group weights). This still leaves open a multitude of possibilities. But beyond three points, we have new constraints arising from unitarity. The amplitude must factorize consistently on all the poles, i.e. when some subset of the external momenta goes on shell, the residue on the corresponding pole must factorize into the product of appropriate lower point amplitudes. In particular, if the exchanged particle is massless, we must have

$$M \to \frac{M_L^{a\,h} M_R^{a\,-h}}{P^2}. \tag{4.47}$$

Here and below, a is an index for the intermediate particle. In cases where there are particles which may have identical helicity and mass, this index distinguishes between them. Similarly for the exchange of a particle with mass m and spin S,

we have

$$M \to \frac{M_L^{a\{I_1,\ldots,I_{2S}\}} M^a_{R\{I_1,\ldots,I_{2S}\}}}{P^2 - m^2} = \frac{M^a_{L\{I_1,\ldots,I_{2S}\}} \epsilon^{I_1 J_1} \ldots \epsilon^{I_{2S} J_{2S}} M^a_{R\{J_1,\ldots,J_{2S}\}}}{P^2 - m^2}. \quad (4.48)$$

For the rest of this section, we will work with four particle amplitudes with particles 1 and 2 incoming and 3 and 4 outgoing. Diagrammatically,

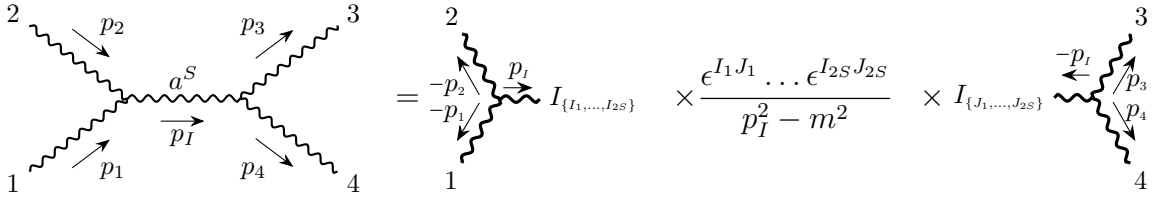

(4.49)

At four points, there are only three possible factorization channels defined by

$$s = (p_1 + p_2)^2 \qquad u = (p_1 - p_3)^2 \qquad t = (p_1 - p_4)^2. \quad (4.50)$$

We must ensure that the four point amplitude factorizes into appropriate three point amplitudes on all these channels. We do this by computing the residues in the s, t and u channels and

$$\left(\frac{R_s}{s - m_s^2} + \frac{R_t}{t - m_t^2} + \frac{R_u}{u - m_u^2} \right),$$

where m_s, m_t, m_u are the masses of the particles exchanged in the s, t, u channels respectively. This procedure will yield local amplitudes for almost all cases. Only in the case of the $W^+W^-\gamma$ amplitude, which has one massless particle and two particles of equal mass, this yields a four point amplitude with x factors

which must be eliminated to get a local expression. We will go into more details in the corresponding section.

This represents only the factorizable part of the four point amplitude. We will find that these need to be supplemented by contact terms which depend on the specific form of the three point vertices. We can determine these by specifying the UV behaviour of the four point amplitudes. For the case of the Standard Model, we demand that they do not have any terms which grow with energy. This lets us determine the required contact terms. The complete four point amplitude is then written as

$$M_4 = \left(\frac{R_s}{s - m_s^2} + \frac{R_t}{t - m_t^2} + \frac{R_u}{u - m_u^2} \right) + P(\lambda_i, \tilde{\lambda}_i),$$

where P is a Lorentz invariant polynomial in the spin spinors corresponding to the four particles with the appropriate number of little group indices.

4.4.1 $W^+W^- \to W^+W^-$

In this section, we analyze the scattering of $W^+W^- \to W^+W^-$. For the sake of explicit calculations, we make the following choice for the 4 particle kinematics (with particles 1, 2, 3 and 4 corresponding to W^-, W^+, W^+, W^- respectively.

$$\begin{aligned} p_1 &= (E, 0, 0, p) & p_2 &= (E, 0, 0, -p) \\ p_3 &= (E, p\sin\theta, 0, p\cos\theta) & p_4 &= (E, -p\cos\theta, 0, -p\cos\theta) \end{aligned} \tag{4.51}$$

We will see that, based on the three point amplitudes listed in Section [4.3.1],

the scattering can occur in the s and t channels via the exchange the Z, A or h.

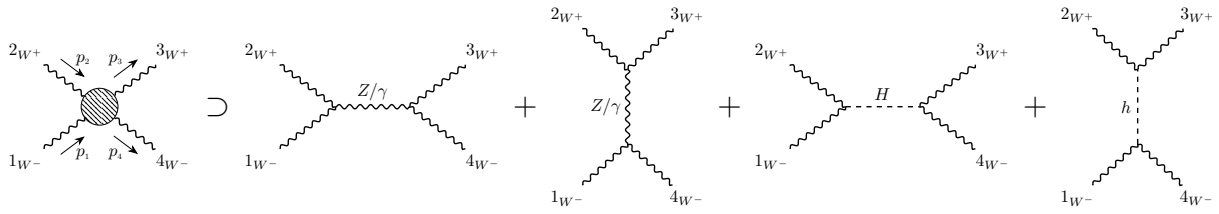

(4.52)

s - Channel

- Z exchange

We can glue together two W^+W^-Z three point amplitudes and construct the residue in the s - channel.

$$(M_L^Z)^{\{I_1 I_2\}} = \frac{e_W}{m_W^2 m_Z} \left(\langle \mathbf{12}\rangle[\mathbf{12}]\langle \mathbf{I}|(-p_1) - (-p_2)|\mathbf{I}] + \text{cyc.}\right)^{\{I_1 I_2\}} \tag{4.53}$$

$$(M_R^Z)_{\{I_1 I_2\}} = \frac{e_W}{m_W^2 m_Z} \left(-\langle \mathbf{34}\rangle[\mathbf{34}]\langle \mathbf{I}|p_3 - p_4|\mathbf{I}] + \text{cyc.}\right)_{\{I_1 I_2\}} \tag{4.54}$$

Here $I = p_1 + p_2$ is the momentum exchanged and we have suppressed the little group indices corresponding to the external particles. The residue on the s - channel is

$$R_s^Z = (M_L^Z)^{\{I_1 I_2\}} (M_R^Z)_{\{I_1 I_2\}}$$

Evaluating this expression yields

$$
\begin{aligned}
R_s^Z = \frac{e_W^2}{m_W^4}\Bigg\{ & 2\,\langle \mathbf{12}\rangle\,[\mathbf{12}]\,\langle \mathbf{34}\rangle\,[\mathbf{34}]\,(p_1-p_2).(p_3-p_4) \\
& + 4\Big(\langle \mathbf{42}\rangle\,[\mathbf{24}]\,\langle \mathbf{1}|p_2|\mathbf{1}]\,\langle \mathbf{3}|p_4|\mathbf{3}] + \langle \mathbf{31}\rangle\,[\mathbf{13}]\,\langle \mathbf{2}|p_1|\mathbf{2}]\,\langle \mathbf{4}|p_3|\mathbf{4}] - (1 \leftrightarrow 2)\Big) \\
& + 2\Big(\langle \mathbf{12}\rangle[\mathbf{12}]\,\langle \mathbf{4}|p_3|\mathbf{4}]\,\langle \mathbf{3}|p_1-p_2|\mathbf{3}] \;+\; \langle \mathbf{12}\rangle\,[\mathbf{12}]\,\langle \mathbf{3}|p_4|\mathbf{3}]\,\langle \mathbf{4}|p_1-p_2|\mathbf{4}] \\
& - (1,2 \leftrightarrow 3,4)\Big)\Bigg\}
\end{aligned}
\tag{4.55}
$$

The full details of the calculation are presented in Appendix [I].

- Photon exchange

This corresponds to gluing together the two $W^+W^-\gamma$ vertices. There are two possibilities

$$
\begin{aligned}
M_L^- &= \frac{e}{m_W} x_{12}^-\,\langle \mathbf{12}\rangle^2 \qquad & M_R^+ &= \frac{e}{m_W} x_{34}^+\,[\mathbf{34}]^2 \\
M_L^+ &= \frac{e}{m_W} x_{12}^+\,[\mathbf{12}]^2 \qquad & M_R^- &= \frac{e}{m_W} x_{34}^-\,\langle \mathbf{34}\rangle^2
\end{aligned}
\tag{4.56}
$$

where the superscripts indicate the helicity of the photon. Note that the definition of x-factors differs slightly from Appendix [H] due to the fact that p_1 and p_2 are now incoming momenta. The appropriate definitions are

$$
\begin{aligned}
\frac{(-p_1+p_2)_{\alpha\dot\alpha}}{2m}\lambda_I^\alpha &= x_{12}^+\;\tilde\lambda_{I\dot\alpha} \qquad & \frac{(p_3-p_4)_{\alpha\dot\alpha}}{2m}\lambda_I^\alpha &= x_{34}^+\;(-\tilde\lambda_{I\dot\alpha}) \\
\frac{(-p_1+p_2)_{\alpha\dot\alpha}}{2m}\tilde\lambda_I^{\dot\alpha} &= x_{12}^-\;\lambda_{I\alpha} \qquad & \frac{(p_3-p_4)_{\alpha\dot\alpha}}{2m}(-\tilde\lambda_I^{\dot\alpha}) &= x_{34}^-\;\lambda_{I\alpha}
\end{aligned}
$$

The extra minus sign that accompanies $\tilde\lambda_{I\dot\alpha}$ in the equations defining $x_{34}^\pm$ is because the momentum I is incoming. The residue corresponding to the photon

exchange is a sum over both the possibilities in eq.(4.58).

$$R_s^A = \frac{e^2}{m_W^2}\left(x_{12}^- x_{34}^+ \langle \mathbf{12}\rangle^2 [\mathbf{34}]^2 + x_{12}^+ x_{34}^- [\mathbf{12}]^2 \langle \mathbf{34}\rangle^2\right) \tag{4.57}$$

We must now eliminate the x - factors in order to obtain a local expression for this residue. There are multiple ways to achieve this and they generally result in different expressions for the residue. It is important to emphasize that while these forms are precisely equal on the factorization channel, they all lead to different expressions away from the pole. Since the physical amplitude must be the same, they yield different contact terms. The complete details of the calculation are delegated to Appendix [I]. Here, we present two different expressions for the residue on the $s-$channel.

$$\begin{aligned} R_s^\gamma = \frac{e^2}{2m_W^4}\Bigg\{ & (p_1-p_2).(p_3-p_4)\,\langle \mathbf{12}\rangle\,[\mathbf{12}]\,\langle \mathbf{34}\rangle\,[\mathbf{34}] \\ & + \Big(\langle \mathbf{12}\rangle[\mathbf{12}]\Big[\langle \mathbf{3}|\,(p_1-p_2)\,(p_1+p_2)\,|\mathbf{4}\rangle\,[\mathbf{34}] - \langle \mathbf{34}\rangle\,[\mathbf{3}|\,(p_1+p_2)\,(p_1-p_2)\,|\mathbf{4}]\Big] \\ & - \langle \mathbf{1}|\,p_1+p_2\,|\mathbf{4}]\,[\mathbf{3}|\,p_1+p_2\,|\mathbf{2}\rangle\,[\mathbf{12}]\,\langle \mathbf{34}\rangle + (1,\,2\leftrightarrow 3,4)\Big)\Bigg\} \end{aligned} \tag{4.58}$$

where $(1,2 \leftrightarrow 3,4)$ means $1 \leftrightarrow 3$ and $2 \leftrightarrow 4$ simultaneously. This expression can be manipulated to look identical to eq.(4.55). This requires the use of the following Schöuten identities

$$\begin{aligned} & \langle \mathbf{3}|\,(p_1-p_2)\,I\,|\mathbf{4}\rangle\,[\mathbf{34}] - \langle \mathbf{34}\rangle\,[\mathbf{3}|\,I\,(p_1-p_2)\,|\mathbf{4}] \\ & = 2\Big(\langle \mathbf{4}|\,p_3\,|\mathbf{4}]\,\langle \mathbf{3}|\,(p_1-p_2)\,|\mathbf{3}]\; - (3\leftrightarrow 4)\Big) \end{aligned}$$

and

$$\begin{aligned}
&\langle \mathbf{1}|\, I\, |\mathbf{4}]\, [\mathbf{3}|\, I\, |\mathbf{2}\rangle\, [\mathbf{12}]\, \langle \mathbf{34}\rangle + (1,\, 2 \leftrightarrow 3,4) \\
&= 4\Big(\langle \mathbf{42}\rangle\, [\mathbf{24}]\, \langle \mathbf{1}|\, p_2\, |\mathbf{1}]\, \langle \mathbf{3}|\, p_4\, |\mathbf{3}] \,+\, \langle \mathbf{31}\rangle\, [\mathbf{13}]\, \langle \mathbf{2}|\, p_1\, |\mathbf{2}]\, \langle \mathbf{4}|\, p_3\, |\mathbf{4}] \,-\, (1 \,\leftrightarrow\, 2)\Big)
\end{aligned}$$

where $I = p_1 + p_2$. These identities are true only on the factorization channel $I^2 = 0$ on which we can write $R_s^\gamma = R_s^Z\, (m_Z = 0)$. This is not true away from the factorization channel. Consequently the contact terms that must be added to achieve the correct UV behaviour differ. This explicitly demonstrates the dependence of contact terms on the specific form of the three point amplitudes.

- Higgs exchange

This is the simplest to compute. We just glue together the following amplitudes.

$$M_L = \frac{e_{WWH}}{m_W}\langle \mathbf{12}\rangle[\mathbf{12}] \qquad M_R = \frac{e_{WWH}}{m_W}\langle \mathbf{34}\rangle[\mathbf{34}] \tag{4.59}$$

which directly yields

$$R_s^h = \frac{e_{WWH}^2}{m_W^2}\langle \mathbf{12}\rangle[\mathbf{12}]\langle \mathbf{34}\rangle[\mathbf{34}] \tag{4.60}$$

The complete contribution of the $s-$ channel is

$$M_s = \left(\frac{R_s^Z}{s - m_z^2} + \frac{R_s^\gamma}{s} + \frac{R_s^h}{s - m_h^2}\right)$$

t - CHANNEL

The computation of the t - channel residues is very similar to that of the s - channel. In fact, we can obtain them from the $s-$ channel ones by the replacement $p_2 \leftrightarrow -p_4$. The results are presented below with $I = p_1 - p_4$.

- Z exchange

$$R_t^Z = \frac{e_W^2}{m_W^4}\Bigg\{2\,\langle\mathbf{14}\rangle\,[\mathbf{14}]\,\langle\mathbf{32}\rangle\,[\mathbf{32}]\,(p_1+p_4).(p_3+p_2) \tag{4.61}$$
$$+4\Big(\langle\mathbf{31}\rangle\,[\mathbf{13}]\,\langle\mathbf{4}|\,p_1\,|\mathbf{4}]\,\langle\mathbf{2}|\,p_3\,|\mathbf{2}] - \langle\mathbf{42}\rangle\,[\mathbf{24}]\,\langle\mathbf{1}|\,p_4\,|\mathbf{1}]\,\langle\mathbf{3}|\,p_2\,|\mathbf{3}] - (1\ \leftrightarrow\ 4)\Big)$$
$$+2\Big(\langle\mathbf{12}\,\rangle[\mathbf{14}]\,\langle\mathbf{2}|\,p_3\,|\mathbf{2}]\,\langle\mathbf{3}|\,p_1+p_2\,|\mathbf{3}] + \langle\mathbf{14}\rangle\,[\mathbf{14}]\,\langle\mathbf{3}|\,p_2\,|\mathbf{3}]\,\langle\mathbf{2}|\,p_1+p_4\,|\mathbf{2}] - (1\ \leftrightarrow\ 4)\Big)\Bigg\}$$

- Photon exchange

The residue on the $t-$ channel resulting from gluing together two $W^+W^-\gamma$ amplitudes is

$$R_t^\gamma = \frac{e^2}{2m_W^4}\Bigg\{-(p_1+p_4).(p_3+p_2)\,\langle\mathbf{14}\rangle\,[\mathbf{14}]\,\langle\mathbf{32}\rangle\ [\mathbf{32}] \tag{4.62}$$
$$+\Big(\langle\mathbf{14}\rangle\,[\mathbf{41}]\,\Big[\langle\mathbf{3}|\,(p_1+p_4)\,(p_1-p_4)\,\mathbf{2}\rangle\,[\mathbf{32}] - \langle\mathbf{32}\rangle\,[\mathbf{3}|\,(p_1-p_4)\,(p_1+p_4)\,|\mathbf{2}]\Big]$$
$$+\langle\mathbf{1}|\,p_1-p_4\,|\mathbf{2}]\,[\mathbf{3}|\,p_1-p_4\,|\mathbf{4}\rangle\,[\mathbf{14}]\,\langle\mathbf{32}\rangle + (1,\,4\leftrightarrow 3,2)\Big)\Bigg\}$$

- Higgs exchange

$$R_t^h = \frac{e_{WWH}^2}{m_W^2}\langle\mathbf{14}\rangle\,[\mathbf{14}]\,\langle\mathbf{23}\rangle\,[\mathbf{23}] \tag{4.63}$$

The total contribution from the $t-$channel is

$$M_t = \left(\frac{R_t^Z}{t - m_z^2} + \frac{R_t^\gamma}{t} + \frac{R_t^h}{t - m_h^2} \right)$$

Contact terms

The quantity $M \equiv M_s + M_t$ has been constructed to have the correct factorization properties. As explained before, the behaviour away from the factorization channels depends on the specific forms of the three point amplitudes. We can impose further constraints on the amplitude to fix it completely. It is evident that the high energy limit of the amplitude is ill defined due to the presence of the $\frac{1}{m_W^4}$ poles which leads to amplitudes which grow with energy as E^4. This violates perturbative unitarity. If we insist that the theory has a well defined high energy limit, we must add contact terms (which by definition have 0 residue on the factorization poles) to cancel this E^4 growth [†]. The form of the contact terms can be deduced by figuring out which components of the amplitude grow in the UV. Plugging in the 4-particle kinematics in 4.51, we find that only the all longitudinal component grows as E^4,

$$M \to \frac{4E^4}{m_W^4} \left(e^2 + e_W^2\right) \left(-5 - 12\cos\theta + \cos 2\theta\right) . \tag{4.64}$$

The following contact term serves to kill these high energy growths

$$c_{WWWW} = \frac{e^2 + e_W^2}{m_W^4} \left(-\langle \mathbf{12}\rangle[\mathbf{12}]\langle \mathbf{34}\rangle[\mathbf{34}] + 2\langle \mathbf{13}\rangle[\mathbf{13}]\langle \mathbf{24}\rangle[\mathbf{24}] - \langle \mathbf{14}\rangle[\mathbf{14}]\langle \mathbf{23}\rangle[\mathbf{23}]\right) \tag{4.65}$$

[†]We thank the authors of [124] for pointing out to us that this contact term can also be derived by UV-IR matching as in Section[4.3.4]

Adding these contact terms, we find that the amplitude still grows as E^2/m_W^2. Demanding that the coefficient of this growing term vanishes enforces $e_{WWH}^2 = 2(e^2 + e_W^2)$.

4.4.2 $W^+Z \to W^+Z$

The 4 particle kinematics appropriate to this situation is

$$p_1 = (E_1, 0, 0, p) \qquad p_2 = (E_2, 0, 0, -p) \tag{4.66}$$
$$p_3 = (E_2, p \sin\theta, 0, p\cos\theta) \qquad p_4 = (E_1, -p\sin\theta, 0, -p\cos\theta)$$

This configuration automatically satisfies momentum conservation. We can rewrite E_2 in terms of E_1 by using the on-shell constraint as $E_2 = \sqrt{E_1^2 - m_W^2 + m_Z^2}$. We can build this amplitude by gluing together two W^+W^-Z amplitudes in two ways and by gluing a W^+W^-h and a ZZh amplitude.

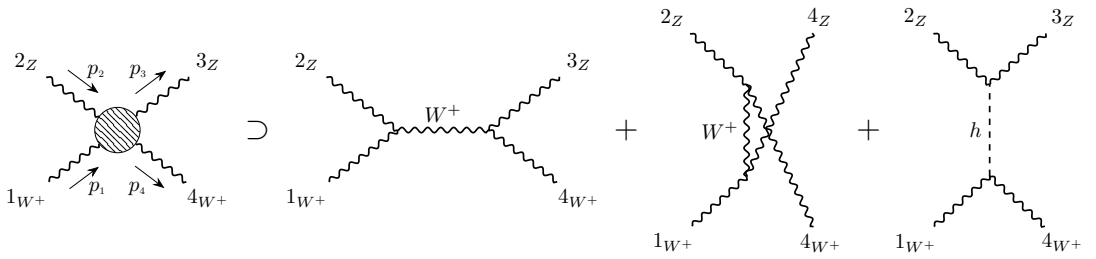

(4.67)

We present the final expressions below. The calculations are very similar to those involved in $W^+W^- \to W^+W^-$.

- $s-$channel W - exchange

$$R_s^W = \frac{e_W}{m_W^4 m_Z^2}\Bigg\{2(m_W^2 - m_Z^2)^2\langle\mathbf{12}\rangle[\mathbf{12}]\,\langle\mathbf{34}\rangle\,[\mathbf{34}] + m_W^2\Bigg(2\langle\mathbf{12}\rangle\,[\mathbf{12}]\,\langle\mathbf{34}\rangle\,[\mathbf{34}]\,(p_1-p_2).(p_3-p_4)$$
$$+ 4\Big[\langle\mathbf{42}\rangle\,[\mathbf{24}]\,\langle\mathbf{1}|p_2|\mathbf{1}]\,\langle\mathbf{3}|p_4|\mathbf{3}] - \langle\mathbf{32}\rangle[\mathbf{23}]\,\langle\mathbf{1}|p_2|\mathbf{1}]\,\langle\mathbf{4}|p_3|\mathbf{4}] + (1,3\leftrightarrow 2,4)\Big]$$
$$+ 2\Big[\langle\mathbf{12}\rangle[\mathbf{12}]\Big(\langle\mathbf{4}|p_3|\mathbf{4}]\,\langle\mathbf{3}|p_1-p_2|\mathbf{3}] - (3\leftrightarrow 4)\Big) + (1,2\leftrightarrow 3,4)\Big]\Bigg)\Bigg\} \tag{4.68}$$

- $u-$channel W - exchange

$$R_u^W = \frac{e_W}{m_W^4 m_Z^2}\Bigg\{2(m_W^2 - m_Z^2)^2\langle\mathbf{13}\rangle[\mathbf{13}]\,\langle\mathbf{24}\rangle\,[\mathbf{24}] + m_W^2\Bigg(-2\langle\mathbf{13}\rangle\,[\mathbf{13}]\,\langle\mathbf{24}\rangle\,[\mathbf{24}]\,(p_1+p_3).(p_2+p_4)$$
$$+ 4\Big[-\langle\mathbf{43}\rangle\,[\mathbf{34}]\,\langle\mathbf{1}|p_3|\mathbf{1}]\,\langle\mathbf{2}|p_4|\mathbf{2}] - \langle\mathbf{32}\rangle[\mathbf{23}]\,\langle\mathbf{1}|p_3|\mathbf{1}]\,\langle\mathbf{4}|p_2|\mathbf{4}] + (1,2\leftrightarrow 3,4)\Big]$$
$$+ 2\Big[-\langle\mathbf{13}\rangle[\mathbf{13}]\Big(\langle\mathbf{4}|p_2|\mathbf{4}]\,\langle\mathbf{2}|p_1+p_3|\mathbf{3}] + (2\leftrightarrow 4)\Big) + (1,3\leftrightarrow 2,4)\Big]\Bigg)\Bigg\} \tag{4.69}$$

- $t-$channel Higgs - exchange

$$R_t^h = \frac{e_{WWH}}{m_W}\frac{e_{ZZH}}{m_Z}\langle\mathbf{23}\rangle[\mathbf{23}]\,\langle\mathbf{14}\rangle[\mathbf{14}]\,. \tag{4.70}$$

- Contact terms

We are again in the familiar situation where the quantity

$$\left(\frac{R_s^W}{s-m_W^2} + \frac{R_u^W}{u-m_W^2} + \frac{R_t^h}{t-m_h^2}\right),$$

factorizes correctly on all the factorization channels. However, the all longitudinal component again grows with energy as can be seen by evaluating this using

the kinematics in eq.(4.66). We find that the following contact term is needed to fix this and have a well behaved theory in the UV,

$$c_{WZWZ} = \frac{e_W^2}{m_W^4}(\langle \mathbf{12}\rangle [\mathbf{12}] \langle \mathbf{34}\rangle [\mathbf{34}] + \langle \mathbf{23}\rangle [\mathbf{23}] \langle \mathbf{14}\rangle [\mathbf{14}] - \mathbf{2}\langle \mathbf{24}\rangle [\mathbf{24}] \langle \mathbf{13}\rangle [\mathbf{13}]) \,. \tag{4.71}$$

Furthermore, to kill growth at $\mathcal{O}(E^2)$, we must also have $e_{WWH}\, e_{ZZH}\, m_W^3 = e_W^2\, m_Z^3$.

4.4.3 $W^+W^- \to Zh$

We next consider the scattering $W^+W^- \to Zh$ with the following kinematics

$$\begin{aligned} p_1^\mu &= (E_1, 0, 0, p_1) & p_2^\mu &= (E_1, 0, 0, -p_1) \\ p_3^\mu &= (E_3, p_2 \sin\theta, 0, p_2 \cos\theta) & p_4^\mu &= (E_4, -p_2 \sin\theta, 0, -p_2 \cos\theta) \end{aligned} \tag{4.72}$$

Using on-shell constraints, we can eliminate p_1, p_2, E_3, E_4 in favor of E_1.

$$p_1 = \sqrt{E_1^2 - m_W^2} \quad p_2 = \sqrt{E_2^2 - m_Z^2} \quad E_3 = \frac{m_z^2 - m_h^2 + 4E_1^2}{4E_1}, E_4 = \frac{4E_1^2 - m_z^2 + m_h^2}{4E_1}$$

We can build this amplitude by gluing together (W^+W^-Z, Zhh) on the $s-$channel and by gluing together (W^+W^-h, ZZh) in the u and t channels as shown

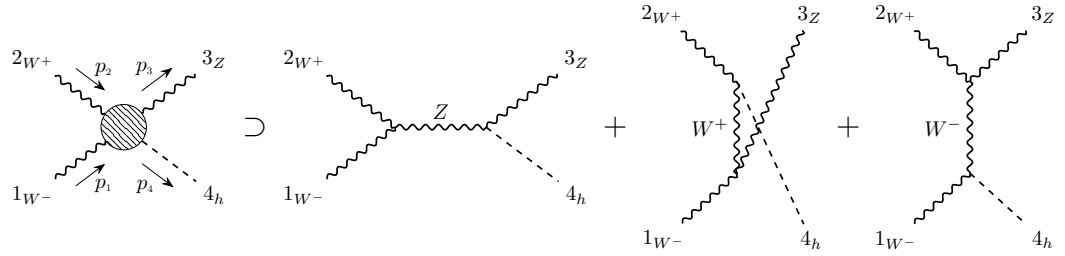

(4.73)

Using the familiar procedure, we get

- $s-$ channel Z exchange

$$R_s^Z = \frac{e_{ZZH}\, e_W}{m_W^2}\left(-\langle \mathbf{12}\rangle\,[\mathbf{12}]\,\langle \mathbf{3}|p_1-p_2|\mathbf{3}] - 2\langle \mathbf{23}\rangle\,[\mathbf{23}]\,\langle \mathbf{1}|p_2|\mathbf{1}] + 2\langle \mathbf{13}\rangle\,[\mathbf{13}]\langle\, \mathbf{2}|p_1|\mathbf{2}]\right) \tag{4.74}$$

- $u-$ channel W exchange

$$R_u^W = \frac{e_W\ e_{WWH}}{m_W m_Z}\left(-\langle \mathbf{13}\rangle\,[\mathbf{13}]\langle \mathbf{2}|p_1+p_3|\mathbf{2}] + 2\langle \mathbf{23}\rangle\,[\mathbf{23}]\langle \mathbf{1}|p_3|\mathbf{1}] - 2\langle \mathbf{12}\rangle\,[\mathbf{12}]\langle \mathbf{3}|p_1|\mathbf{3}]\right) \tag{4.75}$$

- $t-$ channel W exchange

$$R_t^W = \frac{e_W\ e_{WWH}}{m_W m_Z}\left(-\langle \mathbf{23}\rangle\,[\mathbf{23}]\,\langle \mathbf{1}|p_2+p_3|\mathbf{1}] + 2\langle \mathbf{13}\rangle\,[\mathbf{13}]\langle \mathbf{2}|p_3|\mathbf{2}] - 2\langle \mathbf{12}\rangle\,[\mathbf{12}]\,\langle \mathbf{3}|p_2|\mathbf{3}]\right) \tag{4.76}$$

- Contact terms

In this case, the component of the amplitude with W^+, W^-, Z all being longitudinal grows with energy. However, there are no possible contact terms that are compatible with Loretnz invriance and the little group. The vanishing of the growing term imposes a constraint on the couplings e_{WWH}, e_{ZZH}.

$$\frac{e_{ZZH}}{e_{WWH}} = \frac{m_W}{m_Z} \tag{4.77}$$

4.4.4 $W^+W^- \to hh$

To compute this amplitude, we can glue together two W^+W^-h amplitudes in the t and u channels.

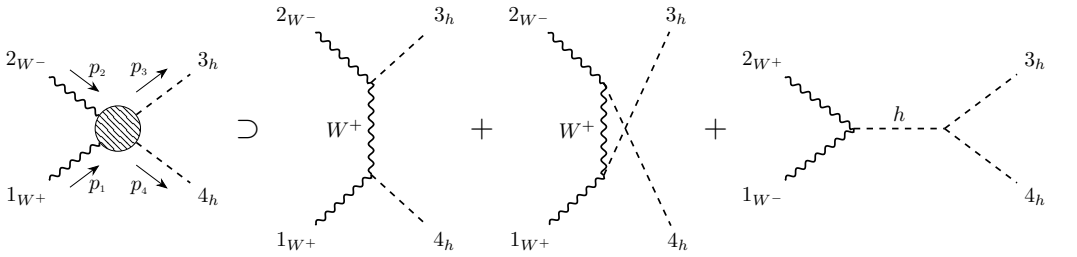

(4.78)

- t-channel W exchange

$$R_t^W = \frac{e_{WWH}^2}{m_W^2}\left(-m_W^2\langle\mathbf{12}\rangle\,[\mathbf{12}] \;-\; \frac{1}{2}\langle\mathbf{1}|\,p_1 \;-\; p_4|\mathbf{1}]\;[\mathbf{2}|p_1 \;-\; p_4\,|\mathbf{2}\rangle\right) \tag{4.79}$$

- $u-$ channel W exchange

$$R_u^W = \frac{e_{WWH}^2}{m_W^2}\left(-m_W^2\langle\mathbf{12}\rangle\,[\mathbf{12}] \;-\; \frac{1}{2}\langle\mathbf{1}|\,p_1 \;-\; p_3|\mathbf{1}]\;[\mathbf{2}|p_1 \;-\; p_3\,|\mathbf{2}\rangle\right) \tag{4.80}$$

- $s-$ channel h exchange

$$R_s^h = \frac{e_{WWH}\,e_{HHH}\,m_H}{m_W}\langle\mathbf{12}\rangle\,[\mathbf{12}] \tag{4.81}$$

- Contact terms

The contact term necessary to kill the $\mathcal{O}(E^2)$ growth is

$$c_{WWHH} = \frac{e_{WHH}^2}{2\,m_W^2}\langle\mathbf{12}\rangle\,[\mathbf{21}] \tag{4.82}$$

4.4.5 $hh \to hh$

The only three point amplitudes which contribute to this are the hhh vertices eq.(4.21). As opposed to the usual, Lagrangian based approach to the Higgs mechanism, where we discover the new triple higgs vertex in the IR, here we must include its contribution simply because it is non zero and contributes to this scattering process.

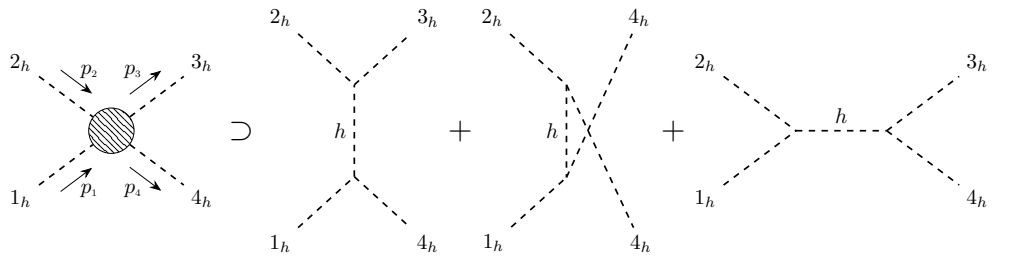

(4.83)

The complete amplitude is

$$e^2_{HHH} m_h^2 \left(\frac{1}{s - m_h^2} + \frac{1}{t - m_h^2} + \frac{1}{u - m_h^2} \right) + \lambda \tag{4.84}$$

where λ is a contact term.

4.5 Conclusions and Outlook

We have presented a completely on-shell description of the higgs mechanism within the Standard Model. We see that all the physics is reproduced by demanding consistent factorization, correct ultraviolet behaviour and consistency of the UV and IR. The precise relations between the masses of the $W^{\pm}, Z$ and θ_w depend on the structures that have been included in the three point W^+W^-Z amplitude. Our choice of the three point amplitude in eq.(4.17) ensured that

we reproduced the usual result. We have constructed four particle, tree-level amplitudes from three particle amplitudes. The construction of higher point amplitudes and extensions to loop amplitudes are the obvious next questions. We have also restricted the particle content of the scalar sector to a single, real scalar transforming under an $SO(4)$ global symmetry. We have studied the Higgs mechanism for $SU(2)_L \times U(1)_Y$ breaking to $U(1)_{\rm EM}$, relevant to electroweak symmetry breaking. It would be interesting to extend this analysis to completely general theories.

This work is a preliminary step in connecting modern methods in scattering amplitudes to the real world. There have been many developments in new ways of thinking about scattering amplitudes. It has proved useful to think of them as differential forms on kinematic space [34]. These differential forms are associated to geometric structures in many cases. The physics of scattering amplitudes emerges from simple properties of the underlying geometry as seen in the few known cases [**?**,16,33,132,133]. It would therefore be useful to rewrite amplitudes in the Standard Model as differential forms. This would lay the groundwork for an attempt to look for hidden geometric structure within these amplitudes.

A

Constraints from projecting positive data

In this appendix, we derive the constraints that result from projecting positive data. We derive the constraints that must be satisfied by 3 dimensional data which are the result of projecting four dimensional positive data. Let us start with $n = 5$. We can add one extra component and turn them into 4D data.

$$Z_i = \begin{pmatrix} \mathbf{z}_i \\ \\ c_i \end{pmatrix} \qquad i = 1, ..5$$

The 3D $\mathbf{z}_i$ can be thought of as coming from positive 4D data if we can add a fourth component such that the resulting 4D data are positive. Thus at 5 points, we need to demand

$$\langle 1234\rangle > 0, \langle 1235\rangle > 0, \langle 1245\rangle > 0, \langle 1345\rangle > 0, \langle 2345\rangle > 0$$

The resulting system of equations can be written in the following way.

$$\begin{pmatrix} -\langle \mathbf{234}\rangle & \langle \mathbf{134}\rangle & -\langle \mathbf{124}\rangle & \langle \mathbf{123}\rangle & 0 \\ -\langle \mathbf{235}\rangle & \langle \mathbf{135}\rangle & -\langle \mathbf{125}\rangle & 0 & \langle \mathbf{123}\rangle \\ -\langle \mathbf{245}\rangle & \langle \mathbf{145}\rangle & 0 & -\langle \mathbf{125}\rangle & \langle \mathbf{124}\rangle \\ -\langle \mathbf{345}\rangle & 0 & \langle \mathbf{145}\rangle & -\langle \mathbf{135}\rangle & \langle \mathbf{134}\rangle \\ 0 & -\langle \mathbf{345}\rangle & \langle \mathbf{245}\rangle & -\langle \mathbf{235}\rangle & \langle \mathbf{345}\rangle \end{pmatrix} \begin{pmatrix} c_1 \\ c_2 \\ c_3 \\ c_4 \\ c_5 \end{pmatrix} = A^T c > 0 \quad \text{(A.1)}$$

Thus, we can think of the 3D data, $\mathbf{z}_i$ as coming from 4D positive data if this system of inequalities as a solution,. The condition for the existence of a solution for a system of linear inequalities is given by Gordan's theorem which states,

Theorem 1 *Exactly one of the following systems has a solution.*

(1) $y^T A > 0$ *for some* $y \in \mathbf{R}^n$

(2) $Ax = 0, x \geq 0$ *for some non zero* $x \in \mathbf{R}^n$

Thus the condition for the existence of a solution to our system is that the null vectors cannot have all positive entries. To find the null eigenvectors of A, we first note that the Schouten identity in three dimensions is

$$\langle \mathbf{123}\rangle \mathbf{4} - \langle \mathbf{234}\rangle \mathbf{1} + \langle \mathbf{341}\rangle \mathbf{2} - \langle \mathbf{412}\rangle \mathbf{3} = 0 \quad \text{(A.2)}$$

$$A = \begin{pmatrix} -\langle \mathbf{234} \rangle & -\langle \mathbf{235} \rangle & -\langle \mathbf{245} \rangle & -\langle \mathbf{345} \rangle & 0 \\ \langle \mathbf{134} \rangle & \langle \mathbf{135} \rangle & \langle \mathbf{145} \rangle & 0 & -\langle \mathbf{345} \rangle \\ -\langle \mathbf{124} \rangle & -\langle \mathbf{125} \rangle & 0 & \langle \mathbf{145} \rangle & \langle \mathbf{135} \rangle \\ \langle \mathbf{123} \rangle & 0 & -\langle \mathbf{125} \rangle & -\langle \mathbf{135} \rangle & -\langle \mathbf{235} \rangle \\ 0 & \langle \mathbf{123} \rangle & \langle \mathbf{124} \rangle & \langle \mathbf{134} \rangle & \langle \mathbf{345} \rangle \end{pmatrix} \tag{A.3}$$

We can easily see that any vector of the form $\begin{pmatrix} \langle \mathbf{5ab} \rangle & -\langle \mathbf{4ab} \rangle & \langle \mathbf{3ab} \rangle & -\langle \mathbf{2ab} \rangle & \langle \mathbf{1ab} \rangle \end{pmatrix}$ is a null eigenvector as a consequence of the Schouten identity. Here $\mathbf{a}$ and $\mathbf{b}$ are any two 3D vectors. From Gordan's theorem, the condition for the existence of a solution and consequently the constraint on the 3D data is that not all entries of the null vector are positive. Let us choose $\mathbf{a} = \mathbf{z}_1$ and $\mathbf{b} = \mathbf{z}_2$. Then $\{\langle \mathbf{512} \rangle, -\langle \mathbf{412} \rangle, \langle \mathbf{312} \rangle\}$ aren't all positive or the sequence $\{\langle \mathbf{125} \rangle, \langle \mathbf{124} \rangle, \langle \mathbf{123} \rangle\}$ has less than 2 sign flips. However, in this case we cannot say anything about the sign flips of the sequences resulting from a different choice of $\mathbf{a}$ and $\mathbf{b}$. Furthermore, any one of them having the wrong flip pattern is sufficient to show that this 3D data cannot arise from positive 4D data.

This can be easily extended beyond $n = 5$. At an arbitrary n, we have to impose positivity of all ordered minors $\langle ijkl \rangle$ with $i < j < k < l$. This results in a similar system of inequalities with null eigenvectors of the form

$$\{(-1)^i \langle (\mathbf{n} - \mathbf{i})\mathbf{ab} \rangle\}, \qquad i = 1, 2...n-1 \tag{A.4}$$

which leads to a similar constraint on the signs.

B

Restricting flip patterns

Consider a pair of sequences $\{a_1, \ldots, a_n\}$ and $\{b_1, \ldots, b_n\}$ which have an equal number of terms. Further suppose that they are connected by the Schouten identity and satisfy a postivity condition, i.e. there exists a relation $a_i b_{i+1} - a_{i+1} b_i = ab > 0$. We will show that the number of sign flips in these sequences, k_1 and k_2 respectively, are related and that the relation depends only on the signs of a_1, a_n, b_1 and b_n.

Firstly, we note that the positivity forces each block in the pair of sequences

$\begin{pmatrix} a_i & a_{i+1} \\ b_i & b_{i+1} \end{pmatrix}$ to take one of the following forms.

Type 1: $\begin{pmatrix} + & + \\ + & + \end{pmatrix}, \begin{pmatrix} + & + \\ - & - \end{pmatrix}, \begin{pmatrix} - & - \\ + & + \end{pmatrix}, \begin{pmatrix} - & - \\ - & - \end{pmatrix}$

Type 2: $\begin{pmatrix} + & - \\ - & + \end{pmatrix}, \begin{pmatrix} + & - \\ + & - \end{pmatrix}, \begin{pmatrix} - & + \\ + & - \end{pmatrix}, \begin{pmatrix} - & + \\ - & + \end{pmatrix}$

Type 3: $\begin{pmatrix} + & + \\ - & + \end{pmatrix}, \begin{pmatrix} - & - \\ + & - \end{pmatrix}$

Type 4: $\begin{pmatrix} + & - \\ + & + \end{pmatrix} \begin{pmatrix} - & + \\ - & - \end{pmatrix},$

Blocks of type 1 and 2 leave $k_1 - k_2$ fixed. A block of type 3 changes $k_1 - k_2$ by -1 and a block of type 4 changes it by 1. Two consecutive blocks of type 3 or 4 are prohibited and a block of type 4 must follow a block of type 3 before the sign of the bottom sequence can be flipped without flipping the sign of the top. Thus, if we know the signs of a_1, a_n, b_1 and b_n, we can determine $k_1 - k_2$. We can list the possibilities by the matrices $\begin{pmatrix} s(a_1) & s(a_n) \\ s(b_1) & s(b_n) \end{pmatrix}$ where $s(x)$ is the sign of x.

- $k_1 = k_2$

$$\begin{pmatrix} + & + \\ + & + \end{pmatrix} \begin{pmatrix} + & - \\ + & - \end{pmatrix} \begin{pmatrix} + & + \\ - & - \end{pmatrix} \begin{pmatrix} + & - \\ - & + \end{pmatrix} \begin{pmatrix} - & - \\ + & + \end{pmatrix} \begin{pmatrix} - & + \\ + & - \end{pmatrix} \begin{pmatrix} - & - \\ - & - \end{pmatrix} \begin{pmatrix} - & + \\ - & + \end{pmatrix}$$

- $k_1 = k_2 + 1$

$$\begin{pmatrix} + & - \\ + & + \end{pmatrix} \begin{pmatrix} + & + \\ + & - \end{pmatrix} \begin{pmatrix} - & + \\ - & - \end{pmatrix} \begin{pmatrix} - & - \\ - & + \end{pmatrix}$$

- $k_1 = k_2 - 1$

$$\begin{pmatrix} - & + \\ + & + \end{pmatrix} \begin{pmatrix} + & + \\ - & + \end{pmatrix} \begin{pmatrix} + & - \\ - & - \end{pmatrix} \begin{pmatrix} - & - \\ + & - \end{pmatrix}$$

C

Cuts of Feynman integrals

A class of integral coming from Feynman parametrizing a 1-loop diagram will are of the form

$$I_n = \int \langle X d^{n-1} X \rangle \frac{(L.X)^{n-D}}{(X.Q.X)^{n-D/2}}$$

We will perform a spherical contour integral in the (ij) directions. Using the transformation in (3.21), the above integral becomes,

$$I_n^{(ij)} = \int dw_i\, dw_j\, \langle X^{(ij)} d^{n-3} X^{(ij)} \rangle \mathcal{R}\, \frac{\left(L_{\{\widehat{ij}\}} X_{\{\widehat{ij}\}} + L_{\{ij\}} (Rw)_{\{ij\}} - L_{\{ij\}} Q^{-1}_{\{ij\}\{ij\}} Q_{\{ij\}\{\widehat{ij}\}} X_{\{\widehat{ij}\}}\right)^{n-D}}{(w_i\, w_j + X^{(ij)} Q^{(ij)} X^{(ij)})^{n-D/2}}$$

where $\mathcal{R}$ =det R. The integral over w_i, w_j to be done over S^2 with an implicit factor of $\frac{1}{2\pi i}$. Using 3.24, we can write the numerator as

$$\left(L_{\{ij\}} R w_{ij} + L^{(ij)} X_{\{\widehat{ij}\}}\right)^{n-D}$$

Since we are integrating over the Riemann sphere with the substitution $w_i = re^{i\phi}$, $w_i = re^{-i\phi}$, only terms containing some power of the product $w_i w_j$ survive the angular integration. This yields,

$$I_n^{(ij)} = \sum_{k=0,\text{even}}^{n-D} \binom{n-D}{k} \binom{k}{k/2} (R.L)_i^{k/2} (R.L)_j^{k/2} \frac{\Gamma\left(1+k/2\right) \Gamma\left(-1-D/2-k/2+n\right)}{2\Gamma\left(n-D/2\right)}$$
$$\int \langle X^{(ij)} d^{n-3} X^{(ij)} \rangle \frac{(L^{(ij)}.X^{(ij)})^{n-D-k/2}}{(X^{(ij)} Q^{(ij)} X^{(ij)})^{(D+k+2-2n)/2}}$$

D

Spherical contour with a quadratic numerator

In this appendix, we sketch out the details of transformation of a quadratic numerator under a spherical residue. Consider the integral in 3.25. The transfor-

mation (3.21) changes the numerator to

$$X.N.X \to \det R \Big((Rw) N_{\{ij\}\{ij\}} (Rw) + X_{\{\widehat{ij}\}} Q_{\{\widehat{ij}\}\{ij\}} Q^{-1}_{\{ij\}\{ij\}} N_{\{ij\}\{ij\}} Q^{-1}_{\{ij\}\{ij\}} Q_{\{ij\}\{\widehat{ij}\}} X_{\{\widehat{ij}\}}$$
$$-2 X_{\{\widehat{ij}\}} Q_{\{\widehat{ij}\}\{ij\}} Q^{-1}_{\{ij\}\{ij\}} N_{\{ij\}\{\widehat{ij}\}} X_{\{\widehat{ij}\}} + X_{\{\widehat{ij}\}} N_{\{\widehat{ij}\}\{\widehat{ij}\}} X_{\{\widehat{ij}\}} \Big)$$

With $\det R = 2\sqrt{-\det Q_{\{ij\}\{ij\}}}$, we can write the cut integral as

$$I_q^{(ij)} = \int \frac{\langle X^{(ij)} d^{n-3} X^{(ij)} \rangle}{2\sqrt{-\det Q_{\{ij\}\{ij\}}}} \frac{dw_i dw_j}{2\pi i} \frac{(Rw) N_{\{ij\}\{ij\}} (Rw) + X_{\{\widehat{ij}\}} N' X_{\{\widehat{ij}\}}}{(w_i w_j + X^{(ij)} Q^{(ij)} X^{(ij)})^{\frac{n}{2}+1}}$$

The first term integrates to

$$\frac{1}{2\pi i} \int_{w_i = \bar{w}_j} \frac{(w.(R^T N R).w) \, \langle X^{(ij)} d^{n-3} X^{(ij)} \rangle dw_i \, dw_j}{(w_i w_j + X_{\{\widehat{ij}\}} Q^{(ij)} X_{\{\widehat{ij}\}})^{\frac{n+2}{2}}} = \frac{\langle X^{(ij)} d^{n-3} X^{(ij)} \rangle Tr(Q^{-1}_{\{ij\}\{ij\}} N_{\{ij\}\{ij\}})}{2\sqrt{-\det Q_{\{ij\}\{ij\}}} n(n-2) \left(X_{\{\widehat{ij}\}} Q^{(ij)} X_{\{\widehat{ij}\}} \right)^{\frac{n}{2}-}}$$

and the second one to

$$\frac{1}{2\pi i} \int_{w_i = \bar{w}_j} \frac{\langle X^{(ij)} d^{n-3} X^{(ij)} \rangle (X_{\{\widehat{ij}\}} N' X_{\{\widehat{ij}\}}) dw_i \, dw_j}{(w_i w_j + X_{\{\widehat{ij}\}} Q^{(ij)} X_{\{\widehat{ij}\}})^{\frac{n+2}{2}}} = \frac{\langle X^{(ij)} d^{n-3} X^{(ij)} \rangle (X_{\{\widehat{ij}\}} N' X_{\{\widehat{ij}\}})}{2\sqrt{-\det Q_{\{ij\}\{ij\}}} n (X_{\{\widehat{ij}\}} Q^{(ij)} X_{\{\widehat{ij}\}})^{\frac{n}{2}}}$$

E

Leading singularities at 6 points

At $n = 6$, we can have leading singularities which correspond to the three box diagrams shown in Figure $E.1$.

We label the leading singularities by the Feynman parameters of the cut propagators. by associating x_i with the propagator $\langle ABii + 1\rangle$. Thus $(ijkl)$ corresponds to the leading singularity which results from setting $\langle ABi - 1i\rangle = \langle ABj - 1j\rangle = \langle ABk - 1k\rangle = \langle ABl - 1l\rangle = 0$. In this notation, the list of singularities is

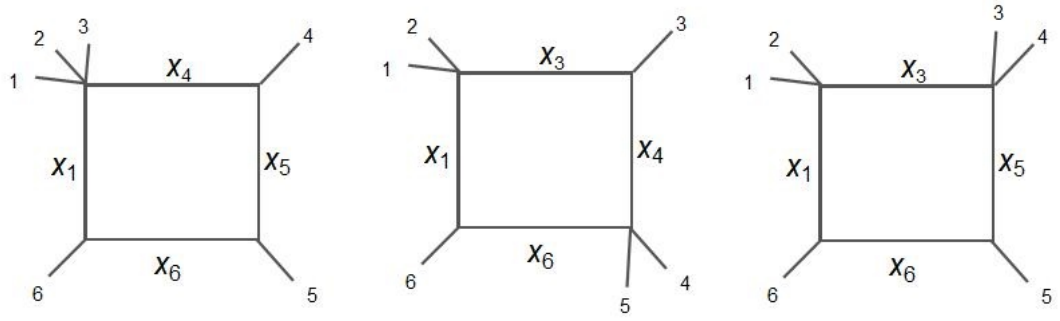

Figure E.1: One-mass, two-mass easy and two-mass hard singularities

- **One mass** (1456), (3456), (1234), (6123), (5612), (2345)
- **Two mass easy** (1356), (6245), (5134), (4623), (3512), (2461)
- **Two mass hard** (3461), (4512), (5623)

The 1-loop, $n-$ point amplitude of $\mathcal{N}=4$ SYM is a sum over all one - mass and two-mass easy leading singularities. Thus the numerator of the full amplitude is constrained to make all the two mass hard singularities vanish and to make all the other singularities equal. The six point amplitude in momentum twistor space must have the form

$$\int_{AB} \frac{\langle ABX\rangle\langle ABY\rangle}{\langle AB12\rangle\langle AB23\rangle\langle AB34\rangle\langle AB45\rangle\langle AB56\rangle\langle AB16\rangle}$$

for some bitwistors X and Y. The corresponding object in Feynman parameter space looks like

$$\int \frac{\langle Xd^5X\rangle(X.N.X)}{(X.Q.X)^4}$$

where the quadric $Q_{ij} \equiv q_{ij} = \langle i-1ij-1j\rangle$ and the numerator is a symmetric

tensor with coefficients to be determined. We can simplify the denominator by making the transformation $x_i \to y_i x_i$ with

$$y = \left(\sqrt{\frac{q_{25}q_{36}}{q_{13}q_{15}q_{26}}}, \sqrt{\frac{q_{15}q_{36}}{q_{13}q_{25}q_{26}}}, \sqrt{\frac{q_{15}q_{26}}{q_{13}q_{25}q_{36}}}, \sqrt{\frac{q_{13}q_{15}q_{26}}{q_{14}^2 q_{25}q_{36}}}, \sqrt{\frac{q_{13}q_{26}}{q_{15}q_{25}q_{36}}}, \sqrt{\frac{q_{25}q_{13}}{q_{15}q_{26}q_{36}}}\right)$$

This transforms the denominator into $X.Q.X \to x_1x_3 + x_1x_4 + x_1x_5 + u_1x_2x_4 + x_2x_5 + x_2x_6 + u_2x_3x_5 + x_3x_6 + u_3x_4x_6$ with $u_1 = q_{24}q_{15}/(q_{25}q_{14})$, $u_2 = q_{35}q_{26}/(q_{36}q_{25})$ and $u_3 = q_{46}q_{13}/(q_{14}q_{36})$.

We demand that all two-mass hard leading singularities vanish and that all the rest are equal to 1. This places some constraints on the numerator N.

F

Feynman parametrizing the 1-loop MHV integrand

In this appendix, we provide the details of Feynman parametrizing the complete one-loop MHV integrand for planar $\mathcal{N} = 4$ SYM. As explained in Section 3.6,

the one-loop integrand is given by

$$\mathcal{A}_n^{\text{MHV}} = \sum_{i<j<i} (ji)$$

More concretely, the expression for the amplitude at n points is

$$\mathcal{A}_n^{\text{MHV}} = \int_{AB} \left(\sum_{i=2}^{n} \frac{1}{\langle ABn1\rangle\langle AB12\rangle\langle AB\star\rangle} \frac{\langle AB(n12 \cap i-1ii+1)\rangle\langle\star 1i\rangle}{\langle ABi-1i\rangle\langle ABii+1\rangle} \right) + \text{cyclic}$$

$$\mathcal{A}_n^{\text{MHV}} = \int_{AB} \frac{\left(\langle n123\rangle\langle\star 12\rangle \prod_{i\neq n,1,2} \langle ABii+1\rangle - \langle 12n-1n\rangle\langle\star 1n\rangle \prod_{i\neq 1,n-1,n} \langle ABii+1\rangle + \sum_{k=2}^{n-1} \langle AB(n12 \cap k-1kk+1)\rangle\langle\star 1k\rangle \prod_{i\neq k-1k,1,n} \langle ABii+1\rangle \right)}{\langle AB\star\rangle \prod_{i=1}^{n} \langle ABii+1\rangle}$$

Combining all the terms in the cyclic sum,

$$\mathcal{A}_n^{\text{MHV}} = \frac{1}{\langle AB\star\rangle \prod_{i=1}^{n} \langle ABii+1\rangle} \left(2\sum_{l=1}^{n} \langle\star ll+1\rangle \prod_{i\neq l-1,l,l+1} \langle ABii+1\rangle\langle l-1ll+1l+2\rangle + \sum_{k=1}^{n} \sum_{l=k+2}^{k-2} \langle\star lk\rangle\langle AB(l-1ll+1) \cap (k-1kk+1)\rangle \prod_{i\neq k-1,k,l-1,l} \langle ABii+1\rangle \right)$$

We can proceed with Feynman parametrization using embedding space techniques. The following formula is useful

$$\frac{\langle ABY_1\rangle \ldots \langle ABY_{n-3}\rangle}{\langle AB12\rangle \ldots \langle ABn1\rangle\langle AB\star\rangle} \xrightarrow{FP} \left(Y_1.\frac{d}{dW}\right) \ldots \left(Y_{n-3}.\frac{d}{dW}\right) \frac{1}{(W.W)^2} \qquad \text{(F.1)}$$

with $W = \sum_{i=1}^{n-1} x_i |ii+1\rangle + x_n |1n\rangle + x|\star\rangle$.

In the 5 point case numerator after performing the cyclic sum is,

$$\langle\star 12\rangle\langle 5123\rangle\langle AB34\rangle\langle AB45\rangle + \langle\star 23\rangle\langle 1234\rangle\langle AB45\rangle\langle AB51\rangle + \langle\star 34\rangle\langle 2345\rangle\langle AB51\rangle\langle AB12\rangle$$
$$+\langle\star 45\rangle\langle 3451\rangle\langle AB12\rangle\langle AB23\rangle + \langle\star 51\rangle\langle 4512\rangle\langle AB23\rangle\langle AB34\rangle + \langle\star 13\rangle\langle AB\bar{1}\bar{3}\rangle\langle AB45\rangle$$
$$+\langle\star 14\rangle\langle AB\bar{1}\bar{4}\rangle\langle AB23\rangle + \langle\star 24\rangle\langle AB\bar{2}\bar{4}\rangle\langle AB51\rangle + \langle\star 25\rangle\langle AB\bar{2}\bar{5}\rangle\langle AB34\rangle$$
$$+\langle\star 35\rangle\langle AB\bar{3}\bar{5}\rangle\langle AB12\rangle.$$

Eq (F.1) adapted to this case reads,

$$\frac{(Y_1.Y_2)(W.W) - 6(Y_1.W)(Y_2.W)}{(W.W)^3}$$

which yields the following Feynman parametrization for $\mathcal{A}_5^{\text{MHV}}$.

$$\langle\star 12\rangle\langle 5123\rangle(-6\langle W34\rangle\langle W45\rangle) + \langle\star 23\rangle\langle 1234\rangle(-6\langle W45\rangle\langle W51\rangle)$$
$$+\langle\star 34\rangle\langle 2345\rangle(-6\langle W51\rangle\langle W12\rangle) + \langle\star 45\rangle\langle 3451\rangle(-6\langle W12\rangle\langle W23\rangle)$$
$$+\langle\star 51\rangle\langle 4512\rangle(-6\langle W23\rangle\langle W34\rangle)$$
$$+\langle\star 13\rangle\left[\langle 5124\rangle\langle 2345\rangle W.W - 6\langle W45\rangle\left(\langle W12\rangle\langle 5234\rangle + \langle W25\rangle\langle 1234\rangle\right)\right]$$
$$+\langle\star 14\rangle\left[-\langle 5123\rangle\langle 3452\rangle W.W - 6\langle W23\rangle\left(\langle W51\rangle\langle 2345\rangle + \langle W25\rangle\langle 1345\rangle\right)\right]$$
$$+\langle\star 24\rangle\left[\langle 1235\rangle\langle 3451\rangle W.W - 6\langle W51\rangle\left(\langle W23\rangle\langle 1345\rangle + \langle W31\rangle\langle 2345\rangle\right)\right]$$
$$+\langle\star 25\rangle\left[-\langle 1234\rangle\langle 4513\rangle W.W - 6\langle W34\rangle\left(\langle W12\rangle\langle 3451\rangle + \langle W31\rangle\langle 2451\rangle\right)\right]$$
$$+\langle\star 35\rangle\left[\langle 2341\rangle\langle 4512\rangle W.W - 6\langle W12\rangle\left(\langle W34\rangle\langle 2451\rangle + \langle W42\rangle\langle 3451\rangle\right)\right] \quad \text{(F.2)}$$

Plugging in W, this evaluates to (3.35)

G

Conventions

In this appendix, we explicitly state all our conventions. We work with the metric signature $(+,-,-,-)$. $\mathrm{SU}(2)_L$ (of the bosons in the UV) and $\mathrm{SL}(2,\mathbf{C})$ spinor indices are raised and lowered using

$$\epsilon_{\alpha\beta} = -\epsilon^{\alpha\beta} = \begin{pmatrix} 0 & -1 \\ 1 & 0 \end{pmatrix} \tag{G.1}$$

We raise and lower the $\mathrm{SL}(2,\mathbf{C})$ as follows

$$\lambda^\alpha = \epsilon^{\alpha\beta}\lambda_\beta \qquad \lambda_\beta = \epsilon_{\beta\alpha}\lambda^\alpha \qquad \tilde{\lambda}^{\dot{\alpha}} = \epsilon^{\dot{\alpha}\dot{\beta}}\tilde{\lambda}_{\dot{\beta}} \qquad \tilde{\lambda}_{\dot{\beta}} = \epsilon_{\dot{\beta}\dot{\alpha}}\tilde{\lambda}^{\dot{\alpha}}$$

We use the same tensor for lowering and raising the indices of the massive little group $\mathrm{SU}(2)_L$ with the convention

$$\lambda_{\alpha I} = \lambda^J_\alpha \, \epsilon_{JI} \qquad \lambda^I_\alpha = \lambda_{\alpha J} \, \epsilon^{JI}.$$

Note that the Greek $\mathrm{SL}(2,\mathbf{C})$ spinor indices are raised and lowered on the left while the Latin little group indices are raised and lowered on the right. We also make use of angle and square spinors which are defined as

$$\begin{aligned} |\mathbf{i}\rangle &:= |\mathbf{i}\rangle^I_\alpha = \lambda^I_\alpha, & \langle \mathbf{i}| &:= \langle \mathbf{i}|^{\alpha I} = \lambda^{\alpha I}, \\ |\mathbf{i}] &:= |\mathbf{i}]^{\dot{\alpha} I} = \tilde{\lambda}^{\dot{\alpha} I}, & [\mathbf{i}| &:= [\mathbf{i}|^I_{\dot{\alpha}} = \tilde{\lambda}^I_{\dot{\alpha}}. \end{aligned} \tag{G.2}$$

With this the momentum can be written as,

$$p_{\alpha\dot{\alpha}} = \epsilon_{JI}|\mathbf{i}\rangle^I[\mathbf{i}|^J = \epsilon_{JI}\lambda^I_\alpha\tilde{\lambda}^J_{\dot{\alpha}}, \qquad p^{\dot{\alpha}\alpha} = \epsilon_{JI}\,\langle \mathbf{i}|^I\,|\mathbf{i}]^J = \epsilon_{JI}\lambda^{\alpha I}\tilde{\lambda}^{\dot{\alpha}J}$$

We follow the convention that undotted indices are contracted from top to bottom while dotted indices are contracted from the bottom to the top.

$$\begin{aligned} \langle \mathbf{ij}\rangle = \langle \mathbf{i}|^{\alpha I}|\mathbf{j}\rangle^J_\alpha, \qquad [\mathbf{ij}] = [\mathbf{i}|^I_{\dot{\alpha}}|\mathbf{j}]^{\dot{\alpha}J} \\ \langle \mathbf{i}|p_k|\mathbf{j}\rangle = \langle \mathbf{i}|^{\alpha I}p_{k\alpha\dot{\beta}}|\mathbf{j}\rangle^{\dot{\beta}J}, \quad [\mathbf{i}|p_k|\mathbf{j}\rangle = [\mathbf{i}|^I_{\dot{\alpha}}p_k^{\dot{\alpha}\beta}|\mathbf{j}\rangle^J_\beta \end{aligned} \tag{G.3}$$

In this notation, the Dirac equation reads

$$\langle \mathbf{i}|p_i = m_i[\mathbf{i}| \qquad p_i|\mathbf{i}] = -m_i|\mathbf{i}\rangle \tag{G.4}$$
$$p_i|\mathbf{i}\rangle = -m_i|\mathbf{i}] \qquad [\mathbf{i}|p_i = m_i\langle \mathbf{i}|$$

We can expand λ_α^I and $\tilde{\lambda}_{\dot{\alpha}I}$ as explained in eq.(4.16)

$$\begin{aligned}\lambda_\alpha^I &= \lambda_\alpha\, \zeta^{-I} + \eta_\alpha\, \zeta^{+I} \qquad (G.5)\\ &= \sqrt{E+p}\, \zeta_\alpha^+(p)\, \zeta^{-I}(k) + \sqrt{E-p}\, \zeta_\alpha^-(p)\, \zeta^{+I}(k)\\ \tilde{\lambda}_{\dot{\alpha}I} &= \tilde{\lambda}_{\dot{\alpha}}\, \zeta_I^+ - \tilde{\eta}_{\dot{\alpha}}\, \zeta_I^- \qquad (G.6)\\ &= \sqrt{E+p}\, \tilde{\zeta}_\alpha^-(p)\, \zeta_I^+(k) - \sqrt{E-p}\, \tilde{\zeta}_{\dot{\alpha}}(p)\, \zeta_I^-(k)\end{aligned}$$

where

$$\zeta_I^+ = \begin{pmatrix}1\\0\end{pmatrix}, \quad \zeta_I^- = \begin{pmatrix}0\\-1\end{pmatrix}, \quad \zeta^{+I} = \begin{pmatrix}0\\1\end{pmatrix}, \quad \zeta^{-I} = \begin{pmatrix}1\\0\end{pmatrix} \tag{G.7}$$

$$\zeta_\alpha^+(p) = \begin{pmatrix}\cos\frac{\theta}{2}\\ \sin\frac{\theta}{2}e^{i\phi}\end{pmatrix}, \quad \zeta_\alpha^-(p) = \begin{pmatrix}-\sin\frac{\theta}{2}e^{-i\phi}\\ \cos\frac{\theta}{2}\end{pmatrix}$$
$$\zeta_{\dot{\alpha}}^+(p) = \begin{pmatrix}-\sin\frac{\theta}{2}e^{i\phi}\\ \cos\frac{\theta}{2}\end{pmatrix}, \quad \zeta_{\dot{\alpha}}^-(p) = \begin{pmatrix}\cos\frac{\theta}{2}\\ \sin\frac{\theta}{2}e^{-i\phi}\end{pmatrix}$$

With this choice, we have have the following contractions

$$\begin{aligned} \lambda^I_\alpha \zeta^+_I &= \lambda_\alpha \qquad \lambda^I_\alpha \zeta^-_I = -\eta_\alpha \\ \tilde{\lambda}^I_{\dot\alpha} \zeta^+_I &= -\tilde{\eta}_{\dot\alpha} \qquad \tilde{\lambda}^I_{\dot\alpha} \zeta^-_I = -\tilde{\lambda}_{\dot\alpha} \end{aligned} \tag{G.8}$$

Furthermore, using G.4 we can deduce following relations between λ and η

$$\begin{aligned} p_{\alpha\dot\alpha}\lambda^\alpha &= -m\,\tilde{\eta}_{\dot\alpha} \qquad p_{\alpha\dot\alpha}\eta^\alpha = m\,\tilde{\lambda}_{\dot\alpha} \\ p_{\alpha\dot\alpha}\tilde{\eta}^{\dot\alpha} &= m\,\lambda_\alpha \qquad p_{\alpha\dot\alpha}\tilde{\lambda}^{\dot\alpha} = -m\,\eta_\alpha \end{aligned} \tag{G.9}$$

H

Amplitudes with one massless particle and 2 equal mass particles

Three particle amplitudes involving one massless particle and two massive particles of equal mass present a difficulty. Consider the three particle amplitude with both particles 1 and 2 having mass m, spins S_1 and S_2 and a third massless particle of helicity h. In order to construct such amplitudes, it is useful to have a Lorentz invariant object which has the correct helicity weight for parti-

cle three and is invariant under the little groups for particles 1 and 2. Unfortunately, the obvious candidates vanish,

$$[3|\, p_1\, |3\rangle = 2\, p_1.p_3 = 0 \qquad [3|\, p_2\, |3\rangle = 2\, p_2.p_3 = 0\,. \tag{H.1}$$

The x-factors defined in massivesh solve this problem. In our paper, we adopt a slightly different definition and notation which we explain below. For all outgoing momenta, we define

$$\frac{(p_1-p_2)_{\alpha\dot\alpha}}{2m}\lambda_3^\alpha = x_{12}^+\ \tilde\lambda_{3\dot\alpha} \qquad \frac{(p_1-p_2)_{\alpha\dot\alpha}}{2m}\tilde\lambda_3^{\dot\alpha} = x_{12}^-\ \lambda_{3\alpha}\,. \tag{H.2}$$

Under little group scaling of particle 3, the helicity spinors scale as $\lambda_3 \to t^{-1}\lambda_3$ and $\tilde\lambda_3 \to t\,\tilde\lambda_3$. It follows that $x_{12}^+ \to t^{-2}\,x_{12}^+$ and $x_{12}^- \to t^2\,x_{12}^-$. An object with helicity h transforms as t^{-2h} under a little group scaling. This justifies the $\pm$ signs on the x-factors.

We can obtain explicit expressions for the x-factors by contracting eq.(H.2) with reference spinors ξ^α or $\tilde{\xi}^{\dot\alpha}$.

$$x_{12}^+ = \frac{\langle 3|p_1-p_2|\xi]}{2\,m[3\,\xi]} \qquad x_{12}^- = \frac{\langle \xi|p_1-p_2|3]}{2\,m\langle \xi\,3\rangle}$$

These are the same as the conventional expressions for polarization vectors of massless particles upto a factor of $\frac{1}{m}$. It is crucial that the x-factors are independent of the reference spinor. To see this, consider two different definitions of x_{12}^+ with reference spinors ξ_1 and ξ_2. Their difference,

$$\frac{\langle 3|p_1-p_2|\xi_1]}{2\,m[3\,\xi_1]} - \frac{\langle 3|p_1-p_2|\xi_2]}{2\,m[3\,\xi_2]} = -\frac{\langle 3|p_1-p_2|3][\xi_1\,\xi_2]}{2\,m[3\,\xi_1][3\,\xi_2]} = 0$$

where the first equality follows from a Schöuten identity and the second from eq.(H.1).

We can build three point amplitudes using the x-factors. Here, we will focus on the amplitude involving two spin 1 particles of mass m and a massless particle of helicity ± 1. The contributing structures are

$$\langle \mathbf{12}\rangle^2\, x_{12}^{\pm} \qquad [\mathbf{12}]^2\, x_{12}^{\pm} \qquad \langle \mathbf{1}3\rangle\, [\mathbf{2}3]\langle \mathbf{12}\rangle \qquad \langle \mathbf{1}3\rangle\, \langle \mathbf{2}3\rangle\langle \mathbf{12}\rangle \qquad \dots \tag{H.3}$$

We pick our amplitudes to be $\langle \mathbf{12}\rangle^2\, x_{12}^{-}$ and $[\mathbf{12}]^2\, x_{12}^{+}$. This corresponds to minimal coupling. For more details about this and amplitudes corresponding to multipole moments, see [116]. We can also compare these with the vertices that we get from the usual Feynman rules (for a photon with positive helicity)

$$\epsilon_3^+ \cdot (p_1 - p_2)\, \epsilon_1 \cdot \epsilon_2 \;+\; \epsilon_1 \cdot (p_2 - p_3)\, \epsilon_2 \cdot \epsilon_3^+ \;+\; \epsilon_2 \cdot (p_3 - p_1)\, \epsilon_3^+ \cdot \epsilon_1, \tag{H.4}$$

where

$$(\epsilon_3^+)_{\alpha\dot\alpha} \equiv \frac{\lambda_{3\alpha}\, \xi_{\dot\alpha}}{[3\,\xi]} \qquad (\epsilon_1)_{\alpha\dot\alpha}^{I_1\, I_2} \equiv \frac{1}{m}\, \lambda_{1\alpha}^{\{I_1}\, \tilde\lambda_{1\dot\alpha}^{I_2\}} \qquad (\epsilon_2)_{\beta\dot\beta}^{J_1\, J_2} \equiv \frac{1}{m}\, \lambda_{2\beta}^{\{J_1}\, \tilde\lambda_{2\dot\beta}^{J_2\}}.$$

Using these definitions in eq.(H.4) and applying Schöuten identities to eliminate the reference spinors, it reduces to

$$\frac{x_{12}^+}{2m}[\mathbf{12}]\left(\langle \mathbf{21}\rangle + \frac{\langle \mathbf{1}3\rangle\langle 3\mathbf{1}\rangle}{m\, x_{12}^+}\right) = -\frac{x_{12}^+}{2m}[\mathbf{12}]^2 \tag{H.5}$$

The following identities are useful in showing this equality

$$\begin{aligned}[\mathbf{12}] &= \langle \mathbf{12} \rangle - \frac{\langle \mathbf{1}|P|\mathbf{2}]}{m} \\ &= \langle \mathbf{12} \rangle + \frac{1}{2m} \left([\mathbf{1}|P|\mathbf{2}\rangle - \langle \mathbf{1}|P|\mathbf{2}] \right),\end{aligned} \tag{H.6}$$

$$[\mathbf{21}] = \langle \mathbf{21} \rangle + \frac{\langle \mathbf{2}3\rangle\langle 3\mathbf{1}\rangle}{mx^+} = \langle \mathbf{21} \rangle + \frac{[\mathbf{2}3][3\mathbf{1}]}{mx^-}. \tag{H.7}$$

Similarly, for a negative helicity photon we have,

$$\frac{-x_{12}^-}{2m}\langle \mathbf{21} \rangle \left([\mathbf{12}] + \frac{[\mathbf{2}3][3\mathbf{1}]}{mx^-} \right) = \frac{x_{12}^-}{2m}\langle \mathbf{21} \rangle^2. \tag{H.8}$$

I

Computation of 4-particle amplitudes

In Sections [4.4.1-4.4.2], we glue together two three point amplitudes to construct the four point amplitude. In cases in which the exchanged particle has spin 1, the following identities are useful

$$\epsilon_{I_1 J_1}\epsilon_{I_2 J_2}\mathbf{I}^{\alpha\{I_1}\tilde{\mathbf{I}}^{\dot{\alpha} I_2\}}\mathbf{I}^{\beta\{J_1}\tilde{\mathbf{I}}^{\dot{\beta} j_2\}} = \frac{1}{2}\left(\epsilon^{\alpha\beta}\epsilon^{\dot{\alpha}\dot{\beta}}m_I^2 - I^{\dot{\alpha}\beta}I^{\dot{\beta}\alpha}\right) = \epsilon^{\alpha\beta}\epsilon^{\dot{\alpha}\dot{\beta}}m_I^2 - \frac{1}{2}I^{\dot{\alpha}\alpha}I^{\dot{\beta}\beta}. \tag{I.1}$$

Note that the second equality can be obtained by using a property of the two dimensional Levi Civita tensor

$$\epsilon_{I_1 J_1}\epsilon_{I_2 J_2} + \epsilon_{I_1 I_2}\epsilon_{J_2 J_1} + \epsilon_{I_1 J_2}\epsilon_{J_1 I_2} = 0. \tag{I.2}$$

The following identities are useful in the computation of the 4 point amplitude in Section [4.4.1]

$$[\mathbf{12}] = \langle \mathbf{12} \rangle - \frac{\langle \mathbf{1}I \rangle \langle I\mathbf{2} \rangle}{m x_{12}^{+}} = \langle \mathbf{12} \rangle - \frac{[\mathbf{1}I][I\mathbf{2}]}{m x_{12}^{-}}, \tag{I.3}$$

$$\langle \mathbf{34} \rangle = [\mathbf{34}] + \frac{\langle \mathbf{3}I \rangle \langle I\mathbf{4} \rangle}{m_{34}^{+}} = [\mathbf{34}] + \frac{[\mathbf{3}I][I\mathbf{4}]}{m x_{34}^{-}} \tag{I.4}$$

and

$$x_{12}^{+} x_{34}^{-} + x_{12}^{-} x_{34}^{+} = \frac{1}{2m^2}(p_1 - p_2) \cdot (p_3 - p_4). \tag{I.5}$$

J

Generators of $SO(4)$ and the embedding of $SU(2) \times U(1)_Y$

The representation of the generators of SU(2)× U(1) as 4×4 matrices was also introduced in [134]. These are derived by identifying the appropriate subgroups

of SO(4) whose generators are

$$A_1 = i\begin{pmatrix} 0 & 0 & 0 & 0 \\ 0 & 0 & -1 & 0 \\ 0 & 1 & 0 & 0 \\ 0 & 0 & 0 & 0 \end{pmatrix}, \quad A_2 = i\begin{pmatrix} 0 & 0 & 1 & 0 \\ 0 & 0 & 0 & 0 \\ -1 & 0 & 0 & 0 \\ 0 & 0 & 0 & 0 \end{pmatrix}, \quad A_3 = i\begin{pmatrix} 0 & -1 & 0 & 0 \\ 1 & 0 & 0 & 0 \\ 0 & 0 & 0 & 0 \\ 0 & 0 & 0 & 0 \end{pmatrix}$$

$$B_1 = i\begin{pmatrix} 0 & 0 & 0 & -1 \\ 0 & 0 & 0 & 0 \\ 0 & 0 & 0 & 0 \\ 1 & 0 & 0 & 0 \end{pmatrix}, \quad B_2 = i\begin{pmatrix} 0 & 0 & 0 & 0 \\ 0 & 0 & 0 & -1 \\ 0 & 0 & 0 & 0 \\ 0 & 1 & 0 & 0 \end{pmatrix}, \quad B_3 = i\begin{pmatrix} 0 & 0 & 0 & 0 \\ 0 & 0 & 0 & 0 \\ 0 & 0 & 0 & -1 \\ 0 & 0 & 1 & 0 \end{pmatrix}.$$

The following combinations can be used to identify the SU(2) and U(1) subgroups

$$\begin{aligned} X^+ &= \frac{1}{2\sqrt{2}}\left(A_1 + iA_2 + B_1 + iB_2\right), & Y^+ &= \frac{1}{2\sqrt{2}}\left(A_1 + iA_2 - B_1 - iB_2\right), \\ X^- &= \frac{1}{2\sqrt{2}}\left(A_1 - iA_2 + B_1 - iB_2\right), & Y^- &= \frac{1}{2\sqrt{2}}\left(A_1 - iA_2 - B_1 + iB_2\right), \\ X^3 &= \frac{1}{2}\left(A_3 + B_3\right), & Y^3 &= \frac{1}{2}\left(A_3 - B_3\right). \end{aligned} \tag{J.1}$$

It is easy to see that they satisfy two copies of the $SU(2)$ algebra

$$\begin{aligned} \left[X^+, X^-\right] &= X^3, \quad \left[X^3, X^+\right] = X^+, \quad \left[X^3, X^-\right] = -X^-, \\ \left[Y^+, Y^-\right] &= Y^3, \quad \left[Y^3, Y^+\right] = Y^+, \quad \left[Y^3, Y^-\right] = -Y^-. \end{aligned} \tag{J.2}$$

We will associate the generators $X^\pm, X^3$ with the symmetry $SU(2)_L$. These are referred to as $T^\pm, T^3$ in the paper, such that $T^\pm \equiv 2X^\pm$. The $U(1)_Y$ is a sub-

group of the $SU(2)$ formed by $Y^{\pm}, Y^3$ and we will set $T^B \equiv 2Y^3$.

References

[1] Stephen J. Parke and T. R. Taylor. Gluonic Two Goes to Four. *Nucl. Phys.*, B269:410–420, 1986.

[2] Stephen J. Parke and T. R. Taylor. An Amplitude for n Gluon Scattering. *Phys. Rev. Lett.*, 56:2459, 1986.

[3] Zvi Bern, Lance Dixon, David C. Dunbar, and David A. Kosower. One-loop n-point gauge theory amplitudes, unitarity and collinear limits. *Nuclear Physics B*, 425(1):217 – 260, 1994.

[4] Ruth Britto, Freddy Cachazo, Bo Feng, and Edward Witten. Direct proof of tree-level recursion relation in Yang-Mills theory. *Phys. Rev. Lett.*, 94:181602, 2005.

[5] Ruth Britto, Freddy Cachazo, and Bo Feng. New recursion relations for tree amplitudes of gluons. *Nucl. Phys.*, B715:499–522, 2005.

[6] Freddy Cachazo, Peter Svrcek, and Edward Witten. MHV vertices and tree amplitudes in gauge theory. *JHEP*, 09:006, 2004.

[7] Edward Witten. Perturbative gauge theory as a string theory in twistor space. *Commun. Math. Phys.*, 252:189–258, 2004.

[8] Nima Arkani-Hamed, Jacob L. Bourjaily, Freddy Cachazo, Simon Caron-Huot, and Jaroslav Trnka. The All-Loop Integrand For Scattering Amplitudes in Planar N=4 SYM. *JHEP*, 01:041, 2011.

[9] Nima Arkani-Hamed, Jacob Lewis Bourjaily, Freddy Cachazo, A. Goncharov, Alexander Postnikov, and Jaroslav Trnka. *Scattering Amplitudes and the Positive Grassmannian.*

[10] Nima Arkani-Hamed, Cameron Langer, Akshay Yelleshpur Srikant, and Jaroslav Trnka. *Deep into the Amplituhedron: Amplitude Singularities at All Loops and Legs. Phys. Rev. Lett.*, **122**(051601), 2019.

[11] Nima Arkani-Hamed and Ellis Ye Yuan. One-Loop Integrals from Spherical Projections of Planes and Quadrics. 2017.

[12] Z. Bern, J. J. M. Carrasco, L. J. Dixon, H. Johansson, and R. Roiban. Manifest ultraviolet behavior for the three-loop four-point amplitude of $\mathcal{N} = 8$ supergravity. *Phys. Rev. D*, 78:105019, Nov 2008.

[13] Charalampos Anastasiou, Ruth Britto, Bo Feng, Zoltan Kunszt, and Pierpaolo Mastrolia. d-dimensional unitarity cut method. *Physics Letters B*, 645(2):213 – 216, 2007.

[14] Ruth Britto, Freddy Cachazo, and Bo Feng. Generalized unitarity and one-loop amplitudes in n=4 super-yang–mills. *Nuclear Physics B*, 725(1):275 – 305, 2005.

[15] Zvi Bern, Lance Dixon, David C. Dunbar, and David A. Kosower. Fusing gauge theory tree amplitudes into loop amplitudes. *Nuclear Physics B*, 435(1):59 – 101, 1995.

[16] Nima Arkani-Hamed and Jaroslav Trnka. *The Amplituhedron. JHEP*, **1410**(030), 2014.

[17] Nima Arkani-Hamed and Jaroslav Trnka. Into the Amplituhedron. *JHEP*, 12:182, 2014.

[18] Andrew Hodges. Eliminating spurious poles from gauge-theoretic amplitudes. *JHEP*, 05:135, 2013.

[19] Nima Arkani-Hamed, Jacob L. Bourjaily, Freddy Cachazo, Andrew Hodges, and Jaroslav Trnka. A Note on Polytopes for Scattering Amplitudes. *JHEP*, 04:081, 2012.

[20] Nima Arkani-Hamed, Freddy Cachazo, Clifford Cheung, and Jared Kaplan. A Duality For The S Matrix. *JHEP*, 03:020, 2010.

[21] L. J. Mason and David Skinner. Dual Superconformal Invariance, Momentum Twistors and Grassmannians. *JHEP*, 11:045, 2009.

[22] Alexander Postnikov. Total positivity, Grassmannians, and networks. *arXiv Mathematics e-prints*, page math/0609764, Sep 2006.

[23] Nima Arkani-Hamed, Hugh Thomas, and Jaroslav Trnka. Unwinding the Amplituhedron in Binary. *JHEP*, 01:016, 2018.

[24] Jacob L. Bourjaily, Jaroslav Trnka, Anastasia Volovich, and Congkao Wen. The Grassmannian and the Twistor String: Connecting All Trees in N=4 SYM. *JHEP*, 01:038, 2011.

[25] Nima Arkani-Hamed, Freddy Cachazo, and Clifford Cheung. The Grassmannian Origin Of Dual Superconformal Invariance. *JHEP*, 03:036, 2010.

[26] Nima Arkani-Hamed, Jacob L. Bourjaily, Freddy Cachazo, and Jaroslav Trnka. Local Integrals for Planar Scattering Amplitudes. *JHEP*, 06:125, 2012.

[27] Cameron Langer and Akshay Yelleshpur Srikant. All-loop cuts from the Amplituhedron. *JHEP*, 04:105, 2019.

[28] Simon Caron-Huot. Loops and trees. *JHEP*, 05:080, 2011.

[29] Nima Arkani-Hamed, Yuntao Bai, and Thomas Lam. Positive Geometries and Canonical Forms. *JHEP*, 11:039, 2017.

[30] Giulio Salvatori. *1-loop Amplitudes from the Halohedron*. 2018.

[31] Giulio Salvatori and Sergio L. Cacciatori. Hyperbolic Geometry and Amplituhedra in 1+2 dimensions. *JHEP*, 08:167, 2018.

[32] Song He, Gongwang Yan, Chi Zhang, and Yong Zhang. Scattering Forms, Worldsheet Forms and Amplitudes from Subspaces. *JHEP*, 08:040, 2018.

[33] Nima Arkani-Hamed, Yuntao Bai, Song He, and Gongwang Yan. *Scattering Forms and the Positive Geometry of Kinematics, Color and the Worldsheet*. *JHEP*, **05**:096, 2018.

[34] Song He and Chi Zhang. *Notes on Scattering Amplitudes as Differential Forms*. *JHEP*, **10**:054, 2018.

[35] David Damgaard, Livia Ferro, Tomasz Lukowski, and Matteo Parisi. The Momentum Amplituhedron. *JHEP*, 08:042, 2019.

[36] Charalampos Anastasiou, Ruth Britto, Bo Feng, Zoltan Kunszt, and Pierpaolo Mastrolia. Unitarity cuts and Reduction to master integrals in d dimensions for one-loop amplitudes. *JHEP*, 03:111, 2007.

[37] Richard John Eden, Peter V. Landshoff, David I. Olive, and John Charlton Polkinghorne. *The analytic S-matrix*. Cambridge Univ. Press, Cambridge, 1966.

[38] R. E. Cutkosky. Singularities and discontinuities of Feynman amplitudes. *J. Math. Phys.*, 1:429–433, 1960.

[39] Tomasz Lukowski. On the Boundaries of the m=2 Amplituhedron. 2019.

[40] Sebastian Franco, Daniele Galloni, Alberto Mariotti, and Jaroslav Trnka. *Anatomy of the Amplituhedron. JHEP*, **03**:128, 2015.

[41] Daniele Galloni. Positivity Sectors and the Amplituhedron. 2016.

[42] Igor Prlina, Marcus Spradlin, James Stankowicz, and Stefan Stanojevic. Boundaries of Amplituhedra and NMHV Symbol Alphabets at Two Loops. *JHEP*, 04:049, 2018.

[43] Igor Prlina, Marcus Spradlin, James Stankowicz, Stefan Stanojevic, and Anastasia Volovich. All-Helicity Symbol Alphabets from Unwound Amplituhedra. *JHEP*, 05:159, 2018.

[44] Tristan Dennen, Igor Prlina, Marcus Spradlin, Stefan Stanojevic, and Anastasia Volovich. Landau Singularities from the Amplituhedron. *JHEP*, 06:152, 2017.

[45] Tristan Dennen, Marcus Spradlin, and Anastasia Volovich. Landau Singularities and Symbology: One- and Two-loop MHV Amplitudes in SYM Theory. *JHEP*, 03:069, 2016.

[46] Igor Prlina, Marcus Spradlin, and Stefan Stanojevic. All-loop singularities of scattering amplitudes in massless planar theories. *Phys. Rev. Lett.*, 121(8):081601, 2018.

[47] Zvi Bern, Enrico Herrmann, Sean Litsey, James Stankowicz, and Jaroslav Trnka. *Logarithmic Singularities and Maximally Supersymmetric Amplitudes. JHEP*, 06:202, 2015.

[48] Zvi Bern, Enrico Herrmann, Sean Litsey, James Stankowicz, and Jaroslav Trnka. *Evidence for a Nonplanar Amplituhedron. JHEP*, 06:098, 2016.

[49] Zvi Bern, Michael Enciso, Chia-Hsien Shen, and Mao Zeng. *Dual Conformal Structure Beyond the Planar Limit. Phys. Rev. Lett.*, 121(12):121603, 2018.

[50] Nima Arkani-Hamed, Jacob L. Bourjaily, Freddy Cachazo, and Jaroslav Trnka. *Singularity Structure of Maximally Supersymmetric Scattering Amplitudes. Phys. Rev. Lett.*, 113(26):261603, 2014.

[51] Livia Ferro, Tomasz Lukowski, Andrea Orta, and Matteo Parisi. *Yangian symmetry for the tree amplituhedron. J. Phys.*, **A50**(29):294005, 2017.

[52] Livia Ferro, Tomasz Lukowski, and Matteo Parisi. *Amplituhedron meets Jeffrey-Kirwan Residue. J. Phys.*, **A52**(4):045201, 2019.

[53] Michael Enciso. *Volumes of Polytopes Without Triangulations. JHEP*, 10:071, 2017.

[54] Michael Enciso. *Logarithms and Volumes of Polytopes. JHEP*, 04:016, 2018.

[55] Steven N. Karp, Lauren K. Williams, and Yan X Zhang. *Decompositions of amplituhedra.* 2017.

[56] Steven N. Karp and Lauren K. Williams. *The $m = 1$ amplituhedron and cyclic hyperplane arrangements.* 2016.

[57] Yuntao Bai and Song He. *The Amplituhedron from Momentum Twistor Diagrams. JHEP*, 02:065, 2015.

[58] Yuntao Bai, Song He, and Thomas Lam. *The Amplituhedron and the One-loop Grassmannian Measure. JHEP*, 01:112, 2016.

[59] Junjie Rao. *4-particle Amplituhedron at 3-loop and its Mondrian Diagrammatic Implication. JHEP*, **06**:038, 2018.

[60] Yang An, Yi Li, Zhinan Li, and Junjie Rao. *All-loop Mondrian Diagrammatics and 4-particle Amplituhedron. JHEP*, **06**:023, 2018.

[61] Junjie Rao. *4-particle Amplituhedronics for 3-5 loops.* 2018.

[62] Jacob L. Bourjaily, Alexander DiRe, Amin Shaikh, Marcus Spradlin, and Anastasia Volovich. *The Soft-Collinear Bootstrap: N=4 Yang-Mills Amplitudes at Six and Seven Loops. JHEP*, 03:032, 2012.

[63] Jacob L. Bourjaily, Paul Heslop, and Vuong-Viet Tran. *Perturbation Theory at Eight Loops: Novel Structures and the Breakdown of Manifest Conformality in $N = 4$ Supersymmetric Yang-Mills Theory. Phys. Rev. Lett.*, 116(19):191602, 2016.

[64] Jacob L. Bourjaily, Paul Heslop, and Vuong-Viet Tran. Amplitudes and Correlators to Ten Loops Using Simple, Graphical Bootstraps. *JHEP*, 11:125, 2016.

[65] Nima Arkani-Hamed, Andrew Hodges, and Jaroslav Trnka. Positive Amplitudes In The Amplituhedron. *JHEP*, 08:030, 2015.

[66] David Simmons-Duffin. Projectors, Shadows, and Conformal Blocks. *JHEP*, 04:146, 2014.

[67] Christian Bogner and Stefan Weinzierl. Feynman graph polynomials. *Int. J. Mod. Phys.*, A25:2585–2618, 2010.

[68] C. Itzykson and J. B. Zuber. *Quantum Field Theory*. International Series In Pure and Applied Physics. McGraw-Hill, New York, 1980.

[69] Vladimir A. Smirnov. Evaluating Feynman integrals. *Springer Tracts Mod. Phys.*, 211:1–244, 2004.

[70] Vladimir A. Smirnov. Analytic tools for Feynman integrals. *Springer Tracts Mod. Phys.*, 250:1–296, 2012.

[71] Hung Cheng and T. T. Wu. *EXPANDING PROTONS: SCATTERING AT HIGH-ENERGIES*. 1987.

[72] Holmfridur Hannesdottir and Matthew D. Schwartz. S -matrix for massless particles. *Physical Review D*, 101(10), May 2020.

[73] Holmfridur Hannesdottir and Matthew D. Schwartz. A finite s-matrix, 2019.

[74] Lance J. Dixon. Gluon scattering in N=4 super-Yang-Mills theory from weak to strong coupling. *PoS*, RADCOR2007:056, 2007.

[75] Lorenzo Magnea. All-order results for soft and collinear gluons. *Pramana*, 72(1):69–81, Jan 2009.

[76] George F. Sterman. Partons, factorization and resummation, TASI 95. In *Theoretical Advanced Study Institute in Elementary Particle Physics (TASI 95): QCD and Beyond*, pages 327–408, 6 1995.

[77] Einan Gardi and Lorenzo Magnea. Infrared singularities in QCD amplitudes. *Frascati Phys. Ser.*, 50:137–157, 2010.

[78] Zvi Bern, Lance J. Dixon, and Vladimir A. Smirnov. Iteration of planar amplitudes in maximally supersymmetric yang-mills theory at three loops and beyond. *Physical Review D*, 72(8), Oct 2005.

[79] Niklas Beisert, Burkhard Eden, and Matthias Staudacher. Transcendentality and crossing. *Journal of Statistical Mechanics: Theory and Experiment*, 2007(01):P01021–P01021, Jan 2007.

[80] Zvi Bern, Michael Czakon, Lance J. Dixon, David A. Kosower, and Vladimir A. Smirnov. The Four-Loop Planar Amplitude and Cusp Anomalous Dimension in Maximally Supersymmetric Yang-Mills Theory. *Phys. Rev.*, D75:085010, 2007.

[81] Rutger H. Boels, Tobias Huber, and Gang Yang. The nonplanar cusp and collinear anomalous dimension at four loops in $\mathcal{N} = 4$ SYM theory. *PoS*, RADCOR2017:042, 2017.

[82] Rutger H. Boels, Tobias Huber, and Gang Yang. The sudakov form factor at four loops in maximal super yang-mills theory. *Journal of High Energy Physics*, 2018(1), Jan 2018.

[83] Rutger H. Boels, Tobias Huber, and Gang Yang. Four-loop nonplanar cusp anomalous dimension in n=4 supersymmetric yang-mills theory. *Physical Review Letters*, 119(20), Nov 2017.

[84] G.P. Korchemsky and A.V. Radyushkin. Loop-space formalism and renormalization group for the infrared asymptotics of qcd. *Physics Letters B*, 171(4):459 – 467, 1986.

[85] G.P. Korchemsky and G. Marchesini. Resummation of large infrared corrections using wilson loops. *Physics Letters B*, 313(3):433 – 440, 1993.

[86] Zvi Bern, Lance J. Dixon, and David A. Kosower. Dimensionally regulated pentagon integrals. *Nucl. Phys.*, B412:751–816, 1994.

[87] Henriette Elvang and Yu-tin Huang. *Scattering Amplitudes in Gauge Theory and Gravity*. Cambridge University Press, 2015.

[88] Nima Arkani-Hamed, Freddy Cachazo, Clifford Cheung, and Jared Kaplan. The S-Matrix in Twistor Space. *JHEP*, 03:110, 2010.

[89] Freddy Cachazo. Sharpening The Leading Singularity. 2008.

[90] Evgeny I. Buchbinder and Freddy Cachazo. Two-loop amplitudes of gluons and octa-cuts in N=4 super Yang-Mills. *JHEP*, 11:036, 2005.

[91] Zvi Bern, Lance J. Dixon, and David A. Kosower. Dimensionally regulated one loop integrals. *Phys. Lett.*, B302:299–308, 1993. [Erratum: Phys. Lett.B318,649(1993)].

[92] Jacob L. Bourjaily, Simon Caron-Huot, and Jaroslav Trnka. Dual-Conformal Regularization of Infrared Loop Divergences and the Chiral Box Expansion. *JHEP*, 01:001, 2015.

[93] Jacob L. Bourjaily, Falko Dulat, and Erik Panzer. Manifestly dual-conformal loop integration. *Nuclear Physics B*, 942:251 – 302, 2019.

[94] Samuel Abreu, Ruth Britto, Claude Duhr, and Einan Gardi. Algebraic Structure of Cut Feynman Integrals and the Diagrammatic Coaction. *Phys. Rev. Lett.*, 119(5):051601, 2017.

[95] Samuel Abreu, Ruth Britto, Claude Duhr, and Einan Gardi. Cuts from residues: the one-loop case. *Journal of High Energy Physics*, 2017, 02 2017.

[96] Lance J. Dixon, Matt von Hippel, Andrew J. McLeod, and Jaroslav Trnka. Multi-loop positivity of the planar $\mathcal{N} = 4$ SYM six-point amplitude. *JHEP*, 02:112, 2017.

[97] Steven Weinberg. *The Quantum theory of fields. Vol. 1: Foundations*. Cambridge University Press, 2005.

[98] Lance J. Dixon. A brief introduction to modern amplitude methods. In *Proceedings, 2012 European School of High-Energy Physics (ESHEP 2012): La Pommeraye, Anjou, France, June 06-19, 2012*, pages 31–67, 2014.

[99] Lance J. Dixon. Calculating scattering amplitudes efficiently. In *QCD and beyond. Proceedings, Theoretical Advanced Study Institute in Elementary Particle Physics, TASI-95, Boulder, USA, June 4-30, 1995*, pages 539–584, 1996.

[100] Johannes M. Henn and Jan C. Plefka. Scattering Amplitudes in Gauge Theories. *Lect. Notes Phys.*, 883:pp.1–195, 2014.

[101] Ruth Britto. Loop amplitudes in gauge theories: modern analytic approaches. *Journal of Physics A: Mathematical and Theoretical*, 44(45):454006, Oct 2011.

[102] Clifford Cheung. TASI Lectures on Scattering Amplitudes. In *Proceedings, Theoretical Advanced Study Institute in Elementary Particle Physics : Anticipating the Next Discoveries in Particle Physics (TASI 2016): Boulder, CO, USA, June 6-July 1, 2016*, pages 571–623, 2018.

[103] Eugene P. Wigner. On Unitary Representations of the Inhomogeneous Lorentz Group. *Annals Math.*, 40:149–204, 1939. [Reprint: Nucl. Phys. Proc. Suppl.6,9(1989)].

[104] R. Kleiss and W. James Stirling. Spinor Techniques for Calculating p anti-p —> W+- / Z0 + Jets. *Nucl. Phys.*, B262:235–262, 1985.

[105] R. Kleiss and W. James Stirling. TOP QUARK PRODUCTION AT HADRON COLLIDERS: SOME USEFUL FORMULAE. *Z. Phys.*, C40:419–423, 1988.

[106] Kaoru Hagiwara and D. Zeppenfeld. Helicity Amplitudes for Heavy Lepton Production in e+ e- Annihilation. *Nucl. Phys.*, B274:1–32, 1986.

[107] Christian Schwinn and Stefan Weinzierl. Scalar diagrammatic rules for Born amplitudes in QCD. *JHEP*, 05:006, 2005.

[108] Christian Schwinn and Stefan Weinzierl. SUSY ward identities for multi-gluon helicity amplitudes with massive quarks. *JHEP*, 03:030, 2006.

[109] S. D. Badger, E. W. Nigel Glover, V. V. Khoze, and P. Svrcek. Recursion relations for gauge theory amplitudes with massive particles. *JHEP*, 07:025, 2005.

[110] S. D. Badger, E. W. Nigel Glover, and Valentin V. Khoze. Recursion relations for gauge theory amplitudes with massive vector bosons and fermions. *JHEP*, 01:066, 2006.

[111] K. J. Ozeren and W. J. Stirling. Scattering amplitudes with massive fermions using BCFW recursion. *Eur. Phys. J.*, C48:159–168, 2006.

[112] Nima Arkani-Hamed, Tzu-Chen Huang, and Yu-tin Huang. Scattering Amplitudes For All Masses and Spins. 2017.

[113] Timothy Cohen, Henriette Elvang, and Michael Kiermaier. On-shell constructibility of tree amplitudes in general field theories. *Journal of High Energy Physics*, 2011(4), Apr 2011.

[114] Alfredo Guevara, Alexander Ochirov, and Justin Vines. Scattering of spinning black holes from exponentiated soft factors. *Journal of High Energy Physics*, 2019(9), Sep 2019.

[115] Alfredo Guevara, Alexander Ochirov, and Justin Vines. Black-hole scattering with general spin directions from minimal-coupling amplitudes. *Physical Review D*, 100(10), Nov 2019.

[116] Ming-Zhi Chung, Yu-tin Huang, and Jung-Wook Kim. Kerr-Newman stress-tensor from minimal coupling to all orders in spin. 2019.

[117] Daniel J. Burger, William T. Emond, and Nathan Moynihan. Rotating Black Holes in Cubic Gravity. 2019.

[118] Ming-Zhi Chung, Yu-tin Huang, Jung-Wook Kim, and Sangmin Lee. The simplest massive s-matrix: from minimal coupling to black holes. *Journal of High Energy Physics*, 2019(4), Apr 2019.

[119] Yilber Fabian Bautista and Alfredo Guevara. From Scattering Amplitudes to Classical Physics: Universality, Double Copy and Soft Theorems. 2019.

[120] Henrik Johansson and Alexander Ochirov. Double copy for massive quantum particles with spin. *Journal of High Energy Physics*, 2019(9), Sep 2019.

[121] Yilber Fabian Bautista and Alfredo Guevara. On the Double Copy for Spinning Matter. 2019.

[122] Aidan Herderschee, Seth Koren, and Timothy Trott. Massive On-Shell Supersymmetric Scattering Amplitudes. *JHEP*, 10:092, 2019.

[123] Aidan Herderschee, Seth Koren, and Timothy Trott. Constructing $\mathcal{N} = 4$ Coulomb branch superamplitudes. *JHEP*, 08:107, 2019.

[124] Yael Shadmi and Yaniv Weiss. Effective Field Theory Amplitudes the On-Shell Way: Scalar and Vector Couplings to Gluons. *JHEP*, 02:165, 2019.

[125] Rafael Aoude and Camila S. Machado. The Rise of SMEFT On-shell Amplitudes. 2019.

[126] Teng Ma, Jing Shu, and Ming-Lei Xiao. Standard Model Effective Field Theory from On-shell Amplitudes. 2019.

[127] Clifford Cheung, Karol Kampf, Jiri Novotny, Chia-Hsien Shen, Jaroslav Trnka, and Congkao Wen. Vector Effective Field Theories from Soft Limits. *Phys. Rev. Lett.*, 120(26):261602, 2018.

[128] Clifford Cheung, Chia-Hsien Shen, and Jaroslav Trnka. Simple Recursion Relations for General Field Theories. *JHEP*, 06:118, 2015.

[129] Gauthier Durieux, Teppei Kitahara, Yael Shadmi, and Yaniv Weiss. The electroweak effective field theory from on-shell amplitudes. 2019.

[130] Neil Christensen and Bryan Field. Constructive standard model. *Phys. Rev.*, D98(1):016014, 2018.

[131] Neil Christensen, Bryan Field, Annie Moore, and Santiago Pinto. 2-, 3- and 4-Body Decays in the Constructive Standard Model. 2019.

[132] Pinaki Banerjee, Alok Laddha, and Prashanth Raman. Stokes polytopes: the positive geometry for ϕ^4 interactions. *JHEP*, 08:067, 2019.

[133] P. B. Aneesh, Mrunmay Jagadale, and Nikhil Kalyanapuram. Accordiohedra as positive geometries for generic scalar field theories. *Phys. Rev.*, D100(10):106013, 2019.

[134] Andreas Helset, Michael Paraskevas, and Michael Trott. Gauge fixing the Standard Model Effective Field Theory. *Phys. Rev. Lett.*, 120(25):251801, 2018.